ЕМИЯ НАУК СССР
EMIA NAUK SSSR

OPTICS AND SPECTROSCOPY

СПЕКТРОСКОПИЯ SPEKTROSKOPIA

APRIL 1959 · VOL. VI · NO. 4
APREL' 1959 · TOM. VI · VYP. 4

Translated on the Initiative of
THE OPTICAL SOCIETY OF AMERICA, INC.
With a Grant-in-Aid from
THE NATIONAL SCIENCE FOUNDATION
by MORRIS D. FRIEDMAN, INC.

RUSSIAN EDITORIAL STAFF

Editor: S. E. FRISH

Assistant Editor: P. P. FEOFILOV

Corresponding Secretary: L. S. SAZONOV

Associate Editors:

M. M. GUREVICH M. A. EL'IASHEVICH A. A. LEBEDEV V. P. LINNIK
S. L. MANDEL'SHTAM I. V. OBREIMOV V. K. PROKOF'EV
N. N. SOBOLEV A. N. TERENIN A. I. TUDOROVSKII

Translation Editorial Staff

MORRIS D. FRIEDMAN

DR. JAMES R. ARONSON, *Arthur D. Little, Inc.*
FRED W. BEHNKE, *Perkin-Elmer Corp.*
DR. A. R. H. COLE, *Massachusetts Institute of Technology*
DR. RICHARD DALVEN, *Raytheon Company, Research Division,*
DR. SUMNER P. DAVIS, *University of California*
CYRUS FELDMAN, *Oak Ridge National Laboratory*
DR. CONRAD J. RAUCH, *Massachusetts Institute of Technology — Lincoln Laboratory*
DR. JOHN S. WAUGH, *Massachusetts Institute of Technology*
DR. ARTHUR W. WINSTON, *Allied Research Corp.*

Published semi-monthly by the Optical Society of America, Inc., 121 Lincoln Avenue, Rochester, New York. Business and Editorial office: 33 University Road, Cambridge 38, Mass. Subscriptions for one year to members of the Society: Associates $13.00; Regular members and Fellows $17.00. Subscriptions for non-members of the Society: One Year U. S. and Possessions, $25.00; Foreign $28.00. Back numbers: $3.00 per copy. Lithoprinted in the USA.

Application for 2nd Class mailing privileges pending at Post Office, Boston, Mass.

АКАДЕМИЯ НАУК СССР
AKADEMIIA NAUK SSSR

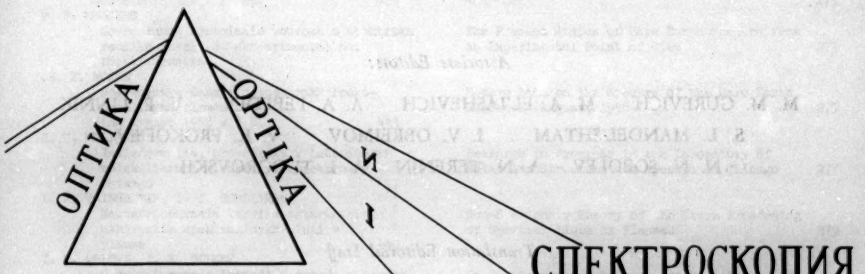

OPTICS AND SPECTROSCOPY

APRIL 1959 - VOL. VI - NO. 4
APREL' 1959 - TOM. VI - VYP. 4

Translated on the Initiative of
THE OPTICAL SOCIETY OF AMERICA, INC.
With a Grant-in-Aid from
THE NATIONAL SCIENCE FOUNDATION
by MORRIS D. FRIEDMAN, INC.

RUSSIAN EDITORIAL STAFF

Editor: S. E. FRISH

Assistant Editor: P. P. FEOFILOV

Corresponding Secretary: L. S. SAZONOV

Associate Editors:

M. M. GUREVICH M. A. EL'IASHEVICH A. A. LEBEDEV V. P. LINNIK
S. L. MANDEL'SHTAM I. V. OBREIMOV V. K. PROKOF'EV
N. N. SOBOLEV A. N. TERENIN A. I. TUDOROVSKII

Translation Editorial Staff

MORRIS D. FRIEDMAN

DR. JAMES R. ARONSON, *Arthur D. Little, Inc.*
FRED W. BEHNKE, *Perkin-Elmer Corp.*
DR. A. R. H. COLE, *Massachusetts Institute of Technology*
DR. RICHARD DALVEN, *Raytheon Company, Research Division,*
DR. SUMNER P. DAVIS, *University of California*
CYRUS FELDMAN, *Oak Ridge National Laboratory*
DR. CONRAD J. RAUCH, *Massachusetts Institute of Technology — Lincoln Laboratory*
DR. JOHN S. WAUGH, *Massachusetts Institute of Technology*
DR. ARTHUR W. WINSTON, *Allied Research Corp.*

Published semi-monthly by the Optical Society of America, Inc., 121 Lincoln Avenue, Rochester, New York. Business and Editorial office: 33 University Road, Cambridge 38, Mass. Subscriptions for one year to members of the Society: Associates $13.00; Regular members and Fellows $17.00. Subscriptions for non-members of the Society: One Year U. S. and Possessions, $25.00; Foreign $28.00. Back numbers: $3.00 per copy. Lithoprinted in the USA.

Application for 2nd Class mailing privileges pending at Post Office, Boston, Mass.

TOM VI, Vyp. 4 OPTIKA I SPEKTROSKOPIIA Aprel , 1959
VOL. VI, No. 4 OPTICS AND SPECTROSCOPY April, 1959

SODERZHANIE

V Mezhdunarodnoi Ob edinennoi komissii po spektroskopii
Doklady na soveshchanii 429
G. HERZBERG
Lembovskie smeshcheniia osnovnykh sostoianii He^4 i He^3 429
W. F. MEGGERS
Sovremennoe sostoianie voprosa o spektrakh redkikh zemel' s eksperimental'noi tochki zreniia 433
CH. E. MOORE
Sovremennye dannye o spektrakh redkozemel nykh elementov (na avgust 1958 g.) 433
R. S. MULLIKEN
Issledovaniia, provodimye v Laboratorii molekuliarnoi struktury i spektrov v Chikago 437
L. A. VAINSHTEIN, I. I. SOBEL'MAN
Nestatsionarnaia teoriia shtarkovskogo ushireniia spektral'nykh linii v plazme 440
I. V. ORLOVA, I. N. GODNEV
O sviazi metoda Larnodi i metoda nulevykh priblizhenii El'iashevicha i Stepanova 447
V. G. VESELAGO
Opredelenie struktury i dipol'nogo momenta molekuly HDSE iz ee mikrovolnovogo spektra 450
V. L. DIANOV-KLOKOV
K voprosu o proiskhozhdenii spektra zhidkogo i szhatogo kisloroda (12,600 - 3000 Å) 457
G. A. KHACHKURUZOV
Kolebatel'nye postoiannye molekuly vody 463
G. S. DENISOV
Ob izmerenii intensivnosti sil nykh polos pogloshcheniia v infrakrasnykh spektrakh zhidkostei 475
M. S. KOZYREVA
Primenenie infrakrasnoi spektroskopii k issledovaniiu polimerizatsii poliizobutilenov 478
L. A. LYZINA, A. T. VARTANIAN
Vliianie parov vody na spektry pogloshcheniia vozognannykh sloev krasitelei 484
IU. V. NABOIKIN, B. A. ZADOROZHNYI, E. N. PAVLOVA
Osobennosti liuminestsentsii orto-dizameshchennykh aromaticheskikh uglevodorodov. II 492
A. S. CHERKASOV
O vliianii zameshchaniushchikh grupp na polozhenie spektrov pogloshcheniia i fluorestsentsii proizvodnykh antratsena 496
A. S. CHERKASOV, T. M. VEMBER
O vliianii kisloroda na fotokhimicheskie prevrashcheniia i kontsentratsionnoe tushenie fluorestsentsii nekotorykh proizvodnykh antratsena 503
Z. A. TRAPEZNIKOVA
O vzaimodestvii "golubykh" i "samarievykh" tsentrov v fosfore ZnS-Sm(Cl) 512

CONTENTS

V International Joint Commission on Spectroscopy
Reports at the Conference 273
Lamb Shifts of the Ground States of He^4 and He^3 273
The Present Status of Rare Earth Spectra from an Experimental Point of View 273
Modern Data on the Spectra of the Rare Earth Elements (August, 1958) 275
Research in Progress in the Laboratory of Molecular Structure and Spectra in Chicago 277
Non-Stationary Theory of the Stark Broadening of Spectral Lines in Plasmas 279
On The Connection Between Larnaudie's Method and the El'iashevich - Stepanov Method of Zero Approximations 284
Determination of the Structure and Dipole Moment of HDSe from its Microwave Spectrum 286
On the Question of the Origin of the Spectrum of Liquid and Compressed Oxygen (12,600 - 3,000 Å) 290
Vibrational Constants of the Water Molecule 294
On the Measurement of Intensities of Strong Absorption Bands in Infrared Spectra of Liquids 301
Application of Infrared Spectroscopy to the Investigation of Polymerization of Polyisobutylene 303
Influence of Water Vapors on the Absorption Spectra of Sublimated Layers of Dyes 307
Peculiarities of the Luminescence of Ortho-Disubstituted Aromatic Hydrocarbons: II 312
On the Influence of Substituting Groups on the Absorption and Fluorescence Spectra of Derivatives of Anthracene 315
The influence of Oxygen on Photochemical Transformations and the Concentration Quenching of Fluorescence of Some Anthracene Derivatives 319
On the Interaction of "Blue" and "Samarium" Centers in the Phosphor ZnS-Sm(Cl) 325

I. V. OBREIMOV, E. F. IAMSHCHIKOV
Krivye dispersii khloroforma i chetyrekhkhloristogo ugleroda v shirokom intervale temperatur 517

V. S. SUKHORUKIKH
Difraktsiia Frenelia ot uzkogo ekrana, shcheli i poluploskosti pri nesfericheskoi volne 523

I. N. SHKLIAREVSKII, A. A. AVDEENKO, V. G. PADALKA
Izmerenie opticheskikh postoiannykh sur'my v infrakrasnoi oblasti spektra pri temperature 290 i 110 528

P. G. KARD
O vliianii tonkikh plenok na polnoe otrazhenie 533

B. V. BOKUT'AND F. I. FEDOROV
K teorii opticheskoi aktivnosti kristallov. III. Obshchee uravnenie normalei 537

B. P. KOZYREV AND O. E. VERSHININ
Opredelenie spektral'nykh koeffitsientov diffuznogo otrazheniia infrakrasnoi radiatsii ot zachernennykh poverkhnostei 542

V. I. MALYSHEV, S. G. RAUTIAN
Ispol'zovanie esheletta pri bol'shikh uglakh difraktsii 550

A. O. SALL
O poroge chuvstvitel'nosti optiko-akusticheskogo priemnika radiatsii. II. Neravnomernoe vydelenie tepla po ob'emu kamery selektivnogo priemnika. Vysokaia chastota obtiuratsii 556

KRATKIE SOOBSHCHENIIA

V. K. ABLEKOV
Ob obrabotke spektrogramm, poluchennykh na interferometre Fabri-Pero 562

N. IA. CHERNIAK, N. N. BUBNOV, L. S. POLIAK, IU. D. TSVETKOV, V. V. VOEVODSKII
O nekotorykh zakonomernostiakh v spektrakh elektronnogo paramagnitnogo rezonansa alkil'nykh radikalov 564

N. N. BUBNOV, V. V. VOEVODSKII, L. S. POLIAK, IU. D. TSVETKOV
O spektrakh elektronnogo paramagnitnogo rezonansa atomov vodoroda, stabilizirovannykh na tverdykh poverkhnostiakh 565

IA. S. BOBOVICH, T. P. TULUB
Temperaturnaia zavisimost' intensivnosti stoksovykh polos kombinatsionnogo rasseianiia v spektrakh nekotorykh tverdykh tel 566

E. F. GROSS, B. V. NOVIKOV, B. S. RAZBIRIN, L. G. SUSLINA
Spektry pogloshcheniia kristallov nekotorykh khalkogenidov galliia 569

Dispersion Curves of Chloroform and Carbontetrachloride in a Wide Temperature Range 329

Fresnel Diffraction of a Non-spherical Wave by a Narrow Screen, a Slit and a Half-plane 332

Measurements of the Optical Constants of Antimony in the Infrared Region of the Spectrum at Temperatures of 290° and 110° 336

On the Influence of Thin Films on Total Reflection 339

On the Theory of Optical Activity in Crystals III. General Equation of Normals 342

Determination of Spectral Coefficients of Diffuse Reflection of Infrared Radiation from Blackened Surfaces 345

Use of an Echelette at Large Diffraction Angles 351

On the Threshold Sensitivity of An Optical-Acoustic Radiation Detector II. Nonuniform Heat Elimination in the Chamber Volume of a Selective Detector. High Modulation Frequency 355

BRIEF REPORTS

On Processing Spectrograms Obtained on a Fabry Perot Interferometer 359

Some Regularities in the Electron Paramagnetic Resonance Spectra of Alkyl Radicals 360

On the Electron Paramagnetic Resonance Spectra of Hydrogen Atoms Stabilized on Solid Surfaces 361

Temperature Dependence of the Intensity of Stokes Bands in the Raman Spectra of Certain Solids 362

Absorption Spectra of Certain Gallium Chalcogenide Crystals 364

Abbreviations Often Encountered and Used Herein 367

Affiliation of Authors from Issue 4 368

Instructions for Authors (Russian) 369

Letter from the Publisher 370

Lithoprinted in the U.S.A. by Blackburn Printing Co., West Concord, Mass.

ТОМ VI, Вып. 4 ОПТИКА И СПЕКТРОСКОПИЯ Апрель, 1959
VOL. VI, No. 4 OPTICS AND SPECTROSCOPY April, 1959

INTERNATIONAL JOINT COMMISSION ON SPECTROSCOPY

Reports at the Conference

As was announced in Optics and Spectroscopy [V, 715 (1958)], there took place in Moscow from August 15, 1958 a conference of the International Joint Commission on Spectroscopy (JCS), at which in addition to organizational matters, a series of scientific ones were discussed. The commission expressed a desire for publication of these discussions in the journals of various countries. In accordance with this decision Prof. G. Herzberg, Dr. W. F. Meggers, Dr. Charlotte Sitterly-Moore, Prof. R. S. Mulliken and Prof. B. Edlen have sent short summaries of their reports to the Editors of Optics and Spectroscopy. Translations of the reports of G. Herzberg, W. F. Meggers, C. Sitterly-Moore and R. S. Mulliken are published below. Prof. B. Edlen sent the text of a report on primary spectroscopic standards which he presented at the conference of commission No. 14 of the International Astronomical Union (IAU). This report discussed the meeting of the International Committee on Weights and Measures, which at its 1957 session adopted as a new spectral standard the $\lambda = 6056$ Å line of Kr^{86} in place of the previously used red line of cadmium. Wavelengths for secondary standards in the infrared (Ne and A) and far ultraviolet (Ge) regions were also taken up. This report will be published in the Proceedings of the International Atomic Congress and therefore is not included in the present issue.

Lamb Shifts of the Ground States of He^4 and He^3

G. HERZBERG

In order to obtain an experimental value for the Lamb shift of the ground state of helium, it is first necessary to know the ionization potential exactly. With this goal in mind, the wavelengths of the far ultraviolet He^4 lines at 543 Å ($1^1S - 2^1P$) 537.0 Å. ($1^1S - 3^1P$) and 591.4 Å ($1^1S - 2^3P_1$) have been redetermined with significantly greater accuracy than before, and the wave lengths for He^3 have been measured for the first time. Lines of C^+ and A^+ in the 610 - 520 Å region, obtained according to the combination principle from lines at longer wavelengths, were used as comparisons. As a result the following values were found for the He^4 wave lengths: 584.3339, 537.0293 and 591.4121 Å, all with a precision of ± .0005 Å. The corresponding numbers for He^3, obtained by combining the measured shifts with the He^4 wavelengths, were found to be: 584.3640, 537.0577 and 591.4466 Å. The term values of the upper states of these lines relative to the ionization limit were redetermined through a new measurement of the Bergmann series $3^3D - n^3F$, the intercombination lines $2^3P - 3^1D$ and the near ultraviolet series $2^2P - n^1D$ and $2^3P - n^3D$. Combining these results with those obtained for the far ultraviolet lines, the following values were found for the ionization potentials of He^4 and He^3:

$$\text{Ion. pot'l } (He^4) = 198310.8_2 \pm 0.15 \text{ cm}^{-1}$$

$$\text{Ion. pot'l } (He^3) = 198300.3_2 \pm 0.15 \text{ cm}^{-1}.$$

The isotope shift of the ground state, $10.50 \pm 0.05 \text{cm}^{-1}$ agrees exactly with the predictions of theory.

An experimental value of the Lamb shift was found by comparing the above ionization potentials with those calculated from Dirac theory, ignoring quantum electrodynamic effects. With the aid of the recent 203-parameter wave function of Pekeris, the Lamb shifts for He^4 and He^3 were found to be -1.1_9 and -1.2_3 cm^{-1}, respectively. The value predicted by Kabir, Salpeter and Sucher is $-1.3_3 + 0.2$ cm^{-1}.

Dept. of Pure Physics
Ottawa, Canada

The Present Status of Rare Earth Spectra from an Experimental Point of View

W. F. MEGGERS

In 1946 the Spectroscopy Section of the National Bureau of Standards undertook the task of compiling and publishing, in four volumes, the compilation "Atomic Energy Levels from the Analysis of Optical Spectra". Besides the relative values of energy levels, this collection contains data on spectral terms, spacings between levels, quantum numbers, magnetic splitting coefficients, electron configurations and ionization potentials.

Volume I embraces data related to the first 23 chemical elements ($_1$H - $_{23}$V), obtained from the analysis of 206 spectra.*

Volume II contains data concerning the 18 elements $_{24}$Cr - $_{41}$Nb, obtained from the analysis of 152 spectra.

Volume III presents data on the 33 elements $_{42}$Mo - $_{57}$La and $_{72}$Hf - 89Ac on the basis of an analysis of 124 spectra.

Volume IV of Atomic Energy Levels, being prepared for publication at the present time is concerned with two separate groups of elements--the so-called rare earths or lanthanides ($_{58}$Ce - $_{71}$Lu) and the actinides (90^{Th} - 102^{No}).

The 14 lanthanides contain among their atomic shells electrons of the 4f type, and the actinides usually possess one or more 5f electrons. In general the presence of the 4f electrons in addition to s, p and d electrons greatly increases the number of energy levels and consequently complicates the spectra of these elements.

* From material in a report to the JCS in Moscow on August 14, 1958

In many cases the 4f electrons are chemically inert, and elements containing f electrons cannot be easily separated inasmuch as the number of s- and d- valence electrons in them is the same. These two circumstances -- the great complexity of the spectra and the difficulty of obtaining pure samples -- have greatly impeded the spectroscopic investigation of these elements in the past, and therefore comparatively little is known about their atomic energy levels to this day. Thus, for example, nearly nothing has been established about the spectra of the singly ionized species of half of these elements, and nothing at all is known about the more highly ionized species of any of them except for CeIII and LuIII. The same is true of the actinides, with the exception of $_{90}Th$, $_{92}U$ and $_{95}Am$. This condition needs to be corrected in order that Volume IV of "Atomic Energy Levels" may contain data comparable to those of the preceding three volumes. The purpose of the present article is to show how the experimental difficulties have been successfully overcome, and to indicate the necessity of further work on these important elements, whose spectra are of particular interest in our atomic age.

Until 1945 the lanthanides were ordinarily separated out of their natural mixture by means of fractional crystallization and, in order to obtain relatively pure samples, it was necessary to repeat this procedure many thousand times. In 1945 a rapid method of separating the lanthanides was found; it is based on the use of absorption columns of organic resins. A great quantity of pure lanthanides has been accumulated as a by-product of the separation and purification of thorium and uranium. Samples of a high degree of purity (99.99%) can now be obtained from various sources at a low price, or even free if rather small quantities are required for research.

Only one of the lanthanides ($_{61}Pm$) is highly radioactive; it has not been found in nature, but has been obtained from the products of U^{235} fission and also from the transmutation of $_{59}Pr$.

All of the actinides are radioactive. With the exception of the first three ($_{90}Th$, $_{91}Pa$ and $_{92}U$) none of them has been found in natural ores or minerals. Nonetheless two or more isotopes of these nine transuranic elements have been successfully isolated, since many of them have sufficiently long half lives so that they can be enriched, purified and studied. Thus, certain characteristic spectra of $_{93}Np$, $_{94}Pu$, $_{95}Am$ and $_{96}Cm$ have already been studied in a cursory fashion, and there is some basis for expecting that these investigations can be completed more exactly and extended to heavier elements. The shortage and high cost of pure samples is no longer an obstacle to spectroscopic investigation of the lanthanides and actinides, but it is still necessary to overcome the difficulty associated with complexity of the spectra and, in certain cases, with the radioactivity of the specimens. Fortunately, recent advances in the field of light sources have substantially alleviated this problem.

Until 1950 the majority of spectra studied were obtained with the usual steady arc or high-voltage alternating-current spark. These hot sources did a good job of atomizing refractory compounds, and exciting their spectra, and permitted the identification of atomic and ionic lines by comparison of their intensities in two different sources; but the high temperatures, appreciable pressures, and strong electric fields in these sources led to a broadening of the lines Significantly narrower lines can be obtained by excitation in a furnace at low pressure, in which case the variation of line intensities with temperature gives useful information. However, heating the furnace to the temperatures necessary to excite ionic lines or other lines with high excitation potentials presents great difficulties.

Gases or metal vapors, excited in evacuated and cooled hollow cathodes, give sharper lines than in furnaces, but the spectra are always mixed with lines belonging to the cathode metal and to rare gases. To date there are in the literature no good spectral data on the lanthanides or actinides obtained with the use of a hollow cathode source.

Apparently the best source for the investigation of complex spectra is an electrodeless lamp, containing traces of volatile metal halides and excited by microwaves [2,3], inasmuch as these lamps work at low pressures and moderate temperatures, they emit narrower lines than the usual arcs and sparks, and without loss of intensity. In order to obtain and isolate the spectra of highly ionized species it is necessary to vary the excitation conditions; this may be accomplished either by going over to a pulsed scheme [4,5] or by adjustment of the temperature or pressure of the vapor [3]. With steady excitation of these lamps the spectra of singly ionized species appear; this is important for the investigation of elements which are mainly ionized in an arc, and in strong magnetic fields. Indeed, the Zeeman effect in ErI (and other lanthanides) in magnetic fields of ~80,000 oersteds has been successfully observed [6] only with the aid of an electrodeless lamp containing metal halides.

The special features of the electrodeless halide lamp include mechanical strength, reliability, small size, insignificant cost of samples, and great brightness -- properties which are exceedingly important for the spectroscopic study of highly radioactive isotopes, inasmuch as they ensure maximum output and reduce to a minimum the danger of working with these materials.

Another virtue of electrodeless halide lamps lies in the fact that they do not prodce a strong background of continuous and molecular spectra, masking the weak lines, as occurs when the light source is an arc at atmospheric pressure. True, this virtue is partly nullified by the appearance of halogen spectra and spectra of new metal-halogen compounds. However the spectra of the unionized halogens are always of the simple one-electron type, and those of the metal halides are usually weak. Moreover it can be seen by comparing the spectra of two or more halogen compounds that their common features belong to the metal, whereas the different features arise either from the halogen itself or from the metal halide molecule. An example of the successful application of this method is found in the investigation of the spectrum of hafnium [7], for which it was possible to detect more than twice as many lines as could be found with arc or spark excitation, and to attain greater accuracy in the measurement of their wavelengths.

The same method has been used to refine the spectrum of ThI, in which 14000 lines were obtained [8].

Inasmuch as the spectra are extraordinarily rich in lines and these lines are sharp, it is necessary to use better comparison spectra for the measurement of wavelengths than the spectrum of an iron arc at atmospheric pressure. More exact reference lines are obtained from the thorium-halogen lamp [9]. If in the future the complex spectra of the lanthanides and actinides are measured with the aid of such comparison spectra, then, using electronic computers [10], it will be possible to determine the atomic energy levels quickly and exhaustively; the accuracy should be sufficient to enable one to reject accidental coincidences between wave length differences and spacings between energy levels.

To summarize, lanthanides and actinides of a high degree of purity are now available for research. Light sources possessing great brightness and mechanical stability can be constructed easily in any laboratory: they are simple in construction and reliable, taking the form of an evacuated quartz tube containing a microscopic quantity of a metal halide. These lamps, fed from a commercial microwave generator, produce atomic spectra with very intense and sharp lines. The use of a pulsed arrangement or regulation of the pressure of the vapor permits the excitation of the spectra of doubly and even more highly ionized species. These lamps are ideal for the observation of the Zeeman effect and for the investigation of highly radioactive elements or isotopes. Thorium-halogen lamps give excellent comparison spectra for the measurement of wavelengths of other complex spectra with exactitude, which is necessary for the latest analysis of atomic energy levels using electronic computers.

Notwithstanding the fact that all the experimental difficulties have been eliminated or reduced to a minimum, very little has been done in the way of determining atomic energy levels on the basis of the analysis of the optical spectra of the lanthanides and actinides. This is explained by a lack of interest in the problem and a reduction in the number of people occupied with it. As far as the author knows at the present moment only one person is working on this problem full time, and three on a part-time basis. If this condition is not changed the spectra of the lanthanides and actinides will remain to a significant extent unknown, and further progress in astrophysics, nuclear physics and spectrochemical analysis will be arrested at the present level since basic data will not be forthcoming.

References

1. C. E. MOORE: Atomic Energy Levels as Derived from Analyses of Optical Spectra. Nat. Bur. Stand. Circ., I, 467, 1949; II, 1952; III, 1958 IV in press.
2. C. H. CORLISS, W. R. BOZMAN, F. O. WESTFALL: JOSA, 43, 398 (1953)
3. F. S. TOMKINS, M. FRED: JOSA, 47, 1087 (1957)
4. L. MINNHAGEN, L. STIGMARK: Ark. f. fys., 13, 27 (1958)
5. R. W. SHORTHILL, G. R. FOWLES: JOSA, 48, 459 (1958)
6. J. W. LINDNER, S. P. DAVIS: JOSA, 48, 542 (1958)
7. C. H. CORLISS, W. F. MEGGERS: J. Res. Nat. Bur. Stand., 61, 269 (1958)
8. R. ZALUBAS: Not published
9. W. F. MEGGERS, R. W. STANLEY: J. Res. Nat. Bur. Stand., 61, 95 (1958)
10. K. G. KESSLER, S. B. PRUSCH, I. A. STEGUN: JOSA, 46, 1043 (1956)

Modern Data on the Spectra of the Rare Earth Elements (August, 1958)

C. E. MOORE

In a classic paper published in 1946, Kiess, Humphrey and Laun [1] showed by analysis of the spectrum of UI that the ground state of this atom is $5f^3 7s^2 6d^5 L_6^o$, which has been completely confirmed by studies of the Zeeman effect. They wrote: The spectrum of uranium can be regarded as the spectrum of a rare earth element analogous to neodymium, in which case uranium is the third member of a second group of rare earths, beginning with thorium. Thus, uranium was for the first time definitely classified in the rare earth category, characteristically governed by the influence of electrons. The second group, beginning with $_{90}$Th, is characterized by the presence of 5f electrons, in contrast with the first group --$_{58}$Ce to $_{71}$Lu -- whose atoms have 4f electrons.

The spectra of these elements are the least known and most complex of all atomic spectra. It is hard to expect that the spectra of many of the ionized species should be investigated in detail. If only four spectra of each element in the first group and in the second group up to element 99 (E) were investigated, that would amount to 96 spectra in all. At the present time the structures of only 22 spectra from the first group and 11 from the second are known, and in the majority of cases their interpretation is far from complete. References to the interpretation of various spectra can be found in two bibliographies, of which one was published by Meggers [2] in 1946 and the other recently by the author of the present article [3].

A short summary of data characterizing the present state of knowledge of the spectra of both groups of rare earth elements is given in Tables 1 and 2, which do not particularly require clarification. It becomes clear that for the majority of spectra the existing lists of lines are neither complete nor of the same kind although the observa- embrace a significant range of wave lengths, for example, the data for Pr I were taken from King's

article on thermal classification. For other spectra not described in the literature data have been obtained such as those for Pm, in whose spectrum 2200 lines have been measured.

Table 1

Summary of data on the spectra of the lanthanide group

Z	Spectrum	Range of observation (in Å)	Zeeman effect	No. of interpreted lines	Ionization potential
58	Ce I	3006—7049			
	Ce II	2592—12000	yes	>3600	
	Ce III	1680—3543	yes	294	20±1
	Ce IV	443—2778	yes	31	36.7
59	Pr I	3218—6738			
	Pr II	2400—8000	yes	312	
	Pr V	2378—2381		2	
60	Nd I	2613—8164	yes	63	
	Nd II	2000—11000	yes	367	
61	Pm	2337—6872			
62	Sm I	2500—8700		> 500	5.6
	Sm II	3008—9264	yes	>1200	11.4
63	Eu I	2428—5326		1156	5.64
	Eu II	2109—10165	yes	467	11.21
	EuIII	2350—2522	yes	7	
64	Gd I	2734—10629		1217	6.16
	Gd II	2141—9004	yes	1177	
65	Tb I	3837—4676			
	Tb II	3841—4651		12?	
66	Dy I	3840—4681			
	Dy II	2300—9000	yes	100	
67	Ho I	3890—4681			
	Ho II	3837—4629			
68	Er I	3181—4745	yes		
	Er II	2915—5133	yes		
69	Tm I	2513—8301		32	
	Tm II	2182—6789	yes	230±	
70	Yb I	2464—10770	yes	88	6.22
	Yb II	2073—9104	yes	856	12.09
71	Lu I	2404—10729		124	6.15
	Lu II	2195—8459	yes	191	14
	LuIII	2236—3057			

Table 2

Summary of data on the spectra of the actinide group

Z	Spectrum	Range of observation (in Å)	No. of observed lines	Zeeman effect	No. of interpreted lines	Ionization potential
90	ThI	2000—11500	12000	yes	1200±	
	ThII	2000—11500	4000	yes	2900 ±	
	ThIII	1450—10702		yes	314	20
	ThIV	797—10875		yes	24	28.6
91	Pa	2640—6379	323			
92	UI	2900—11000	9000	yes	2000	4
	UII	2400—8504		yes	743	
93	Np	2655—4363	114	yes *		
94	PuI	2790—6887	1400	yes *		
	PuII	2500—8000	600	yes	5	
95	AmI	2953—8497			112	6.0
	AmII	2527—8234	3000		173	
96	Cm	2516—5250	300			

In column 4 the existence of Zeeman effect investigations is indicated. In the last column the ionization potentials, taken from various articles, are given.

In a number of the spectra isotope shifts are observed; they have been used for confirmation or broadening of the interpretation of the spectrum. The isotope shift in the spectrum of Ce II, observed by Brix and Frank [4], has for the first time been connected with the 6s and 6p electrons. In the spectrum of Sm I analogous data have been used to group the odd levels into terms and to determine electron configuration [5]. Wilets and Bradley connected the negative isotope shift in Er II with transitions depending on a double electron jump [6].

In Table 3 are given the number of terms and levels predicted from theory for numbers of f electrons ranging from 1 to 14. The figures under both headings signify the possible number of terms of the given type. Until now very little has been known about the terms of higher multiplicity, with the exception of the lowest ones. Moreover the terms with electron configurations d^2, p^2, s^2, fsp, fsd and fpd need to be examined. All these factors, taken together, result in serious complications in rare earth spectra, and explain the paucity of data in Tables 1 and 2.

Table 3

No. of electrons	Predicted Terms and Levels — Equivalent f-electrons			No. of terms	No. of levels
f^1	$^2(F)$			1	2
f^2	$^1(SDGI)$	$^3(PFH)$		7	13
f^3	$^2(PDFGHIKL)$	$^4(SDFGI)$		17	41
f^4	$^1(SDFGHIKLN)$	$^3(PDFGHIKLM)$	$^5(SDFGI)$	47	107
f^5	$^2(PDFGHIKLMNO)$	$^4(SPDEGHIKLM)$	$^6(PFH)$	73	198
f^6	$^1(SPDFGHIKLMNQ)$	$^3(PDFGHIKLMNO)$	$^5(SPDFGHIKL)$ $^7(F)$	119	295
f^7	$^2(SPDFGHIKLMNOQ)$	$^1(SPDFGHIKLMN)$	$^5(PDFGHI)$ $^7(S)$	119	389
f^8	$^1(SPDFGHIKLMNQ)$	$^3(PDFGHIKLMNO)$	$^5(SPDFGHIKL)$ $^7(F)$	119	295
f^9	$^2(PDFGHIKLMNO)$	$^4(SPDFGHIKLM)$	$^6(PFH)$	73	198
f^{10}	$^1(SDFGHIKLN)$	$^3(PDFGHIKLM)$	$^5(SDFGI)$	47	107
f^{11}	$^2(PDFGHIKL)$	$^4(SDFGI)$		17	41
f^{12}	$^1(SDGI)$	$^3(PFH)$		7	13
f^{13}	$^2(F)$			1	2
f^{14}	$^1(S)$			1	1
				648	1682

On the basis of the above outline it is possible to make some brief general remarks. Zeeman effect data are very scanty for the singly ionized rare earths, owing to their comparatively low ionization potentials. With the exception of the more highly ionized rare earth spectra has hardly begun. From Ce to Yb (excepting $_{61}$Pm) the basic terms of the trivalent ions are known only from fluorescence and absorption spectra of rare earth salt crystals at low temperatures. It is well known that the absorption lines are caused by transitions among various levels of the $4f^n$ configurations, where n takes on values from 1 (for Ce^{+++}) to 13 (for Yb^{+++}) 7. At least in one case -- that of divalent europium Eu^{++} -- it has been shown that there is a state coinciding with one well known from optical spectra -- $4f^7\ ^8S^o_{7/2}$.

In the second group analogous observations have been made for various ions having a $5f^n$ configuration, for example:

U^{+4} — $5f^2$
UU^{+3} — $5f^3$
Np^{+3} — $5f^4$
Pu^{+3} — $5f^5$
Am — $5f^6$

* One value for the g-factor, obtained from atomic beam magnetic resonance.

A more detailed review of this question may be found in Jorgensen [8].

In view of the extreme importance of rare earth spectra for physicists, astrophysicists, chemists and others, it is entirely necessary that spectroscopists of all countries accept the challenge contained in this paper. An interpretation of these spectra, based on complete, accurate and uniform lists of lines, is needed, as well as observations of the Zeeman effect. For the majority of spectra the observations must embrace the region from the ultraviolet to the far infrared. In planning these investigations we must of course avoid duplication of effort. Modern computers of the IBM type will be able to lighten the work if a treatment of the data is set up by the experimental spectroscopists. It is the duty of spectroscopists to take up the gauntlet without delay.

Washington, D. C. November 21, 1958

References

1. C. C. KIESS, C. J. HUMPHREYS, D. D. LAUN: J. Res. Nat. Bur. Std., 37, 57, RP 1729 (1946)
2. W. F. MEGGERS: JOSA, 36, 431 (1946)
3. C. E. MOORE: Nat. Bur. Std. Circ. 467, 3, XXXIII (1958)
4. P. BRIX, H. FRANK: Zs. Phys., 127, 209 (1950)
5. P. BRIX: Zs. Phys., 126, 431 (1949)
6. L. WILETS, L. C. BRADLEY, III: Phys. Rev. (2), 84, 1055 (1951)
7. H. GOENECHT: Ann. der Phys. (5), 28, 673 (1937) (5), 31, 600, 755 (1938)
8. C. K. JØRGENSEN: Mat. Fys. Medd. Kgl. Danske Videnskab. Selskab. 29, No. 7 (1955)

Research in Progress in the Laboratory of Molecular Structure and Spectra in Chicago

R. S. MULLIKEN

It occurs to me that a short outline of the work in progress at the Laboratory of Molecular Structure and Spectroscopy in Physics Department at the University of Chicago will be more appropriate than a report on any special topic. Our work consists of several interconnected parts, both theoretical and experimental, in the general field of chemical physics, of which the theoretical calculation of molecular structures occupies the greatest number of workers. Basically the work may be categorized in the following four divisions.

HIGH-RESOLUTION SPECTROSCOPY

The equipment for work on experimental spectroscopy consists of a 30 foot installation of the Paschen type with a diffraction grating having 1200 lines/mm, a 21 foot apparatus of the same type, and a 21 foot vacuum spectrograph of normal incidence with a 1200 line/mm grating, having a resolving power in the vicinity of 30,000 in the third order. Dr. P. G. Wilkinson is in charge of the laboratory. At the present time particular significance is attached to vacuum spectroscopy. Using the continuous emission spectrum of Kr_2 and X_2 excited by microwaves, as a light source in the region 1200 - 2200 Å, the spectra of N_2, CO, O_2, NO, CO_2, C_2H_2 and C_2D_2, C_2H_4 and C_2D_4, C_6H_6 have been ed and interpreted. The results are published in the articles of Wilkinson, Wilkinson and Mulliken, and others; a series of further articles on this subject is in preparation. The Vigard-Kaplan bands have been obtained for the first time in the absorption spectrum of nitrogen, and also two new remarkably weak absorption band systems in that substance. Moreover, data have been published on the emission spectra of certain diatomic molecules. Dr. Wilkinson has obtained new standard wavelengths in the vacuum region. He is also working on the determination of the refractive indices of H_2, He and N_2, measuring the wavelength shift in gases at high and low pressures. T. Namioka is carrying on a large project on the theory of concave diffraction gratings with reference to characteristics of spectral lines for various arrangements of apparatus. He has corrected some serious errors made in previous work.

ABSORPTION SPECTRA OF SOLUTIONS

The spectrophotometric work includes the visible and ultraviolet spectra of molecules in solutions, including the spectra of complexes in which electron transfer occurs. (Dr. Tsubomura is doing this work under a grant from Prof. Mulliken and Prof. V. G. Brown of the Chemistry Department.) Work in this field opens a breadth and diversity of possibilities for the understanding of chemical reactions and their mechanisms, photochemical reactions of analytical chemistry, and certain solid state effects of interest in biochemistry.

THEORY OF CONJUGATED AND HYPERCONJUGATED SYSTEMS

In connection with a recent conference on hyperconjugation, Prof. Mulliken focused his attention on certain questions, moot at that conference, having to do with the factors determining bond lengths and energies of conjugated and hyperconjugated organic molecules. In an article written jointly with N. Mueller, and also in an article in Tetrahedron, he suggested that these molecules be divided into those having sacrificial and those having isovalent conjugation or hyperconjugation. In another article,

which will appear in Tetrahedron, he critically exmmined the role of π-π conjugation and other factors in determining bond lengths and energies in the presence of conjugation and hyperconjugation.

HIGH-SPEED THEORETICAL CALCULATIONS ON ATOMS AND MOLECULES

Beginning in 1950 the Laboratory has focused its efforts more and more on obtaining good electronic wave functions for molecules in order to achieve, with the aid of quantum mechanical calculations, a better understanding of the electronic structure of molecules, valence, and other related matters. This work now is approaching a successful conclusion, thanks mainly to the efforts of Prof. C. J. Roothaan and those students and scientific collaborators who are working with him.* Two difficult problems confronted them: 1)the obtaining of mathematical expressions for the values of interelectronic repulsion integrals when the electrons concerned are in orbits about different nuclei; 2) the elaboration of methods of rapid calculation on a large electronic computer.

From the very beginning of the existence of quantum mechanics the difficulties of solving the first of these problems and the great volume of the calculations necessary, delayed the determination of electronic structures of molecules, except for the simplest cases, and forced them to remain on a qualitative and semiempirical basis. However, at the present time these difficulties have been removed for diatomic molecules; and it is possible to consider that the main problem remaining unsolved: namely, the development of rapid and accurate methods of evaluating interelectronic repulsion integrals for three and four centers, will soon be solved.

The most general integral of the above-mentioned type may be written thus:

$$(1)\quad I = \int dv_1 \int dv_2 \, [\chi_a(1)\chi_b^*(1)]\, e^2/r_{12}[\chi_c^*(2)\, \chi_d^*(2)]$$

where each χ is an atomic orbital (AO) of the Slater type: $r^m e^{-\zeta} Y(\theta,\varphi)$ about one of the four nuclei a, b, c, d, each of the four χ's being labelled according to type (i.e. represented by 1s, 2pσ, 3d or 4fπ) and according to the value of the orbital exponent ζ. In two-center integrals (two atoms) the configuration abcd in equation 1 can be replaced by the configurations aabb, aaab or abab. The configuration aaaa is still simpler, corresponding to integrals over a single atom [the Coulomb integrals $1s_a(1)\, 1s_a(1)\, 2s_a(2)\, 2s_a(2)$ and the exchange integrals $1s_a(1)\, 2s_a(1)\, 1s_a(2)\, 2s_a(2)$].

The possibility of quickly calculating interelectronic (and other simpler) integrals permits one to construct molecular wave functions from two or more antisymmetrized molecular orbitals (MO); each MO is approximated by a linear combination of atomic orbitals (LCAO-MO) with one or more AO's on each atom. Then to determine the best wave function one uses the self consistent field (SCF) or other variational methods, leading to a minimum energy.

It is a very important fact that we are beginning to accumulate tests for the determination of optimal values of ζ for each AO in each MO. Great successes have been attained in the determination of SCF-LCAO-MO wave functions for LiH, BH, NH, HF, Li_2, N_2, F_2, CO and LiF. The application of comparatively small electronic computers shortens the time required for a full determination of the form and energy of the MO and the total energy, using wave functions constructed from MO's of the simple LCAO-SCF type, to 10 minutes for hydrides, 35 minutes for first-row homopolar molecules, and 100 minutes for first-row heteropolar molecules. It may be pointed out by way of comparison that a few years ago Dr. C. V. Sherr in our laboratory spent roughly two man-years on the N_2 calculation using conventional (hand) methods of computation.

Soon perfected programs will be ready for these calculations, including those for molecules containing atoms with higher orbital quantum numbers. Although similar calculations have been carried out in other places, the majority of them make use of diferent approximations. Before beginning the calculation of particular molecules, we wish to establish accurate and reliable programs for fast machine computations.

Apart from the investigation of LCAO-MO-SCF wave functions, Prof. Roothaan and his collaborators are devoting a large amount of work to the calculation of correlated electron wave functions for simple atoms and for H_2, using detailed functions of the interelectron distance r_{ij}. The possibility of applying methods which take configuration interaction into account is being studied. Further, for diatomic molecules they are continuing to make use of functions in elliptic coordinates, with which a better wave function for H_2 has already been obtained than that calculated by James and Coolidge. They are attempting to carry similar calculations over to the case of atoms and molecules containing 3 and 4 electrons.

---

* See C.C.J.ROOTHAAN. J.Chem. Phys. 28 , 982, (1958); R.S. MULLIKEN. C.C.J.ROOTHAAN. Proc. Nat. Acad. Sci., 1959.

TOM VI, Vyp 4
VOL. VI, No.4

OPTIKA I SPEKTROSKOPIIA
OPTICS AND SPECTROSCOPY

Aprel', 1959
April, 1959

Non-Stationary Theory of the Stark Broadening of Spectral Lines in Plasmas

L. A. VAINSHTEIN AND I. I. SOBEL'MAN

Abstract: The broadening of atomic spectral lines by charged particles is considered in the non-adiabatic approximation. Taking account of the non-adiabatic character of the process allows one to obtain a series of new results even within the limits of a relatively simple quasi-classical model. For the velocities characteristic of electron plasmas, the Weisskopf broadening mechanism has little effect and the broadening is due instead to inelastic processes. It is shown that for large velocities the width and displacement of the lines decrease approximately as v^{-1}. For this reason the ions play an important role. For determining the plasma parameters in a series of cases it is more convenient to use the displacement of the line, rather than its width.

INTRODUCTION

Collisions of atoms with charged particles --electrons and ions-- play an important role in the broadening of atomic spectral lines in plasmas. The theory of this effect is, however, in an unsatisfactory state. This may be seen from an analysis of the experimental data [1] as well as from the results of a series of theoretical papers connected with the quantum mechanical theory of broadening by electrons [2-6]. The basic inadequacy of the theory is its assumption of an adiabatic perturbation [7]. But investigations of the broadening of a series of H and He lines in the Born approximation show that inelastic collisions play a fundamental role, which cannot be taken into account in the adiabatic approximation (cf. formulae (17) in reference [3] and (11.40) in reference [9]). Moreover using the general expression for the effective broadening cross-section σ, found in reference [6], it is possible to show that for large electron velocities the Weisskopf broadening mechanism becomes ineffective. In the Born approximation, valid for large velocities, $\sigma \sim v^{-2}$, and hence the line width $\gamma \sim v^{-1}$, instead of $\gamma \sim v^{1/3}$ as given by the adiabatic theory.

The present article is concerned with the construction of a non-stationary quasi-classical theory which is free of the defect of the adiabatic approximation. It turns out that within the limits of a relatively simple quasi-classical model* it is possible to reveal the fundamental nature of the mechanism of broadening by fast charged particles. For velocities characteristic of electron plasmas the broadening is due to inelastic collisions. The results obtained may easily be generalized to the case where quasi-classical motion no longer obtains. Thus the quasi-classical approximation allows one to obtain fundamental results in simple analytic form without limiting the generality of the theory.

CALCULATION OF THE EFFECTIVE CROSS-SECTIONS FOR BROADENING AND DISPLACEMENT

In the quasi-classical approximation the influence of a perturbing particle on an atom is determined by the time dependence of the potential V(t). Before the collision let the atom be in a state n. Let us expand the wave function $\psi_n(t)$ in unperturbed functions:

$$\psi_n(t)=\sum_s a_{ns}(t)\psi_s^{(0)}\exp\left[-\frac{i}{\hbar}E_s t\right]. \tag{1}$$

The coefficients a_{ns} are determined by the usual equations of perturbation theory. It is convenient however to introduce the phase α_n, putting $a_{nn}=e^{-i\alpha_n}$. One then obtains the system of equations

$$\hbar\dot{\alpha}_n = V_{nn} + \sum_s{}' e^{i\alpha_n}\alpha_{ns}V_{ns}e^{i\omega_{ns}t}, \tag{2}$$

$$i\hbar a_{nk} = \exp[-i\alpha_n]\,V_{kn}\exp[i\omega_{kn}t]+\sum_s{}' a_{ns}V_{ks}\exp[i\omega_{ks}t],$$

with the initial conditions $a_{nk}(-\infty)=\delta_{nk}$; $\alpha_n(-\infty)=0$.

Integrating equation (2) to second order perturbation theory we find

$$\alpha_n(t) = \frac{1}{\hbar}\int_{-\infty}^{t} V_{nn}(t')dt' - \frac{1}{\hbar^2}\sum_s{}'\int_{-\infty}^{t} dt' V_{ks}(t')e^{i\omega_{ks}t'} \tag{3}$$

$$\int_{-\infty}^{t'} dt'' V_{ns}^*(t'')\exp[-i\omega_{ns}t''] = \frac{1}{\hbar}\int_{-\infty}^{t} V_{nn}(t')dt'$$

$$-\frac{i}{\hbar^2}\sum_s{}'\int_0^{\infty} d\tau e^{i\omega_{ns}\tau}\int_{-\infty}^{t} dt' V_{ns}(t')\,V_{ns}^*(t'-\tau).$$

The matrix element of the dipole transition, calculated with the help of the functions in equation (1), will be

$$\langle n'|r|\,n\rangle \exp\,[-i\omega_{nn'}t-i\alpha(t)]; \quad \alpha(t)=\alpha_n(t)-\alpha_{n'}^*(t). \tag{4}$$

[in evaluating (4) one takes account only of those terms corresponding to the undisplaced frequency $\omega_{nn'}$]. Thus the phase of the equivalent atomic oscillator changes during collision by the quantity which is in general complex:

$$\alpha = \eta - i\Gamma = (\eta_n - \eta_{n'}) - i\,(\Gamma_n + \Gamma_{n'}). \tag{5}$$

* In addition to the assumption of quasi-classical character, use is made below of a series of further simplifying assumptions. Similar assumptions are always made in carrying out actual calculations.

Within the limits of the adiabatic theory the expression (4) leads to the usual dispersion formula for the shape of the spectral line, where the width and displacement γ are determined by the relations **

(6)[2]

$$\gamma = 2\pi N v\sigma'; \quad \sigma' = 2\pi \int [1 - \exp[-\Gamma(\rho)]\cos\eta(\rho)]\rho d\rho,$$

$$\Delta = Nv\sigma'' ; \quad \sigma'' = 2\pi \int \exp[-\Gamma(\rho)]\sin\eta(\rho)\rho d\rho.$$

Here σ' and σ'' are the effective cross-sections of broadening and displacement, and ρ is the collision parameter.

The imaginary part of the phase corresponds to damping of the oscillator. Insofar as the damping leads to a symmetric broadening of the levels there is an increase in the width and a decrease in the displacement of the line, as is quite obvious from (6). From (3) it is not difficult to obtain

(7)

$$2\Gamma_n = -\mathrm{Im}\, 2\alpha_n(\infty) = \frac{1}{\hbar^2}\sum_s{}' \left| \int_{-\infty}^{\infty} V_{ns} \exp[i\omega_{ns}t]dt \right|^2$$

The right member of (7) coincides with the usual expression for the transition probability in a field V(t) [9].

In the case of a slowly varying perturbation it is possible to take $V^*_{ns}(t'')$ out of the integral sign in (3) and, assuming that $V(-\infty)=0$, obtain the usual phase shift of the stationary theory

(8)

$$\alpha_n(\infty) = \eta_n - i\Gamma_n = \frac{1}{\hbar}\int_{-\infty}^{\infty}\left[V_{nn}(t) + \sum_s{}' \frac{V_{ns}}{\hbar\omega_{ns}}^2\right] dt; \quad \Gamma_n = 0.$$

Let us consider now arbitrarily fast passages. We will assume that the trajectory of the perturbing particle is rectilinear, the z axis is directed along the path of the particle (i.e.) we are neglecting transitions between the M-components of the level, and we are limiting ourselves to the dipole approximation for the potential. As a rule, a similar assumption is made in the theory of spectral line broadening. Then, for passage at the collision distance ρ,

$$V_{ns} = \frac{Ze^2 \left\langle n\left|\sum z_i\right|s\right\rangle}{\sqrt{\rho^2 + v^2t^2}},$$

and after integrating in (3) we find

(10)

$$\alpha_n(\infty) = \eta_n - i\Gamma_n = \sum_s{}' \frac{\pi C_4^s}{2v\rho^3}\left[F\left(\frac{\rho}{\rho_\tau}\right) - iF_1\left(\frac{\rho}{\rho_\tau}\right)\right],$$

$$\rho_\tau = \frac{v}{2\omega_{ns}} = \frac{\hbar v}{2\Delta E_{ns}}; \quad F(x) = \frac{x}{2}\left[e^{-x}\mathrm{Ei}(x) - e^{x}\mathrm{Ei}(-x)\right];$$

(11)

$$F_1(x) = \frac{x}{2}\exp[-|x|].$$

The parameters C_4^s define the constant of the quadratic Stark effect, averaged over M,

$$C_4 = \sum_s C_4^s$$

(12)

$$C_4^s = \frac{Ze^2\langle n|\sum z_i|s\rangle|^2}{\hbar^2\omega_{ns}} = \frac{2^2 4}{3\hbar^2\omega_{ns}g_n} S,$$

where S is the line strength of the transition ns [10].

For $\rho \gg \rho_\tau$ $F(\rho/\rho_\tau) = 1$, $F_1(\rho/\rho_\tau) = 0$. and (10) goes over into the usual expression of stationary theory: $\eta = \pi C_4/2v\rho^3$, $\Gamma = 0$.

There is a divergence from "stationarity" for those passages having a collision parameter $\rho < \rho_\tau$. For $\rho \ll \rho_\tau$ η turns out to be much less than in stationary theory. At the same time the role of inelastic collisions increases substantially.

In order to simplify the later calculations we assume that the fundamental contribution to α is made by only one of the levels n and n'. Moreover we omit the summation $\sum_s{}'$, attributing the total perturbation to the nearest level having a non-zero matrix element for the dipole transition. In the cases of interest in practice this is usually possible (cf. footnote ** on page 281). Let us rewrite (10) in dimensionless form:

(13)

$$\eta = \frac{\pi\beta^2}{\chi^3}F(x); \quad \Gamma = \frac{\pi\beta^2}{2\chi^2}\exp[-|x|]; \quad \chi = \frac{\rho}{\rho_\tau},$$

(14)

$$\beta = \frac{2C_4^{\frac{1}{3}}(\Delta E)^{\frac{1}{3}}}{\hbar^{\frac{4}{3}}v^2} = \frac{2\mu}{m}\cdot\frac{\Delta E}{kT}\left(\frac{S}{3a_0^2 g}\right)^{\frac{1}{2}},$$

where μ is the mass of the perturbing particle. Substituting (13) in (6) we find:

(15')

$$\sigma' = \sigma'_0 I'(\beta); \; I'(\beta) = b\beta^{-\frac{2}{3}}\int_0^\infty [1 - \exp[-\Gamma(\chi)]\cos\eta(\chi)]\chi d\chi,$$

(15'')

$$\sigma'' = \sigma''_0 I''(\beta); \; I''(\beta) = \frac{b}{\sqrt{3}}\beta^{-\frac{2}{3}}\int_0^\infty \exp[-\Gamma(\chi)]\sin\eta(\chi)\chi d\chi,$$

where $\sigma'_0 = aC_4^{2/3}v^{1/3}$ and $\sigma''_0 = \sqrt{3/2}\,\sigma'_0$ — are the cross-sections for broadening and displacement in the usual stationary theory [7]; $a = 2\frac{2}{3}\pi\frac{5}{3}\Gamma(\frac{1}{3}) = 11.4$;

$b = 4 - \pi\frac{2}{3}\Gamma(\frac{1}{3}) = 0.695$.

** The method of calculation of the width and displacement is practically the same as in the case of real phases (cf. references [6 and 7]. The designation of the effective cross-sections σ' and σ'' differs from that used in references [6] and [7].

The factors I' and I'' give a correction for non-stationarity and depend only on β. It is not difficult to show that for $\beta \gg 1$ we find $I' = I'' = 1$. For $\beta \ll 1$ we have instead the asymptotic expressions *

$$\sigma' = 2\pi^3 \left(\frac{S}{3\alpha_{og}^2}\right)\left(\frac{\hbar}{mv}\right)^2 \ln \frac{2mv^2}{\Delta E c} \; ; \quad c = 9.6\left(\frac{S}{3\alpha_{og}^2}\right)^{\frac{1}{2}}, \tag{16}$$

$$\sigma'' = 38.4\left(\frac{S}{3\alpha_{og}^2}\right)\left(\frac{\hbar}{mv}\right)^2 . \tag{17}$$

DISCUSSION OF RESULTS

The integrals I' and I'' were computed on an electronic computing machine for a series of values of β (cf. the Table and figure 1). At the same time, with the aim of estimating the relative contribution of Γ and η to the broadening, the integral I was calculated for $\eta = 0$ and I'' for $\Gamma = 0$. The calculations show that for $\beta > 1$ the integrals I' and I'' $\sim$ 1 and that the cross-section has the same value as in the stationary theory.

β	I'	I''
12.78	1.00	—
4.52	0.98	0.964
1.60	1.105	0.885
0.565	1.222	0.783
0.200	1.247	0.594
$7.06 \cdot 10^{-2}$	1.123	0.396
$2.50 \cdot 10^{-2}$	0.885	0.228
$0.883 \cdot 10^{-2}$	0.626	0.122
$0.312 \cdot 10^{-2}$	0.410	0.0632
$0.110 \cdot 10^{-2}$	0.255	0.0324
$3.90 \cdot 10^{-4}$	0.153	0.0166
$1.38 \cdot 10^{-4}$	0.089	0.0084
$0.488 \cdot 10^{-4}$	0.051	0.0042
$0.172 \cdot 10^{-4}$	0.029	0.0021

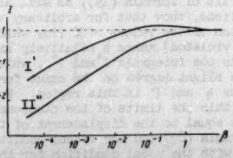

Figure 1. Dependence of the correction factors I' and I'' on the parameter β.

As β decreases the integrals I' and I'' decrease rapidly. For $\beta < 0.5$ the line width is almost totally due to inelastic collisions**. This is because for small β the Weisskopf broadening mechanism becomes ineffective due to the rapid decrease of η. It is important that the non-adiabatic character leads simultaneously to the presence of inelasticity and to a decrease in η. If one keeps the same expression for η as in the stationary theory, then a calculation taking account of the inelastic processes leads only to a small correction [11]. Inelastic transitions have practically no effect on the displacement of the line. The decrease in I'' for small β is entirely due to the decrease in η. For small β we have $\gamma_\Delta \sim \nu^{-1}$ [cf. (16), (17)], which is in good agreement with the results of quantum mechanical calculations, (cf. Introduction). Moreover the asymptotic formula (16) essentially agrees with formula (10) in reference [3].

According to (15') and (15'') the total broadening due to electrons and ions is determined by the expressions

$$\gamma = N_e v_e \sigma'_{oe} \left\{ I'(\beta_e) + \left(\frac{m}{M}\right)^{1/4} I'(\beta_i) \right\} ;$$

$$= N_e v_e \sigma''_{oe} \left\{ I''(\beta_e) + \left(\frac{m}{M}\right)^{1/4} I'' (\beta_i) \right\} . \tag{18}$$

Here m is the electron mass, and M is the charge and mass of an ion. The Table allows one to calculate γ and Δ if the parameters ΔE, C_4, and S are known. **

The factor $\left(\frac{S}{3\alpha_{og}^2}\right)$ in (14) is close to unity, and hence the parameter

$$\beta \approx \frac{Z\mu}{m} \cdot \frac{\Delta E}{kT},$$

has significantly different values for electrons and ions. For this reason the broadening by electrons and ions may differ in character. In figure 2 is shown the dependence of γ on $\theta = kT/\Delta E$ for electrons ($Z\frac{\mu}{m} = 1$) and ions N^{++} ($Z\frac{\mu}{m} = 30{,}000$); the dotted line gives the results of the stationary theory. For $\theta \leq 10$ the total cross-section is $\gamma = \gamma_e + \gamma_i$, the same as in the stationary theory. This case occurs extremely rarely, for example for $\Delta E \sim 1$ eV in an arc discharge. In the region $10 < \theta < 10^4$ (T is of the order of several tens of thousands of degrees for ΔE (0.1 eV), $\gamma_e \sim \nu^{-1}$ where γ_e and γ_i are of the same order of magnitude. For $\theta \approx 10^4$ we have $\gamma \approx \gamma_i \gg \gamma_e$ and up to $\theta \approx 10^6$ we have $\gamma_i \sim \nu^{-\frac{1}{2}}$. Finally for $\theta > 10^6$ (for not very small value of ΔE this corresponds to temperatures of tens of

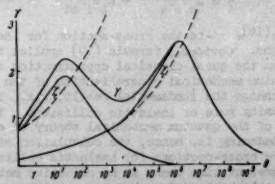

Fig. 2. The line width due to electrons (γ_e) ions (γ_i), and the total width (γ) as functions of the temperature of the plasma $\theta = \frac{kT}{\Delta E}$. The dotted lines give γ_e and γ_i according to the stationary theory.

* The cross-section for displacement σ'' for $\beta \ll 1$ does not depend on ΔE. Hence taking account of the single perturbing level with the smallest value of ΔE may turn out to be unallowable. However as will be shown below the case $\beta \ll 1$ for σ'' is not of practical interest.

** In the general case inelastic collisions lead also to a change in the integrated line intensity. We will not consider this effect more closely since it depends strongly on concrete cases and in part on the distribution of the atoms among the levels.

** Any two of these parameters are independent.

millions of degrees) γ decreases rapidly. Over the whole range of temperature $10 < \theta < 10^7$ the quantity γ changes monotonically and by less than a factor of two. From the point of view of an experimental verification of the theory it is more interesting to compare γ and Δ for various lines. In connection with the fact that $\Delta\xi$ varies within considerably wider limits than S, the integrals I' and I'' in the majority of cases decrease with increasing C_4, although they do not have a single-valued dependence on C_4. For ions, as in the stationary theory, $\gamma = 1.15, \Delta_i \sim C_4^{2/3}$. Calculations using formula (18) for a series of lines of ArII for T=40,000° show that γ changes from line to line in a manner practically independently of C_4 and that Δ increases with C_4, but considerably more slowly than according to a $C_4^{2/3}$ law. The latter is related to the fact that the ionic contribution to the displacement is relatively larger than to the width.

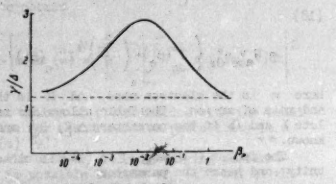

Fig. 3. Dependence of the ratio of the width to the displacement on β_e.

In the stationary theory the ratio $\gamma/\Delta = 1.15$ for all lines. In the present theory it depends on β_e (figure 3) and is approximately 1.15 only in the two limiting cases: $\beta_e > 1$ (both electrons and ions are described by the stationary theory) and $\beta_e < 10^{-4}$ (where electrons generally do not play a role.) *

All of these results agree qualitatively with the experimental data [1]. Quantitative comparison is hardly possible at present. Actually $\beta_e < 1$ the electronic contribution to the width is connected with inelastic processes. Hence for not too high temperatures, when $\beta_i > 1$, the formula for γ has the form

$$\gamma = N_e v_e \sigma_e^{(in)} + N_i v_i \sigma_{oi}' \qquad (19)$$

where $\sigma^{(in)} = \sigma'$-is the cross-section for inelastic collisions. Obviously formula (19) applies to more than the quasi-classical approximation since the quantum mechanical generalization of the theory cannot change the fundamental result, viz. The overwhelming role of inelastic collisions. The problem of the quantum mechanical theory of electron broadening is, hence, the calculation of the effective cross-sections for inelastic collisions. At the present time there is no effective method for the calculation of such cross-sections. Hence in the cases where the first term in (19) may not be neglected, it is difficult to expect quantitative agreement of the theoretical value for γ with the experimental value. Hence from this point of view it follows that one should use the displacement of the spectral lines rather than their width for the determination of plasma parameters since the displacement does not depend on inelastic processes.

* In taking account of several perturbing levels as a result of random compensation of displacements it is possible that $\gamma/\Delta \gg 3$.

ON THE APPLICABILITY OF PERTURBATION THEORY

We now consider the extent to which it is allowable to use perturbation theory for the integration of the system (2). For simplicity we again limit ourselves to a single perturbing level and omit the term $V_{nn'}$ which is equal to 0 in the dipole approximation. The formal solution of the system (2) may then be written in the form

$$a(t) = \frac{1}{i\hbar^2} \int_{-\infty}^{t} dt' V_{12}(t') \exp[i\alpha(t') + i\omega t'] \int_{-\infty}^{t} dt'' V_{12}^*(t'') \exp[-i\alpha(t'') - i\omega t''] \qquad (20)$$

$$= \frac{1}{i\hbar^2} \int_{-\infty}^{t} dt' V_{12}(t') \exp[\Gamma + i] \int (\dot\eta + \omega) dt' \int_{-\infty}^{t'} dt'' V_{12}^*(t'') \exp[\Gamma - i \int (\dot\eta + \omega) dt''].$$

The expression (2) reduces to (3), if we put $\exp[i\alpha + i\omega t]$, i. e. if we require

$$\Gamma \ll 1; \qquad \dot\eta \ll \omega \equiv \frac{\Delta E}{\hbar}. \qquad (21)$$

An analysis of formula (15), as well as numerical calculations, show that for arbitrary values of β the region of the values of χ [for which condition (21) is violated] makes a relatively small contribution to the integrals I' and I'', which depend in the same slight degree on the exact form of the functions $\dot\eta$ and Γ in this region. For $\beta > 1$, i. e. within the limits of the stationary theory, $\hbar\dot\eta$ is equal to the displacement of the level [cf. formula (8)] and the second condition (21) coincides with the usual condition for the applicability of the theory of the quadratic Stark Effect. Generalizing the terminology of the stationary theory to the case of small β, one may say that the theory developed above describes the quadratic Stark effect, since η and $\Gamma \sim e$.

Within the limits of the stationary theory one may obtain formulas for the broadening which are suitable in the same degree for the quadratic as well as the linear effect (i. e. also for line displacements larger than $\Delta\xi$). It turns out that the transition to the linear effect can play a role only for $\beta < 1$. However under these conditions a Weisskopf mechanism in general plays practically no role and the broadening is determined by inelastic processes.

The solution (3) was obtained on the assumption that there was no degeneracy, which is obviously not true if the line width becomes greater than $\Delta\xi$. It is necessary therefore to impose one additional requirement:

(22) $\hbar\nabla v \ll \Delta E$.

For hydrogen-like levels condition (22) is usually not fulfilled. In this case, as in the stationary theory, one must expect the linear effect in the non-stationary theory.

In conclusion we express our thanks to S. L. Mandel'shtam and M. A. Mazing for their interest in this work and a discussion of the results.

April 15, 1958.

References

1. M. A. MAZING, S. L. MANDEL'SHTAM, V. G. KOLOSHNIKOV: Sbornik pamiati akad. G. S. LANDSBERGA. (Collection in memory of Acad. G. S. LANDSBERG) Akad. Nauk Press, 1959
2. B. KIVEL, S. BLOOM, H. MARGENAU: Phys. Rev., 98, 495 (1955)
3. B. KIVEL: Phys. Rev., 98, 1055 (1955)
4. H. MARGENAU, B. KIVEL: Phys. Rev. 98, 1822 (1955)
5. R. E. MEYEROTT, H. MARGENAU: Phys. Rev., 99, 1851 (1955)
6. I. I. SOBEL'MAN: OIS, 1, 617 (1956); ZETF, 31, 519 (1956) (See Soviet Physics JETP)
7. I. I. SOBEL'MAN: UFN, 54, 551 -586(1954); Fortsch. der Phys., 5, 175 (1957)
8. N. F. MOTT, H. S. W. MASSEY: The theory of atomic collisions. Oxford, Clarendon Press, 1949 (IL, Moscow, 1951)
9. L. D. LANDAU, E. M. LIFSHITZ: London, Pergamon Press; Reading, Mass., Addison-Wesley Publ. Co., 1958
10. E. U. CONDON; G. H. SHORTLEY: The theory of atomic spectra. Cambridge, Eng. Univ. Press, 1935 (IL, Moscow, 1949)
11. H. M. FOLEY: Phys. Rev., 69, 616 (1946)

TOM VI, Vyp. 4 OPTIKA I SPEKTROSKOPIIA Aprel', 1959
VOL. VI, No. 4 OPTICS AND SPECTROSCOPY April, 1959

On The Connection Between Larnaudie's Method and the El'iashevich - Stepanov Method of Zero Approximations

I. V. ORLOVA AND I. N. GODNEV

Abstract: A transformation of the fundamental equations of Larnaudie to the secular equation of El'iashevich shows that Larnaudie's method is one variation of the El'iashevich-Stepanov method of zero approximations. Application of this method to second-order blocks allows us, in the case where "progressive rigidity" may be assumed, to establish the relation $D_{12} \approx 0$ and to obtain an approximate equation for calculating the force constants.

Quite recently Larnaudie [1] put forward an approximate procedure for calculating the frequencies and force constants of molecules; this is the so-called "method of progressive rigidity". It is of interest to establish the connection between this method and the method of zero approximations [2,3]. It is shown in this paper that Larnaudie's method is one of the variations of the El'iashevich-Stepanov method of zero approximation [2], useful for approximate solution of certain problems.

Let $Q_1, Q_2, \ldots, Q_n$ be normal coordinates corresponding to the n vibrational degrees of freedom of a given symmetry type, and let $S_1, S_2, \ldots, S_n$ be the symmetry coordinates, A the matrix of kinematic coefficients, K the matrix of force constants, and W the transformation matrix carrying the normal coordinates into the symmetry coordinates,

$$S = WQ. \tag{1}$$

Larnaudie's method is based on a special choice of the matrix W, in which in order to solve the problem of molecular vibrations one uses the equations

$$WW = A, \tag{2}$$

$$WKW = \Lambda, \tag{3}$$

where Λ is the diagonal matrix of the squares of the frequencies, arranged in descending order of magnitude,

$$\lambda_1 > \lambda_2 > \cdots > \lambda_n.$$

In equations (2) and (3) it is assumed that the matrix W has the form

$$W = \begin{pmatrix} w_{11} & 0 & 0 & \ldots & 0 \\ w_{21} & w_{22} & 0 & \ldots & 0 \\ \vdots & \vdots & \vdots & & \vdots \\ w_{n1} & w_{n2} & \ldots & \ldots & w_{nn} \end{pmatrix}. \tag{4}$$

This choice of the elements of the matrix W is based on the idea of "progressive rigidity", which amounts to assuming that as the frequency of the normal vibrations of the molecule increases, so also the rigidity of the molecule increases; that is, as the frequency increases one may neglect an increasingly larger number of the non-diagonal elements of the matrix W.

Equations (2) and (3) were applied by Larnaudie to solve both the direct problem of determining the frequencies of oscillation of molecules and the inverse problem of determining the force constants.

Let us now consider the connection between Larnaudie's method, as just described, and the El'iashevich-Stepanov method of zero approximations. For this purpose we shall determine the form of the secular equation corresponding to equations (2) and (3).

Multiplying the left and right hand sides of equation (3) by W and W^{-1}, we obtain

$$WWK = WAW^{-1}, \tag{5}$$

since

$$WW^{-1} = E.$$

Because of equation (2), equation (5) has the form

$$AK = WAW^{-1} \tag{6}$$

The product of the matrices A and K is the matrix D of interaction coefficients [2].

Accordingly,

$$D = WAW^{-1} \tag{7}$$

The matrix W is triangular, and therefore (see [4]) the matrix W^{-1} is also triangular. Multiplying such triangular matrices by the diagonal matrix Λ in the order indicated in (7), we obtain

$$AK = D = \begin{pmatrix} D_{11} & 0 & 0 & \ldots & 0 \\ D_{21} & D_{22} & 0 & \ldots & 0 \\ \vdots & \vdots & & & \vdots \\ D_{n1} & D_{n2} & & & D_{nn} \end{pmatrix} \tag{8}$$

The secular equation in the form given by El'iashevich [2,5] is

$$\begin{vmatrix} D_{11} - \lambda & 0 & \ldots & 0 \\ D_{21} & D_{22} - \lambda & \ldots & 0 \\ \vdots & \vdots & & \vdots \\ D_{n1} & D_{n2} & \ldots & D_{nn} - \lambda \end{vmatrix} = 0 \tag{9}$$

whence

$$\lambda_1 = D_{ii} \tag{10}$$

Thus, for the solution of the direct problem Larnaudie's method is equivalent to the El'iashevich-Stepanov method of zero approximations, and is a variation of the latter in which the non-diagonal elements D_{ij} adjacent to the diagonal are set equal to zero in the development of D according to (8).

The secular equation (9) corresponding to the Larnaudie equations (2) and (3) allows us also to examine the possibility of representing the roots of second-order blocks as combinations of two partial frequencies. In fact, when Larnaudie's method is applicable (when "progressive rigidity" may be assumed) the matrix D takes the form

(11)
$$D = \begin{pmatrix} D_{11} & 0 \\ D_{21} & D_{22} \end{pmatrix} = \begin{pmatrix} A_{11}k_{11}+A_{12}k_{12} & 0 \\ A_{12}k_{11}+A_{22}k_{12} & A_{12}k_{12}+A_{22}k_{22} \end{pmatrix}$$

whence we obtain immediately the relations*

(12) $$D_{12}=A_{11}k_{12}+A_{11}k_{22}\approx 0,$$
(13) $$D_{21}=A_{12}k_{11}+A_{22}k_{12}\neq 0.$$

The roots of the secular equation corresponding to the matrix (11) are

(14) $$\lambda_1\approx D_{11}=A_{11}k_{11}+A_{12}k_{12},$$
(15) $$\lambda_2\approx D_{22}=A_{12}k_{12}+A_{22}k_{22}.$$

These solutions, for $D_{12}\approx 0$, can be represented as combinations of the partial frequencies [6]

(16) $$\lambda_1 \approx \frac{A_{11}}{k_{11}^*} = M_1$$

(17) $$\lambda_2 \approx \frac{k_{22}}{t_{22}} = B_2$$

where k_{11}^* and t_{22} are elements of the matrices of force constants and of kinetic energies respectively. Eliminating A_{12} from (14) and k_{12} from (15) with the aid of (12), we obtain (16) and (17)**.

Equations (12), (14), (15) allow us to complete the approximate calculation of the three force constants of a second-order block on the basis of the experimental values of two frequencies. In fact, the solution of equations (12), (14) and (15) with respect to the force constants yields

(18) $$k_{11}\approx\frac{\lambda_1}{A_{11}}+\frac{A_{12}^2}{A_{11}}\frac{\lambda_2}{|A|}$$

(19) $$k_{12}\approx -\frac{A_{12}}{|A|}\lambda_2$$

(20) $$k_{22}\approx\frac{A_{11}}{|A|}\lambda_2.$$

The approximate formulae (18) -- (20) have been obtained previously by other methods [6--8], but the method given here seems simpler and physically more fundamental.

Force constants	Values of the force constants (in 10^6 cm^{-2})	
	Calculated by eqs (18)--(20)*+	Exact values obtained by Stepanov [2,10]**
$k_{11}=k_q$ -- h	11.86	11.65
$k_{12}=\nu 2a$	2.59	2.55
$k_{22}=k_\mu$	2.49	2.47

The table illustrates the application of these formulae to the case of CF_4. The calculation of the force constants is carried out on the basis of experimental values of the frequencies [9] which are close to the values calculated by Stepanov [2, 10].

Equations (18)--(20) are well satisfied for other tetrahedral molecules of the form XY_4 (for $Y \neq H$) and also in a variety of other cases. The conditions of applicability amount to the existence of "progressive rigidity" of the corresponding frequencies in second order blocks.

March 31,1958

References

1. M. LARNAUDIE: J. Phys. et Rad., 15, 365 (1954)
2. M. V. VOL'KENSHTEIN, M. A. EL'IASHEVICH, B. I. STEPANOV: Kolebaniia molekul (Vibrations of molecules), vol. 1, GITTL, Moscow, 1949
3. A. S. SVERDLIN, I. N. GODNEV: ZFKh, 29, 1807 (1955)
4. A. I. MAL'TSEV: Osnovy lineinoi algebry (Principles of linear algebra). GITTL, Moscow, 1956
5. M. A. EL'IASHEVICH: ZFKh, 15(7-8), 847-864 (1941) (See RT-1141, 23 pp. from LC)
6. A. S. SVERDLIN: Cand. Dissertation, Ivanov Chemical-Technological Inst., 1956
7. G. GLOCKLER, J. Y. TUNG: J. Chem. Phys., 13, 388 (1945)
8. V. P. MOROZOV: Cand. Dissertation, Ivanov Chem.-Tech.- Inst., 1953
9. H. H. CLAASSEN: J. Chem. Phys., 22, 50 (1954)
10. B. I. STEPANOV: ZETF, 15, 43 (1945)

* Equation (12) was found empirically by Sverdlin [6]. He applied it in calculating the force constants of tetrahedral molecules.

** $k_{11}^* = \frac{k_{22}}{|k|}$, $t_{22} = \frac{A_{11}}{|A|}$.

*+ Cf. [6].

+* In [2,10] values of the individual force constants k_q, h, a, k_μ are obtained

TOM VI, Vyp. 4 OPTIKA I SPEKTROSKOPIIA Aprel' , 1959
VOL. VI, No. 4 OPTICS AND SPECTROSCOPY April , 1959

Determination of the Structure and Dipole Moment of HDSe from its Microwave Spectrum

V. G. VESELAGO

Abstract: The rotational spectrum of the HDSe molecule was measured in the centimeter region. The dipole moment of the molecule was determined and found to be 0.62 debye. The molecular structure was determined taking centrifugal distortion into account. The effective Se-H and Se-D distances are not equal and are respectively 1.452 and 1.446 Å. The H-Se-D angle is 90°17' ± 50'. The structures of the HDO and HDS molecules were determined on the basis of previously measured spectra.

INTRODUCTION

The spectra of hydrogen selenide H_2Se, and its deuterated analogues, D_2Se and HDSe, have been investigated by many authors [1-4]. In all these investigations calculations were made of the molecular structure, but the results obtained by different authors vary greatly. One of the reasons for such divergences is the fact that centrifugal distortion was not taken into account and the structural parameters obtained therefore represent some sort of average over many rotational states.

In order to determine the structure of the molecule of hydrogen selenide considering centrifugal distortion it is most advantageous to use the microwave spectrum. This spectrum is sufficiently rich in lines and at the same time is rather easy to decipher. It is interesting to compare the results obtained for HDSe with those which have been obtained in the investigation of the spectra of D_2Se and H_2Se [1,3,4], as well as with the data of references [5,8] where the spectra of HDO and HDS, which are related to HDSe, were analyzed.

In order to obtain the microwave spectrum of HDSe we have used a microwave spectrograph of the usual Stark-modulated type. The operating range was from 8000 to 44,000 megacycles while the electronics allowed observation of the absorption lines on an oscilloscope as well as on an EPP-09 recorder. The klystron frequency was stabilized by a modulation scheme using a resonant cavity [9].

Altogether in the range 8000-44,000 megacycles we detected 10 transitions of the pure rotation spectrum of HDSe. The frequencies of these transitions are given in Table 1 ([10]).

Table 1

Transitions	Frequencies of lines (in megacycles)				
	$HDSe^{82}$	$HDSe^{80}$	$HDSe^{78}$	$HDSe^{77}$	$HDSe^{76}$
$1_{10} - 1_{11}$	41476.1	41504.5	41534.1	41549.0	41565.4
$2_{20} - 2_{21}$	9127.75	9138.55	9148.65	9155.85	9161.5
$3_{31} - 3_{32}$	43068.4	43106.8	43156.8	43183.1	43206.8
$4_{31} - 4_{32}$	8756.7	8771.05	8786.05	8793.95	8801.85
$5_{32} - 5_{33}$	33023.0	33075.4	33129.7	33157.4	33188.2
$7_{43} - 7_{44}$	22184.4	22230.0	22277.6	22302.3	22327.7
$9_{54} - 9_{55}$	13827.7	13862.65	13899.3	13918.3	13937.8
$10_{55} - 10_{56}$	—	38629.0	38724.0	—	—
$11_{65} - 11_{66}$	8215.8	8240.6	8266.6	8280.0	8293.6
$12_{66} - 12_{67}$	—	23249.8	—	—	—

1. DIPOLE MOMENT

The dipole moment of HDSe was determined from the Stark splitting of lines in a constant electric field [11], and turned out to be 0.62 debye. Since this figure is in contradiction with the value 0.24 debye found for D_2Se [3] we have attempted to calculate the dipole moment from the ionic character of the Se-H bond. If we designate this value by p then the dipole moment μ (in debyes) is

$$\mu = rlp \cdot \cos\varphi/2 \cdot 4.8 \qquad (1)$$

Here l is the length of the selenium-hydrogen bond, φ is the H-Se-D bond angle, and the coefficient 4.8 represents the charge on the electron. The value of p is connected with the difference in electronegativity between the atoms which constitute the bond, albeit different authors regard this dependence in different ways [12, 13].

It should be pointed out that none of the suggested dependences permits a satisfactory calculation of the dipole moments for the related molecules HDO, HDS, HDSe. Therefore the work of Nekrasov [14] is of special interest since in it the author suggests the use of different values of of electron affinity for the same element forming various bonds.* Tmus, for the bond between hydrogen and elements which have an 18-electron filled shell Nekrasov suggests that the electron affinity of hydrogen be taken equal 334 kcal/g.atom and not 312 kcal./g-atom as is usually done. Then the calculated value μ (HDSe) turns out to be 0.69 debye which is very close to the value we obtained; calculation of the dipole moments of water and hydrogen sulfide gives the values 1.91 and 1.16 debye respectively, which also correspond well to experimental results [5, 15].

2. DETERMINATION OF ROTATIONAL CONSTANTS

Proceding from the observed frequencies we have calculated the rotational constants of the HDSe molecule in the rigid asymmetric rotor approximation. Since for a plane molecule the rotational constants are connected by the relation

$$\frac{1}{C} = \frac{1}{A} + \frac{1}{B},$$

in order to establish A, B and C it is sufficient to know the frequencies of only two transitions. Knowing A, B and C we can calculate the frequencies of all the remaining transitions for the given isotopic combination. In the third and fourth column of Table 2 are given the results of such calculations for the $HDSe^{80}$ molecule. As can be seen from the data given, the discrepancies between calculated and experimental frequencies are so great that the rigid rotor approximation must be considered as definitely unsuitable.

* Nekrasov uses the electron affinity in relative units so that actually they coincide with values of electro-negativity.

Table 2

Transitions	ν_{obs}	Rigid rotor approximation ν_{calc}	Rigid rotor approximation $\nu_{calc.}-\nu_{obs}$	Method of 7 lines ν_{calc}	Method of 7 lines $\nu_{calc}-\nu_{obs}$	Method of 10 lines ν_{calc}	Method of 10 lines $\nu_{calc}-\nu_{obs}$
$1_{10}-1_{11}$	41508.5	—	—	—	—	41508.5	0
$2_{20}-2_{21}$	9138.55	—	—	—	—	9138.55	0
$3_{21}-3_{22}$	43104.4	43104.4	−2.4	—	—	43108.3	1.7
$4_{31}-4_{32}$	8771.05	8801.3	30.25	—	—	8771.34	0.29
$5_{41}-5_{42}$	33075.4	33138.4	63.0	—	—	33071.3	−4.1
$7_{61}-7_{61}$	22230.0	22368.2	138.2	—	—	22229.0	−0.4
$9_{81}-9_{82}$	13862.65	14043.1	180.45	—	—	13863.79	1.14
$10_{91}-10_{92}$	38629.0	38846.0	217	38672	43	38629.5	0.5
$11_{10}-11_{10}$	8240.6	8424.5	183.9	8237	−3.6	8240.3	−0.3
$12_{10}-12_{11}$	23249.8	23483.3	233.5	23274	24.2	23238.1	−13.7
S . . .	—	—	—	—	$5\cdot10^{-4}$	—	$0.6\cdot10^{-4}$

In order to determine the rotational constants including the effects of centrifugal distortion it is usually necessary to perform extremely complicated and long calculations to find the eigenvalues of the Hamiltonian [17]

$$(2)\qquad H=\sum_{\alpha}^{P_\alpha^2}\frac{P_\alpha^2}{2I_\alpha}+\sum_{\beta\gamma\delta\varepsilon}\tau_{\beta\gamma\delta\varepsilon}P_\beta P_\gamma P_\delta P_\varepsilon$$

In our case, however, it is possible to simplify the task considerably since all the observed transitions are of the type $J_\tau \rightarrow J_{\tau+1}$ and an approximate equation can be obtained for their frequencies [5]:

$$(3)\qquad \begin{aligned}\nu=&\frac{A-C}{2}\left[\Sigma(\varkappa)-\Sigma(\varkappa)\right]\{1+2KJ(J+1)\delta_J/H+(K-1)J(J+1)D_{JK}/(G-F)+\\&+\frac{2}{3}K(K+2)\left[D_K/(G-F)-2R_5/H\right]+\left[\frac{16(G-F)}{H^2}-\right.\\&\left.-R_6-4D_K/(G-F)\right]_{K\text{ even}}+\left[\frac{64(G-F)}{H^2}R_6\right]_{K\text{ odd}\geq 3}-\\&-\left[2D_K/(G-F)\right]_{K\text{ odd}}.\end{aligned}$$

According to this formula the frequency is a function of seven unknowns: the asymmetry parameter $\varkappa=\frac{2B-A-C}{A-C}$, $U=\frac{A-C}{2}$ and five centrifugal distortion constants D_{JK}, D_K, δ_J, R_5 and R_6. All other quantities in (3) have the same meaning as in reference [5]. To determine these seven unknowns we have employed two methods. First we have solved the system of seven equations of the type (3) (method of seven lines); second, by the method of least squares we found the values of all the unknown quantities which best fit all the 10 equations (method of ten lines). The results obtained by the first method are given in Table 3 and those obtained by the second in Table 4. In solving the problem by the method of seven lines we began with those which corresponded to the lowest values of J. The frequencies of the transitions $10_{55}-10_{56}$, $11_{65}-11_{66}$, $12_{66}-12_{67}$, were then calculated and compared with the experiment (cf. the fifth and the sixth columns of Table 2). In the seventh and the eighth columns of Table 2 a comparison is made with the experimental frequencies calculated by the method of ten lines.

Table 3

	$HDSe^{82}$	$HDSe^{80}$	$HDSe^{78}$	$HDSe^{77}$	$HDSe^{76}$	average
$\frac{A-C}{2}$ (in mc)	79744	79760	79782	79785	79799	—
$\varkappa$	−0.47911	−0.47884	−0.47862	−0.47843	−0.47829	—
$\delta_J\cdot10^3$ . .	0.513	0.549	0.541	0.633	0.583	0.56
$D_{JK}\cdot10^3$ . .	0.283	0.294	0.291	0.310	0.315	0.30
$R_5\cdot10^3$ . .	0.133	0.124	0.132	0.119	0.125	0.13
$D_K\cdot10^3$ . .	−0.115	−0.107	−0.117	−0.118	−0.088	−0.11
$R_6\cdot10^3$ . .	−0.874	−0.897	−0.886	−0.900	−0.937	−0.90

Table 4

	$HDSe^{82}$	$HDSe^{80}$	$HDSe^{78}$	$HDSe^{77}$	$HDSe^{76}$	average
$\frac{A-C}{2}$ (in mc)	79772	79785	79808	79812	79830	—
$\varkappa$	−0.47959	−0.47926	−0.47906	−0.47889	−0.47882	—
$\delta_J\cdot10^3$ . .	0.310	0.385	0.364	0.410	0.356	0.37
$D_{JK}\cdot10^3$ . .	0.215	0.217	0.212	0.224	0.229	0.22
$R_5\cdot10^3$ . .	0.299	0.272	0.298	0.275	0.308	0.29
$D_K\cdot10^3$ . .	−0.372	−0.338	−0.358	−0.357	−0.371	−0.36
$R_6\cdot10^3$ . .	−0.543	−0.600	−0.575	−0.587	−0.571	−0.58

In the last line of the table is given the mean-square error for one transition

$$S=\sqrt{\frac{1}{10}\sum\left(\frac{\nu_{obs.}-\nu_{calc.}}{\nu_{calc.}}\right)^2}$$

which for the method of seven lines turns out to be approximately ten times greater than for the method of ten lines. The error in the determination of value $\frac{A-C}{2}$ is ± 3 megacycles and the error in the determination of $\varkappa$ is ± 0.00005.

3. STRUCTURE OF THE HDSe MOLECULE

The rotational constants of a triangular molecule are connected with its structural parameters (see the drawing) by the following simple relations:

$$(4)\qquad \begin{aligned}&\frac{K}{C}=\frac{M_1M_3a^2+M_1M_2b^2+M_2M_3c^2}{\Sigma},\\&\frac{K}{\sqrt{AB}}\sqrt{\frac{M_1M_2M_3}{\Sigma}}\cdot ab\cdot\sin\varphi,\end{aligned}$$

here $\Sigma=M_1+M_2+M_3$, and K is a conversion factor whose value is 505531 if we take A,B and C in megacycles, a, b, and c in Å, and M_1, M_2, M_3 in atomic mass units. The asymmetry parameter $\varkappa$ and the value of U for planar molecules are simply related to the rotational constants:

$$(5)\quad A=U\left(\sqrt{2}(1+\varkappa)+2\right),\ B=U\left(\sqrt{2}(1+\varkappa)+1+\varkappa\right),\ C=U\sqrt{2}(1+\varkappa).$$

Combining equations (4) and (5) we obtain the following relation between κ and the structural parameters:

$$(6)\quad \sqrt{2+\frac{3+\kappa}{\sqrt{2}(1+\kappa)}}=\frac{M_1M_2a^2+M_1M_3b^2+M_2M_3(a^2+b^2-2ab\cos\varphi)}{\sqrt{\Sigma M_1M_2M_3}\cdot ab\cdot\sin\varphi}$$

This equation is simplified if we suppose that the Se-H and Se-D are equal, i.e. that $a=b$ and the angle φ is near 90° so that $\sin\varphi$ and $\cos\varphi$ can be expanded in powers of $X=90^\circ-\varphi$ keeping only the linear and quadratic terms.

$$(7)\quad \sqrt{M_1M_2M_3}\sum\sqrt{2+\frac{3+\kappa}{\sqrt{2}(1+\kappa)}}-|M_1(M_2+M_3)+2M_2M_3|=-2M_2M_3X+|M_1(M_2+M_3)+2M_2M_3|\frac{X^2}{2}.$$

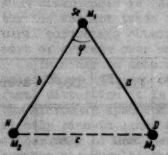

Structural parameters of a triangular molecule

Substituting into the quadratic equation which we obtain the values of κ, M_1, M_2 and M_3 for any of the isotopic combinations of the molecule it turns out that only complex values of the angle κ are obtained. In order to overcome this obstacle it is necessary to assume that the distances Se-H and Se-D which we considered equal are in reality not the same. If we now introduce into our calculations a quantity $\alpha=\frac{r(Se-D)}{r(Se-H)}-1$, then equation (7) is transformed in the following way:

$$(8)\quad \sqrt{M_1M_2M_3}\sum\sqrt{2+\frac{3+\kappa}{\sqrt{2}(1+\kappa)}}-|M_1(M_2+M_3)+2M_2M_3|=-2M_2M_3X+|M_1(M_2+M_3)+2M_2M_3|\frac{X^2}{2}-M_1(M_2-M_3)\alpha.$$

From the two equations of type (8) which correspond to any two isotopic variants of the molecule HDSe it is easy to find values of α and X. a and b are then determined from the second equation (4). The results obtained are shown in Table 5.

Table 5

	Method of seven lines	Method of ten lines
α	-0.0045 ± 0.0007	-0.0042 ± 0.0007
r(Se—H)	1.4521 ± 0.0005 Å	1.4519 ± 0.0005 Å
r(Se—D)	1.4456 ± 0.0005 Å	1.4458 ± 0.0005 Å
φ	$90°17\pm50'$	$90°10'\pm50'$

As can be seen from the data given, the solutions obtained by the methods of seven and ten lines result in practically identical structures for the HDSe molecule. The fact that distances a and b determined from the spectrum are different can easily be explained if we consider that these distances are not equilibrium but effective distances corresponding to the lowest vibrational state of the molecule.

Since in references [1,3,4] centrifugal distortion was not taken into consideration it is natural that the structure of the molecule of hydrogen selenide as determined by us differs greatly from the structures quoted in those papers.

4. STRUCTURE OF MOLECULES HDS AND HDO

While the rotational spectra of HDS and HDO have been analyzed rather thoroughly structures of these molecules have not yet been determined and calculations have been limited to establishing U and κ [5-7]. In order to determine the structure of each of these molecules it is necessary to know U and κ for two isotopic combinations. In the case of HDS, U and κ are known only for HDS^{32}; for HDS^{34} they have not been determined since the number of lines observed in the spectrum HDS^{34} is only 5 [5], which is not sufficient for the solution of the system of seven equations of type (3). However the calculation of U and κ for HDS^{34} must be practically identical.

Let ν_1 be the frequency of a certain transition for the molecule HDS^{32}, and ν_1 the frequency of the same transition for HDS^{34} [we speak here, of course, only of the transitions of the Q-branch for which equation (3) is valid]. Then

$$(9)\quad \frac{\nu_1}{\nu_1}=\frac{U p_1(1+q_1x)(1+\beta_1)}{U' p_1(1+q_1x')(1+\beta_1)}=\frac{U(1+q_1x)}{U'(1+q_1x')}$$

here p_1 and q_1 are coefficients which present the value $[E(\kappa)-E'(\kappa)]$ in equation (3) as linear functions of κ, and β_1 is an overall correction for centrifugal distortion. In expression (9) all values marked by an asterisk belong to HDS^{34}. An equation similar to (9) can be written for any other transition:

$$(10)\quad \frac{\nu_1}{\nu_2}=\frac{U(1+q_1x)}{U'(1+q_1x')}$$

Knowing U and κ for HDS^{32} and having solved equations (9) and (10), we obtain the following results for HDS^{34}: U = 97715 megacycles, $\kappa=-0.478205$. The structure of the HDS molecule which is now determined from the system of equations (8) is the following: $\varphi=92°06'$, r(S — H) = 1.3283 Å, r(S — D) = 1.3215 Å, $\alpha=-0.0051$.

For HDO, only the spectrum of the isotopic combination HDO^{16} has been measured. Therefore in order to solve the equation (8) we have to assume values $\kappa=-0.6830$ [6] and $\varphi=104°27'$ [18], whereupon we obtain the structural parameters: r(O — H) = 0.9458 Å, r(O — D) = 0.9405 Å, $\alpha=-0.0056$. Thus we see that the effective length of the bond with deuterium turns out to be smaller than the length of the bond with hydrogen not only for the HDSe molecule but also for the molecules HDS and HDO, whose structure is similar to that of HDSe. It is also natural that the structures of HDS and HDO which we found differ somewhat from the commonly accepted ones which are determined from infrared spectra

without consideration of centrifugal distortion [18].

5. CENTRIFUGAL DISTORTION CONSTANTS

The centrifugal distortion coefficients D_{JK}, D_K, δ_J, R_5 and R_6 can easily be determined from the structural parameters of the molecule and its vibrational frequencies [19].

Table 6

	Calculated values	Experimental values	
		Method of seven lines	Method of ten lines
$\delta_J \cdot 10^6$ . .	0.58	0.56	0.37
$D_{JK} \cdot 10^6$ . .	0.10	0.30	0.22
$R_5 \cdot 10^6$ . .	—0.4	0.13	0.39
$D_K \cdot 10^6$ . .	—0.15	—0.11	—0.36
$R_6 \cdot 10^6$ . .	—0.66	—0.90	—0.58

In Table 6 theoretical values for HDSe are compared with experimental ones obtained by the method of seven and ten lines. As can be seen from Table 6, calculated and experimental values of constants of the centrifugal distortion constants agree only in order of magnitude while the values of the constant R_6 differ even in sign. It is interesting to note that an analogous change in the sign of R_6 is observed also for the HDS molecule [5]. The striking discrepancy between the calculated and experimental values of centrifugal distortion constants forces one to conclude that experimentally determined values of these constants actually cannot be quantitatively discussed in terms of the physical characteristics of the molecule. They should be considered only as coefficients which allow us to determine values of U and κ for a non-rotating molecule and also to calculate the frequencies of new lines of the spectrum from the measured frequencies of the lines already found.

Table 7

Calculated frequencies of lines of $HDSe^{80}$ (in megacycles)

Transition	Method of seven lines	Method of ten lines
$6_{45}-6_{43}$	6385	6389
$8_{44}-8_{45}$	61052	61016

In Table 7 is shown the result of such a calculation for lines $6_{42} - 6_{43}$ and $8_{44} - 8_{45}$ of the spectrum of $HDSe^{80}$. As can be seen from Table 7, frequencies calculated by the methods of seven and of ten lines differ very little although in calculating these two we have used substantially different centrifugal distortion constants. Since the frequencies of these transitions lie beyond the frequency limits of our spectrograph they have not been observed.

In conclusion I would like to express my sincere gratitude to my scientific adviser, A. M. Prokhorov, for the constant support and help which he gave me in the course of this work.

April 18, 1958

References

1. D. M. CAMERON, W. C. SEARS, H. H. NIELSEN: J. Chem. Phys., 7, 994 (1939)
2. E. D. PALIK: J. Chem. Phys., 23, 980 (1955)
3. A. W. JACHE, P. W. MOSER, W. GORDY: J. Chem. Phys., 25, 209 (1956)
4. E. D. PALIK, R. A. OETJEN: J. Mol. Spect., 1, 223 (1957)
5. R. E. HILLIGER, M. W. P. STRANDBERG: Phys. Rev., 83, 575 (1951)
6. S. WEISBAUM. Y. BEERS, G. HERRMANN: J. Chem. Phys., 23, 1601 (1955)
7. D. W. POSENER, M. W. P. STRANDBERG: Phys. Rev., 95, 374 (1954)
8. G. ERLANDSSON, J. COX: J. Chem. Phys., 25, 778 (1956)
9. V. G. VESELAGO, N. A. IRISOVA: RiE, 2, 484 (1957) (See Radio Engineering and Electronics)
10. V. G. VESELAGO: IAN USSR FS, 22, 1150 (1958) (See CTT, Bulletin)
11. V. G. VESELAGO: ZETF, 32, 620 (1957) (see Soviet Physics JETP)
12. C. H. TOWNES, A. L. SCHAWLOW: Microwave Spectroscopy. McGraw-Hill Co. N.Y., 1955
13. L. PAULING: The nature of the chemical bond. Ed. 2, 1940, Ithaca, N.Y. Cornell Univ. Press (Goskhimizdat, 1947, Moscow-Len.)
14. B. V. NEKRASOV: ZOKh, 16, 1797 (1946)
15. M. W. P. STRANDBERG: J. Chem. Phys., 17, 901 (1949)
16. V. G. VESELAGO, A. M. PROKHOROV: ZETF, 31, 731 (1956) (See Soviet Physics JETP)
17. D. KIVELSON, E. B. WILSON, Jr.,: J. Chem. Phys., 21, 1229 (1953)
18. LANDOLT-BORNSTEIN: I, 2 Teil, Auflage 5, Berlin, Springer Verlag, 1951
19. H. H. NIELSEN: Rev. Mod. Phys., 23, 90 (1951)

TOM VI, Vyp. 4 OPTIKA I SPEKTROSKOPIIA Aprel', 1959
VOL. VI, No. 4 OPTICS AND SPECTROSCOPY April, 1959

On the Question of the Origin of the Spectrum of Liquid and Compressed Oxygen (12,600 - 3,000 Å)

V. I. DIANOV-KLOKOV

Abstract: The temperature dependence of the absorption band intensity of condensed oxygen at constant density has been measured in the 80 - 250° K range. The distribution of the intensities and the temperature coefficients agrees with the assumption that the absorption spectrum of condensed oxygen in the 12600 - 3000 Å region corresponds almost completely to dipole transitions in statistical $(O_2)_2$ complexes.

INTRODUCTION

In order to explain the origin of the absorption spectrum of condensed oxygen in the 12600 - 3000 Å region, it is important to resolve the question of whether bands of a pair of interacting $(O_2)_2$ molecules or a single O_2 molecule belong to it. Various hypotheses on this score have been made mainly on the basis of studying the behavior of the spectrum as a function of the mixture composition, the pressure and also by comparing it with changes in the magnetic susceptibility under analogous conditions. Such considerations are too indirect and, consequently, a definite answer to this question has not yet been obtained. In this connection, it is expedient to make a more detailed analysis of the distribution of the band intensities in the spectrum in addition to their dependences on the temperature and density. The present research is such an attempt.

EXPERIMENTAL SECTION AND RESULTS OF MEASUREMENTS

The influence of temperature on the spectrum of oxygen at constant density has been investigated by using cells able to withstand a pressure to 5000 atm. (fig. 1)*.

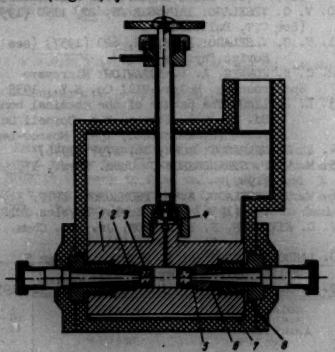

Figure 1

1-cell (45X HM A steel); 2-modulator (45X HM A steel); 3-inner window (fused quartz); 4-needle (silvered steel); 5-gasket (teflon); 6-seal (teflon); 7-jacket (sheet iron); 8-heat insulator (felt)

* I am grateful to L.D.Lifshits for a number of comments on constructing the cell.

That it would be air-tight at pressures below atmospheric (evacuation) was guaranteed by thin, 80 μ teflon gaskets 5, compressed at 150° C between internal windows of fused quartz 3 (12mm, diameter, 10 mm thickness) and the ground faces of the choppers 2 (opening diameter 5 mm). The length of the absorbing layer, l_1 = 2.05 cm, could be decreased by using a quartz bushing.

After the cell had been cooled by liquid nitrogen poured into the heat insulated outer jacket 7, oxygen of 99 - 98.5% purity was liquefied in the channel. After a certain time (10 - 20 min.) sufficient for the reduction of channel temperature, the needle valve was closed. During the natural warming of the cell (1 - 1.5 hours), a series of successive spectrograms (15 - 30 exposures) was recorded which corresponded to the various oxygen temperatures (T = 80 - 250° K). The stability of the spectrum band intensities as the temperature slowly rose near 230 - 250°K indicated the absence of leaks. The temperatures were measured by a thermocouple soldered to the cell frame. A certain temperature drop (~10°) between the outer and inner parts of the cell was not taken into account since the temperature dependences of the absorption coefficient ϵ_m seemed to be very shallow. The oxygen density ρ_{O_2} was determined by means of the first spectrograms of the series, taken in the presence of liquid nitrogen in the jacket, on the basis of curves obtained earlier [4,5]. The influence of thermal broadening and cell deformation on the quantity ρ_{O_2} was not taken into account for l_1 = 2.05 cm.** The maximum pressure in the cell

**As follows from [5], $\epsilon_{m6290} \sim \rho^{4.7}$ for liquid oxygen at T = 80-90°K. Taking the cell deformation into account would lead to a still greater rise in the curves on figure 2. In order to estimate the magnitude of the possible correction, measurements were made with a quartz bushing in the cell (l_1=1.2 cm). A rough computation of the deformation shows that an increase in the cell volume is related principally to the compression of the basic teflon gaskets. Hence, it follows that the relative change in the density for $\frac{\Delta\rho}{\rho} \cong \frac{\Delta l_1}{l_1}$ (l_1 = 1.2 cm) must be approximately twice that for l_1 = 2.05 cm. Actually, a lag in the growth of intensity with temperature was observed in the spectrum with the bushing inserted. A decrease in ϵ_m of ~10% even occurred for the 6290 and 3803 Å bands near T = 250 - 270 °K. (It is essential that the relation of the band intensities for each value of T should agree with that obtained for l_1 = 2.05 cm.) Linear extrapolation to an infinite layer yields an increase in the ϵ_m of the bands for T = 250° K of not more than 10% in comparison with those shown on figure 2. Because of the low precision in determining $\frac{\Delta\rho}{\rho}$, it was resolved not to introduce this correction.

reached 3500 atm. for $\rho_{O_2} = 1.17\ g/cm^3$ ($\sim$ 820 Amagat)*

The double-beam, high speed spectrophotometer [6] is similar to that we used earlier.

Results of measurements of the absorption coefficient at the maximum $\epsilon_m = \frac{1}{l_1} \log_{10} \frac{I_0}{I}$ and the half-width $\Delta\nu_{1/2}$ of certain bands are shown in figures 2 and 3 as a function of the temperature for $\rho_{O_2} = 1.17\ g/cm^3$. The results of Robin et al for the 7620 Å band [7] are in satisfactory agreement with those obtained herein (figure 2).

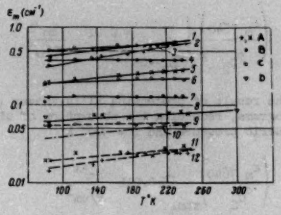

Figure 2. Temperature dependence of the absorption coefficient at the band maxima $\rho_{O_2} = 1.17 g/cm^3$; $l_1 = 2.05$ cm.
A-Band of the allowed groups; B-head bands of the forbidden groups; C-vibrational repetitions in the forbidden groups; D-Data of Robin [7] for the 7620 Å band. Wave lengths in Å : 1-12 600; 2-5769; 3-10 600; 4-6290; 5-4773; 6-3612; 7-3808; 8-7640 9-5325; 10-7640 (induced); 11-4472; 12-9190 (Dashed lines refer to measurements with reduced accuracy; dot-dash line is computed)

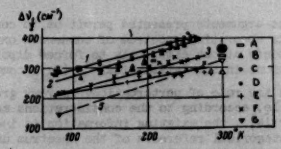

Figure 3. Change in the band half-width with temperature. Wavelengths in Å: A-3808; B-4773; C-5769; D-6290; E-10600; F-12600; G-7620. For T = 300°K, according to the data of Robin [3,7]. The lines 1 refers to points C and D, 2 to points A and B, 3 to F, 4 to E, 5 to G. The large size symbols refer to Robin data.

The measurements of the half-widths values are exaggerated, especially for $T \leq 100°$ K, because of the low spectrophotometer resolving power ($\sim$80 cm^{-1}). Nevertheless, noticeable broadening of the band is seen on figure 3 for increasing T.

DISCUSSION OF THE RESULTS

As had been mentioned in [4], experimental and theoretical investigations of the forced, simultaneous ("combination") transitions of vibrational-vibrational and electronic-vibrational type permit the Ellis-Kneser hypothesis on "two-electron" transitions in condensed oxygen to be considered as very probable, now. For not too strong intermolecular interactions, the terms of the system ("complex"), or the generator, are approximately equal to a linear combination of the terms of the free molecules [9].

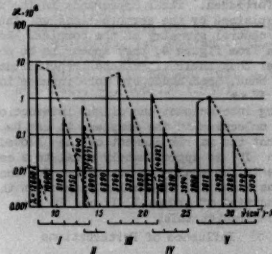

Figure 4. Absorption band intensities of liquid oxygen in the 12600-3000 Å region (T=77.8° K, 99 % purity)

Consequently, the Ellis-Kneser "two-electron" terminology should be understood as a transition of the aforementioned system at an energy level whose value equals approximately the sum of two appropriate free molecule levels. As has been shown [4,5,10], despite the classification of Robin and Robin [3], all the absorption bands in the 12600-3000 Å region in liquid and condensed oxygen are basically related to intermolecular interaction. Consequently, it can be assumed that the spectrum under consideration corresponds principally to dipole transitions in $(O_2)_2$ complexes, where the direction of the transition matrix element coincides with lines connecting the centers of both O_2 molecules. The transitions can be denoted thus in the Ellis-Kneser terminology (see fig. 4 also)

I $\quad {}^3\Sigma_g + {}^3\Sigma_g \rightarrow \Delta + {}^3\Sigma_g$

II $\quad {}^3\Sigma_g + {}^3\Sigma_g \rightarrow {}^1\Sigma_g + {}^3\Sigma_g$

III $\quad {}^3\Sigma_g + {}^3\Sigma_g \rightarrow \Delta + \Delta$

IV $\quad {}^3\Sigma_g + {}^3\Sigma_g \rightarrow {}^1\Sigma_g + \Delta$

V $\quad {}^3\Sigma_g + {}^3\Sigma_g \rightarrow {}^1\Sigma_g + {}^1\Sigma_g$

Such an assumption permits a number of peculiarities of the spectrum to be explained satisfactorily.

a) Intensity Distribution

The presence of a center of symmetry in the $(O_2)_2$ complex can be assumed approximately. Then it follows from symmetry considerations that the transitions I, II and IV can be allowed but the transitions III and V are forbidden ($g \leftrightarrow g$). If the weakening of the prohibition under an additional vibrational excitation is taken into account then only the purely electronic (head) bands of the groups III and V (6290 and 3808 Å) seem to be more strictly forbidden. Their appearance in the spectrum is explained by the perturbations and the imperfect central symmetry of the complex. Actually, as is seen from figure 4, they appear to be noticeably weaker than their vibrational repetitions. On the other hand, head bands are more intense in groups I, II and IV **

Taking into account the slight interaction between the molecules in the complex, it can be thought that the matrix element of the allowed transition IV is approximately equal to a certain difference in the analogous quantities for the transitions I and II. The relation between the band intensities of groups I, II and IV (fig. 4) does not contradict this.

b) Influence of Perturbations

The distortion of the eigen functions of the complex by perturbations can be separated into two groups of components: Those not violating the symmetry of the system***(s) and those violating the symmetry (as). Hence, it follows that only the second group of components can cause the appearance of transitions, forbidden from symmetry considerations, with noticeable intensity. On the other hand, both groups of perturbation components can affect the band intensity of the allowed transitions. Hence, it should be expected that the greatest rise in the intensity will occur for allowed bands as the temperature rises and the least for the most strictly forbidden transitions. Figure 2 shows that a higher temperature intensity coefficient actually corresponds to the groups of allowed bands I, II and IV than to the forbidden bands III and V. It can also be noted that the temperature exerts the least influence in groups III and V on the head bands which are most strictly forbidden. The corresponding changes in the ratio of the band intensities are detected also as the pressure increases, which is illustrated by the following results compiled on the basis of [3] :

$P_{atm.}$	...	700	1200
$\epsilon_{m6290}/\epsilon_{m5769}$	...	0.72	0.70
$\epsilon_{m6290}/\epsilon_{m4773}$	...	1.19	1.14

It can be expected that the temperature intensity coefficient will increase for allowed bands in the $(O_2)_2$ complex with the growth of the effective dipole moment of the transition since the influence of the s -components of the perturbation herewith increases[9]. As is seen from figure 2, the group IV , with less intensity than group I, actually corresponds to a lower temperature coefficient. As regards the 7640 Å band, an investigation of liquid mixtures of O_2-N_2, O_2-Ar has shown [4] that approximately 40% of its intensity is related to the "independent" transitions in the O_2 molecules:

$$\left(\frac{\epsilon_m\ 7640}{\rho_{O_2}}\right)\Bigg|_{\rho_{O_2}\to 0} = 0.018\ \frac{cm^{-1}}{g/cm^3}$$

The result of processing Ellis-Kneser [12] spectrograms, recording the absorption of air at atmospheric pressure and T = 300° K

$$\left(\frac{\epsilon_m\ 7640}{\rho_{O_2}}\right)_{atm.} \cong 0.012\ \frac{cm^{-1}}{g/cm^3}$$

convinces us of the reasonableness of this quantity.

Taking this fact into account, the temperature dependence of the "forced" part of the band intensity agrees satisfactorily with the statements explained above. In conformance with the 12600 Å band intensity which is less than expected, its temperature coefficient appears to be lower than for the vibrational repetition 10600 Å. This fact can indicate the role of the vibrational perturbation in increasing the transition probability.

CONCLUSIONS

The arguments presented permit us to consider that the absorption spectrum of condensed oxygen corresponds almost completely to forced dipole transitions in the "statistical" $(O_2)_2$ complexes, wherein the role of perturbations is very great*+ Meanwhile, according to the considerations mentioned earlier [4] , the existing information is inadequate to a categorical reference of the spectrum under consideration to complexes of just one completely definite kind (for example, with anti-parallel spins). An investigation of this side of the question can possibly explain the reason for the somewhat larger than could be expected intensities of the forbidden III and V groups of bands.

A noticeable influence of the transitions in the unperturbed O_2 molecules in condensed oxygen occurs only in the II group of bands (7640 and apparently 6890 Å). This is illustrated on figure 4 where the intensities of the "atmospheric" bands of oxygen 12600 and 7620 Å, calculated approximately from the data of Ketelaar [10] and the spectrograms of Ellis and Kneser [12] for $\rho_{O_2} = 1.20$ g/cm³ are

*Extrapolation of Amagat [8] results.

** Such a distribution, for free O_2 molecules, corresponds to a small change in the equilibrium internuclear distance r_e [11] .

***More exactly, to that group of symmetry which the corresponding transition forbids.

*+In particular, the deviation from the quadratic law of intensity growth [3,7] observed at high densities can be related to an increase in the perturbations.

denoted by short dashes. Let us note that the intensities of the vibrational repetitions in both "atmospheric" systems are radically weakened in comparison with the purely electronic bands. The reasons for a certain distortion in such a regularity for group I in condensed oxygen have not yet been clarified.

I consider it my duty to express my gratitude to I. V. Obreimov for interest in the research and a number of comments, to L. S. Maiants and CH. K. Mukhtarov for valuable discussions, to D. D. Brezhnev and R. V. Rumiantseva for assistance in preparing the cell and to N. A. Chumaevskii for aid in recording the spectra.

April 30, 1958

References

1. R. GUILLIEN: Ann. phys., 8, 555 (1937)
2. J. ROBIN, S. ROBIN: C.R., 236, 792 (1953)
3. J. ROBIN, S. ROBIN: J. Phys. et Rad., 15, 331 (1954)
4. V. I. DIANOV-KLOKOV: OiS, 4, 448 (1958)
5. V. I. DIANOV-KLOKOV: OiS, 1, 650 (1956)
6. V. I. DIANOV-KLOKOV: PiTE (in press)
7. J. ROBIN, M. DESMARET, E. UBELMANN: C.R., 243, 1750 (1956)
8. E. H. AMAGAT: Ann. chim. Phys., 29, 68 (1893)
9. CH. K. MUKHTAROV: XI Vsesoiuznoe soveshchanie po spektroskopii (XI All-Union Conference on Spectroscopy), 1957
10. J. A. A. KETELAAR: Nuovo Cim., 2, Suppl. N3, 763 (1955)
11. G. HERZBERG: Spectra and structure of diatomic molecules, Van Nostrand. (IL, Moscow, 1949, p. 321)
12. J. W. ELLIS, H. O. KNESER: Publ. Astron. Soc. Pac., 46, 106-108 (1934)

TOM VI, Vyp. 4 OPTIKA I SPEKTROSKOPIIA Aprel', 1959
VOL. VI, No. 4 OPTICS AND SPECTROSCOPY April , 1959

Vibrational Constants of the Water Molecule

G. A. KHACHKURUZOV

Abstract: Results of an investigation of the vibrational-rotational spectra of water vapor allow the determination of forty vibrational energy levels of H_2O. It is shown that the values of these levels, within the limits of accuracy of their determination, are described by a complete cubic expression for $G_o^o(v_1, v_2, v_3)$ by successive calculation of the Darling-Dennison resonance. The values of the vibrational constants of H_2O were determined anew taking into account all second order anharmonicity constants.

INTRODUCTION

The introduction of semiconducting photoresistors into the practice of spectroscopic measurements has allowed detailed investigations to be carried out during the last ten years of the fine structure of a large number of vibrational-rotational bands of water vapor situated in the near infrared region (1 - 6.5μ). Previously this region of the spectrum was poorly studied due to the low sensitivity of thermal detectors of infrared radiation. The new spectral data together with the best experimental results obtained in the past were not subjected until now to systematic examination with the object of making more precise the values derived earlier of the vibrational constants of the water molecule and of determining by computational means those vibrational energy levels whose values cannot be established according to the existing spectral data.

Attempts at utilizing the new spectral data for the determination of the vibrational constants of H_2O were undertaken in 1954 [1,2] and in 1956 [3]. However, these attempts cannot be acknowledged as satisfactory for the following reasons: 1) the vibrational energy levels of H_2O calculated with the help of the vibrational constant [1,3] are very significantly different from the experimental values; 2) in [2,3] it was asserted without proof that between the vibrational states of H_2O, a Fermi resonance also occurs in addition to the Darling-Dennison resonance; 3) in the work [3] the value of the anharmonicity constant, y_{222}, is presented but the remaining quantities of the same order are not taken into account; 4) in [2] and [3] new values for the Darling-Dennison resonance constant γ are adduced, while in [4] [5] it is asserted that the value of γ for H_2O must be a function of the vibrational quantum numbers; 5) it is not known in exactly what manner and which initial data were utilized by the authors for the determination of the vibrational constants of H_2O.

In the present work a complete cubic expression for the unperturbed values is used for the description of the vibrational energy levels

$$(1)\quad G_o^o(v_1,v_2,v_3) = \sum_{i=1}^{3} \omega_i^o v_i + \sum_{\substack{i=1 \\ i>j}}^{3}\sum_{j=1}^{3} x_{ij}^o v_i v_j + \sum_{\substack{i=1 \\ i\geq j\geq k}}^{3}\sum_{j=1}^{3}\sum_{k=1}^{3} y_{ijk}^o v_i v_j v_k$$

hence the Darling-Dennison resonance is taken into account. Nothing is assumed about the nature of the resonance interaction. The question of the dependence of γ on the vibrational quantum numbers is not determined beforehand.

In the work [6] results of investigations of the vibrational-rotational spectra of H_2O were examined in detail and a summary was compiled of selected experimental values of the vibrational energy levels of the water molecule (see Table 1). A direct analysis of the dependence of the vibrational energy levels of H_2O on v_1, v_2, v_3 showed that these data can not be satisfactorily described without taking into account the cubic terms [6]. The selection of the cubic expression (1) for $G_o^o(v_1,v_2,v_3)$ was influenced by this.

Table 1

Selected values of the vibrational energy values of H_2O based on spectral data (in cm^{-1})

$v_1v_2v_3$	$G_o(v_1,v_2,v_3)$	$\pm \Delta G_o^*$	Literature Source	$v_1v_2v_3$	$G_o(v_1,v_2,v_3)$	$\pm \Delta G_o$	Literature Source
000	0	—	—	121	10328.85	± 0.15	[8], [11], [14]
010	1594.78	± 0.02	[2]	022	10523	> ± 1	[8], [11]
020	3151.53	± 0.02	[6]	300	10599.7	± 0.5	[8], [11]
100	3656.65	± 0.05	[3], [9]	201	10613.12	± 0.02	[16]
001	3755.79	± 0.02	[9]	102	10868.8	± 0.5	[8], [11], [14]
030	4666.65	± 0.15	[8], [10], [11]	003	11032.36	± 0.02	[16]
110	5235.0	± 0.1	[13]	051	11248.4	± 0.7	[8], [11]
011	5331.19	± 0.02	[15]	013	11813.44	± (0.5)	[14]
040	6136.4	± 1.7	[8], [11]	032	12012	> ± 1	[8], [11]
120	6775.0	± (0.5)	[16]	211	12151.22	± 0.02	[16]
021	6871.65	± 0.02	[13]	112	12497.65	± (0.5)	[14]
200	7201.4	± 0.2	[11]	013	12565.01	± 0.02	[16]
101	7249.8	± 0.2	[17]	221	13652.65	± (0.5)	[14]
002	7445.0	± 0.5	[12]	301	13830.92	± 0.02	[17]
130	8273.98	± (0.5)	[16]	103	14318.77	± 0.02	[17]
031	8373.6	± 0.3	[8], [11]	311	15347.91	± 0.02	[17]
210	8761.5	± 0.5	[11]	113	15832.47	± 0.02	[17]
111	8867.05	± 0.05	[13]	321	16821.61	± (0.02)	[17]
012	9000.10	± 0.02	[15]	401	16898.01	± 0.02	[17]
041	9833.5	± 0.1	[8], [11]	203	17495.49	± 0.02	[17]

* Approximate error according to [6].

To expression (1) for the vibrational energy levels, counted from the level (0,0,0), corresponds the following expression for the levels counted from the potential energy minimum:

$$(2)\quad G(v_1,v_2,v_3) = \sum_{i=1}^{3} \omega_i\left(v_i+\tfrac{1}{2}\right) + \sum_{\substack{i=1 \\ i>j}}^{3}\sum_{j=1}^{3} x_{ij}\left(v_i+\tfrac{1}{2}\right)\left(v_j+\tfrac{1}{2}\right) + \sum_{\substack{i=1 \\ i\geq j\geq k}}^{3}\sum_{j=1}^{3}\sum_{k=1}^{3} y_{ijk}\left(v_i+\tfrac{1}{2}\right)\left(v_j+\tfrac{1}{2}\right)\left(v_k+\tfrac{1}{2}\right).$$

Expression (2) is the generalization of the quadratic expression obtained in the second approximation of perturbation theory [18]. It can be shown that expression (2) corresponds to the third approximation of perturbation theory and to taking into account terms proportional to the fifth and sixth powers of the relative displacements of the atoms in the expansion of the potential energy.

The constants ω_i, x_{ij}, y_{ijk} have the meaning of the normal vibrational frequencies and the first and second order anharmonicity constants, respectively. The following relations hold between ω_i^0, x_{ij}^0, y_{ijk}^0 and ω_i, x_{ij}, y_{ijk}:

$$\omega_i^0 = \omega_i + x_{ii} + \tfrac{1}{2}(3y_{iii} + y_{123}) + \tfrac{1}{2}\sum_{l \neq i}(x_{il} + y_{iil} + \tfrac{1}{2}y_{iil}),$$

$$x_{ii}^0 = x_{ii} + \frac{3}{2}y_{iii} + \frac{1}{2}\sum_{l \neq i} y_{iil}, \qquad (3)$$

$$x_{ij}^0 = x_{ij} + y_{iij} + y_{ijj} + \tfrac{1}{2}y_{123},$$

$$y_{ijk}^0 = y_{ijk};\ i, j, k, l = 1, 2, 3.$$

Darling-Dennison resonance takes place between the states $(v_1 \geqslant 2, v_2, v_3)$ and (v_1-2, v_2, v_3+2). It can be shown according to the spectral data (see [6]) that within the limits of accuracy of the determination of the vibrational energy levels of H_2O the Darling-Dennison resonance is the only perturbing influence. Therefore all these levels may be broken up into two classes: the non-resonating levels $(v_1 < 2,\ v_2, v_3 < 2)$, representable by formula (1), and the resonating levels $(v_1 > 2,\ v_2, v_3)$ not immediately representable by formula (1). The latter may be sub-divided into levels participating in pairwise resonance interaction

$$(v_1 = 2, 3;\ v_2;\ v_3 = 0, 1) - (v_1 = 0, 1;\ v_2;\ v_3 = 2, 3),$$

and into levels participating in triplet resonance interaction

$$(v_1 = 4, 5;\ v_2;\ v_3 = 0, 1) - (v_1 = 2, 3;\ v_2;\ v_3 = 2, 3) - (v_1 = 0, 1;\ v_2;\ v_3 = 4, 5)$$

etc. The corresponding cases of resonance interactions will be denoted as the pair resonance case, triplet resonance case, etc.

Let E_k^0, E_l^0, E_m^0, ... be the unperturbed values of the energy levels found in resonance interaction, and let W_{kl}, W_{lm}, ... be the matrix elements of the perturbing energy operator. Then according to the first approximation of degenerate perturbation theory the perturbed energy level values E_k, E_l, E_m, ... are defined by the roots of a secular equation of the following form:

$$\begin{vmatrix} E_k^0 - E & W_{kl} & 0 & \dots \\ W_{lk} & E_l^0 - E & W_{lm} & \dots \\ 0 & W_{ml} & E_m^0 - E & \dots \\ \dots & \dots & \dots & \dots \end{vmatrix} = 0 \qquad (4)$$

where W_{lk} is the complex conjugate of W_{kl}. If it is agreed to understand by the level k the level $(v_1 \geqslant 2, v_2, v_3)$, and by l, the level (v_1-2, v_2, v_3+2), then in the Darling-Dennison resonance case $|W_{kl}|^2$, according to [19,20], is equal to

$$|W_{kl}|^2 = \tfrac{1}{64}\gamma^2 . v_1(v_1-1)(v_3+1)(v_3+2), \qquad (5)$$

where γ is the resonance interaction constant.

In the case of pair resonance interaction, equation (4) reduces to the quadratic equation

$$E^2 - (E_k^0 + E_l^0).E + E_k^0 E_l^0 - |W_{kl}|^2 = 0. \qquad (6)$$

An application of the theorem of Viete to equation (6) gives the following relation between the perturbed and unperturbed energy values of the pairwise resonating levels:

$$E_k + E_l = E_k^0 + E_l^0; \qquad (7)$$

$$E_k E_l = E_k^0 E_l^0 - |W_{kl}|^2, \qquad (8)$$

which are equivalent to the following:

$$E_k - E_k = E^0 - E_l \qquad (9)$$

$$(E_k - E_l)^2 = (E_k^0 - E_l^0)^2 + |4\,W_{kl}|^2. \qquad (10)$$

The relations (9) and (10) imply that as a result of pair resonance the levels would be repelled from each other by identical distances. When three levels participate in the resonance reaction the determinantal equation (4) reduces to the cubic equation

$$E^3 - (E_k^0 + E_l^0 + E_m^0)E^2 + (E_k^0 E_l^0 + E_l^0 E_m^0 + E_m^0 E_k^0 - |W_{kl}|^2 - |W_{lm}|^2)E - (E_k^0 E_l^0 E_m^0 - E_k^0|W_{lm}|^2 - E_m^0|W_{kl}|^2) = 0. \qquad (11)$$

The application of the theorem of Viete to equation (11) allows the following relations to be written down between the perturbed and unperturbed values of the energy levels sharing in the triplet resonance:

$$E_k + E_l + E_m = E_k^0 + E_l^0 + E_m^0; \qquad (12)$$

$$E_k E_l + E_l E_m + E_m E_k = E_k^0 E_l^0 + E_l^0 E_m^0 + E_m^0 E_k^0 - |W_{kl}|^2 - |W_{lm}|^2; \qquad (13)$$

$$E_k E_l E_m = E_k^0 E_l^0 E_m^0 - E_k^0|W_{lm}|^2 - E_m^0|W_{kl}|^2. \qquad (14)$$

Analogous relations may be deduced for levels taking part in more complex resonance interactions.

DETERMINATION OF THE VIBRATIONAL CONSTANTS

Starting from the experimental values of the vibrational energy levels of H_2O, adduced in Table 1, and the theoretical results expounded in the previous section, one may proceed to the successive determination of the numerical values of the vibrational constants found in the cubic expression (1) for $G_o^o(v_1,v_2,v_3)$.

Expression (1) is directly applicable for the representation of the non-resonating vibrational levels of H_2O:

$$G_o(100)=\omega_1^o+x_{11}^o+y_{111}^o=3656.65\ cm^{-1};$$

$$G_o(001)=\omega_3^o+x_{33}^o+y_{333}^o=3755.79\ cm^{-1};$$

$$G_o(0v_2^0)=\omega_2^o\cdot v_2+x_{22}^o\cdot v_2^2+y_{222}^o\cdot v_2^3;$$

$$G_o(1v_2^0)=G_o(100)+G_o(0v_2^0)+(x_{12}^o+y_{112}^o)v_2+y_{122}^o\cdot v_2^2;$$

$$G_o(0v_2^1)=G_o(001)+G_o(0v_2^0)+(x_{23}^o+y_{233}^o)\cdot v_2+y_{223}^o\cdot v_2^2;$$

$$G_o(1v_2^1)=G_o(1v_2^0)+G_o(0v_2^1)-G_o(0v_2^0)+x_{13}^o+y_{113}^o+y_{133}^o+y_{123}^o\cdot v_2.$$

Setting v = 1,2,3 in (17) and utilizing the data of Table 1 for the (010) (020) and (030) levels, we obtain the following values of the constants ω_2^o, x_{22}^o, y_{222}^o:

(21) $\omega_2^o = 1612.60\ cm^{-1}$; $x_{22}^o = -17.22\ cm^{-1}$;

$y_{222}^o = -0.60\ cm^{-1}$.

Equation (18) and the data of Table 1 for the levels $(1, v_2, 0)$ allow the determination of the values $x_{12}^o + y_{112}^o$ and y_{122}^o:

(22) $x_{12}^o + y_{112}^o = -16.30\ cm^{-1}$,

(23) $y_{122}^o = -0.10^{-1}$.

Equation (19) and the data of Table 1 for the levels of the type $(0, v_2, 1)$ allow the determination of the values of $x_{23}^o + y_{233}^o$ and y_{233}^o:

(24) $x_{23}^o + y_{233}^o = -20.92\ cm^{-1}$,

(25) $y_{223}^o = +1.55\ cm^{-1}$.

Equation (20) and the data of Table 1 for the levels (101) and (111) allow the determination of the values of $x_{13}^o + y_{113}^o + y_{133}^o$ and y_{123}^o:

(26) $x_{13}^o + y_{113}^o + y_{133}^o = 162.64\ cm^{-1}$,

(27) $y_{123}^o = -1.72\ cm^{-1}$.

For the next step in the determination of the vibrational constants of H_2O it is necessary to utilize the data of Table 1 for the levels participating in the pair resonance interaction. Here we shall be guided by relations (7) and (8) between the perturbed and unperturbed values of these levels. In order to use these relations it is necessary to plot the experimental values for both levels participating in the pair resonance. The corresponding data are presented in Table 1 for the following seven pairs of resonating levels: (200)-(002), (210)-(012), (300)-(102), (201)-(003), (211)-(013), (301)-(103) and (311)-(113). The relation (7) suitable for these data may be written down in the following form:

(28) $G_o^o(v_1,v_2,v_3)+G_o^o(v_1-2,\ v_2,v_3+2)=G_o(v_1,v_2,v_3)+G_o(v_1-2,\ v_2,v_3+2)$,

where v_1, v_2, v_3 = 200; 210; 300; 201; 211; 301; 311.

The quantities on the left-hand side of equation (28) may be represented, according to (1) and (15), (16), (21)-(27), in the following form:

(29) $G_o^o(200)=7313.30+2(x_{11}^o+3y_{111}^o)$,

$G_o^o(002)=7511.58+2(x_{33}^o+3y_{333}^o)$,

$G_o^o(210)=8875.28+2(x_{11}^o+3y_{111}^o+y_{112}^o)$,

$G_o^o(113)=15951.20+6(x_{33}^o+4y_{333}^o+y_{133}^o+y_{233}^o)$.

After substituting the corresponding expression of (29) in the left-hand side of equation (28) and the corresponding values from Table 1 in the right-hand side, it turns out that of the seven equations (28) only six are independent. These latter equations are equivalent to the following:

(30) $y_{112}^o+3y_{233}^o = -2.53\ cm^{-1}$;

(31) $y_{112}^o+y_{233}^o = -0.91\ cm^{-1}$;

(32) $x_{11}^o+x_{33}^o = -89.30\ cm^{-1}$;

(33) $y_{111}^o+y_{333}^o = +0.02\ cm^{-1}$;

(34) $y_{113}^o+y_{133}^o = +1.85\ cm^{-1}$;

(35) $2x_{33}^o+9y_{333}^o+y_{113}^o = -93.61\ cm^{-1}$.

It can be shown [6] that the equations (28) corresponding to $v_1v_2v_3$ = 200 and 210 reduce to each other. This circumstance makes it possible to make more accurate the value for $G_o^o(210)$ quoted in Table 1:

(36) $G_o(210)=8762.5\ cm^{-1}$.

From (30) and (31) we determine

(37) $y^o_{112} = -0.10\ cm^{-1}$; $y^o_{233}=-0.81\ cm^{-1}$.

From (37), (22) and (24) we determine

(38) $x^o_{12}= -16.20\ cm^{-1}$; $x^o_{23}= -20.11\ cm^{-1}$.

From (34) and (26) we determine

(39) $x^o_{13}= -164.49\ cm^{-1}$.

One may make up corresponding equations also for other pairs of resonating levels. However they all reduce to the above-cited equations (30)-(35). On the strength of this it turned out to be possible to determine the values of the vibrational levels (220), (230), (310), (023) and (123), having at our disposal only the data of Table 1 for the levels (022), (032), (112), (221) and (321):

(40)
$$G_o(220)=10286\ cm^{-1};$$
$$G_o(230)=11765\ cm^{-1};$$
$$G_o(310)=12140.41\ cm^{-1};$$
$$G_o(023)=14070.33\ cm^{-1};$$
$$G_o(123)=17325.02\ cm^{-1}.$$

Of the 19 vibrational constants entering into the cubic expression (1) there still remained the eight undetermined constants (ω^o_3, a^o_{11}, x^o_{33}, y^o_{111}, y^o_{113}, y^o_{133}, y^o_{333}) for which were obtained the six equations (15), (16), (32)-(35). For the determination of these constants it is necessary to supplement these six equations by two more independent equations.

In order to do this it is natural to make use of relation (12) between the perturbed and unperturbed values of the vibrational levels participating in the triplet resonance. Here it is necessary to know the experimental values of all three levels found in the triplet resonance interaction. However the spectral data known for H_2O make it possible to determine only two of them - (401) and (203) (see Table 1). But the existing data do not allow the determination of the energy value of the third level (005). To complete the solution of the problem of the determination of the vibrational constants of H_2O we could only rely on relation (8) or (10) for the levels between which the pair resonance takes place, which is connected with the clarification of the dependence of the quantity γ on the vibrational quantum numbers and to the determination of the form of this dependence. According to Table 1 and the results (40) the perturbed energy values of twelve pairs of resonating levels are known for H_2O. Of these the most precise values are known for the four pairs of levels:

(41) (201)-(003); (211)-(013); (301)-(103); (311)-(113).

The least precise values are known for the levels: (220)-(022) and (230)-(032), which consequently will not be used in the sequel. Moreover, the perturbed (observable) values are known for six more pairs of resonating levels:

(42) (200)-(002); (210)-(012); (300)-(102); (310)-(112); (221)-(023); (321)-(123).

Insofar as the quantity γ may depend on the vibrational quantum numbers of the resonating states, we shall write $\gamma(v_1v_2v_3)$ instead of γ. The relations (5) and (10) make it possible to determine this quantity by the following formula:

$$(43)\quad \gamma^2_{v_1v_2v_3} = \frac{1}{a_{v_1v_3}}\left[\left(\Delta_{v_1v_2v_3}\right)^2-\left(\Delta^o_{v_1v_2v_3}\right)^2\right],$$

where $\Delta_{v_1v_2v_3}$ and $\Delta^o_{v_1v_2v_3}$ are the absolute values of the differences between the perturbed and unperturbed values of the pairwise resonating levels and

$$(44)\quad a_{v_1v_3} = v_1(v_1 - 1)(v_3+1)(v_3+2).$$

In formulas (43) and (44) $v_1=2,3$; $v_3=0$, 1 and $v_2= 0, 1, 2, \ldots$. The expression of $\Delta^o_{v_1v_2v_3}$ in terms of the quantum numbers may be derived in general form starting from the definitions of these quantities in terms of the unperturbed values of the pairwise resonating levels and the expressions (1) for $G^o_o(v_1,v_2,v_3)$. If we carry out corresponding calculations and take advantage of the obtained results of the determinations of the vibrational constant and also of the relations (15), (16), (32)-(35), having made use of them for the elimination of ω^o_1, ω^o_3, and express the constants x^o_{11}, y^o_{111}, y^o_{113} and y^o_{133} through x^o_{33} and y^o_{333}, then we obtain the following expression for $\Delta^o_{v_1v_2v_3}$ in terms of x^o_{33} and y^o_{333}:

$$(45)\quad \Delta^o_{v_1v_2v_3} = A_{v_1v_2v_3} + a_{v_1v_3}x^o_{33} + b_{v_1v_3}y^o_{333},$$

where $b_{v_1v_3}$ has the following values:

(46) $b_{20}=12$; $b_{30}=b_{21}=48$; $b_{31}= 156$,

and the quantities $A_{v_1v_2v_3}$ are determined by the following expressions:

$$A_{2v_2^o} = 376.76-10.66\ v_2+ 3.30\ v_2^2,$$
$$A_{3v_2^o} = 699.24 - 13.70\ v_2+3.30\ v_2^2,$$
(47)
$$A_{2v_2^1} = 889.26 - 10.46\ v_2+3.30\ v_2^2,$$
$$A_{3v_2^1} = 1868.02 - 13.50\ v_2+3.30\ v_2^2.$$

In connection with (45), expression (43) may be transformed to the form:

$$\gamma^2_{(v_1v_2v_3)} = -a_{v_1v_3}\left(x^o_{33} + c_{v_1v_3}\, y^o_{333} + d_{v_1v_2v_3}\right)$$

(48)

$$\left(x_{33} + c_{v_1v_3}\, y_{333} + e_{v_1v_2v_3}\right),$$

$$c_{v_1v_3} = \frac{b_{v_1v_3}}{a_{v_1v_3}}\,; \quad d_{v_1v_2v_3} = \frac{A_{v_1v_2v_3} + \Delta_{v_1v_2v_3}}{a_{v_1v_3}}\,;$$

(49)

$$e_{v_1v_2v_3} = \frac{A_{v_1v_2v_3} - \Delta_{v_1v_2v_3}}{a_{v_1v_3}}$$

Let us assume the independence of the quantities $\gamma^2_{v_1v_2v_3}$ of the vibrational quantum numbers, then for the determination of x^o_{33} and y^o_{333} the following equations may be set up:

$$a_{v_1'v_3'}\left(x^o_{33} + c_{v_1'v_3'}\, y^o_{333} + d_{v_1'v_2'v_3'}\right)\left(x^o_{33} + c_{v_1'v_3'}\, y^o_{333} + e_{v_1'v_2'v_3'}\right) =$$

$$= a_{v_1''v_3''}\left(x^o_{33} + c_{v_1''v_3''}\, y^o_{333} + d_{v_1''v_2''v_3''}\right)\chi \qquad (50)$$

$$\chi\left(x^o_{33} + c_{v_1''v_3''}\, y^o_{333} + e_{v_1''v_2''v_3''}\right);$$

$$v_1', v_1'' = 2,3;\ v_2', v_2'' = 0, 1, 2\ldots;\ v_3', v_3'' = 0,1.$$

It was pointed out that Table 1 and the results (40) allow the determination of the ten pairs of pairwise resonating levels (41) and (42). Consequently, the known values $\Delta_{v_1v_2v_3}$ and according to (47) and (49), $d_{v_1v_2v_3}$ and $e_{v_1v_2v_3}$ correspond to $v_1v_2v_3$ = 200, 210, 201, 300, 211, 301, 310, 221, 311, 321. These data allow the composition of 45 equations of the type (50). Analysis of these [6] showed that within the limits of accuracy of the determination of the quantities $d_{v_1v_2v_3}$ and $e_{v_1v_2v_3}$ according to the formulas (49), the values of the constants x^o_{33} and y^o_{333} are defined in a completely unique manner by the equations (50). To this degree of accuracy the quantity γ does not depend on the vibrational quantum numbers.

The most accurate values of x^o_{33}, y^o_{333} and γ on the basis of the data of Table 1 for the levels (41) equal:

(51) $x^o_{33} = -45.12\ \text{cm}^{-1}$; $y^o_{333} = -0.45\ \text{cm}^{-1}$;

(52) $\gamma = 76.02\ \text{cm}^{-1}$.

The results (51) in conjunction with equations (15), (16), (32)-(35) determine the value of the rest of the vibrational constants:

(53) $\omega^o_1 = 3700.36\ \text{cm}^{-1}$; $x^o_{11} = -44.18\ \text{cm}^{-1}$;

$y^o_{111} = +0.47\ \text{cm}^{-1}$; $\omega^o_3 = 3801.36\ \text{cm}^{-1}$;

$y^o_{113} = +0.68\ \text{cm}^{-1}$; $y^o_{133} = +1.17\ \text{cm}^{-1}$.

The determination of the constants entering into the cubic expression (1) for the unperturbed vibrational energy levels of H_2O is completed with the results (53). The values of these constants and the values of the resonance interaction constants corresponding to them are presented in Table 2.

Table 2

Vibrational constants of the H_2O molecule (in cm^{-1})

i	ω^o_i	ij	x^o_{ij}	jk	y^o_{ik}	ijk	y^o_{ijk}
1	3700.36	11	− 44.18	111	+1.55	223	+0.47
2	1812.60	22	− 17.22	222	−0.81	233	−0.80
3	3801.36	33	− 45.12	333	+0.68	113	−0.45
		12	− 16.20	112	−1.72	123	−0.10
γ = 76.02		23	− 20.11	122	+1.17	133	−0.10
		13	−164.49				

DISCUSSION OF THE RESULTS OBTAINED

We proceeded from the experimental values of the non-resonating and pairwise resonating vibrational energy levels, cited in Table 1. In Table 3 the experimental values of the non-resonating vibrational levels of H_2O from Table 1 are compared with the corresponding calculated values based on formula (1) and the data of Table 2. An analogous comparison is carried out in Table 4 for the pairwise resonating levels. Together with the experimental values of $G_o(v_1,v_2,v_3)$ for the pairwise resonating levels from Table 1, in Table 4 the values of (40) are quoted whose accuracy of determination equals the accuracy of determination of their partners in resonance according to the spectral data.

Table 3

Experimental and calculated energy values of non-resonating vibrational levels of H_2O (in cm^{-1})

$v_1v_2v_3$	$G_o(v_1,v_2,v_3)$ experimental	$G_o(v_1,v_2,v_3)$ calculated	$v_1v_2v_3$	$G_o(v_1,v_2,v_3)$ experimental	$G_o(v_1,v_2,v_3)$ calculated
010	1594.78*	1594.78	021	6871.65*	6871.68
020	3151.53*	3151.53	101	7249.8*	7249.80
100	3656.65*	3656.65	130	8273.98*	8273.50
001	3755.79*	3756.79	031	8373.8*	8373.63
030	4666.65*	4666.65	111	8807.05*	8807.09
110	5235.0*	5235.03	041	9833.5	9833.39
011	5331.19*	5331.20	121	10328.85	10329.04
040	6136.4	6136.48	051	11248.4	11247.44
120	6775.0*	6775.18	131	11813.44	11812.85

The experimental values of $G_o(v_1,v_2,v_3)$ are directly utilized for the determination of the numerical values of the vibrational constants noted in Tables 3 and 4 by asterisks.

Tables 3 and 4 show that the cubic expression (1) for $G_o^o(v_1,v_2,v_3)$ makes possible the reproduction of the experimental values of the non-resonating vibrational energy levels of H_2O for $v_2 \leqslant 5$, within the limits of error of their determination according to the spectral data.

The frequency of the vibrational transition of the H_2O molecule from the state (061) to the state (050) was determined in the works [11,13]. Combining this result with the calculated value of $G_o(050)$, we obtain for the energy level (061)

$$G_o(061)=12624 \text{ cm}^{-1}, \tag{54}$$

the inaccuracy of which may be estimated to be ± 5 cm^{-1}. But on direct calculation, according to (1) and Table 4, we obtain

$$G_o(061)_{calc} = 12612 \text{ cm}^{-1}. \tag{55}$$

The results (54) and (55) show that in using the cubic representation (1) the divergence between the experimental and calculated values of the levels corresponding to $v_2 = 6$ becomes approximately 10 cm^{-1}. For levels corresponding to larger values of v_2 the magnitude of this divergence must become progressively larger, since for a precise reproduction of the actual values of such levels it is necessary to take into account terms of the fourth and higher degrees in the expansion of $G_o^o(v_1,v_2,v_3)$.

It follows from Tables 4 and 1 that the difference between the calculated energy values of the pairwise resonating levels and the corresponding experimental values does not in large part exceed the error of determination of the latter according to the spectral data. In the remaining cases, besides the cases with levels (321) and (123), the divergence between the experimental and the calculated values is small and may be explained easily by insufficient accuracy in the values of the vibrational constants of Table 2.

A sharper distinction between the experimental and calculated values occurs for $G_o(321)$ and $G_o(123)$. The value of $G_o(123)$ quoted in Table 4 is based on the experimental value of $G_o(321)$. The latter was determined by Freudenburg and Mecke [17] on the basis of an analysis of the rotational structure of the band $3\nu_1 + 2\nu_2 + \nu_3$. However these authors remark that the band $3\nu_1+2\nu_2+\nu_3$ is superposed on the considerably more intense band $4\nu_1+\nu_3$, which makes the analysis of its structure more difficult. It may now be considered proven that Freudenburg and Mecke mistakenly interpreted the fine structure of the band $3\nu_1+2\nu_2+\nu_3$ and, in particular, erred in the determination of the center of this band by 10 cm^{-1}. This is evident on comparison of the distances between the observed and unperturbed values of the levels participating in the pairwise resonance (see [6]).

In the determination of the vibrational constants of H_2O we have not used the experimental values of $G_o(401)$ and $G_o(203)$, insofar as the levels (401), (203), (005) are found in resonance coupling, and the value of $G_o(005)$ has not yet been determined by spectral data. Now, according to (1) and the data of Table 4, we may calculate the unperturbed energy values of these levels:

$$G_o^o(401) = 17238.03 \text{ cm}^{-1}; \quad G_o^o(203) = 17255.89 \text{ cm}^{-1}; \tag{56}$$

$$G_o^o(005) = 17822.55 \text{ cm}^{-1}$$

Table 4

Experimental and calculated energy values of pairwise resonating vibrational levels of H_2O (in cm^{-1})

$v_1v_2v_3$	$G_o(v_1,v_2,v_3)$ experimental	$G_o(v_1,v_2,v_3)$ calculated	$v_1v_2v_3$	$G_o(v_1,v_2,v_3)$ experimental	$G_o(v_1,v_2,v_3)$ calculated
200	7201.4*	7201.18	201	10613.12*	10613.11
002	7445.0*	7445.22	003	11032.36*	11032.37
210	8762.5[1]	8762.14	211	12151.22*	12151.26
012	9000.10	9000.46	013	12565.01*	12564.98
220	10286[3]	10285.40	221	13652.65	13654.85
022	10523	10523.14	023	14070.33[2]	14068.13
230	11765[3]	11767.33	301	13830.92*	13830.83
032	12012	12009.84	103	14318.77*	14318.87
300	10599.7*	10601.33	311	15347.91*	15347.94
102	10868.8*	10867.17	113	15832.47*	15832.44
310	12140.41[2]	12141.72	321	16821.61	16831.67
112	12407.85	12406.34	123	17325.03[2]	17314.97

The results (52) and (56) permit the calculation of the coefficients in equation (11) for the levels (401), (203), (005). The solutions of these equations follow:

$$G_o(401)=16899.01 \text{ cm}^{-1}; \quad G_o(203)=17495.48 \text{ cm}^{-1}; \tag{57}$$

$$G_o(005)=17921.98 \text{ cm}^{-1}.$$

The values (57) for the levels (401) and (203) turn out to agree in accuracy with the corresponding experimental values quoted in Table 1. This indicates that even the calculated value (57) for $G_o(005)$, apparently, reproduces very accurately the actual value of the vibrational energy of H_2O for this state. It is easy to verify that the results (56) and (57) satisfy equations (12)-(14) with a high degree of accuracy.

The high accuracy of reproduction of the experimental values of the vibrational energy levels of H_2O corresponding to $v_1,v_2,v_3 \leqslant 5$, with the help of the cubic expression (1) for $G_o^o(v_1,v_2,v_3)$ and the apparatus of first order perturbation theory permit the confirmation that within the indicated limits according to Table 2 many vibrational levels of H_2O may be very accurately determined by calculation which have been heretofore undetermined due to the absence of the corresponding spectral data (see [6]). The successful application of Table 4

for calculating the levels (401), (203), (005) permits the calculation of the lower most vibrational energy levels of H_2O between which there must be triple resonance interaction (see Table 5).

Table 5

Calculated values of the vibrational energy levels of H_2O between which triplet resonance interaction occurs.

$v_1v_2v_3$	$G^o_o(v_1v_2v_3)$	$G_o(v_1v_2v_3)$	$v_1v_2v_3$	$G^o_o(v_1v_2v_3)$	$G^o(v_1v_2v_3)$
400	14124.64	13858.77	420	17141.76	16833.36
202	14003.24	14227.27	222	17000.08	17226.20
004	14454.72	14528.57	024	17444.24	17526.52
410	15652.62	15350.89	500	17456.05	16889.95
212	15517.78	15735.67	302	17174.13	17471.26
014	15962.30	16046.15	104	17474.85	17743.82

We note that very great difficulties were encountered in the works [3, 19] in attempts to reproduce the observed values of the vibrational energy levels (401) and (203) by means of calculations. The resonance between these levels was treated as pairwise and a quadratic representation was used for the unperturbed energy values. Having obtained a considerable divergence between the experimental and calculated values of the levels by such an approach, it was explained as evidence for the presence in H_2O of a still higher anharmonic resonance analogous to Fermi resonance [2,3], in addition to the Darling-Dennison resonance.

Up to the present time the vibrational constants of H_2O were determined on the basis of a quadratic expression for the unperturbed vibrational energy values, which was justified by the insufficient ability to study the molecular spectrum of water in the infrared region, and also by the relative smallness of the second anharmonicity constants y_{ijk}. The values of the vibrational constants ω_i^o and x_{ij}^o quoted in Table 2 are close to the corresponding values of these constants in the work [3]. The largest difference occurs in the values of x_{11}^o and x_{33}^o, since in the determination of these constants on the basis of the quadratic expression for $G^o(v_1,v_2,v_3)$ the values actually found are $x_{11}^o + 4y_{111}^o$ and $x_{33}^o + 4y_{333}^o$. The value (52) for the resonance interaction constant γ is intermediate between the values found in [3] and [19].

Values of the normal vibration frequencies ω_i and of the anharmonicity constants x_{ij} are quoted in Table 6 which were calculated according to [3] according to the corresponding data of Table 2. The value of the zero point vibrational energy of the water molecule is here determined to be $G(000) = 4634.00\ cm^{-1}$.

Table 6

Normal vibrational frequencies and anharmonicity constants of H_2O (in cm^{-1}).

i	ω_i	ii	x_{ij}	ij	x_{ij}
1	3835.37	11	−45.18	12	− 15.14
2	1647.59	22	−17.44	23	− 19.99
3	3938.74	33	−44.82	13	−165.48

CONCLUSIONS

1. Numerical values of nineteen vibrational constants entering the complete expression for the vibrational energy levels of the water molecule were determined, as was the value of the resonance interaction constant.

2. New values of the vibrational constants of H_2O allow the calculation of the vibrational energy levels corresponding to $v_1,v_2,v_3 \leqslant 5$, with an accuracy of the same order as that done on the basis of spectral data.

3. By using a complete cubic expression for $G^o_o(v_1,v_2,v_3)$ and by successive calculation of the Darling-Dennison resonance, the necessity no longer arises for assuming a dependence of the resonance interaction constant γ on the vibrational quantum numbers and for assuming that a Fermi resonance occurs in the water molecule.

4. The vibrational levels of H_2O taking part in triplet resonance interaction have been determined by means of calculations for the first time.

5. The values of the normal oscillation frequencies and of the anharmonicity constants have been made considerably more precise.

April 9, 1958

References

1. A. S. FRIEDMAN, L. HAAR: J. Chem. Phys., 22, 2051 (1954)
2. H. W. WOOLEY: J. Res. Natl. Bur. Stand., 54, 299 (1955)
3. W. S. BENEDICT, N. GAILAR, E. K. PLYLER: J. Chem. Phys., 24, 1139 (1956)
4. H. C. ALLEN, Jr., L. R. BLAINE, E. K. PLYLER: J. Res. Natl. Bur. Stand., 56, 279 (1956)
5. H. C. ALLEN, Jr., E. K. PLYLER: J. Chem. Phys., 25, 1132 (1956)
6. G. A. KHACHKURUZOV: Tr. GIPKh, No. 42, 51 (1959)
7. F. W. DALBY, H. H. NIELSEN: J. Chem. Phys., 25, 934 (1956)
8. W. S. BENEDICT, H. H. CLAASSEN, J. H. SHAW: J. Res. Natl. Bur. Stand., 49, 91 (1952)
9. W. S. BENEDICT, E. K. PLYLER: J. Res. Natl. Bur. Stand., 46, 246 (1951)
10. O. C. MOHLER, W. S. BENEDICT: Phys. Rev., 74, 702 (1948)
11. W. S. BENEDICT, E. K. PLYLER: Energy Transfer in Hot Gases. Natl. Bur. Stand. Circ. 523, Washington, 1954, p. 57
12. R. C. NELSON, W. S. BENEDICT: Phys. Rev., 74, 703 (1948)
13. W. S. BENEDICT, A. M. BASS, E. K. PLYLER: J. Res. Natl. Bur. Stand., 52, 161 (1954)
14. W. S. BENEDICT: Phys. Rev., 74, 1246 (1948)
15. R. MECKE: Z. f. Phys., 81, 313 (1933)
16. W. BAUMANN, R. MECKE: Z. f. Phys., 81 445 (1933)
17. K. FREUDENBERG, R. MECKE: Z. f. Phys., 81, 465 (1933)
18. H. H. NIELSEN: Rev. Mod. Phys., 23, 90 (1951)
19. B. T. DARLING, D. M. DENNISON: Phys. Rev., 57, 128 (1940)
20. G. HERZBERG: Vibrational and rotational spectra of polyatomic molecules (IL, Moscow, 1949)

TOM VI, Vyp. 4
VOL. VI, No. 4

OPTIKA I SPEKTROSKOPIIA
OPTICS AND SPECTROSCOPY

Aprel', 1959
April, 1959

On the Measurement of Intensities of Strong Absorption Bands in Infrared Spectra of Liquids

G. S. DENISOV

Abstract: A method is described for preparation and measurement of thicknesses of absorption cells 1 - 5μ thick to obtain infrared spectra of highly absorbing liquids. Selective reflection is discussed as a possible source of errors in measuring the integral intensity and the band contour.

The investigations of intensities of infrared absorption spectra of many pure liquids are hampered due to the high absorption coefficient of some bands. Therefore, in the literature, data are missing on band intensities of pure ketones and esters of organic acids in the region of 1700 cm^{-1}, of alcohols in the region of 3000 cm^{-1}, of chloroform and bromoform in the region of 1200 cm^{-1}. To obtain these one needs layers of substances with thicknesses of the order 1 - 5μ. The problem of preparation and measurement of such layers becomes topical for the investigation of intermolecular interactions. One can make certain deductions from the change of intensity about the mechanics of these interactions [1] while going from pure liquids to solutions. While investigating the dependence of the band intensity of νC=O ketones on the solvent, we found it indispensable to make absorption cells of small thickness and to take into account errors in quantitative measurements which are specific for this case: errors due to influence of selective reflection in regions of strong absorption bands and due to influence of capillary forces on the thickness.

The basic difficulty which arises, when we try to make cells of such thicknesses, lies in the high demands on the quality of polishing the windows. Keussler [2] succeeded in making cells for ultraviolet absorption spectra with thicknesses of 0.3 - 4.0μ from quartz plates polished with the same accuracy as the plates of a Fabry-Perot etalon. We tried to work out a similar method for infrared absorption spectra using rock-salt as window material. The plates were polished with an accuracy to about 0.5 fringes. A ring-shaped aluminum layer, deposited by vacuum evaporation, served as a gasket. The cell windows were adjusted to be plane-parallel by varying the pressure of the holder screws with the aid of interference fringes from a Hg lamp. The liquid was introduced through an opening drilled into the upper window. The thickness was obtained by an interferometric method from transmission spectra of empty cells. In the region 4000 - 7500 Å the thickness was measured with the spectro-photometer SF-2M* which made it possible to measure thicknesses from 1 to 7μ. The accuracy of these measurements exceeds by almost one order that of determining the optical density, so that the error in measuring the absorption coefficient depends only on the accuracy with which the transmission is measured. The errors are apparently much larger when one obtains the layer thickness from the optical density using the fall-off of the band investigated [3]. Since the light beam of the spectrometer SF-2M was narrow, the cell thickness could be measured at several points. The layer proved to be plane-parallel within 2%. A wedge of this magnitude can not have any influence on the accuracy of measurement of the absorption coefficient.

In measurements of the spectra of liquids in such cells one can have systematic errors due to variations of the thickness when filling the cell. The relative magnitude of these errors will increase with decreasing layer thickness and this must lead to a violation of Lambert's law which can be interpreted as a proportion between the observed optical density and the thickness. We obtained absorption spectra of dipropylketone in the region of the valence oscillation band of C=O in the spectrometer IKS-6 with a NaCl prism (the spectral width of the slit was 4.5 cm^{-1}) with the aid of cells of thicknesses 1.19; 2.04; 3.48; 4.04μ. The dependence of the optical density on the thickness is shown in Figure 1. The points lie on a straight line passing through the origin, which means that the influence of capillary forces in this case is small. An attempt to introduce the liquid into the cell from the edge also does not cause a variation of thickness.

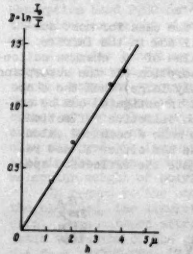

Figure 1 Dependence of the optical density in the band maximum of ν C=O $(n\text{-}C_3H_7)_2CO$ on the layer thickness.

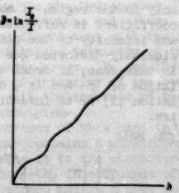

Figure 2

One has to pay special attention to the influence on the accuracy of measurement by selective reflection in the region of the absorption band where the refraction index of the investigated liquid varies greatly. The expression for the intensity of the normally incident beam passing through a plane-parallel layer of thickness h of the substance, characterized by a complex index of refraction, n - iκ, can be derived from the equations introduced by A. G. Vlasov[4]:

* The author is grateful to A. N. Mironova and Prof. A. N. Zaidel' for giving him the opportunity to use the spectrometer SF-2M.

$$J=J_0 e^{-\frac{4\pi h\kappa}{\lambda}} \cdot \frac{1+\rho^2-2\rho\cos\varphi}{1+\rho^2 e^{-\frac{8\pi h\kappa}{\lambda}} - 2\rho e^{-\frac{4\pi h\kappa}{\lambda}} \cos\left(\frac{4\pi h\kappa}{\lambda}-\varphi\right)}$$

where $\rho = \frac{(n-n_1)^2+\kappa^2}{(n+n_1)^2+\kappa^2}$, $\tan\frac{\varphi}{2} = -\frac{2\kappa n_1}{n^2-n_1^2+\kappa^2}$,

n_1 is the index of refraction of the cell window.

A dependence of the optical density D on the thickness according to (1) is shown in Figure 2. The observed optical density is linearly dependent on the thickness - strictly speaking only for $\rho=0$ i.e. for $n=n_1$ and $\kappa=0$. If the variation of ρ is not large (the corresponding oscillator strength is weak) in the limits of the band investigated, then for not too small thicknesses the term D_o, added to the optical density stipulated by reflection, is taken into account by measuring the optical density outside the absorption band and by calculation using the formulae from [5]. If in this case ρ is small, the D_o is virtually independent of the wavelength and the absorption coefficient can be calculated without substantial error from the relation:

$$\kappa = \frac{\lambda}{2\pi}\frac{D-D_o}{h} \qquad (2)$$

This is apparently the case for most substances investigated until nov in the infrared region. However, if the value of ρ changes noticeably in the region of absorption (if the absorption coefficient is sufficiently large) then the shape and intensity of the band investigated can be considerably distorted due to selective reflection. In this case, in order to make a combined calculation of n and κ, one has either to use relation (1) or to investigate the reflection spectra.

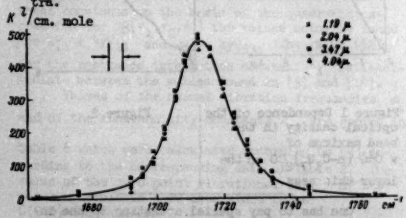

Figure 3 Plot of the absorption coefficient of the band of $\nu C=O$ $(n\text{-}C_3H_7)_2CO$ vs. frequency for samples of various thickness.

Recent attempts to determine the absorption coefficient of strong bands ($\kappa \sim 0.1 - 1.0$) of liquids from transmission spectra [3,6] were not accompanied by an analysis of the applicability of equation (2), used for calculation of κ, which depreciates considerably the results obtained. A numerical estimate of the value of κ, where the deviations from Lambert's law are considerable, is difficult, since it requires the knowledge of the index of refraction in the absorption band. However, a good experimental criterion for the influence of selective reflection can be the shape of the band $\kappa(\lambda)$ calculated from spectra obtained at various thicknesses. The independence of the function $\kappa(\lambda)$ on the thickness means the validity of Lambert's law for any other wave length. As one can see from Figure 3 for $\nu C=O$ of dipropylketone the deviations from Lambert's law are beyond the accuracy of spectro-photometric measurement.

The author thanks Prof. V. M. Chulanovskii for his guidance in this work and for discussion of the results.

May 7, 1958

References

1. V. M. CHULANOVSKII M. P. BURGOVA, G. S. DENISOV, E. L. ZHUKOVA: Fiz. sb. L'vov Univ., No. 3(8), 42 (1957)
2. V. VON KEUSSLER: Spectr. Acta, 6, 185 (1954)
3. M. P. LISITSA, V. N. MALINKO: PITE, No. 3, 52 (1957)
4. I. V. GREBENSHCHIKOV, A. G. VLASOV, B. S. NEPORENT, N. V. SUIKOVSKAIA: Prosvetlenie optiki (Enlightenment of optics) 27 (1946)
5. H. O. MC MAHON: JOSA, 40, 376 (1950)
6. R. M. ADAMS, J. J. KATZ: JOSA, 46, 895 (1956)

TOM VI, Vyp. 4 OPTIKA I SPEKTROSKOPIIA Aprel', 1959
VOL. VI, No. 4 OPTICS AND SPECTROSCOPY April , 1959

Application of Infrared Spectroscopy to the Investigation of Polymerization of Polyisobutylene

M. S. KOZYREVA

Abstract: The polymerization process of polyisobutylene was investigated by means of infrared spectra. The samples had a degree of polymerization n=2, 3, 4, 5, ~15, ~20, ~36. It was shown that at the polymerization the intensities of the absorption bands at 3075, 1640 and 888 cm^{-1} increase.

At the present time the methods of molecular spectral analysis are successfully employed for the study of polymerization processes, for determination of the number of double bonds and their position in unsaturated compounds [1-5]. In particular, in the papers [1, 2] on the study of the polymerization process of polyisobutylenes by means of the Raman spectra, it was found that as a result of polymerization of isobutylenes, there are formed polymeric molecules $\left[\begin{matrix} CH_3 \\ CH_2\ C \\ CH_3 \end{matrix}\right]_n$ with a double bond at the end and that with the increase of the degree of polymerization of polyisobutylenes to n=15, the statistical weight of branched isomers grows in relation to transisomers.

The present work also deals with the study of the polymerization process of polyisobutylenes. For this purpose there were taken infrared absorption spectra. Unlike in the papers [1, 2], the polyisobutylene samples were taken with a larger range of molecular weights (112-2000) and they were investigated within a wider range of the spectrum (10,000-800 cm^{-1}).

The investigated samples had a degree of polymerization n=2,3,4,5, ~15, ~20, ~36. The preparation of monodisperse fractions presents considerable difficulties and they can be obtained only for low molecular polyisobutylenes. We had at our disposal polyisobutylenes known to be heteregenous in composition. Each sample presented a mixture of homologues with various chain lengths.

The employed samples and some data on their physico-chemical properties are given in Table 1.*

Table 1

Sample	Average molec. weight	Index of Refr. at D_{Na} and 20°C	Spec.gravity at 20°C rel. to dens. of water at 4°C
Dimer	112	—	—
Trimer	168	1.4420	0.7859
Tetramer	224	1.4470	0.7932
Pentamer	280	1.4532	0.8037
Polyisobutylene P-1	850	1.4942	0.8804
Polyisobutylene P-V	1160	1.4990	0.8890
Polyisobutylene P-Z	2000	—	—

The infrared spectra were obtained with a IKS-11 spectrometer with LiF (region 10000-2000 cm^{-1}) and NaCl (region 2000-800 cm^{-1}) prisms. In figure 1 there are given spectra of several samples of polyisobutylenes in the region 2000-800 cm^{-1}. Figures 2 and 3 show correspondingly the spectra of polyisobutylenes in the region of 2900-3300 cm^{-1} and 2800-3100 cm^{-1}. The spectra in the regions 2800-3100 cm^{-1} and 1150-1500 cm^{-1} (with the exception of the pentamer) were obtained in solution. Carbontetrachloride was used as a solvent.

From figures 1, 2 and 3 it can be seen that the spectra of the low molecular isobutylenes, the tetramer and pentamer, sharply differ from the spectra of the higher molecular polyisobutylenes, the spectra of the other polyisobutylenes are similar. The spectra of the pentamer and tetramer strongly differ in the region of 800-1300 cm^{-1} (the spectrum of the tetramer is not shown in figure 1, because it is similar to the spectrum of the pentamer), where a larger number of bands appears as compared with the high molecular polyisobutylenes.

The polymerization process of polyisobutylenes can be expressed by a decrease in the number of the $=CH_2$ bonds and, consequently, is manifest in the infrared spectra by a decrease in the intensities of the corresponding absorption bands. These absorption bands lie in polyisobutylenes at 3075, 2980, 1640 and 888 cm^{-1}. In figures 1 - 3, it is seen that the intensity of these absorption bands changes with the transition from low to high molecular weight polymers, and namely the intensity of the bands 3075, 1640 and 888 cm^{-1} decreases while the intensity of the band 2980 cm^{-1} increases with the increase of the molecular weight of the sample, i. e. with the decrease in the number of the $=CH_2$ group per unit volume. Thus, the intensity of the absorption band 2980 cm^{-1} grows with the growth of the molecular weight which is not in agreement with the content of the group $=CH_2$.

A similar behaviour of this band has been observed by Fox and Martin [6] in the hydrocarbon series: ethylene, propylene, 1-butene and cetene. Their infrared spectra also showed that with the increase of the molecular weight the intensity of the absorption band at 2980 cm^{-1} grows. Nelson [2] also observed the increase of intensity of the same band in the Raman spectra with the increase of the molecular weight of polyisobutylene.

In regard to the occurrence of this band in the olefines, the literature contains contradictory data. Some authors attribute it to the characteristic vibration of the group $=CH_2$ in compounds of the form $R_1R_2C=CH_2$ [7], others maintain that it is not characteristic and that its location depends on whether it belongs to the spectrum of a cis- or trans-isomer [8]. It is evidently impossible to consider the band to be characteristic for the vibrations $=CH_2$ groups, just as it is impossible to attribute it to a strong branching, since in the hydrocarbon series ethylene-cetene (where no branching occurs), a similar change of that band was observed. Thus, Sverdlov's [7] conclusion about the band at 2980 cm^{-1} being characteristic for the $=CH_2$ bond in compounds of the form $R_1R_2C=CH_2$ is not confirmed, neither by our data, nor by those of Fox and Martin.

*The investigated samples and their physico-chemical data were given to us by T. F. Danilova.

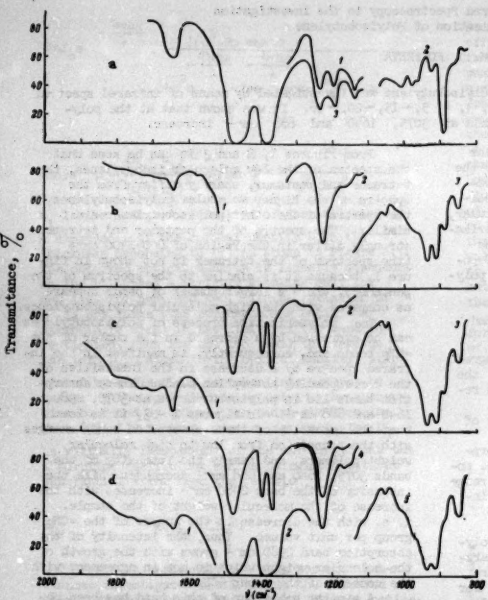

Figure 1. Infrared absorption spectra of polyisobutylenes in the region 800 - 2000 cm^{-1}.
[l thickness of the layer (in mm): C- concentration (in %)]
a. pentamer (M = 280): 1- l = 1.2, C = 5.1: 2- l = 0.11, C = 100; 3- 0.06, C = 100.
b. polyisobutylene P-1 (M = 850): 1- l = 0.11, C = 100; 2- l = 1.2, C = 2; 3- l = 0.11, C = 100;
c. polyisobutylene P-F (M = 1200): 1- l = 0.8, C = 100; 2- l = 0.62, C = 1.5; 3- l = 0.11, C = 100.
d. Polyisobutylene P-Z (M = 2000): 1- l = 0.8, C = 100; 2- l = 0.11, C = 100; 3- l = 0.62, C = 1.5; 4- l = 1.2 , C = 1.5, 5- l = 0.11, C = 100.

Figure 1 shows also that on polymerization, together with the above shown bands, the intensities of the absorption bands at 909, 940, 848 and 1225 cm^{-1} change. The absorption band at 909 cm^{-1} is usually attributed to the vinyl group CH_2 . According to Gruzdev [8] olefines, with a complex branching, show two bands: at 910 and 940 cm^{-1}, occurring as a result of splitting of the 925 cm^{-1} band, characteristic for the given type of branching. As seen in figure 1, in the spectrum of the pentamer whose molecules differ from the higher polyisobutelenes by smaller branching, there appears one band lying at 924 cm^{-1}. On the same figure one can see that in that region the higher molecular weight polyisobutylenes show two bands, of equal intensity, at 909 and 940 cm^{-1} . Apparently they appeared in the higher molecular polyisobutylenes as a result of branching at ~ 925 cm^{-1}. The increase of intensity of these bands with the increase of the molecular weight is not in agreement with the decrease of the number of vinyl groups per unit volume. Therefore, according to Gruzdev [8] , and in accord with our data, the intensification of these bands can be attributed to the increased number of groups C-C-R .
C

According to the literature [9] - the absorption bands at 848 and 1225 cm^{-1} in aliphatic hydrocarbons can also be attributed to the vibration of the groups C-C-R.
C

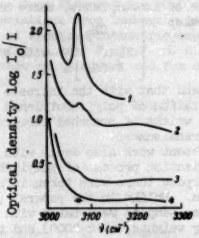

Figure 2. Absorption spectra of polyisobutylenes in the region 2900-3200 cm^{-1} (Thickness of the examined layer l=0.104mm).
1- dimer(n=112); 2- pentamer(M=280); 3- polyisobutylene P-F (M=1200); 4- polyisobutylene P-Z(M=2000).
For clearness the spectra are shifted along the vertical axis by 1- 1.0; 2- 0.8; 3- 0.2.

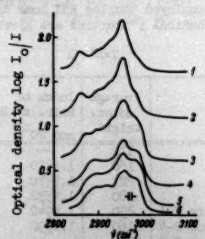

Figure 3. Absorption spectra of polyisobutylenes in the region (2800-3200 cm^{-1}) [l thickness of the layer (in mm); C- concentration (in %)]; the spectra were obtained in CCl_4 solution: 1- tetramer (M = 224) l = 0.212, C = 1; 2- pentamer (M = 280) l = 0.212, C = 1; 3- polyisobutylene P-1 (M = 850) l = 0.104. C = 2; 4- polyisobutylene P-Z (M = 1200) l = 0.104, C = 1.5; 5- polyisobutylene P-V (M = 1160) l = 0.104, C = 2; 6- polyisobutylene P-Z (M = 2000) l = 0.104, C = 1.5. For better clearness the spectra are shifted along the ordinate by: 1- 1.6; 2- 1.1; 3- 0.6; 4- 0.3; 5-0.1.

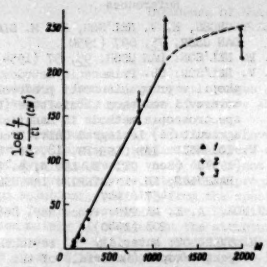

Figure 4. Absorption coefficient of the band $\nu = 1225$ cm^{-1} as a function of the molecular weight: 1- absorption coefficients calculated from spectra given in the work [10]; 2- absorption coefficients calculated from polyisobutylene spectra; 3- absorption coefficients calculated from spectra of polyisobutylenes in CCl_4 solutions.

The structure of polyisobutylenes is characterized by the presence of such groups. As can be seen from their structural formula, with the increase of the degree of polymerization n, the number of groups $\begin{matrix} & C & \\ & | & \\ C & - & C \end{matrix}$ in the molecule grows (table 2). However, the number of molecules per unit volume will be different, depending on the molecular weight, namely, with the increase of the molecular weight the number of molecules per unit volume diminishes.

Thus, the number of groups $\begin{matrix} & C & \\ & | & \\ C & - & C \end{matrix}$ will depend on the molecular weight and on the number of molecules per unit volume. In table 2 are given n_1 - number of groups $\begin{matrix} & C & \\ & | & \\ C & - & C \end{matrix}$ in one molecule and calculations of the molecule number $\left(n_0 = N_0 \frac{d}{M}\right)$ and of the number $m = n_1 n_0$ of the group $\begin{matrix} & C & \\ & | & \\ C & - & C \end{matrix}$ in the unit volume with the density d, the molecular weight M and the Avogadro number N_0 taken into account.

The table shows that with the increase of the molecular weight the number of groups $\begin{matrix} & C & \\ & | & \\ C & - & C \end{matrix}$ per unit volume also grows, and, consequently, the absorption of 1225, 909, 940 and 848 cm^{-1} bands has to grow too, which is the case. It has been noticed that with an insignificant depolymerization of polyisobutylenes with the molecular weight 2000, effected by heating at 150° for about 200 hours (without the access of air), the intensity of the band at 1225 cm^{-1} decreases, while at the same time no other change was observed in other regions of the spectrum. The absorption spectra of the polyisobutylenes given in table 1 were investigated in detail according to this band.

Table 2

Sample	Degree of polymerization	n_1	$\frac{n_0}{N_0} \cdot 10^2$	$\frac{m}{N_0} \cdot 10^2$
Dimer	2	1	0.64	0.64
Trimer	3	2	0.47	0.94
Tetramer	4	3	0.35	1.05
Pentamer	5	4	0.287	1.15
Polyisobutylene P-1	15	14	0.104	1.46
Polyisobutylene P-V	20	19	0.077	1.54

The absorption spectra in the region of 1250-1170 cm^{-1} for these substances were obtained in 1-3 % solution *. As a solvent CCl_4 was used which had three absorption bands in that region: at 1210, 1252, and 1280 cm^{-1}. The absorption of the solvent was excluded by consecutive measurements of the solution (intensity I) and of the solvent (intensity I_0) in one and the same cell. For the samples in table 1 the absorption coefficient of the maximum of the band were calculated and are also given by dots in figure 4 as a function of the molecular weight **.

The figure shows that there is a scatter in the values of the absorption coefficient. This is greater than a measurement error and is caused by the nonuniform polydisperse nature of the solutions used. In the same figure the triangles show absorption coefficients calculated from polyisobutylene spectra presented in the paper [10]. It can be seen from the figure that the curve of the function $k = f(M)$ does not go through the origin but cuts the abscissa at $M = 60$. Actually, at a molecular weight of 56 (monomer), the absorption coefficient has to be zero, since the number of the groups $\begin{matrix} & C & \\ & | & \\ C & - & C \end{matrix}$ in the monomer is zero. From the figure it is also apparent that the coefficient of absorption is a linear function of molecular weight in the range of 100-1000.

In the range of molecular weight M = 1000-2000 the curve bends; however, because of an insufficient number of samples for this region, the subsequent behavior of that curve is not clear.

RESULTS

1. A decrease of intensity has been observed in the absorption bands at 3075, 1640 and 888 cm^{-1} for the transition from the dimer towards polyisobutylene with a molecular weight $M = 2000$. The loss of intensity of these bands has been connected with the drop in the number of vinyl groups per unit volume with polymerization.

* The spectra of the dimer and the trimer were not taken in solution due to the very low bond intensity. Beforehand it had been established that the absorption coefficients of the tetramer and pentamer are nearly identical for the substances as well as for their solutions.

** For the low molecular weight polyisobutylenes (dimer-pentamer) the absorption band at 1225 cm^{-1} is shifted towards the higher frequencies (1232 cm^{-1}).

2. When the pentamer changes into polyisobutylenes with a higher degree of polymerization, the band at 924 cm^{-1} splits into two bands of equal intensity: 909 and 940 cm^{-1}.

3. With the increase of the degree of polymerization of polyisobutylenes an increase of intensity of the absorption bands at 2980, 940, 909, 848, and 1225 cm^{-1} takes place. The absorption bands at 940, 909, 848, and 1225 cm^{-1} are attributed to vibrations of the groups C-C-R in polyisobutylenes whose number per unit volume grows with the increase of the degree of polymerization.

4. The absorption coefficient of the band at 1225 cm^{-1} grows with the growth of the molecular weight of polyisobutylene; in the range of the molecular weight (100-1000) it grows linearly.

May 7, 1959

References

1. E. F. GROSS, K. V. NEL'SON, IA. M. SLOBODIN: DAN USSR, 75, 697 (1950)
2. K. V. NEL'SON: DAN USSR, 95, 57 (1954)
3. K. V. NEL'SON: Sb. Primenenie metodov spektroskopii v promyshlennosti prodovol'stvennykh tovarov i sel'skom khoziaistve (Use of spectroscopic methods in manufacturing and agriculture) Leningrad Univ. Press, 1957,
4. A. V. IOGANSEN: IAN USSR FS, 18, No. 6, 708 (1954) (See CIT BULLETIN, p. 707, 1954)
5. P. A. BAZHULIN, KH. E. STERIN: IAN USSR FS, 11, 457 (1947)
6. J.J.FOX, A. E. MARTIN: Proc. Roy. Soc. 175A, 208 (1940)
7. L. M. SVERDLOV: Materialy X coveshchaniia po spektroskopii (Materials of the X Conf on Spectroscopy), 1, 278, 1957. L'vov Univ. Press
8. P. F. GRUZDEV: ZFKh, 28, 507 (1954)
9. H. L. MC MURRY, V. THORNTON: Anal. Chem., 24, No. 2, 318 (1952)
10. LANDOLT-BORNSTEIN: Zahlenwerte und Funktionen aus Physik, Chemie, Astron., Geophy., 1(2), 377 (1951) Auflage 6

TOM VI, Vyp. 4 OPTIKA I SPEKTROSKOPIIA Aprel', 1959
VOL. VI, No. 4 OPTICS AND SPECTROSCOPY April, 1959

Influence of Water Vapors on the Absorption Spectra of Sublimated Layers of Dyes

L. A. LYZLNA AND A. T. VARTANIAN

Abstract: Investigated were changes of absorption spectra of sublimated layers of dyes with addition of water vapors. The presence of various absorbing centers in the layers was established.

In a previous article [1] it was shown that the absorption layers of sublimated layers of a series of dyes measured in vacuo differ not only from the spectra of layers obtained by precipitation from solutions, but also from the spectra of sublimated layers measured in air. The difference was caused mainly by changes in the structure of the layer under the influence of air humidity. A detailed study of the changes taking place in the spectra with introduction of water vapor on the evaporated layer was of interest.

The method for preparation of sublimated layers and the apparatus for measurement of their absorption spectra in vacuo were described in [1]. After the absorption spectra in vacuo have been measured, water vapors of predetermined pressure were introduced into the vessel. The measurements were performed - as a rule - 20-30 minutes after admission of vapor. Dyes of various classes were investigated.

RESULTS AND DISCUSSION

The absorption spectra of the majority of dyes which we investigated changed considerably upon the introduction of water vapor onto sublimated layers.

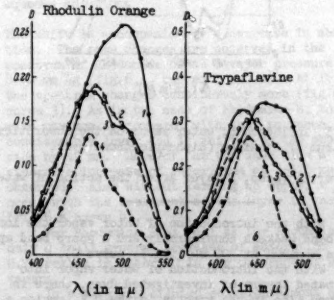

Fig. 1. Influence of water vapor on the absorption spectra of acridine dyes

a - Rhoduline Orange; b - Trypaflavine 1-layer in vacuo, 2-layer after acted upon by water vapor at 6 mm Hg pressure, 3-same at 12 mm Hg pressure, 4-concentrated aqueous solutions

Under the conditions of a vacuum, in the spectrum of a layer of Rhodulin Orange a longwave band with a maximum at 504 mμ (fig.1,a, curve 1) predominates; in the presence of water vapor at a pressure of 6 mm Hg the height of this maximum is almost halved (fig.1,a,curve 2). The curve 2 shows a maximum at 470 mμ. At the same time the absorption on the short wave length side of the spectrum grows. A further increase of water vapor (to 12 mm Hg) leads to a general broadening of the band and to a small decrease of absorption in the region 465-500 mμ (fig.1,a, curve 3). Under these conditions the absorption curve of the layer is very similar to the curve of the concentrated aqueous solution (fig.1,a, curve 4), and to that of the sublimated layer measured in air [2]. Similar changes are observed also when the layer is in humid air.

The absorption spectrum of trypaflavine in vacuo shows two maxima of about the same height (fig.1,b, curve 1). As in the previous case, with the addition of water vapor the absorption in the longwave part of the spectrum decreases, while in the shortwave part it increases (fig.1,b, curve 2 and 3). At 6 mm Hg pressure the position of the shortwave maximum approximately coincides with that of the concentrated aqueous solution of trypaflavine (fig.1,b, curve 4). The curve 2 in figure 1, b, again strongly recalls the curve of the sublimated layer measured in air.

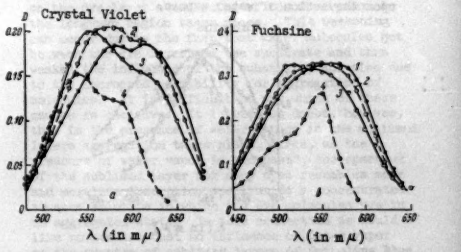

Fig. 2. Influence of water vapor on the absorption spectra of triphenylmethane dyes.

a - Crystal Violet. 1-layer in vacuo, 2-layer after acted upon by water vapor for ½ hour, 3-same for 2 hours, 4-concentr. aqueous solutions.
b - Fuchsine. 1-layer in vacuo, 2-layer after acted upon by water vapor at 6 mm Hg pressure, 3-same at 15 mm Hg, 4-concentr. aqueous solutions.

Figure 2 shows the spectral changes of a layer of Crystal Violet in contact with humid air. The absorption band of the layer in vacuo shows two clear maxima at 580 and 620 mμ (fig.2,a, curve 1). In the absorption curve obtained 2 hours after the introduction of humid air, a shortwave band with a maximum at 550 mμ clearly prevails (fig.2,a, curve 3). In general, the curves 3 and 4 coincide (fig.2,a), except that the curve 3 deviates into the longwave side.

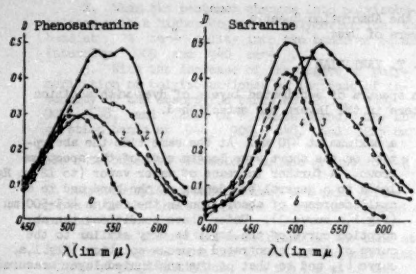

Fig. 3. Influence of water vapor on the absorption spectra of azine dyes.

a - Phenosafranine, b - Safranine
1-layer in vacuo, 2-layer after acted upon by water vapor at 10 mm Hg (a) and 6 mm Hg (b), 3-same at 16 mm Hg, 4-concentr. aqueous solutions

An analogous redistribution of absorption with introduction of water vapors into a sublimated layer is observed with Fuchsine (fig.2,b), Phenosafranine (fig.3,a) and Safranine (fig.3,b). In figure 4 are shown changes observed in the spectrum of Thionine upon the action of water vapors.

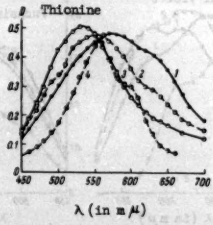

Fig. 4. Influence of water vapor on the absorption spectrum of Thionine (a thiazine dye)

1-layer in vacuo, 2-layer after acted upon by water vapor at 6 mm Hg, 3-same at 14 mm Hg, 4-concentr. aqueous solutions.

In vacuo the layer is characterized by a wide absorption curve consisting of at least three bands (fig.4, curve 1). With introduction of water vapors (fig.4, curve 2 and 3) again a decrease of absorption in the longwave region (600-650 mμ) takes place and an increase occurs on the shortwave side (500-550 mμ). However, now the shortwave maximum (530 mμ, fig.4, curve 3) is shifted considerably towards the shortwave side in comparison with the shortwave maximum of the concentrated aqueous solution. (557 mμ, fig.4, curve 4). Similar changes are observed in the spectrum of the Methylene Blue layer [2]. The shift of the shortwave maximum in this case reaches 30 mμ.

For the spectrum of the sublimated layer of Auramine in vacuo two clearly defined bands are characteristic with maxima at 430 and 370 mμ (fig.5)[1]. Under these conditions the spectrum of the layer is very close to the spectrum of the aqueous and alcoholic solutions. The spectrum of the sublimated layer is very sensitive to water vapor and the temperature of the substrate. In air it changes noticeably within the first minutes; after the layer remains longer in air, the maximum of the longwave band appears at about 450 mμ, and the maximum of the shortwave at 390 mμ. Sometimes also in vacuo the maximum of the shortwave band appears not at 370 mμ, but at somewhat longer wave lengths. This can be caused either by traces of humidity or by the influence of the temperature of the substrate*, since if the temperature of the substrate at sublimation is kept at room or a lower temperature, the maximum of the shortwave band is always at 370 mμ. In the curve 1 (fig.5) this maximum appears at 385 mμ which is evidence of a partial change of the layer in vacuo. This has been achieved by slight heating of the layer.

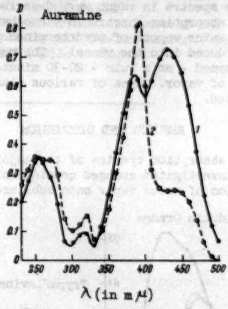

Fig. 5 Influence of water vapor on the absorption spectrum of Auramine (diphenylmethane dye).

1-layer in vacuo, 2-layer after the action of water vapor

With the introduction of water vapor the longwave band weakens considerably and a sharp band appears with a maximum at 392 mμ (fig.5, curve 2).

With the introduction of water vapor into sublimated layers of investigated dyes, there is observed also in the spectra in the U.V. region a redistribution of absorption, analogous to that taking place in the visible region.**

In all the investigated dyes, with the exception of triphenylmethane dyes, with the action of humidity on the layer a decrease in area takes place together with the change in the shape of the curve. In Auramine the absorption band area decreases 20-30%, in the rest of the dyes 6-10%.

The changes taking place in the absorption spectra of layers of Rhodamine B and Rhodamine 6G under the action of humidity have a somewhat different character. In the layer of Rhodamine B as the

*During the sublimation of the dye, the temperature of the substrate usually increases a little.
**This question will not be studied in the present paper.

water vapor is introduced a shift of the longwave absorption band occurs basically towards the shortwave side (fig.6,b, curves 2 and 3).

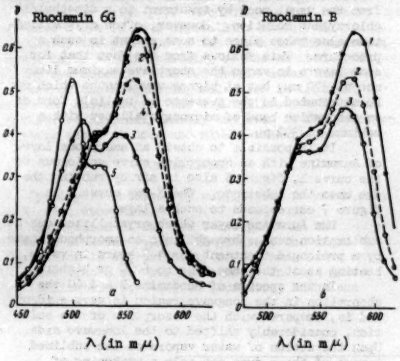

Fig. 6 Influence of water vapor on the absorption spectra of xanthene dyes

a - Rhodamin 6G, b - Rhodamin B
1-layer in vacuo, 2-layer after acted upon by water vapor at 9 mm Hg (a) and 10 mm Hg (b), 3-same at 16 mm Hg, 4-after treatment in vacuo, 5-concentr. aqueous solutions

The shift is accompanied by a decrease in absorption. The same changes are observed in the spectrum of Rhodamine 6G at a vapor pressure of 8-10 mm Hg (fig.6,a, curves 1 and 2). At 16 mm Hg the spectrum changes considerably more (fig.6,a, curve 3). As in the case of Rhodamine B, the longwave maximum as compared with that in vacuo, is considerably lower and is shifted to the shortwave side by 19 mμ. However, at the same time a considerable increase of absorption at λ=510 mμ is observed. Also without warming up opposite changes occur with the treatment of the layer in vacuo (fig.6,a curve 4).

For Rhodamine B as well as for Rhodamine 6G only a small general decrease of absorption in the U.V. region is observed in the presence of water vapors.

In a strongly diluted solution almost all molecules of a dye are under identical conditions (monomers). In high concentrations of a dye an interaction between neighboring molecules can take place. In aqueous solution, as well known, such interaction often leads to the formation of dimers and more complex aggregates which is followed by well known changes in the absorption spectrum. In solid layers the dye molecules are under the influence of the closely arranged identical molecules. The influence of identical molecules on each other ought to be accompanied by broadening and shifting of the absorption band towards the longwave side, similar to that which takes place with some compounds of the aromatic series e.g. with anthracene. In dye layers deposited on a substrate, single molecules are not only under the influence of the perturbing action of identical molecules, but also under that of the substrate, whereby for such thin layers with which we dealt (~0.1 μ) the portion of the molecules under the influence of the substrate sometimes could be sufficient for their spectral evidence.

If it is assumed that the absorption of molecules under the influence of the substrate is also displaced towards the longwave side as compared with absorption of molecules free from the influence of the substrate, then it follows that the shift will depend on the distance of the molecules from the substrate. Then the observed absorption curve will be the envelope of the absorption of molecules perturbed to different extents.

A comparison of absorption spectra of dye solutions and layers obtained in vacuo and by deposition from solutions [1], and also the investigation of changes observed in the spectra of sublimated layers with introduction of water vapor, leads to a conclusion about the presence of absorption centers of different origin in dye layers. The absorption caused by such centers depends on the condition of the layer. With the sublimation of the dye in vacuo the obtained layer is as a rule amorphous.

The spectrum of a dye sublimed in vacuo is basically caused by an absorption of separate randomly distributed molecules, both free of the influence of the substrate, or influenced by the substrate. With the introduction of water vapors on the dye layer a weakening of the absorption in the longwave region takes place. This weakening can occur due to the fact that water molecules get between the dye layer and the substrate and thus weaken the influence of the substrate, and also due to the increased possibility for aggregation of molecules. It is difficult to say which of these causes is decisive. It is without doubt, however, that in the presence of water vapors in the sublimed layers aggregation takes place, since, as the pressure of water vapor is increased, the spectrum of the sublimed layer for many dyes resembles more and more the absorption spectrum of a concentrated aqueous solution in which the dye molecules are in an aggregated state. In this connection we would like to mention that no influence of water vapor on the spectra of sublimed layers of Quinoline Blue, Indigo and Riboflavine was observed. This is obviously explained by the fact that the first two dyes are insoluble in water, and the last one does not aggregate. The formation of molecular aggregates upon the introduction of water vapor on sublimated layers is observed in acridine-, triphenylmethane- and azine dyes. Actually, when the curves 3 in figures 1,a, 1,b, 2,a and 3,b are compared with curves 4 in the same figures, obtained for concentrated aqueous solutions, then it can easily be seen that they very much resemble each other. Consequently, in layers of these dyes the aggregation in the presence of water vapor can reach almost the same degree which is present in aqueous solutions at high concentrations of these dyes. Fuchsine does not belong to the dyes which are highly aggregated in solution (fig.2,b, curve 4). The shortwave maximum of the layer subjected to the action of water vapor at 15 mm Hg pressure (fig. 2, curve 3), unlike the solution, is higher than the longwave maximum. Apparently, in the presence of water

vapor there are more aggregated molecules in the layer than in solution, but the degree of aggregation is smaller. Therefore, the absorption curves of the layer subjected to the action of water vapor does not coincide with the concentrated aqueous solution.

At the same time, while in the layers of the examined classes of dyes the degree of aggregation in the presence of water vapor was approximately the same as in concentrated aqueous solutions, in thiazine and diphenylmethane dye layers it apparently was higher.

In the presence of water vapor the spectra of sublimed layers of Thionine, Methylene Blue and Auramine show new absorption bands with the maximum shifted several tens of millimicrons towards the short wavelength as compared with the maximum of the shortwave band of the concentrated aqueous solution. It can be assumed that the Thionine band with a maximum at 530 mμ and the Methylene Blue at 570 mμ are caused to a considerable degree by the crystalline state of the dye [3,4]. However, x-ray measurements have not disclosed the presence of a crystalline state in the Thionine layer. It is possible that the size of the particles formed was very small.

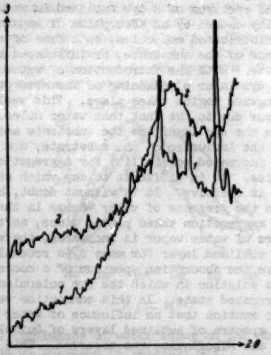

Fig. 7. X-ray diagrams of Auramine layers.

1-The layer after the action of water vapor, 2-layer obtained by rubbing

On introduction of water vapor on sublimated layers of Auramine there appears a sharp band with a maximum at 392 mμ. The appearance of this band has been attributed to crystallization of the form I of the dye, characterized by a band with a maximum at 430*. This is confirmed by x-ray measurements (fig.7, curve 1).** In order to prevent crystallization of Auramine in vacuo, it is necessary to perform the sublimation rapidly and the layer should be as thick as possible. It is expedient to use a hydrophobic substrate obtained from the usual ones by treatment in a dimethyldichlorxylene solution. However, often crystallization also takes place to some extent in such a procedure. This follows from the fact that for some layers in vacuo the shortwave maximum lies not at 370 mμ, but at higher wavelengths which can be attributed to the presence in implicit form of an absorption band of microcrystallites with a maximum at 392 mμ.

It is possible to obtain an amorphous layer of Auramine with an absorption curve analogous to the curve 1, figure 5 also in air by rubbing the dye onto the substrate. The X-ray curve 2 in figure 7 corresponds to such a layer.

The Auramine layer which crystallizes out at sublimation can be brought into an amorphous state by a prolonged treatment for 4-5 hours in vacuo, heating it at the same time to 60°C or higher.

In the spectra of Rhodamine B and 6G the absorption in the longwave region is very evident and is, compared with the absorption of the solution, considerably shifted to the longwave side. Upon the action of water vapors on the sublimed layers of these dyes not only a weakening of absorption in that region takes place, but also a shift of the maximum into the shortwave side, while no considerable increase of absorption in the shortwave region takes place (fig.6). The change observed in the longwave region with introduction of water vapors is connected with the weakening of the influence of the substrate, since the decrease of the absorption in the longwave region is not accompanied by any considerable increase of absorption in the shortwave region. For Rhodamine 6G only at a water vapor pressure of the order of 16 mm Hg is a comparatively small increase of absorption in the shortwave band with a maximum at 510 mμ observed (fig.6,a,curve 3), connected with aggregation. This maximum compared to the shortwave maximum of the concentrated aqueous solution, is displaced 10 mμ to the longwave side (fig.6, curve 5) which is probably evidence of a higher degree of aggregation for Rhodamine 6G in solution than in the layer with the introduction of water vapor. It is characteristic that with the removal of humidity from the Rhodamine layer, the band with the maximum at 510 mμ disappears and the curve becomes similar to the curve in vacuo (fig.6,a, curve 4).

When humidity is removed from sublimed layers of other dyes subjected to the action of water vapors, some disaggregation is also observed, however the curve obtained for sublimed layers which are not subjected to the action of water vapors is not fully reproduced.

For a series of dyes (Quinoline Blue, Erythrosine etc.) when some conditions are observed, a layer can be obtained showing diffuse reflection [5]. The transition from solutions of these dyes to the deposition of diffuse reflecting layers is also accompanied by a shift of absorption towards the longwave side. However these bands are attributed to the absorption of colloidal particles of dyes. It is quite possible that a similar effect takes place also with a series of other dyes. Thus, e.g. the absorption shift into the longwave side observed with the transition from Indigo solutions

*Later on, speaking about Auramine, we will deal only with the form I [1]. In the crystallization of the form II, characterised by an absorption band at 370 mμ, there appears a band with a maximum at 320 mμ. The form II crystallizes more slowly than form I and in another system.

**The X-rays were obtained by A. G. Alekseev. We take the opportunity to express our gratitude.

to layers, has been explained by Weinstein and Wyman [6] in an analogous manner.

Our explanation of the nature of absorption bands of solid layers of dyes does not agree with that given by Weigl [7]. According to the latter, in vacuo a dye is in a crystalline state. He attributes the presence of two bands in the spectrum of the layer to the splitting of the excited level of the dye molecule into two levels under the influence of the neighboring molecules in the cell. As it was shown above, the crystallization in vacuo is observed extremely rarely and even in the presence of water vapor it does not always take place.

CONCLUSIONS

1. Dye layers obtained by sublimation in vacuo are, as a rule, amorphous.
2. Aggregation of the dye takes place in the presence of water vapor. In general, the degree of aggregation is approximately of the same order as in concentrated aqueous solutions. In some dyes crystallization is observed (Auramine, Methylene Blue, Thionine).
3. In solid dye layers, according to the state in which they are,(vacuum, water vapor) different absorption centers can exist - "free" molecules, molecules under the influence of the substrate, aggregated molecules and microcrystallites. The shape of the absorption curve of a solid dye layer is determined by the relation between these absorption centers.

April 23, 1958

References

1. L. A. LYZINA, A. T. VARTANIAN: OiS, 6, 172 (1959) (See this journal, p. 110)
2. A. T. VARTANIAN: ZFKh., 30, 1028 (1956)
3. L. A. LYZINA: OiS, 4, 501 (1958)
4. M. M. MELANKHOLIN: OiS, 3, 104 (1957)
5. L. A. LYZINA: OiS, 5, 428 (1958)
6. J. WEINSTEIN, G. WYMAN: J. Am. Chem. Soc., 78, 2387 (1956)
7. J. WEIGL: J. Chem. Phys., 24, 364 (1956)

TOM VI, Vyp. 4 OPTIKA I SPEKTROSKOPIIA Aprel', 1959
VOL. VI, No. 4 OPTICS AND SPECTROSCOPY April , 1959

Peculiarities of the Luminescence of Ortho-Disubstituted Aromatic Hydrocarbons:

II. The Fluorescence of the Methyl Esters of 2-hydroxy and 2-methoxy-naphthoic Acids.

U. V. NABOIKIN, B. A. ZADOROZHNYI AND E. N. PAVLOVA

Abstract: The appearance of three bands in the fluorescence spectrum of the methyl ester of 2-hydroxy-3-naphthoic acid is postulated to result from intramolecular hydrogen bonding. The spectrum of the methyl ester of 2-methoxy-3-naphthoic acid, on the other hand, shows only a single band which is weakly pertrubed by solvent effects.

The structural formula of the methyl ester of 2-hydroxy-3-naphthoic acid (I), shown below, suggests the presence of an intramolecular hydrogen bond in this compound. Thus, we might expect the physical properties (including the fluorescence spectrum) to be influenced by this type of interaction. In the corresponding methoxy-compound (II) such a bond obviously is impossible.

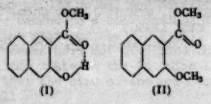

Bergman et al. [1] decided on the basis of the electronic absorption spectrum of the methyl ester of 2-hydroxy-3-naphthoic acid and related compounds that an internal hydrogen bond does occur in these substances. This conclusion was suggested by the fact that there is a shift of the 3600 Å absorption band to longer wavelengths on going from the methyl ester of methoxy-naphthoic acid (II) to the corresponding hydroxy-compound (I). The ultraviolet results, however, were not entirely satisfactory, and furthermore this data did not provide a measure of the strength of the intramolecular forces.

The fluorescence spectra of methyl salicylate and o-methoxy-benzoic acid were recorded by Weller [2, 3], who reported some of the features of these spectra. It seemed worthwhile, therefore, to compare the fluorescence spectrum of methyl salicylate with that of the corresponding derivatives of 2-hydroxy-3-naphthoic acid, and to estimate the intramolecular forces present in these molecules in addition to establishing the effect of these interactions on the spectra.

The experimental method and apparatus employed in this work have been described in a previous communication [4]. The fluorescence spectra in the red region were recorded using a FEU-22 photomultiplier. The substances investigated were synthesized from 2-hydroxy-3-naphthoic acid by the usual methods. The absorption spectrum of the methyl ester of 2-hydroxy-3-naphthoic acid observed in ethanol, heptane, and in an alcoholic solution of sodium hydroxide is shown in Figure 1. The spectrum of the methyl ester as given by Bergman [1] is in good agreement with our data.

Figure 2 shows the fluorescence spectrum of the methyl ester of 2-hydroxy-3-naphthoic acid. As this diagram indicates, there are some differences in the bands appearing in the different solvent systems. At low concentration in the inert solvents, benzene and heptane, the fluorescence spectrum has a maximum at 4200 Å. This

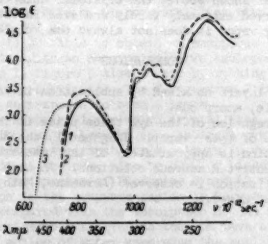

Figure 1. Absorption spectrum of the methyl ester of 2-hydroxy-3-naphthoic acid.
1. In ethanol 2. In heptane 3. In ethanol containing NaOH at pH 11.3.

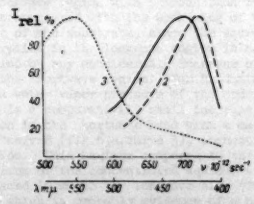

Figure 2. The fluorescence spectrum of the methyl ester of 2-hydroxy-3-naphthoic acid.
1. In ethanol 2. In benzene 3. In ethanol plus NaOH at pH 11.3.

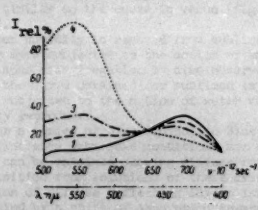

Figure 3. The fluorescence spectrum of solutions of 2-hydroxy-3-naphthoic acid methyl ester in alcoholic NaOH at various pH's.
1. pH 8.2 2. pH 10.7 3. pH 11.0 4. pH 11.3

maximum appears to be shifted slightly to longer wavelengths in ethanol. In alcoholic sodium hydroxide, this band was found to diminish in intensity with increasing pH, and at the same time to be replaced by a more intense band with a maximum around 5500 Å. The fluorescence curves as a function of pH are shown in Figure 3. It may be observed that at pH 11.3 the band in the blue region has almost vanished. The change in the fluorescence spectrum is accompanied by a corresponding change in the absorption spectrum as may be seen from Figure 1.

In benzene and heptane solution the methyl ester exhibited a strong concentration dependence of the fluorescence quantum yield as observed by the band with maximum at 4200 Å. This effect is shown in Figure 4. Concentration quenching of the blue fluorescence is accompanied, however, by the appearance of weak emission in the 6500 Å region, which is detectable even at a concentration of 1 g/l . This band also is found in the fluorescence spectrum of the crystalline ester, as shown in Figure 5.

In carbon tetrachloride solution similar changes in the fluorescence spectra were observed.

The fluorescence spectrum of the methyl ester of 2-methoxy-3-naphthoic acid was found to be almost independent of the nature of the solvent. On increasing the concentration, a very small shift of the fluorescence band to longer wavelengths was observed. The fluorescence spectrum of this substance in solution is given in Figure 6.

In order to estimate the strength of the intramolecular hydrogen bond, the infrared spectrum of the methyl ester of 2-hydroxy-3-naphthoic acid was observed in the -OH stretching region. As may be seen from Figure 7, the hydroxyl band, which occurs at 3280 cm^{-1} , has been shifted to longer wavelengths when compared with the stretching frequency of a free hydroxyl group. If we employ the data of Shigorin [5] for the frequency of the free -OH group and estimate the energy of the intramolecular hydrogen bond, the result is 5.0 kcal./mol. The position and intensity of this band are not dependent on the concentration throughout the range 0.01 to 1 g/l., i.e., even when the red fluorescence appears.

The above results enable us to reach the general conclusion: that the peculiarities found in the spectrum of the methyl ester of 2-hydroxy-3-naphthoic acid are associated with the presence of the hydroxyl group. Because, in the case of the corresponding methoxy-compound, none of these differences were observed.

The changes in the fluorescence spectrum of the methyl ester of 2-hydroxy-3-naphthoic acid in alcoholic sodium hydroxide can be easily explained inasmuch as they are accompanied by the appearance of a long wavelength band in the absorption spectrum. Thus, we are observing a typical bathochromic shift in both absorption and fluorescence which results from the formation of organic anions in solution.

If we compare our results for the naphthalene derivatives with those of Weller [2, 3], for methyl salicylate and the corresponding methoxy compound, the changes observed are completely

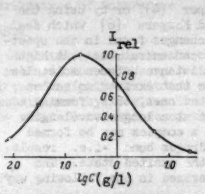

Figure 4. Dependence of the relative fluorescence yield of fluorescence of the methyl ester of 2-hydroxy-3-naphthoic acid in concentration. Solution in benzene.

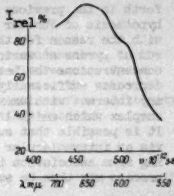

Figure 5. Fluorescence spectrum of crystalline methyl 2-hydroxy-3-naphthoate.

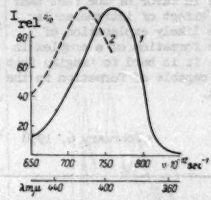

Figure 6. Fluorescence spectrum of methyl 2-methoxy-3-naphthoate. 1. In benzene 2. In ethanol.

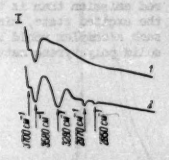

Figure 7. Infrared absorption spectra. 1. Pure CCl_4 2. Solution of methyl 2-hydroxy-3-naphthoate in CCl_4.

analogous. It should be noted that the red emission of the methyl ester of 2-hydroxy-3-naphthoic acid appears only at high concentrations, where there is a noticeable quenching of the short wavelength fluorescence band. The careful purification of the compound rules out the possibility that the long wavelength emission comes from impurities. On the contrary, the more careful the purification the more noticeable is this fluorescence.

The appearance of the 6500 Å band might be ascribed to the formation of dimers. Because of this possibility the absorption spectrum was measured at different concentrations in benzene. No changes in the long wavelength region of the spectrum were observed, and the absorption band was coincident with that observed in heptane solution. A cryoscopic determination of molecular weight in benzene using different concentrations of the ester also showed no detectable change such as would be expected on association. Furthermore, as mentioned above, varying the concentration of the substance in carbon tetrachloride has little effect on the infrared spectrum between 2.5 and 4.5 μ .

Thus, the red emission does not result from the formation of a dimer. Obviously the fluorescence yield in the red region must be very low because it is detectable only at high concentrations, when the blue luminescence is already quenched. In this case, it is possible to explain the long wavelength band on the basis of the considerations set

forth in the previous paper [4], or by using the hypothesis of Förster and Kaspers [6] which deal with the reason for the changes found in the spectrum of pyrene at various concentrations. At high concentrations the mean distance between molecules decreases sufficiently so that excited molecules may interact with unexcited ones, thus, forming a complex which emits light at a longer wavelength. It is possible that such a complex may be formed via an intermolecular hydrogen bond -i.e. resulting from association in the excited state. The process may then be summarized in the following way:

$$A^* + A \rightarrow AA^* \rightarrow 2A + h\nu_f.$$

Investigations of the fluorescence spectrum of the methyl ester of 2-hydroxy-3-naphthoic acid in polystyrene, at various concentrations have shown that the red fluorescence appears at lower concentrations than is the case for liquid solutions. This is evidence in favor of the fact that in the present case the effect of intramolecular hydrogen bonds is a more likely explanation of red emission than is the formation of a complex in the excited state, since it is hard to imagine that such a complex would be capable of formation in the solid polystyrene matrix.

February 6, 1958

References

1. E. D. BERGMANN, Y. HIRSHBERG, S. PINCHAS: J. Chem. Soc., No. 9, 2351 (1950)
2. A. WELLER: Naturwiss., 42, 175 (1955)
3. A. WELLER: Zs. Elektrochemie, 60, No. 9, 1144 (1956)
4. IU. V. NABOIKIN, E. N. PAVLOVA, B. A. ZADOROZHNYI: OiS, 6, 366 (1959) (see this journal p.)
5. D. N. SHIGORIN, M. M. SHEMIAKIN, et al.: DAN USSR, 108, 672 (1956)
6. TH. FÖRSTER, K. KASPER: Zs. Elektrochemie, 59, 976 (1955)

TOM VI, Vyp. 4 OPTIKA I SPEKTROSKOPIIA Aprel', 1959
VOL. VI, No. 4 OPTICS AND SPECTROSCOPY April, 1959

On the Influence of Substituting Groups on the Position of the Absorption and Fluorescence Spectra of Derivatives of Anthracene

A.S.CHERKASOV

Abstract: The influence of various substituents and their positions in the anthracene nucleus on the displacement of the absorption and fluorescence spectra relative to the absorption and fluorescence spectra of anthracene was investigated. It was established that for many polysubstituted anthracenes the value of the shift is equal to the sum of shifts caused by each substituent by itself. The deviations from additivity observed for some anthracene derivatives are explained by steric interactions of the substituents.

Upon studying the absorption and fluorescence spectra of meso derivatives of anthracene, it was established that the introduction of various substituents in the meso position of the anthracene nucleus leads to a shift of the spectra towards lower frequencies, and the value of the displacement in the case of disubstituted derivatives was shown to be equal to the sum of the shifts caused by each substitutent by itself [1-3].

It was of interest to determine whether independence in the influence of the substituents on the displacement of the absorption and fluorescence spectra would be observed for more than two substituents, and, also, in the case where they were located on the side rings of the anthracene nucleus. For this purpose we carried out an investigation of a series of α and β methyl-meso-aryl derivatives of anthracene.

The compounds used in the investigation were synthesized in the following way. 1-Methylanthracene (m.p. 85-85.5°) was obtained by distillation of 1-chloro-4-methyl-anthraquinone with zinc dust [4]; 2-methylanthracene (m.p. 202-204°), 2,3-dimethylanthracene (m.p.248-249°), 1,3-dimethylanthracene (m.p.80-80.5°) and 1,4-dimethylanthracene (m.p. 72-73°) were obtained by zinc dust and ammonia [6] reduction of the corresponding methylanthraquinones; 2-methyl-9, 10-diphenyl-anthracene (m.p. 216-218°), 2,3-dimethyl-9,10-diphenyl-anthracene (m.p.246-248°), 1,3-dimethyl-9,10-diphenyl-anthracene (m.p. 165-167°), 1,4-dimethyl-9,10-diphenyl-anthracene (m.p. 182.5-184.5°), 2-methyl-9,10-di-(o-tolyl)-anthracene (m.p. 202.5-204°) 2,3-dimethyl-9,10-di-(o-tolyl) anthracene (m.p. 199.5-201°), 1,3-dimethyl-9,10-di-(o-tolyl) anthracene (m.p. 182-189°) were obtained by reduction with stannous chloride and HCl of the corresponding methyl-meso-aryl-9,10-dihydroxy-dihydro-anthracenes, obtained in turn from the organo-magnesium compounds.

The preparations used for the spectral investigations were carefully purified beforehand by repeated recrystallizations and chromatography on alumina.

The absorption spectra were taken on an SF-4 spectrophotometer; the fluorescence spectra were taken with the help of a UM-2 monochromator with an FEU-17 photomultiplier as the energy receiver. The spectral sensitivity of the latter arrangement was determined with the aid of a light source of known energy distribution.

Absorption and fluorescence spectra were investigated at room temperature (~20°C.). Ethanol was used as the solvent.

Comparison of the absorption spectra of 1-2-, and 9-methylanthracenes shows (see figure) that position of the substituents in the anthracene nucleus has appreciable influence on the displacement of the spectrum relative to the anthracene spectrum, the value of the shift being different for the short and long wavelength bands.

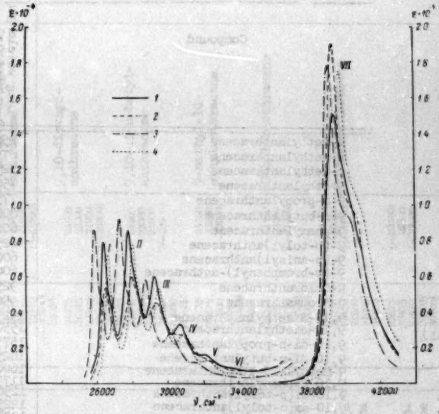

Absorption spectra of solutions of methyl derivatives of anthracene in ethanol.

1) 1-methylanthracene, 2) 2-methylanthracene, 3) 9-methylanthracene, 4) anthracene; I, II, ... VII - ordinal numbers of the maxima.

Thus, the presence of a methyl group in the meso position causes a significant displacement of both bands, but the long wavelength band is shifted somewhat more (150 cm^{-1}) than the short wavelength band; in the case of 1-methylanthracene the shift of the long and short wavelength bands are equal (250 cm^{-1}), but introduction of a methyl group into the β-position leads to a shift mainly of the short wavelength band (325 cm^{-1}) and has almost no influence on the long wavelength position (table 1).

The primary influence of meso substituents on the long wavelength absorption band, and of β-substituents on the short wavelength absorption band was noted earlier by Jones [7] for the case where the substituent groups were capable of conjugating with the anthracene nucleus (nitro, cyano, aldehyde and acetyl groups), and was explained by the fact that the short wave length band was connected with the electric moment directed along the axis of the anthracene nucleus (x-band), while the long wavelength band has to do with the electric moment directed along the shorter axis (y-band).*

*Calculations of polyacene molecules by the molecular orbital method lead to analogous results.

Table 1

Shifts of the absorption and fluorescence maxima of anthracene derivatives relative to the corresponding maxima of anthracene*.

Compound	Shift** relative to anthracene (cm^{-1})			Departure from additivity (cm^{-1})		
	Absorption			Absorption		
	Long wavelength band	Short wavelength band	Fluorescence	Long wavelength band	Short wavelength band	Fluorescence
1-methylanthracene	250	250	325			
2-methylanthracene	75	325	375			
9-methylanthracene	725	575	725			
9-ethylanthracene	750	575	725			
9-n-propylanthracene	775	575	750			
9-n-butylanthracene	800	650	775			
9-phenylanthracene	600	475	825			
9-(p-tolyl)anthracene	625	525	1025			
9-(p-anisyl)anthracene	600	575	1425			
9-(p-bromphenyl)-anthracene	600	475	1025			
9-Chloranthracene	925	500	925			
9-Bromanthracene	950	575	975			
9,10-dimethylanthracene	1525	1225	1550	+75	+75	+100
9,10-diethylanthracene	1550	1275	1575	+50	+125	+125
9,10-di-n-propylanthracene	1575	1325	1625	+25	+175	+125
9,10-di-n-butylanthracene	1625	1350	1675	+25	+50	+125
9-methyl-10-ethylanthracene	1600	1275	1575	+125	+125	+125
9,10-diphenylanthracene	1175	975	1650	-25	+25	0
9,10-di(p-tolyl)anthracene	1250	1125	1875	0	+75	-175
9,10-di(o-tolyl)anthracene	1225	1175	1325			
9,10-di(p-anisyl)anthracene	1300	1225	2025	+100	+75	-825
9,10-di(p-bromphenyl)anthracene	1200	925	1725	0	-25	-325
9,10-dichloranthracene	1700	1025	1725	-150	+25	-125
9,10-dibromanthracene	1775	1200	1825	-125	+50	-125
9-methyl-10-bromanthracene	1675	1275	1725	0	+125	+25
9-ethyl-10-bromanthracene	1675	1200	1725	-25	+50	+25
9-n-propyl-10-bromanthracene	1700	1250	1725	-25	+100	0
9-phenyl-10-bromanthracene	1575	1125	1775	+25	+75	-25
1,4-dimethylanthracene	500	475	650	0	-25	0
1,3-dimethylanthracene	300	575	975	-25	0	-25
2,3-dimethylanthracene	150	675	375	0	+25	-375
1,9-dimethylanthracene***	1320	960		+345	+135	
2,9,10-trimethylanthracene***	1600	1480		+75	-95	
2,3,9,10-tetramethylanthracene***	2090	2120		+490	+320	
2-methyl 9,10-diphenylanthracene	1300	1425	1825	+25	+150	-200
2-methyl-9,10-di(o-tolyl)anthracene	1250	1525	1625	-25	0	-75
2,3-dimethyl-9,10-diphenylanthracene	1300	1575	1825	-50	-25	-575
2,3-dimethyl-9,10-di(o-tolyl)anthracene	1300	1875	1650	-50	+25	-425
1,3-dimethyl-9,10-diphenylanthracene	1575	1775	2125	+50	+250	-225
1,3-dimethyl-9,10-di(o-tolyl)anthracene	1575	1975	2025	+50	+200	0
1,4-dimethyl-9,10-diphenylanthracene	1900	2275	3425	+200	+825	+1225
1,4-dimethyl-9,10-di(o-tolyl)anthracene	1925	2375	2725	+225	+675	+750

*Departures from additivity in 9,10-diacetoxyanthracene, 9,10-dimethoxyanthracene, 9-chlor-and 9-brom-10-methoxyanthracene, 9-methyl-10-methoxyanthracene, 9-chlor- and 9-brom-10-anthracenecarboxylic acids are (see ref.[3]): for the long wavelength absorption band -150 to +25, for the short wavelength absorption band 0 to +175, and for fluorescence -25 to +225.

**Shown in the table are the values of the displacements of the weak maximum (maximum II, fig. 1) of the long wavelength absorption band, of the maximum of the short wavelength absorption band, and of the weak maximum in the fluorescence spectrum relative to the corresponding maxima in the absorption and fluorescence spectra of anthracene.

***According to ref.[7].

Table 2

Positions of absorption and fluorescence maxima of anthracene derivatives.

Compound	Position of maxima (cm^{-1})		Compound	Position of maxima (cm^{-1})		Compound	Position of maxima (cm^{-1})	
	Absorption	Fluorescence		Absorption	Fluorescence		Absorption	Fluorescence
Anthracene	26650 28050 29500 30875 32250 (~33750) 30725	26400 25125 23800 22200 (~20800)	9,10-di(o-tolyl) anthracene	25425 26825 28250 29650 (~31100) 38350	25000 23700 22400 21100	1,4-dimethyl-9,10-diphenylanthracene	24800 26150 27500 (~29000) 37450	(~22800) 21600
1-methylanthracene	26400 27800 29250 30700 32100 30475	26100 24700 24300 22800 (~20500)	9,10-di(p-tolyl) anthracene	25400 26800 28175 29575 (~31050) 38600	24250 23150 (~22000)	2-methyl-9,10-di (o-tolyl)anthracene	25400 26800 28200 29550 (~31000) 38200	24750 23400 22050 (~20600)
2-methylanthracene	26500 27975 29400 (~30750) (~32200) 29400	26050 24650 23250 (~21850) (~20500)	9,10-dichlor-anthracene	24850 26350 27800 29200 (~30600) (~32000) 38700	24750 23300 21900 20800	2,3-dimethyl-9,10-di (o-tolyl)anthracene	25350 26750 28125 29500 (~30900) 37850	24700 23375 (~22100) (~20600)
1,3-dimethylanthracene	26300 27750 29100 (~30600) (~32000) 29150	25675 24350 23000 (~21500)	9,10-dibrom anthracene	24800 26275 27700 29125 (~30500) (~32000) 38525	24400 23200 21450 (~20700)	9,10-di(p-anisyl) anthracene	25400 26750 28150 (~29500) (~31200) 38500	(~23750) 23000
1,4-dimethylanthracene	26100 27550 29050 30550 (~31750) 30250	25675 24375 23000 (~21700)	9-methyl-10-bromanthracene	25000 26375 27775 29175 (~30600) 38550	24400 23300 21950 (~20900)	9,10-di(p-bromphenyl) anthracene	25450 26850 28250 29600 (~31000) 38800	24400 23300 (~22100) (~20950)
2,3-dimethylanthracene	26450 27900 29300 30700 32150 38650	26075 24650 23300 (~22000) (~20500)	9-ethyl-10-bromanthracene	24975 26375 27800 29200 (~30600) 38525	24600 23300 21950 (~20900)	9,10-diethyl-anthracene	25100 26500 27925 29375 (~30800) 38450	24800 23450 22050 (~20700)
1,3-dimethyl-9,10-di (o-tolyl)anthracene	25100 26475 27800 (~29150) (~30700) 37750	24300 23000 (~21700)	9-phenyl-10-bromanthracene	25000 26350 27750 29150 (~30600) 38475	24500 23300 21900 (~20600)	9,10-di-n-butyl-anthracene	25025 26425 27850 29250 (~30700) 38375	24750 23350 21950 (~20600)
1,4-dimethyl-9,10-di (o-tolyl)anthracene	24775 26125 27500 (~28800) (~30300) 27350	(23200) 22300 (21000)	9-n-propyl-10-bromanthracene	25075 26475 27900 29350 (~30700) 38600	24450 23250 (~22000)	9-methyl-10-ethylanthracene	25050 26450 27900 29300 (~30800) 38450	24850 23450 23100 (~20750)
9-(p-tolyl)anthracene	29650 27425 28825 30250 (~31650) 30200	25150 24000 (~22400) (~21300)	2-methyl-9,10-diphenylanthracene	25350 26750 28150 (~29500) (~31000) 38475	24400 23200 (~21900)	9-chloranthracene	25700 27125 28575 29950 31325 39225	25500 24100 (~22700) (~21350)
9-(p-anisyl)anthracene	28050 27450 28850 30240 31600 39150	24800 23600 (~22300)	2,3-dimethyl-9,10-diphenylanthracene	25375 26750 28150 29500 (~31000) 38150	24450 23300 (~22000)	9-bromanthracene	25675 27100 28500 29875 31300 (~32700) 39150	25450 24050 22850 20800
9-(p-bromphenyl) anthracene	28050 27450 28850 30250 (~31650) 39250	25250 24000 (~22700) (~21300)	1,3-dimethyl-9,10-diphenylanthracene	25075 26475 27850 (~29200) (~30700) 37950	(~23400) 22900 (~22000)			

The resemblance which was found between the regularities of the influence of the methyl group and the conjugation of substituents can, evidently, be explained by the fact that in methyl substituted anthracenes there is the influence of hyperconjugation [7], i.e., interaction takes place between the σ-electrons of the methyl groups and π-electrons of the anthracene nucleus, which leads to an apparent increase in the length of the chain of conjugation, and, consequently, to a shift of the absorption spectrum to a region of lower frequencies.

The values of the displacements of absorption and fluorescence spectra both for meso substituted anthracenes** and also for derivatives of anthracene having methyl substituents on the side ring of the anthracene nucleus are given in table 1.*** In table 1 are also listed the values of the differences between the experimentally determined shifts and the calculated shifts, based on the assumption that the shifts of the spectra of polysubstituted derivatives of anthracene relative to the corresponding spectra of anthracene arise from shifts caused by each substituent by itself (deviations from additivity).****

From the data of table 1 it is evident that deviations from additivity in the shifts of the absorption spectra for nearly all the compounds are very small, and, for the most part, do not exceed the precision of the determination.

Anomalously higher deviations are found only for 1,4-dimethyl-9,10-diphenylanthracene (+250 cm^{-1}) and in 1,3-dimethyl-0,10-di(o-toly)-anthracene (+200 cm^{-1}), in which one of the methyl groups is found in the α-position also.

For meso substituted anthracenes, additivity in the displacements of the fluorescence spectra is observed to be satisfactory. However, for groups of compounds having methyl substituents in the side ring of the anthracene nucleus significant deviations are found. As in the absorption spectra, the greatest deviations are in meso substituted anthracenes having methyl substituents in the α-positions of the anthracene nucleus, and moreover, in compounds with the methyl groups in the 2 and 3 positions. In the latter the failure of the experimental and calculated values to coincide is caused by the fact that introduction of a second methyl group into 2-methylanthracene, or into 2-methyl-mesoarylanthracene has almost no influence on the position of the fluorescence spectrum, and, for example the fluorescence spectra of each pair of the following coincide: 2-methyl and 2,3-dimethyl-, 2-methyl-9,10-diphenyl and 2,3-dimethyl-9,10-diphenyl-, 2 methyl-9,10-di(o-tolyl)-and 2,3-dimethyl-9,10-di(o-tolyl)anthracenes.

Our attention is attracted by the fact that the characteristic feature of the compounds for which a deviation from additivity is found in the influence of substituents on the shift of absorption and fluorescence spectra is the presence of substituents whose spheres of action overlap in space.

Evidently, there are close spatial locations of the substituents which lead to interaction between them, and, consequently, to some change in their state in comparison with that which they have when in isolated positions (for example, when they are found in the 1 and 3 positions, or 1 and 4), and are the reason for the observed departures from additivity. That these deviations are connected on the whole with spatial interaction of the substituting groups, and not with a mutual influence which occurs across the anthracene nucleus, is shown by the good agreement of calculated and observed values of maxima of absorption and fluorescence spectra for di-meso derivatives of anthracene with substituents of different kinds.

The deviations from additivity in the fluorescence spectra are much more pronounced than in the absorption spectra. Thus, for example, in 1,4-dimethyl-9,10-diphenyl-anthracene and 1,4-dimethyl-9,10-di(o-tolyl)-anthracene, these deviations are equal to +1125 cm^{-1} and + 750 cm^{-1} respectively in the fluorescence spectra, while in the absorption spectra (long wavelength band) they are only +200 cm^{-1} and +225 cm^{-1}. Evidently this is evidence for the view that the spatial interaction of the substituents is intensified in the excited state.

Thus, from an examination of the influence of substituents on the shift of the absorption and fluorescence spectra, it follows that if, in the anthracene, there are substituents which are separated in space, then their combined influence arises from the influence of each of the substituents by itself.

The positions of the maxima of absorption and fluorescence spectra of such polysubstituted anthracenes can be calculated from the positions of the corresponding maxima in the spectrum of anthracene and the value of the displacement caused by the substituents. On the other hand, by the presence of a deviation from additibity in the influence of substituents, it is possible to observe the presence of interactions between them.

April 26, 1958

**Data on the spectra of meso derivatives of anthracene have, in part, been published earlier [1,3].

***Frequencies of the separate maxima of absorption and fluorescence are presented in table 2.

****The deviation from additivity is defined as the difference between the displacements actually found and the sum of displacements caused by each substituent by itself.

References

1. A. S. CHERKASOV: ZFKh., 29, 2209 (1955)
2. A. S. CHERKASOV: IAN USSR FS, 20(4), 478 (1956) (See CTT Bulletin, 20, p. 436)
3. A. S. CHERKASOV, T. M. VEMBER: OiS, 1, 663 (1956)
4. O. FISCHER, A. SAPPER: J. Prakt. Chem., Neue Folge, 83, 201 (1911)
5. G. HELLER, K. SCHULKE: Deutschen chemischen Gesellschaft, Berichte, 41, 3627 (1908)
6. J. V. BRAUN, O. BAYER: Deutschen chemischen Gesellschaft, Berichte 59, 914 (1926)
7. R. N. JONES: Chem. Rev., 41, 353 (1947)
8. C. A. COULSON: Proc. Phys. Soc., 60, 257 (1948)

TOM VI, Vyp. 4 OPTIKA I SPEKTROSKOPIIA Aprel', 1959
VOL. VI, No. 4 OPTICS AND SPECTROSCOPY April , 1959

The Influence of Oxygen on Photochemical Transformations and the Concentration Quenching of Fluorescence of Some Anthracene Derivatives

A.S. CHERKASOV and T.M. VEMBER

Abstract: The effect of oxygen on the quantum yields of the fluorescence, photo-oxidation and photo-dimerization process have been studied for 9-methyl, 9-ethyl, 9-n-propyl, and 9-methyl-10-methoxymethyl anthracene at various concentrations in solution. It has been shown that the results obtained may be fitted to a kinetic scheme in which photo-dimerization results from excited singlet molecules, the photo-oxide from excited molecules in the triplet state, and concentration quenching from the interaction of excited molecules in the singlet state with unexcited molecules of the same substance.

It has been shown by us previously [1] that the concentration quenching of fluorescence in meso-monoalky anthracenes results from the interaction of excited and unexcited molecules, as a result of which a stable photodimer may be formed. In order to clarify further the mechanism of the processes occurring when light energy is absorbed by these substances we have undertaken a study of the effect of oxygen on the quantum yield of fluorescence and on the quantum yields of photodimerization and photo-oxidation.

The substances studied were 9-methyl, 9-ethyl, 9-n-propyl and 9-methyl-10-methoxymethyl anthracene.

The monoalkyl anthracenes were obtained from anthrone and the corresponding alkyl magnesium halides [2], and the methylmethoxymethyl anthracene by the action of hydrochloric acid on a solution of 9, 10-dimethyl-9, 10-dihydroxydihydroanthracene in methanol [3]. Carefully purified samples were used for the investigation (recrystallized and chromatographed on Al_2O_3), and had the following melting points: 9-methylanthracene 80-81°, 9-ethylanthracene 58-58.5°, 9-n-propylanthracene 68-69°, and 9-methyl-10-methoxymethylanthracene, 110-111° C.

The procedure for measuring the quantum yields of fluorescence and of the photo-oxidation and dimerization reactions was as described previously [1]. The work was carried out at 20° C. Ethanol was used as solvent. The solutions were irradiated by means of a mercury lamp SVD-120 with filters to isolate the 365 mm group of lines. Different oxygen concentrations were obtained by saturating with oxygen, air or with a mixture of oxygen and nitrogen at atmospheric pressure. Removal of oxygen from solutions was achieved by bubbling nitrogen through them for long periods* (the solutions were heated to boiling several times and then cooled) or by first freezing the solutions in liquid air and then pumping off the air with a fore-pump.

All the monoalkyl anthracenes studied gave both a photo-oxide and a photo-dimer when their alcohol solutions were irradiated in the presence of oxygen. 9-methyl-10 methoxymethyl anthracene, however, gave only the photo-oxide, as was shown by the fact that in the absence of oxygen, prolonged irradiation of the solution did not lead to a decrease in the concentration of the starting material** With increasing concentration of the substance under study, the quantum yield of fluorescence fell, but that of both the photo-dimerization and photo-oxidation reactions rose.

The observed values of the quantum yields of all three processes are set forth in table 1.

It may be seen that oxygen has a quenching effect on the fluorescence, the quantum yield of which falls with increasing oxygen concentration.

It should be noted that the parallelism between the amount of quenching by oxygen and the amount of photo-oxide formed which was observed for benzene and some of its methyl derivatives [5] is not present in the anthracenes. The sum of the quantum yields of fluorescence and photo-oxidation is not equal to the fluorescence quantum yield of oxygen-free solutions at the same concentration, as would be the case if quenching by oxygen always resulted in the formation of photo-oxide. For example at a concentration of 2×10^{-2} mol/l. this sum for an oxygen-saturated solution of 9-methyl anthracene is 0.357, and for 9-methyl-10-methoxymethyl anthracene is 0.730, while the fluorescence yields of oxygen free solutions are 0.156 and 0.390, i. e. only about half. At low concentrations of the substances, however, (about 10^{-5} molar) the fluorescence yield is 2.5 times greater for an oxygen-free solution of 9-methyl anthracene than for a corresponding solution saturated with oxygen, and is 3.5 times greater for the case of 9-methyl-10-methoxymethyl anthracene; i. e. the oxygen quenching is very considerable, although at this concentration the formation of photo-oxide is almost absent.

Quenching by oxygen decreases with increasing concentration of the substance under investigation, but at the same time concentration quenching decreases with increasing concentration of dissolved oxygen, which shows that the two processes compete with each other.

Plotting the variation of the reciprocal of the quantum yield of fluorescence as a function of the concentration of dissolved oxygen (Fig. 1-a) and of the concentration of the substance itself

*Cylinder nitrogen was purified of traces of oxygen by passing it over heated copper turnings.

**As we have shown, 9, 10-dimethyl- and 9, 10-dipropyl-anthracene in alcoholic solutions also give only the photo-oxide. It is also well known [4] that 9, 10-diphenyl-anthracene also gives only the photo-oxide. Apparently the formation of the photodimer from meso-disubstituted anthracenes is hindered by the steric effect of the substituent in both meso positions.

TABLE I

Quantum yield of fluorescence (B) and quantum yield for the photo-oxidation reaction (φ_{ph}) and photo-dimerization reaction (φ_d) at different concentrations of substance studied (A), and of oxygen (O_2).

Substance	$[O_2]\ 10^3$	$[A]\ 10^2$	φ_{ph}	φ_d	B	$B+\varphi_{ph}$	$B+\varphi_d$	$B+\varphi_{ph}+\varphi_d$
9-methyl-anthracene	0	0.001	0	0	0.390	0.390	0.390	0.390
		0.3	0.008	0.031	0.295	0.303	0.326	0.334
		0.6	0.006	0.042	0.290	0.296	0.332	0.348
		1.0	0.005	0.063	0.230	0.235	0.313	0.318
		1.5	0.005	0.115	0.187	0.192	0.302	0.307
		2.0	0.009	0.130	0.156	0.165	0.286	0.295
	1.34	0.001	0	0	0.290	0.290	0.290	0.290
		0.3	0.058	0.026	0.240	0.298	0.266	0.324
		0.6	0.095	0.046	0.220	0.315	0.266	0.361
		1.0	0.125	0.068	0.185	0.310	0.253	0.378
		1.5	0.155	0.081	0.160	0.315	0.241	0.396
		2.0	0.180	0.088	0.135	0.315	0.223	0.403
	6.4	0.001	0	0	0.150	0.150	0.150	0.150
		0.3	0.089	0.004	0.150	0.240	0.154	0.244
		0.6	0.138	0.027	0.135	0.273	0.162	0.300
		1.0	0.191	0.022	0.120	0.311	0.144	0.333
		1.5	0.223	0.086	0.106	0.329	0.172	0.395
		2.0	0.250	0.070	0.097	0.357	0.167	0.417
9-ethyl-anthracene	1.34	0.001	0	0	0.300	0.300	0.300	0.300
		0.3	0.042	0.008	0.262	0.304	0.270	0.312
		0.6	0.088	0.012	0.240	0.328	0.252	0.340
		1.0	0.135	0.014	0.214	0.349	0.228	0.363
		1.7	0.177	0.024	0.180	0.357	0.204	0.381
		2.0	0.210	0.030	0.165	0.375	0.195	0.405
9-n-propyl-anthracene	1.34	0.001	0	0	0.310	0.310	0.310	0.310
		0.3	0.027	0.015	0.280	0.307	0.295	0.322
		0.6	0.058	0.026	0.253	0.311	0.279	0.337
		1.0	0.078	0.028	0.230	0.308	0.258	0.336
		1.7	0.081	0.038	0.180	0.271	0.228	0.308
		2.0	0.106	0.034	0.180	0.286	0.214	0.319
9-methyl-10-methoxymethyl-anthracene	0	0.001	0	0	0.930	0.930	0.930	0.930
		0.3	0	0	0.770	0.770	0.770	0.770
		0.6	0	0	0.665	0.665	0.665	0.665
		1.0	0	0	0.560	0.560	0.560	0.560
		1.5	0	0	0.475	0.475	0.475	0.475
		2.0	0	0	0.390	0.390	0.390	0.390
	1.34	0.001	0	0	0.600	0.600	0.600	0.600
		0.3	0.088	0	0.535	0.623	0.535	0.623
		0.6	0.167	0	0.490	0.657	0.490	0.657
		1.0	0.258	0	0.435	0.693	0.435	0.693
		1.5	—	—	0.375	—	0.375	—
		2.0	0.431	0	0.310	0.741	0.310	0.741
	6.4	0.001	0	0	0.270	0.270	0.270	0.270
		0.3	0.144	0	0.250	0.394	0.250	0.394
		0.6	0.242	0	0.230	0.472	0.230	0.472
		1.0	0.380	0	0.220	0.580	0.220	0.580
		1.5	—	—	0.203	—	0.203	—
		2.0	0.547	0	0.183	0.730	0.183	0.730

gives fairly good straight lines * ; this indicates the diffusion-limited character of these processes **

For anthracene it has been shown that the drop in fluorescence yield on increasing the anthracene concentration is almost equal to the increased yield of photodimerization [4, 10] .

However, in the meso monoalkyl-anthracenes the quantum yield of dimerization in both oxygen free solutions and in solutions saturated with air is significantly less than the amount of concentration quenching at the same concentration***, and the sum of the fluorescence and dimerization yields falls with increasing concentration of the substance (Table 1). This shows that the collision of an excited and an unexcited molecule does not always form a stable dimer. This is also clearly shown by the fact that 9-methyl-10-methoxymethyl-anthracene, the fluorescence of which shows very strong concentration quenching, does not form a stable dimer, and concentration quenching is especially strong in oxygen-free solutions, where no photo-decomposition is observed.

The sum of the quantum yields of fluorescence and of the photo-oxidation and photo-dimerization reactions, as may be seen from Table 1, increases with increasing concentration of the substance

---

* We examined solutions of concentration up to 2×10^{-2} molar. At concentrations higher than this there is a small deviation from linearity, and a new band is observed in the fluorescence spectrum [6] on the long wavelength side of the usual spectrum. A similar band has also been observed in the fluorescence spectrum of concentrated pyrene solutions [7] and has been ascribed to the fluorescence spectrum of unstable dimers formed from one excited and one unexcited molecule.

** The diffusion-limited character of the concentration quenching of the fluorescence of anthracene had been decided earlier on the basis of its dependence on the viscosity of the solvent.

*** It should be noted that in the presence of oxygen (or any other quencher) the yield of dimers may also exceed the amount of concentration quenching of fluorescence which occurs. (The latter is calculated as the difference between the fluorescence yield in the absence of concentration quenching and at the concentration studied.) This may occur because in this case, the increase in the yield of dimers with increasing concentration of reagent occurs not only because of reduced fluorescence yield, but because of a decrease in the "quantum yield" of oxygen quenching as well.

(except in the case of the oxygen-free systems); at the highest concentration investigated, 2×10^{-2} molar, it is greater than the limiting quantum yield of fluorescence (B_0) attained in oxygen-free solution at low concentration -i.e.- with no concentration quenching or oxygen quenching. It is well known that the photo-oxidation of anthracene and some of its derivatives in carbon disulfide occurs with a quantum yield close to unity [4], although the limiting fluorescence yield in this solvent is very low. We may conclude that the processes leading to a low value of limiting fluorescence quantum yield do not involve direct transition from the excited to the ground state, but that an intermediate active molecule, no longer capable of fluorescence, but able to react with oxygen to form photo-oxides must, be involved.

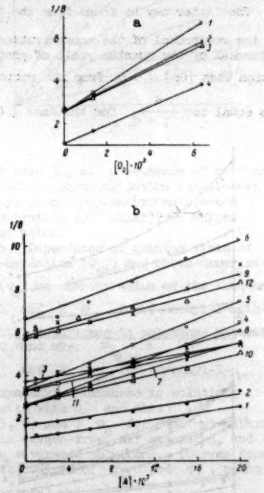

Figure 1. Dependence of the reciprocal of the fluorescence quantum yield on concentration of Oxygen (a), and of the substance itself (b)

a: 1- 9-methyl-anthracene; 2- 9-ethyl-anthracene; 3- 9-n-propyl-anthracene; 4- 9-methyl-10-methoxymethylanthracene. (Concentrations all 10^{-5} molar).

b: 1- 9-methyl-10-methoxymethyl-anthracene in oxygen-free solution; 2- same saturated with air; 3- same saturated with oxygen; 4- 9-methyl-anthracene, oxygen-free; 5- same saturated with air; 6- same saturated with oxygen; 7- 8- 9- same 3 situations for 9-ethyl-anthracene; 10- 11- 12- ditto for 9-n-propyl-anthracene.

The formation of reactive molecules capable of further reaction with oxygen to form the photo-oxide must occur both during concentration and oxygen quenching. A survey of the results obtained with 9-methyl-10-methoxy-methylanthracene demonstrates this since the high quantum yield of photo-oxidation (which was obtained at 2×10^{-2} mol/l). and an oxygen saturation of 0.547 with a limiting fluorescence yield close to unity (0.93) cannot be explained by the formation of photo-oxide by only one of the above processes.

Thus the results of the investigation of the effect of oxygen on the quantum yields of fluorescence and of the photo-dimerization and -oxidation processes show that our earlier kinetic proposal [1] in which photo-oxide formation results from concentration quenching, is insufficient to explain the results observed.

Bowen , in an investigation of the photochemical decomposition and concentration quenching of anthracene and some of its derivatives, assumed that the photodimers of these substances are formed from singlet excited molecules, while the photo-oxide results from molecules in the triplet state [4, 11]. According to his proposed kinetic mechanism [4] the excited molecules interacting with the solvent either go over to the triplet state, or remain in the singlet state and simply lose excess vibrational energy and arrive at a distribution of vibrational levels characteristic of the temperature of the surroundings. Singlet excited molecules lose their remaining energy either by fluorescence, or by oxygen quenching, or by concentration quenching: it is assumed that the last two processes may also lead to the formation of molecules in the triplet state

$$
\begin{aligned}
A + h\nu &\longrightarrow {}^*A, && 1,\\
{}^*A + S &\longrightarrow {}^1A + S, && \alpha,\\
{}^*A + S &\longrightarrow {}^3A + S, && 1-\alpha,\\
{}^1A &\longrightarrow A + h\nu', && f',\\
{}^1A + O_2 &\longrightarrow {}^3A + O_2, && q'[O_2],\\
{}^1A + A &\longrightarrow {}^3A + A, && p'[A],\\
{}^1A + A &\longrightarrow A_2, && d'[A],
\end{aligned}
$$

Here A is the ground state and ^1A AND ^3A excited singlet and triplet molecules, resp. ; S refers to solvent molecules; α is the probability of transition from the excited state to the equilibrium excited singlet configuration, and f , q', p', and d' are the rate constants for the corresponding processes, [A] and $[O_2]$ are concentrations. In this formulation we postulate "instantaneous" quenching sufficiently great in amount to reduce the limiting fluorescence quantum yield to 0.2-3 in the case of anthracene,for example. However, as was shown in [12] in the case of anthracene and its alkyl derivatives there also exists a quenching process, occurring in a time significantly less than the excited state lifetime, it cannot be very considerable, since the lifetime of the excited state in the absence of any kind of quenching (τ_0) defined as the ratio of the experimentally found fluorescence lifetime to the experimental quantum yield is for these substances very close to the value of τ_0 computed from the long wavelength absorption band.

From the above considerations it seems to us that the following kinetic scheme is more reasonable.

$$
\begin{aligned}
{}^*A + S &\longrightarrow {}^1A + S, && 1,\\
{}^1A + S &\longrightarrow {}^3A + S, && t,\\
{}^1A &\longrightarrow A + h\nu, && f,\\
{}^1A + O_2 &\longrightarrow {}^3A + O_2, && q[O_2],\\
{}^1A + A &\longrightarrow {}^3A + A, && p[A],\\
{}^1A + A &\longrightarrow A_2, && d[A],\\
{}^3A + S &\longrightarrow A + S, && K_1[{}^3A],\\
{}^3A + O_2 &\longrightarrow AOO, && K_2[{}^3A][O_2],\\
AOO &\longrightarrow A + O_2, && K_3,\\
AOO + A &\longrightarrow AO_2 + A, && K_4[A].
\end{aligned}
$$

This picture differs from that of Bowen in that here oxygen quenching and concentration quenching compete with formation of the triplet state by interaction of excited molecules with the solvent, whereas in Bowen s scheme this is not the case *.

According to the above the quantum yield of fluorescence takes the following form

$$B = \frac{f}{f + t + (p + d)[A] + q[O_2]}$$

or

$$B = \frac{\frac{f}{f + t}}{1 + \frac{p + d}{f + t}[A] + \frac{q}{f + t}[O_2]}$$

from which we obtain

$$\frac{1}{B} = \frac{f + t}{f} + \frac{p + d}{f + t}\,\frac{f + t}{f}[A] + \frac{q}{f + t}\,\frac{f + t}{f}[O_2]$$

from which it may be seen that the reciprocal of the quantum yield of fluorescence must depend linearly on the concentration of the substance concerned and on the oxygen concentration. As was noted above such linearity fits the observations reasonably well (fig. 1) and by a graphical solution of (2) when $[O_2] = 0$ (oxygen quenching absent) and also when [A] is very small (concentration quenching absent), the constants $\frac{f + t}{f}$ $\frac{p + d}{f + t}$ and $\frac{q}{f + t}$ are readily

The expressions for the photo-dimerization quantum yield φ_d and for the photo-oxidation quantum yield φ_{ph}, take the form

$$\varphi_d = \frac{\frac{d}{f + t}[A]}{1 + \frac{p + d}{f + t}[A] + \frac{q}{f + 1}[O_2]}$$

$$\varphi_{ph} = \left(\frac{\frac{K_4}{K_3}[A]}{1 + \frac{K_4}{K_3}[A]}\right)\left(\frac{\frac{K_2}{K_1}[O_2]}{1 + \frac{K_2}{K_1}[O_2]}\right) X$$

$$X\left(\frac{\frac{f}{f + t} + \frac{p}{f + t}[A] + \frac{q}{f + t}[O_2]}{1 + \frac{p + d}{f + t}[A] + \frac{g}{f + t}[O_2]}\right)$$

The constant $\frac{d}{f + t}$ in expression (3) is determined using the value of $\frac{p + d}{f + t}$ and the ratio $\frac{d}{p + d}$. The latter may be found from the dependence of the reciprocal of the concentration ** on the reciprocal of the quantum yield of photo-dimerization when $[O_2] = 0$ or from the ratio $\frac{d}{d + ph}$ which is equal to $\frac{d}{f + d}$ for the case $[O_2] = 0$. ***

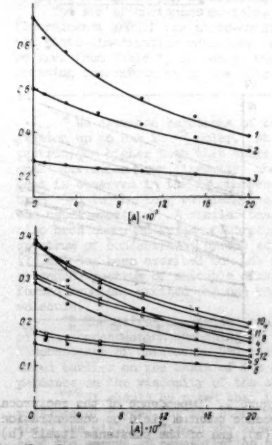

Figure 2. Dependence of quantum yield of fluorescence on concentration of substance.
1- 9-methyl-10-methoxymethyl-anthracene in oxygen-free solution; 2- same saturated with air; 3- same saturated with oxygen; 4- 9-methyl-anthracene, oxygen-free; 5- same saturated with air; 6- same saturated with oxygen; 7- 8- 9- same 3 situations for 9-ethyl-anthracene; 10- 11- 12- ditto for 9-n-propyl-anthracens. (Curves constructed from computed quantum yields. Points . experimental values) .

* The mechanism of photo-oxide formation is assumed the same as in Bowen's scheme.

** This dependence is linear.

*** $\varphi_{ph}\varphi_d$. (sum of quantum yields of steps ${}^1A + A$) at a given concentration in absence of O_2 equals the ratio $(B_o - B)/B_o$.

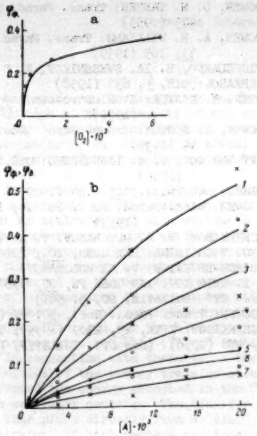

Figure 3., a. Dependence of quantum yield of the photo-oxidation reaction of 9-methyl-10-methoxy-methyl anthracene (concentration 10^{-2} molar), on oxygen concentration.

b. Dependence of quantum yield of photo-oxidation (φ_{ph}) and photo-dimerization (φ_d) on concentration of the substance.

1 and 2 φ_{ph} for 9-methyl-1-meth-oxymethyl-anthracene in solutions saturated with O_2 and air.

3 and 4 φ_{ph} for 9-methyl-1-methoxymethyl-anthracene in solutions saturated with O_2 and air.

5, 6, and 7 φ_d for 9-methyl-anthracene in oxygen-free, air saturated, and oxygen saturated solutions. (Curves from computed values of φ_{ph} and φ_d, points experimental values).

Having experimentally determined the quantum yield of photo-oxidation for a given concentration of the substance concerned at different concentrations of oxygen, or for a fixed oxygen concentration and varying concentration of the substance, the values of the constants $\frac{K_4}{K_3}$ and $\frac{K_2}{K_1}$ which occur in (4) may readily be found.

It should be noted that the expressions introduced above for the quantum yields of fluorescence, photo-dimerization and photo-oxidation are in our view completely analogous to the corresponding expressions obtained from Bowen's formulation. Thus for example the quantum yield of fluorescence obtained from Bowen's expressions takes the form:

$$B = \frac{\alpha}{1 + \frac{p'+d'}{f'}[A] + \frac{q'}{f'}[O_2]}$$

A comparison of this expression with (1) shows that the constants α, $\frac{p'+d'}{f'}$, and $\frac{q'}{f'}$ in (5) correspond to the constants $\frac{f}{f+t}$, $\frac{p+d}{f+t}$, and $\frac{q}{f+t}$ in (1). The experimentally determined numerical values of the corresponding constants must be the same in both cases, but their physical interpretation is different.

The numerical values of the constants in (1), (3), and (4), for the substituted anthracenes which we have studied are given in Table 2++.

The limiting fluorescence yield (B_o), as may be seen from Table 2 is identical for the three monoalkyl anthracenes studied. Some increase in the fluorescence yield is observed with increasing molecular weight of the alkyl substituent for non-deoxygenated solutions [15], resulting from the fact that the substances with heavier alkyl groups are less susceptible to oxygen quenching, as the data show. The relative and absolute constants for concentration quenching and for oxygen quenching for monoalkyl anthracenes are very close to those found earlier for anthracene in benzene [14].

TABLE 2

Values of the constants appearing in the expressions for quantum yields of fluorescence and of photo-chemical reactions for various substituted anthracenes.

Substance	$\frac{f}{f+t}$ (B_o)	$\frac{p+d}{f+t}$*	$\frac{q}{f+t}$	$\frac{K_2}{K_1}$	$\frac{K_4}{K_3}$	τ_o x10^9	$\frac{(f+t)}{}$ x10^{-7}	$\frac{(p+d)}{}$ x10^{-10}	$\frac{q}{}$ x10^{-10}
9-methyl-anthracene	0.39	74.5	254	1700	34	7.0	14.4	1.07	3.6
9-ethyl-anthracene	0.38	50.5	190	-	-	6.5	15.4	0.78	2.8
9-n-propyl-anthracene	0.38	45.0	178	--	-	6.7	14.9	0.67	2.7
9-methyl-10-methoxymethyl anthracene	0.93	69.0	396	11800	86.5	13.5	7.4	0.51	2.9
anthracene (in benzene) (14)	0.24	30.0	128	2100	2.38	13.4**	7.45	0.93	4.0

* The value of the constants $\frac{d}{f+t}$ and $\frac{p}{f+t}$ were computed separately only for 9-methyl anthracene. They are equal respectively to 15.5 and 59.0. In 9-methyl-10-methoxymethyl-anthracene dimerization is absent and consequently the value in the column is itself $\frac{p}{f+t}$.

**Computed from the long wavelength absorption band.

++ Table 2 also gives absolute values of the constants p + d, and q. The values of the constants f + t required for calculation of the absolute values of p + d and q were obtained by dividing unity by τ_o, the mean lifetime of the excited state of the oxygen-free solution of the substance, as determined on the fluorimeter [13] at a concentration of 10^{-5} mols/liter.

On the basis of the constants given in Table 2, the quantum yield of fluorescence as a function of concentration was computed for all the compounds studied: for 9-methyl-anthracene and 9-methyl-10-methoxymethyl-anthracene the quantum yields of photo-oxidation and photo-dimerization were also calculated as a function of concentration of the substance and of oxygen. As may be seen from figures 2 and 3 the computed curves are in satisfactory agreement with the experimental points. We can therefore say that the kinetic mechanism proposed above describes essentially correctly the processes brought about by the light energy absorbed by substituted anthracenes of the types studied, although possibly it does not cover all of them.

April 2, 1958

References

1. A. S. CHERKASOV, T. M. VEMBER: OiS, 4, 203 (1958)
2. F. KROLLPFEIFFER, F. BRANSCHEID: Ber. Deutsch. chem. Gesell., 56, 1617 (1923)
A. SIEGLITZ, R. MARX: Ber. Deutsch. chem. Gesell., 56, 1619 (1923)
3. G. M. BADGER, R. S. PEARCE: J. Chem. Soc., 2314 (1950)
4. E. J. BOWEN, D. W. TANNER: Trans. Farad. Soc., 51, 475 (1955)
5. E. J. BOWEN, A. H. WILLIAMS: Trans. Farad. Soc., 35, 765 (1939)
6. G. A. TISHCHENKO, B. IA. SVESHNIKOV, A. S. CHERKASOV: OiS, 4, 631 (1958)
7. T. FÖRSTER, K. KASPER: Z. Elektrochem., 59, 976 (1955)
8. E. J. BOWEN, A. NORTON: Trans. Farad. Soc., 35, 44 (1939)
9. B. IA. SVESHNIKOV, G. A. TISHCHENKO: OiS, 1, 155 (1956)
10. F. WEIGERT: Naturwiss., 15, 124 (1927)
11. E. J. BOWEN: Disc. Farad. Soc., No. 14, 143 (1953)
12. A. S. CHERKASOV, V. A. MOLCHANOV, T. M. VEMBER, K. G. VOLDAIKINA: DAN USSR, 109, 292 (1956)
13. A. M. BONCH-BRUEVICH, V. A. MOLCHANOV, V. I. SHIROKOV: IAN USSR FS, 20, 596 (1956) (See CTT Bulletin, 20, p. 541)
14. E. J. BOWEN: Trans. Farad. Soc., 50, 97 (1954)
15. A. S. CHERKASOV: ZhKh, 29, 2209 (1955); IAN USSR FS, 20, 478 (1956) (See CTT BULLETIN, 20, p. 436)

TOM VI, Vyp. 4 OPTIKA I SPEKTROSKOPIIA Aprel', 1959
VOL. VI, No. 4 OPTICS AND SPECTROSCOPY April, 1959

On the Interaction of "Blue" and "Samarium" Centers in the Phosphor ZnS-Sm(Cl)

Z. A. TRAPEZNIKOVA

Abstract: An investigation has been made of the luminescent intensity of "blue" and activator centers as a function of the intensity of the exciting illumination in the phosphors ZnS-Sm and ZnS-Sm(Cl). The temperature dependence of the luminescence spectra of these phosphors has also been investigated. An interpretation of the results is given, and a proposal is made for the mechanism by which energy is transferred from the "blue" centers to the "samarium" centers.

In previous papers [1,2] on excitation spectra it was shown that in zinc sulphide luminophors, both without an activator and with various activators, certain centers are formed which absorb light of wavelengths between 332-342 mμ; moreover it was shown that the energy absorbed in these centers can be transferred to the activator centers. On the basis of a comparison of our results with those of other workers, it was concluded that these centers are responsible also for the blue fluorescence of nonactivated zinc sulphide ("blue" centers).

In connection with these facts there arose the question of the energy transfer mechanism which transferred the energy absorbed in the "blue" centers to the activator centers. The transfer of energy might take place directly from a "blue" center to an activator, if both centers are located directly next to one another. Or the transfer might take place through the lattice of the host material if the "blue" and activator centers were distributed independently of each other in the ZnS lattice.

On the other hand, the observed increase of the quantum yield of activator luminescence during absorption of light in the "blue"centers in relation to the absorption by the lattice of the zinc sulfide pointed to the fact that the "blue" and activator centers were located quite close together. For such a distribution of the centers the losses during energy transfer would be smaller than for the case of transfer via the host lattice. Moreover, it was discovered that on introducing allogenic zinc sulphide anions ($O^=$, $Se^=$, Cl^-, etc.) the activator luminescence spectrum changed and at the same time the maximum of the excitation shifted. This also pointed to the "blue" and activator centers being located side by side.

On the other hand it is very improbable that activators of different valences could be located alongside the same lattice defect, which is a "blue" center.

Hence the experimental data presented in previous papers did not give a definite answer to the question of the distribution of the "blue" and activator centers in zinc sulphide.

In order to resolve this question the present work was undertaken. An investigation was made of the dependence of the intensity of the fluorescence of the "blue" and activator centers on the intensity of the exciting light. If a "blue" center and an activator center form a single unit then their brightness as a function of the intensity of the exciting light should vary according to the same law, since the presence of other excited or ionized centers could not influence the probability for energy distribution inside one and the same center. If the centers exist independently then the variations could be different.

We investigated two phosphors, ZnS-Sm and ZnS-Sm(Cl). At room temperature the luminescence of ZnS-Sm and ZnS-Sm(Cl) was reddish-blue and the spectrum consisted of a blue band and the fluorescence lines of Sm^{3+}. The phosphor ZnS-Sm showed only the Sm^{3+} fluorescence at room temperature. We obtained the phosphors in the following manner. Zinc sulphide of "luminophor" purity was treated with hydrogen sulphide at a temperature of 900°C to eliminate zinc sulphate. To the phosphor we then added an activator in the form of samarium sulphide. In the preparation of the phosphor ZnS-Sm(Cl) the chlorine ion was added in the form of $ZnCl_2$. The samarium Sm^{3+} and the chlorine Cl^- were introduced in quantities of 10^{-3} gram-atom per gram mole of ZnS. A carefully ground charge of the phosphor was placed in an ampoule from which the air was evacuated to a pressure of $2 \cdot 10^{-5}$mm Hg. The pumping-out took place while the ampoule was heated to 130°C. Then the ampoule was sealed off and the phosphor was annealed at 1150°C for an hour.

The brightness of the blue and orange-red bands was recorded by a photomultiplier. The blue light was completely separated from green and red with the help of two BG2 + BG12 Schott filters (the spectrum of samarium has a group of lines in the green). The phosphors were excited through an ultra-violet filter which transmitted basically the mercury line λ = 365 mμ, which falls at the cut-off of the absorption of the blue centers The intensity of the excitation illumination could be varied by a factor of 65.7.

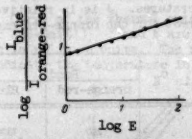

Fig. 1. Curve of the dependence of the ratio of the brightness of the blue emission to the brightness of the orange-red emission on the intensity of the exciting light plotted in log-log coordinates. I and E are in relative units. Temperature is 293°K.

In figure 1 we have shown in log-log coordinates the dependence of the ratio of the blue to orange-red luminescence on the intensity of the exciting light, for the phosphor ZnS-Sm(Cl).

It is clear from figure 1 that this ratio does not remain constant when the intensity of the excitation is varied. Hence it follows that the "blue" and "samarium" centers do not form a single unit but instead are distributed in the lattice independently of one another.

The mechanism for transferring energy from

"blue" to "samarium" centers may be represented in the following way. The "blue" centers absorb light with λ = 332-342 mμ and are ionized. As a result of thermal vibrations, electrons from the filled zone may fall into the empty ground state of the "blue" centers. This leaves holes in the filled zone which may migrate through the crystal. When the holes encounter "samarium" centers the latter become ionized.

Naturally this mechanism requires that there be a definite activation energy and one may expect that at sufficiently low temperatures there will be only the blue luminescence.

"In order to support this idea we carried on experiments on the temperature dependence of the luminescence spectra of ZnS-Sm(Cl) and ZnS-Sm. During the experiments the phosphors were placed in a Dewar flask which had a flat quartz bottom, through which passed the excitation illumination of wavelength 334 mμ, i.e. at the maximum of the absorption by the "blue" centers (this line was separated from the spectrum of the mercury lamp by means of a double monochromator). The emission from the phosphor fell on the slit of the spectrograph which was carefully protected from stray light. The spectra were recorded at room temperature, the temperature of dry ice, and the temperature of liquid nitrogen. For the phosphor ZnS-Sm(Cl), when the temperature was lowered, there was an increase in intensity of the blue emission and a simultaneous decrease in the intensity of the samarium lines. Quantitative measurements of the brightness of the blue and orange-red luminescence as a function of the temperature were made with the help of a photo multiplier and filters, as described above, with an excitation illumination of λ = 365 mμ. The data obtained are shown in Table 1."

Table 1

Brightness of the orange-red and blue emission from the phosphor ZnS-Sm(Cl) at various temperatures. J is in relative units, different for the orange-red and blue bands.

Temperature in °K	Band	
	Orange-red	Blue
293	250	7370
195	15	21300
77	15	11100

From the data in Table 1 it is clear that the brightness of the blue band goes through a maximum when the temperature is lowered. The brightness of the orange-red band falls monotonically with decreasing temperatures, although the decrease is less sharp in the region 293-195°K than in the region 195-77°K. This type of variation in the brightness of the blue and orange-red fluorescence shows that at temperatures below 195°K in this phosphor additional factors come into operation which decrease the number of ionized "blue" centers. In the phosphor ZnS-Sm an analogous temperature dependence of the brightness of the "Blue" luminescence is not found. In this case, on the contrary, the brightness of the blue band at 77°K is much higher than at 195°. This may be seen from Table 2.

Table 2

Brightness of the orange-red and blue emission from the phosphor ZnS-Sm at various temperatures. J is in relative units, different for the orange-red and blue bands.

Temperature in °K	Band	
	Orange-red	Blue
293	95	<1
195	30	<1
77	<1	300

In addition it was discovered that these two phosphors behave differently under the influence of infra-red light. Thus when the phosphor ZnS-Sm(Cl) is excited at liquid nitrogen temperature, it gives off, under the influence of infra-red light, a bright flash of blue light which turns rapidly to orange-red upon heating. This is due to passage of holes from the "blue" centers to the "samarium" centers. The same change in color is present during thermal luminescence. When the phosphor ZnS-Sm(Cl) is excited at room temperature it does not give off a flash. On the other hand, the phosphor ZnS-Sm, when excited at liquid nitrogen temperature, does not give off a flash; upon heating an orange-red flash appears, and when excited at room temperature this phosphor gives off a bright flash of orange-red light.

The different temperature dependences of the intensity of the blue band in the phosphors ZnS-Sm(Cl) and ZnS-Sm, and the different behaviour of these phosphors under the influence of infra-red light indicate that they differ from one another not only by the relative number of "blue" and "samarium" centers, but also in the number and depth of trapping levels.

To explain this we measured curves of the thermal emission. The heating of the phosphor took place uniformly at the rate of about 10 degrees per minute from the temperature of liquid nitrogen, at which the phosphor was excited, up to the temperature +180°C. The brightness was measured by a photomultiplier, and the data recorded automatically. In figure 2 we give the curve of the thermal luminescence of the phosphor ZnS-Sm. As may be seen this phosphor has several trapping levels of various depths.

In figure 3 we give the curve of the thermal luminescence of the phosphor ZnS-Sm(Cl). Here it is possible to discover one, or perhaps two, low temperature trapping levels in the absence of deep levels.

As may be seen from figures 2 and 3, the areas under the thermal emission curves for the phosphors ZnS-Sm(Cl) and ZnS-Sm are equal, but this does not prove the equality of the total amount of light emitted by these phosphors for the following

reason. The curve of the thermal luminescence of the phosphor ZnS-Sm was taken with increased voltage on the photomultiplier tube (almost twice the voltage used with the other phosphor). This was necessary because the phosphor ZnS-Sm gives off principally orange-red light, in which region the sensitivity of the photomultiplier falls rapidly.

If one takes account of the increase in photomultiplier sensitivity with increasing voltage and the decreasing sensitivity of the multiplier in the orange-red region of the spectrum then the total light emitted by the phosphor ZnS-Sm(Cl) is found to be some ten times larger than was emitted by the ZnS-Sm.

Thus as may be seen from figures 2 and 3 the phosphor ZnS-Sm(Cl) differs from ZnS-Sm by the almost total absence of deep trapping levels and also by the capability of emitting a larger total amount of light. The emission of the larger amount of light by the phosphor ZnS-Sm(Cl) may be connected with an increase in the number of shallow trapping levels and hence with an increase in the amount of stored light. On the other hand, the thermal emission of a large total amount of light may be connected with the absence in ZnS-Sm(Cl) of just those deep levels from which ejection of electrons takes place at the quenching temperature of the "samarium" centers.

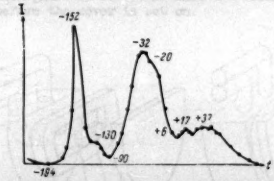

Figure 2. Curve of the thermal emission of the phosphor ZnS-Sm. I and t are the brightness and time in relative units. The numbers on the curve indicate the temperature (in°C).

The phosphors ZnS-Sm and Zn-Sm(Cl) are capable of storing a large amount of light. As is well-known, for phosphors of this type the emission of radiation falls in the presence of a sufficiently intense exciting light. This takes place because not all of the light being absorbed goes into the ionization of the luminescent centers; a part of it for example may be used up uselessly in the ejection of electrons from trapping levels. The fall in brightness for the phosphor ZnS-Sm(Cl) at temperatures below 195°K can be explained by a decrease in the emission of light by the phosphor at these low temperatures due to the emission stimulated by the excitation illumination, since this phosphor stores a large total amount of light only at temperatures below 195°K. This action is not present in ZnS-Sm since in this phosphor the trapping levels are deeper and the emissive action would take place at all temperatures.

We also investigated the dependence of the intensity of the blue and orange-red light of the phosphor ZnS-Sm(Cl) on the intensity of the excitation light at temperatures of 293, 195, and 77°K. The resulting curves are given in log-log coordinates in figure 4.

From figure 4 it is clear that the brightness of the blue light increases faster than linearly at the temperatures 293 and 77° (for T = 293°, $I_{Blue} \sim E^{3/2}$), and linearly at the intermediate temperature 195°K; the brightness of the orange-red light increases linearly at room temperature and somewhat more slowly than linearly at temperatures of 195 and 77°K. Fok [3] has theoretically analyzed the case of phosphors with two sorts of luminescence centers under the conditions that holes are exchanged between them via the valence band and that light may be absorbed only by one sort of center, and he has obtained the dependence of the brightness of the luminscence from both centers as a function of the intensity of the excitation. These calculations agree qualitatively with our results. However their quantitative use to determine the separation of the ground states of the luminescence centers from the top of the valence band does not give a reasonable magnitude for the respective energies. This indicates that the phosphor ZnS-Sm(Cl) is a more complicated system than simply a phosphor with two luminescence centers and one trapping level, as Fok assumed in his calculations.

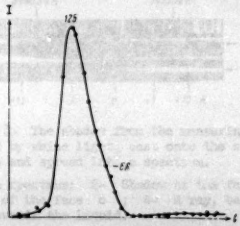

Fig. 3. Curve of the thermal emission of the phosphor ZnS-Sm(Cl) I and t are the brightness and time in relative units. The numbers on the curve indicate the temperature in °C.

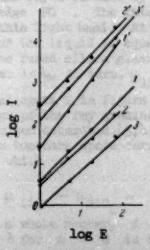

Fig. 4. Curves of the dependence of the brightness of the blue and orange-red emission from the phosphor ZnS-Sm(Cl) on the intensity of the exciting light at various temperatures. I and E in relative units. The blue emission (in°K: 1' - 293, 2' - 195 3' - 77); orange-red emission 1 - 293, 2 - 195, 3 - 77.

CONCLUSIONS

1. In zinc sulphide the "blue" and the activator centers are distributed in clusters in the lattice independently of one another.
2. The transfer of holes from the "blue" centers to the activator centers requires the existence of activation energy.
3. The introduction of chlorine into zinc sulphide which has been activated by samarium changes the spectrum of the trapping levels, and in particular the deep trapping levels vanish; it is also possible that the number of shallow levels increases. The total amount of emitted light increases by a factor of ten.
4. The storing of light by the phosphor ZnS-Sm(Cl) at low temperatures in the absence of deep trapping levels leads to a decrease in the brightness of the phosphor's blue luminescence at temperatures below 195°K. because of stimulated emission due to the exciting light.

The author extends his deep thanks to T. Voznesenskaia for help with this work, and to L. A. Vinokurov for the quantitative brightness measurements, and to M. V. Fok for his constant interest in this work and for useful advice during the discussion of the results.

April 29, 1958

References

1. Z. A. TRAPEZNIKOVA, V. V. SHCHAENKO: DAN USSR, 106, 230 (1956) (See Soviet Physics Doklady)
2. Z. A. TRAPEZNIKOVA: Materialy V Soveshchaniia po liuminestsentsii (kristallofosfory) [Materials from the V Conf. on Lumin. (crystal phosphors)] Akad. Nauk ESSR Press. Tartu, 1957, p. 17
3. L. A. VINOKUROV, M. V. FOK: OiS, 4, 118 (1958) M. V. FOK: OiS, 2, 475 (1957)

TOM VI, Vyp. 4 OPTIKA I SPEKTROSKOPIIA Aprel', 1959
VOL. VI, No. 4 OPTICS AND SPECTROSCOPY April, 1959

Dispersion Curves of Chloroform and Carbon-tetrachloride in a Wide Temperature Range

I. V. OBREIMOV AND E. F. LAMSHCHIKOV

Abstract: The dispersion curve of CCl_4 and $CHCl_3$ in the range 2800 – 6200Å is given in a temperature range from 0° to 77° for CCl_4 and from −3 – 53°C for $CHCl_3$.

The present work is a continuation of the work [1, 2] . It is devoted to the study of CCl_4 and $CHCl_3$, widely used as solvents. We have perfected the apparatus somewhat.

1. THE CELL.

The previously employed cell suffered from the shortcoming of too large a "dead" space of the liquid. This shortcoming has been removed in the cell shown in figure 1. The whole cell is made of high quality silica glass transparent to U. V. It consists of the body of the cell 1 , a silica glass spacer 2 and a silica glass cover 3 . The body of the cell has two openings provided with silica glass tubes cemented into these openings. One of them is used to pour in the solution to be measured, the second as an air exit. The spacer 2 is cemented with an insoluble substance to the cell body and the cover 3 is glued on. A measuring silica glass block 4 is inserted within the cell, before the cover is set on.

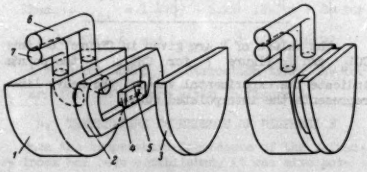

Figure 1.

The Silica Glass Cell

On the left is given the schematic view, on the right- the external view. 1- the body of the cell; 2- the spacer; 3- cover; 4- measurement block; 5- the working face of the measurement block; 6- the input tube connected with the cell body; 7- a tube for air exit.

2. THE MEASURING BLOCK.

The measuring block (fig. 2) is made of the same plane-parallel silica plate as in the paper [1, 2] . A bundle of light falls normally on the faces a and a' and grazes the interface ABCD , perpendicular to the faces a and a' . The face c forms an angle of about 45° with the face a ; thus the faces a and c form a prism bending the ray towards the base, if $\mu_{liquid} < \mu_{block}$ and upwards, if $\mu_{liquid} > \mu_{block}$ (here the letter μ designates the index of refraction.)

A ray of light passing through the face c and a ray deflected by the face c , on being superimposed gave interference bands. This interference pattern could easily be seen by illuminating the block with white light and throwing the shadows (see fig. 3) cast by the block onto the slit of the spectroscope, situated perpendicular to the edge CD of the block. In figure 3 the wave length increases from right to left.

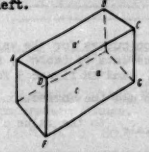

Figure 2. The Measuring Block

(Explanations in the text.)

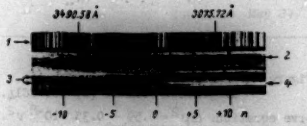

Figure 3. The shadow from the measuring block, illuminated by white light, cast onto the slit of the spectograph and spread into a spectrum.

1- Fe spectrum; 2- Shadow of the face ABCD; 3- Shadow of the face c ; 4- A ray, bent by the face c towards the liquid.

The slit was placed vertically; the dark band is the shadow of the face c, spread into a spectrum. The light band crossing this dark band at $\lambda = \lambda_0$ corresponds to the ray deflected by the dihedral angle with the edge FG . The interference bands are visible on this light band. At $\lambda = \lambda_0$ the refractive index of the liquid is equal to the refractive index of the fused silica glass, at $\lambda > \lambda_0$, $\mu_{liqu.} < \mu_{SiO_2}$ at $\lambda < \lambda_0$, in turn, $\mu_{liqu.} > \mu_{SiO_2}$.

The chain of oval spots 2 in figure 3, is the Fresnel diffraction image of the ray grazing the face ABCD, which has been often described [3,4]. The average interval between two dark spots corresponds to that wavelength, for which

$$(1) \qquad \mu_{liqu.} - \mu_{SiO_2} = n\frac{\lambda}{d}$$

where n - is a whole number, d - the thickness.

Since the λ for n = 0 is known, we can construct the whole dispersion curve by means of the diffraction picture. We interpolated the experimentally obtained values with the help of a formula of the Sellmeyer type with three constants

$$\mu^2 = A + \frac{B}{\nu_0^2 - \nu^2}.$$

The values A, B and ν_0^2 for $t = 20°$ are given in table 1:

TABLE 1

Substance	A	B (in 10^9 cm^{-2})	$\nu_0^2 \cdot 10^{-9}$ (in cm^{-2})	Interpolation limits
CCl_4	1.3507$_4$	4.236$_5$	5.786	6.2—2.8 · 10^{-3} cm
$CHCl_3$ . . .	1.2729$_5$	4.979$_4$	6.396	6.2—2.80 · 10^{-3} cm

The correction curves for the values μ^2, calculated from the data of table 1, are given in figure 4 for CCl_4 and in figure 5 for $CHCl_3$.

It is necessary to add the correction $\Delta\mu^2 = \mu^2_{meas.} - \mu^2_{calc.}$ to the value μ^2.

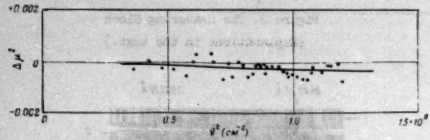

Figure 4. The correction curve for the dispersion formula (2) for CCl_4.

The curve equation: $\Delta\mu^2 = 0.59 - 0.35 \cdot 10^{-8} \nu^2$.

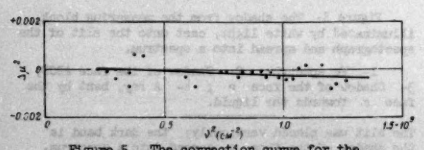

Figure 5. The correction curve for the dispersion formula (2) for $CHCl_3$.

The curve equation: $\Delta\mu^2 = 0.73 - 0.22 \times 10^{-8} \nu^2$.

3. TEMPERATURE DEPENDENCE OF THE REFRACTIVE INDEX AND THE DISPERSION

Among spectroscopists, the opinion is widely held neither theoretically nor experimentally confirmed, that the dispersion is much less dependent on temperature than the index of refraction. The measurements of Rinne [5] on the temperature behaviour of the refractive index of silica glass could be a confirmation of this opinion from which it follows that the dispersion curve within the measurement limits of λ from 4360 to 6563 Å is shifted parallel to itself when the silica glass is heated from 0 to 800°. It has been shown in the papers [1, 2] that with a 2° change in the temperature, the dispersion curves of hydrocarbons investigated in these papers, are displaced parallel to themselves. It has been shown, in the work [6], that in the interval for λ from 4340 to 6363 Å the dispersion curve $\mu(\lambda)$ changes slope for some organic compounds, for other compounds the dispersion curve is shifted parallel to itself. As will be shown later, the dispersion curve is also shifted parallel to itself for CCl_4 and $CHCl_3$.

In the beginning we measured, by means of an apparatus described in [7], the temperature change of the quantity n in formula (1) at a fixed wavelength $\lambda = 5461$ Å, and then, on the basis of the performed measurements, we calculated the change in μ with temperature. The quantity n is approximately a linear function of the temperature. Only few deviations from a straight line were observed on a graph but they existed. Therefore, we expressed them as a curve of the correction to the formula, giving a linear dependence between t and n,

$$t = -pn + t_0 - \tau. \tag{3}$$

The coefficients p and t_0 are given in table 2.

TABLE 2

Substance	p (in °t)	t_0 (in °C)	Temperature interval (in C)
CCl_4 . .	+ 0.825	17.40	0—+77
$CHCl_3$ . .	+ 0.812	— 0.46	−3—+53

TABLE 3

Substance	a'	b'
CCl_4 . .	+4.08 · 10^{-2}	−8.22 · 10^{-4}
$CHCl_3$ . .	−2.9 · 10^{-4}	−8.32 · 10^{-4}

The values of τ are given in figure 6 for CCl_4 and in figure 7 for $CHCl_3$; the points indicate the experimental values, the heavy line represents the interpolated curve.

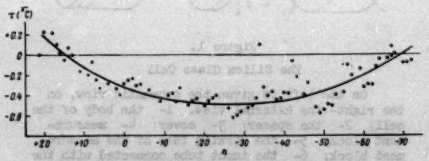

Figure 6. The function $\tau(n)$ for CCl_4.

To formula (3). The points designate experimentally obtained values.

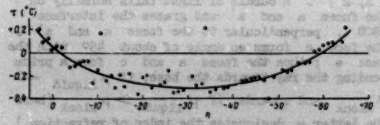

Figure 7. The function τ (n) for $CHCl_3$.

To formula (3). The points designate experimental values.

From formulas (1) and (3) it is easy to obtain the temperature dependence of μ_{liqu} (for λ 5461 Å) in the form

$$(4) \qquad \mu_{liqu.} = \mu_{SiO_2} + a' + b' t + \Delta\mu ,$$

where

$$(5) \qquad b' = -\frac{\lambda}{pd} , \quad a' = \frac{t_0\lambda}{pd} , \quad \Delta\mu = -\frac{\tau\lambda}{pd} .$$

In our case $d = 1.063_5 \cdot 10^{-1}$ cm, $\lambda = 5461$ Å, $\mu_{SiO_2} = 1.4601$ for $t = 20^o$, $\frac{d\mu_{SiO_2}}{dt} = 1 \cdot 10^{-6}$ (from the paper [8]). The values for the coefficients from the formula (4), calculated on the basis (5), are given in table 3 .

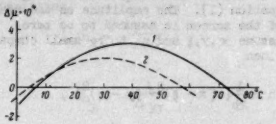

Figure 8. Correction Curves to formula (4).
1 - for CCl_4; 2 - for $CHCl_3$.

Thus, $\mu_{liqu.} = 1.4709 - 6.22 \cdot 10^{-4} t + \Delta\mu$ for CCl_4 for $\lambda = 5461$ Å and $\mu_{liqu} = 1.4598 - 6.32 \cdot 10^{-4} t + \Delta\mu$ for $CHCl_3$. Correction terms $\Delta\mu$ for CCl_4 and for $CHCl_3$ are given in figure 8.

4. TEMPERATURE DEPENDENCE OF DISPERSION

Once the temperature dependence of the refractive index had been established, it was also possible to determine the temperature dependence of dispersion.

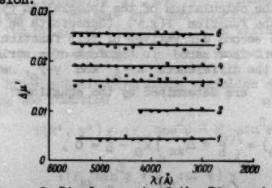

Figure 9. Displacement of the Dispersion Curve of CCl_4 with temperature change.
Temperature (in °C): 1- 26.8, 2- 36.7, 3- 46.9, 4- 52.4, 5- 60.0, 6- 63.5.

The values μ (for λ 5461 Å) have been calculated with the above values of the coefficients a' and b' and the correction curve; from these values of μ the whole dispersion curve was constructed. In figures 9 and 10 there is shown the dependence of $\Delta\mu = \mu(19.0^o) - \mu(t)$ on the wavelength for CCl_4 and $\Delta\mu = \mu(20.2^o) - \mu(t)$ for $CHCl_3$, respectively.

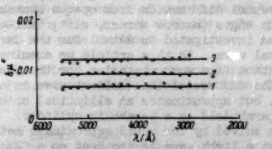

Figure 10. Displacement of the Dispersion Curve of CCl_3 with temperature change.
Temperature (in °C): 1- 80.7, 2- 34.7, 3- 39.0.

It can be assumed that the dispersion curve for these substances shifts with a temperature change parallel to itself.

May 29, 1958

References

1. I. V. OBREIMOV, T. N. SHKURINA: IAN USSR FS, 17, 757 (1953)
2. I. V. OBREIMOV, T. N. SHKURINA: IAN USSR OKhN, 890 (1955) (See CB Bulletin p. 805)
3. I. V. OBREIMOV: O prilozhenii frenelevoi difraktsii dlia fizicheskikh i tekhnicheskikh izmerenii (On the use of Fresnel diffraction for physical and engineering measurements) Akad. Nauk Press, 1945
4. I. V. OBREIMOV: Tr. GOI, 24, No. 147 (1957)
5. R. B. SOSMAN: The properties of silica. The Chem. Catalog Co. N.Y., 1927
6. G. D. GAL'PERN, L. A. KONOVALOVA, M. M. KUSAKOV: Tr. Inst. nefti AN USSR, 1, No. 2, 223 (1950)
7. A. N. NIKITINA, I. V. OBREIMOV: IAN USSR FS, 14, 557 (1950)
8. I. V. OBREIMOV: ZETF, 16, 253 (1946)

TOM, VI, Vyp. 4 OPTIKA I SPEKTROSKOPIIA Aprel', 1959
VOL. VI, No. 4 OPTICS AND SPECTROSCOPY April, 1959

Fresnel Diffraction of a Non-spherical Wave by a Narrow Screen, a Slit and a Half-plane

V. S. SUKHORUKIKH

Abstract: An approximate method for solving diffraction problems, based on Huygens' concepts, is applied to the problem of Fresnel diffraction from a narrow screen, a slit and a half-plane for a non-spherical incident wave. Certain characteristics of these diffraction phenomena are determined. Basic data obtained from calculations are checked experimentally.

Fresnel diffraction from opaque obstacles with straight edges (narrow screen, slit, half-plane) has been investigated in detail for the case of a spherical wave. In this article we examine Fresnel diffraction from such obstacles for the case in which the surface of the incident wave is not a sphere, but approximates an elliptical or hyperbolic paraboloid or a parabolic cylinder. The problem is solved by the usual approximate methods.

1. Let a light wave be incident on a flat opaque screen. (Fig. 1).

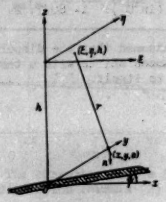

Figure 1

The amplitude of this light wave, in the plane passing through the rear surface of the screen (the xOy plane of the rectangular coordinate system xyz), for free wave-propagation is determined by the relation:

$$v(x,y)=\exp\left[i\frac{2\pi}{\lambda}\Delta(x,y)\right], \tag{1}$$

where

$$\Delta(x,y)=\frac{\Delta_{xx}}{2}x^2+\frac{\Delta_{yy}}{2}y^2 \tag{2}$$

is a function describing the phase distribution in the xOy plane.

We wish to determine the light intensity at points in a plane located behind the screen at a distance z=h ($h>0$). The abscissae and ordinates of these points will be designated by ξ and η.

According to the approximate diffraction theory based on Huygens' concepts we have [1].

$$v(\xi,\eta,h)=-\frac{i}{\lambda}\int\frac{\exp\left(i\frac{2\pi}{\lambda}r\right)}{r}\cos(n,r)v(x,y)\,dx\,dy, \tag{3}$$

where $v(\xi,\eta,h)$ is the amplitude of the wave in the plane $z=h$; r is the distance from the point (ξ,η,h) to the point $(x,y,0)$; (n,r) is the angle formed by the outer normal to the surface of integration and the straight line from the point (ξ,η,h) to the point $(x,y,0)$. The integration is performed over the region σ, which is the part of the plane xOy not covered by the opaque screen. The amplitude of the wave in this part of the plane is assumed to be equal to the right side of the equation (1). The amplitude on the rear surface of the screen is assumed to be zero.

We assume x, y, ξ and η to be small compared with h. Then

$$r=h+\frac{1}{2h}\left[(x-\xi)^2+(y-\eta)^2\right], \tag{4}$$

$$\frac{\cos(n,r)}{r}=\frac{1}{h}.$$

Substituting (1), (2) and (4) into (3) we find:

$$v(\xi,\eta,h)=\frac{\exp(iC)}{\lambda h}\int_{\sigma}\exp\left[i\frac{2\pi}{\lambda}F(x,y)\right]dx\,dy \tag{5}$$

where

$$F(x,y)=\frac{1}{2}\left(\frac{1}{h}+\Delta_{xx}\right)x^2+\frac{1}{2}\left(\frac{1}{h}+\Delta_{yy}\right)y^2-\frac{\xi}{h}x-\frac{\eta}{h}y. \tag{6}$$

For the calculation of the integral in (5) let us write the function F(x,y) (henceforth we will assume the second derivatives of this function to be different from zero) in the form of a series in powers of the differences $x-x_0$ and $y-y_0$, where x_0 and y_0 are determined by the equations:

$$F_x(x_0)=\left(\frac{1}{h}+\Delta_{xx}\right)x_0-\frac{\xi}{h}=0,$$
$$F_y(y_0)=\left(\frac{1}{h}+\Delta_{yy}\right)y_0-\frac{\eta}{h}=0. \tag{7}$$

Making use of the series expansions thus obtained, we have:

$$v(\xi,\eta,h)=\frac{\exp(iC_1)}{\lambda h}\int_{\sigma}\exp\left(i\frac{\pi}{\lambda}\left[F_{xx}(x-x_0)^2+F_{yy}(y-y_0)^2\right]\right)dx\,dy. \tag{8}$$

The right sides of the equations

$$F_{xx} = \frac{1}{h} + \Delta_{xx}, \tag{9}$$

$$F_{yy} = \frac{1}{h} + \Delta_{yy}$$

contain second derivatives of the function $\Delta(x\,y)$; we will consider the first derivatives of this function to be small in the region of the plane xOy not covered by the screen. Under this assumption, the equation

$$z = -\Delta(x, y) \tag{10}$$

can be taken as the equation of the envelope of the wave near the indicated part of the plane xOy, and the quantities

$$h_x = -\frac{1}{\Delta_{xx}} \tag{11}$$

and

$$h_y = -\frac{1}{\Delta_{yy}}$$

can be taken as the z-axis of the centers of curvature of the principal normal sections going through the top of the wave envelope. The condition applied above to the function $F(x,y)$ (i.e. that its second derivatives be different from zero) thus means that the plane $z = h$ does not pass through the centers of curvature of the principal normal sections. Equations (7) thus acquire a graphical meaning: they are the equations which establish the relationship between the points of planes xOy and $z = h$ required by geometrical optics.

Let us choose as a screen in the plane xOy a narrow screen of width d. The center of the screen passes through the origin; the sides form the angle ψ with the axis Ox.

Calculation of the integral (8) is performed for this screen position by introducing new integration variables x' and y'. These are the abscissa and ordinate of a new coordinate system with its origin at (x_o, y_o); this system is rotated through the angle ψ with respect to the old system.

After substituting these variables and introducing the function

$$f(x', y') = (F_{xx}\cos^2\psi + F_{yy}\sin^2\psi)\,x'^2 \tag{12}$$

$$+(F_{xx}\sin^2\psi + F_{yy}\cos^2\psi)\,y'^2$$

$$+ 2(F_{yy} - F_{xx})\sin\psi\cos\psi\,x'y',$$

we obtain, instead of (8), the equation

$$v(\xi,\eta,h) = \frac{\exp(ikl)}{\lambda h}\left[\int_{-\infty}^{\infty}\int_{-\infty}^{y'_0-\frac{d}{2}} \exp\left[i\frac{\pi}{\lambda}f(x'y')\right]dx'dy' + \int_{-\infty}^{\infty}\int_{y'_0+\frac{d}{2}}^{\infty} \exp\left[i\frac{\pi}{\lambda}f(x',y')\right]dx'dy'\right]. \tag{13}$$

where y'_o in formula (13) is the ordinate of the center of the strip. The integration is carried out over the whole region of the plane xOy not covered by the screen. This is permissible in spite of the assumption about the region of integration being small [2].

Two different distributions of light intensity can occur, depending whether or not the plane $z = h$ passes through the center of curvature of the normal section forming the angle ψ with the xOy plane in the top of the wave surface:

a) The plane $z = h$ does not pass through the center of curvature of the normal section $O\psi$: In this case

$$\frac{1}{h} \neq \frac{\cos^2\psi}{h_x} + \frac{\sin^2\psi}{h_y},$$

and consequently the coefficient for x'^2 in equation (12) is not zero.

After calculating the integrals in formula (13), we obtain the following expression for the light intensity in the plane $z=h$:

$$I(\xi,\eta,h) = \frac{1}{2}\cdot\frac{|h_x h_y|}{|h-h_x|\,|h-h_y|}\left[\left(1 - \int_{u_1}^{u_2}\sin\frac{\pi}{2}t^2dt\right)^2 + \left(1 - \int_{u_1}^{u_2}\cos\frac{\pi}{2}t^2dt\right)^2\right] \tag{14}$$

where

$$u_{1'2} = (y'_o \mp \frac{d}{2})\sqrt{\frac{2}{\lambda}\cdot\frac{|h-h_x|\,|h-h_y|}{h|h_x|\,|h_y|\,|1 - h\left(\frac{\cos^2\psi}{h_x} + \frac{\sin^2\psi}{h_y}\right)|}}. \tag{15}$$

From formulas (14), (15), and (7), it follows that the light intensity in the plane $z = h$ is constant along lines having the slope

$$k = \operatorname{tg}\psi\,\frac{(h-h_y)h_x}{(h-h_x)h_y}. \tag{16}$$

The line passing through the axis Ox is the symmetry axis of the diffraction pattern.

Let us designate the distance between the point (ξ,η) and the symmetry axis of the diffraction pattern by the letter l, taken with a definite sign. Geometrical optics establishes the following relation between the quantities l and y'_o :

$$y'_o = l\sqrt{\left(\frac{h_x}{h-h_x}\right)^2\sin^2\psi + \left(\frac{h_y}{h-h_y}\right)^2\cos^2\psi}. \tag{17}$$

Substituting the right side of this equation for y'_o in (15) we obtain :

(18)
$$u_{1,2} = \mp d \sqrt{\frac{1}{2\lambda} \cdot \frac{|h-h_x||h-h_y|}{h|h_x||h_y|\left|1-h\left(\frac{\cos^2\psi}{h_x}+\frac{\sin^2\psi}{h_y}\right)\right|}} + \sqrt{\frac{2}{\lambda} \cdot \frac{(h-h_x)^2 h_y^2\cos^2\psi + (h-h_y)^2 h_x^2 \sin^2\psi}{h|h_x||h_y||h-h_x||h-h_y|\left|1-h\left(\frac{\cos^2\psi}{h_x}+\frac{\sin^2\psi}{h_y}\right)\right|}}\,.$$

One can see from formulas (14) and (18) that the diffraction patterns described by these coincide with the well-known Fresnel diffraction patterns from a narrow screen for an incident spherical wave. The form of the diffraction pattern depends on the numerical value of the first term in equation (18). Diffraction patterns with the same value of this term are geometrically similar. The width of the diffraction pattern is proportional to the square root of the wavelength of the light and to the square root of the quantity

$$\frac{h|h_x||h_y||h-h_x||h-h_y|\left|1-h\left(\frac{\cos^2\psi}{h_x}+\frac{\sin^2\psi}{h_y}\right)\right|}{(h-h_x)^2 h_y^2\cos^2\psi + (h-h_y)^2 \sin^2\psi}\,.$$

We obtain similar results if we investigate diffraction patterns from slits and half-planes.

b) The plane $z = h$ passes through the center of curvature of the normal section C_ψ.

Consequently

(19)
$$\frac{1}{h} = \frac{\cos^2\psi}{h_x} + \frac{\sin^2\psi}{h_y}\,,$$

and the coefficient for x'^2 in equation (12) is equal to zero.

In this case calculation of the integrals from formula (13) gives us the equations

$$I = \frac{|h_x h_y|}{|h-h_x|\,|h-h_y|}$$

for $I(\xi,\eta,h)$ at points in the $z = h$ plane lying outside the geometrical shadow; this is the light intensity for free wave propagation and $I = 0$ at points of the $z = h$ plane lying inside the geometrical shadow.

Thus, according to our calculation, if we move the plane $z = h$ so that it passes through the center of curvature of the normal section C_ψ, then the Fresnel diffraction pattern in the plane $z = h$ reduces to the geometrical shadow.

Let us note that this deduction can be made directly from formula (18), without calculating the integrals in (13). Actually, for

$$\frac{1}{h} \longrightarrow \frac{\cos^2\psi}{h_x} + \frac{\sin^2\psi}{h_y}$$

the denominator of the expressions under the root in this formula tends toward zero, which also occurs for $\lambda \to 0$, i.e. in the transition to geometrical optics.

The width of the geometrical shadow is determined from (17) and (19). It equals :

(20)
$$D = d\sqrt{\frac{|h-h_x||h-h_y|}{|h_x h_y|}}$$

The angle between the geometrical shadow and the screen is a right angle, as follows from (16) and (19).

Substitution of a slit or a half-plane for the narrow screen does not change the result. According to our calculation, each of these obstacles also casts a geometrical shadow which is perpendicular to its edge.

2. The experimental part of this work was performed with an arrangement which allowed us to observe the diffraction of an incident spherical wave. In order to obtain a cylindrical wave we used a collimator and a special cell. The collimator consisted of a meniscus system 230 mm in diameter, with a focal length of 1917 mm. An incandescent lamp served as the light source. The width of the collimator slit was 0.02 mm. A filter having its transmission maximum at $\lambda = 5.46 \cdot 10^{-5}$ cm. was placed in front of the slit.

The walls of the cell which transformed the plane waves from the collimator into converging cylindrical waves consisted of a plane-parallel plate and a plano-convex lens of K8 glass with a radius of curvature of 2250 mm. The convex side of the lens faced the inside of the cell. We mounted spacers between the plate and the lens; all parts of the cell were cemented together. The effective width and height of the cell were 200 mm. The cell was filled with water. The radius of curvature of the converging cylindrical waves leaving the cell was 1225 cm. This value was determined by direct measurement of the distance from the last cell wall to the plane of the minimum cross section of the light beam. At a distance of 60 cm from the last cell wall we mounted an opaque screen 5mm wide. The diffraction patterns were photographed on a panchromatic film of type 10-800. The photographic film was mounted 2330 cm from the plane of the screen. The angle between the envelope of the cylindrical wave and the edge of the screen was 25° and 45°. In the latter case, the plane of the photographic film was the plane in which, according to our calculation, the geometrical shadow was expected.

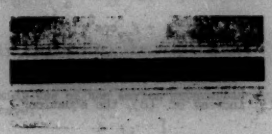

Figure 2. Diffraction pattern from a screen 5mm wide.

$h = 2330$ cm, $h_x = 1165$ cm, $h_y = \infty$, $\psi = 65°$.

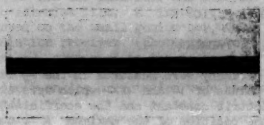

Figure 3. Shadow from a 5mm wide screen observed in a plane passing through the center of curvature of a normal section C_ψ .

$h = 2330$ cm, $h_x = 1165$ cm, $h_y = \infty$, $\psi = 45^\circ$.

Figures 2 and 3 show the photographs obtained. Figure 2 (screen at an angle of 25° to the enveloping surface) shows a typical Fresnel diffraction pattern from a narrow screen. In Figure 3 (screen at an angle of 45° to the enveloping surface) we have no Fresnel diffraction pattern; instead we observe a geometrical shadow.

The experimental results are thus in good agreement with the calculations.

The author takes this opportunity to express his gratitude to I. V. Obreimov for his interest in this work and for much valuable advice.

March 22, 1958

References

1. A. SOMMERFELD: Lectures on theoretical physics. vol. 4. Optics, N.Y., Academic Press, 1956 (IL, Moscow, 1953)
2. M. PLANCK: Introduction to theoretical physics. vol. 4. Theory of light. London, Macmillan Co. 1932 (ONTI, Moscow-Leningrad, 1934)

TOM VI, Vyp. 4 OPTIKA I SPEKTROSKOPIIA Aprel', 1959
VOL. VI, No. 4 OPTICS AND SPECTROSCOPY April, 1959

Measurements of the Optical Constants of Antimony in the Infrared Region of the Spectrum at Temperatures of 290° and 110° K

I. N. SHKLIAREVSKII, A. A. AVDEENKO, AND V. G. PADALKA

Abstract: The indexes of refraction μ and absorption $\mu\chi$ of antimony were measured in the spectral region from 1-12 μ at temperatures of 290° and 110°.* From the values of μ and $\mu\chi$ which were found, the dependence on wavelength of the real and imaginary parts of the dielectric constant and the coefficient A, of energy absorption, was constructed for both temperatures. From the position of the maximum A, the value of the energy gap between zones was calculated.

INTRODUCTION

In a previous work the results of measurements of the optical constants of silver [1], gold, copper, and nickel [2] in the spectral region from 1-12 μ were presented. In these metals in the given region of the spectrum the indexes of refraction μ are significantly smaller than the indexes of absorption $\mu\chi$, and at least for the first three of them the inequality

$$(1) \qquad \nu_0^2 \ll \omega^2 \ll \omega_0^2$$

is satisfied, where ν_0 is the frequency of collision of electrons with the lattice, and ω_0 is the frequency which corresponds to the upper limit of the internal photo-effect.

In some metals (bismuth, antimony) in the region of the spectrum from 1-12 μ the indexes of refraction and absorption are of the same order. In this case the inequality [Eq.(1)] can hardly be satisfied. The optical properties of such metals in the infrared region of the spectrum have scarcely been investigated. Besides, if quantum transitions play a significant role in the absorption of light in this region of the spectrum, then by the position of the maximum of the absorption coefficient one may find the amount of the energy gap between bands.

1. METHOD OF MEASUREMENT

The determination of the optical constants of antimony was done with the help of the method of Avery [3], which consists of measurements of the quantity

$$(2) \qquad \rho^2 = \frac{R_p}{R_s}$$

at two angles of incidence φ. Here R_p and R_s are the coefficients of reflection, polarized, respectively, in and perpendicular to the plane of incidence. A system of two equations was obtained for calculations of the optical constants μ and $\mu\chi$ from the results of the measurements

$$\left.\begin{aligned} \rho_1^2 &= f_1(\mu, \mu\chi, \varphi_1) \\ \rho_2^2 &= f_2(\mu, \mu\chi, \varphi_2) \end{aligned}\right\}$$

which cannot be solved explicitly. The unwieldy calculations, a considerable amount of which are necessary for determination of the optical constants with the help of Avery's original method of calculation, require a large expenditure of time. The problem of finding μ and $\mu\chi$ from measured values of ρ^2 was considerably refined with the solution of Afanas'eva, Noskov, Cherepanov [4]. We also utilized the method of "intersecting circles" of Noskov in calculations of the optical constants of antimony.

Usually the quantity ρ^2 is measured not at two but at three angles of incidence; the third measurement is a check. It is better when one of the angles of incidence is larger than the principal angle, and the two others somewhat smaller.

The described method of measurement of the optical constants we applied to those metals in which $\mu \approx \mu\chi$. The optical constants of antimony satisfy this condition.

2. APPARATUS FOR MEASUREMENTS

The scheme of the apparatus for measurements of the optical constants of metals in the infrared region of the spectrum was presented in an earlier paper [1]. The apparatus used in the present work is no different in principle from that described in reference [1]. The difference is that on the small goniometer table instead of two samples located parallel to each other, in the latter case one sample was located inside the cryostat. A photograph of the apparatus is presented in Figure 1.

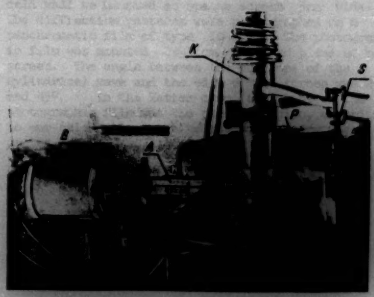

Fig. 1. External View of the Apparatus
S - Monochromator Slit; P - Polarizer; A - Analyzer
K - Cryostat; B - Receiver of Radiation.

* Here and in the future temperatures are given in degrees Kelvin.

Here S is the slit of the ZMR-2 monochromator P and A are the polarizer and analyzer stops of free selenium film, K is the cryostat, rigidly mounted on the small goniometer table, B is the radiation receiver (photoconductor) or (bolometer) connected to the mochromator. The selenium stops are easily revolved around their axes; their angles or rotation were measured with a precision of 2' with the help of the limb. The polarizer was fastened to the fixed arm of the goniometer, and the analyzer and radiation receiver to the rotating arm. The angle of rotation of the radiation receiver could be measured with a precision of 3' .

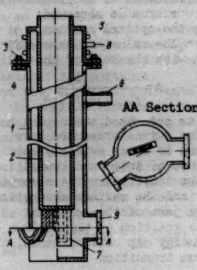

Fig. 2. The Cryostat

1 - Outer Cylinder; 2 - Inner Cylinder; 3 - Screws 4 - Rubber Gasket; 5 - Coil; 6 - Tap; 7 - Tap with Channels; 8 - Opening for insertion of the Thermocouple; 9 - Window.

In figure 2 is presented a schematic diagram of the cryostat which consists of external 1, and internal 2, cylinders fastened together with the help of screws 3. The rubber gasket 4 serves as a vacuum seal. The upper part of the cryostat was warmed by the coil 5 (seen in fig. 1), through which running water was passed. The space between the cylinders 1 and 2 was pumped out to a high vacuum through the tap 6. After the evacuation a vacuum rubber tube was put on the tap and the clamp was tightened. To the bottom of the inside cylinder 2 was welded a tap 7 , in the body of which were drilled channels; thus, the cooling liquid directly washed the wall of the tap. Clamped to the tap, the sample -a glass plate with antimony precipitated on it- was placed approximately in the center of the outer vessel (see section AA , figure 2). The temperature of the outer surface of the sample was measured with the help of a thermocouple, brought out of the cryostat through the opening 8 . On the outer cylinder on a level with the tap were placed two windows 9 , covered by plane parallel plates of sylvite. The sylvite plates were glued to the frame of the window with vacuum putty. In order to avoid fogging of the plates the body of the window was warmed with the help of a nichrome spiral to temperatures somewhat above room temperature.

The goniometer table, on which the cryostat was fastened (fig. 1) , was provided with a special carriage and three adjusting screws. During the alignment of the apparatus the sample was set exactly vertical with the help of the adjusting screws, and with the help of the carriage - exactly in the center of the goniometer.

3. ADJUSTMENT OF THE APPARATUS AND THE TECHNIQUE OF MEASUREMENT

The alignment of the system was a very crucial stage of the work, since poor execution of it might introduce significant errors. It was convenient to proceed in two stages: first, to adjust the stops, and then to adjust the sample. Usually the free selenium film would deteriorate and have to be replaced after 3-4 months. Hence, the installation and adjustment is done comparatively seldom. However, before every series of measurements it should be checked and in case it is necessary done anew.

The polarizer was placed such that one of its principal directions formed an angle $\psi_P = 45°$ with the plane of incidence. If now for a straight path of light the analyzer is next placed so that the angle ψ_A would equal 0, 90, 180, and 270° , then with the correct adjustment of the stop the intensity of light, passing through the analyzer in all these cases, must be equal. If the stop analyzer was placed incorrectly then the beams passing through it in some positions will be cut and the mentioned intensities turn out to be unequal. The correctness of the adjustment of the polarizer may be checked by placing it at an angle $\psi_P = -45°$. The relation of the intensity of light transmitted by the analyzer must not be changed here.

The second part of the adjustment -the installation of the sample- is no less crucial. The results of the measurements may be very strongly distorted if the sample is not installed vertically and exactly in the center of the goniometer. The correctness of its installation is easily checked at the time of conducting the measurements: the intensity of the passing light must not change when the analyzer is turned 180° .

For carrying out the measurements of the quantity ρ^2 by Avery's method, one stop was sufficient. However, at the same time corrections had to be introduced, connected with the fact that partially polarized light usually issued from the monochromator. Corrections were determined experimentally for every wavelength at which measurements of the optical constants were made, and naturally, these corrections may serve as an additional source of error. We eliminated the necessity of introducing corrections by placing on the slit of the monochromator a polarizer fixed at the angle $\psi_P = 45°$

The optical constants of antimony were determined by three values of the quantity ρ^2 measured at angles of incidence equal to 70, 77, and 87°. After measurement of ρ^2 at room temperature liquid oxygen was put into the cryostat. Measurements of the quantity ρ^2 at low temperatures were done at the very same adjustment of the apparatus. The temperature of the layer of antimony was about 20° higher than the temperature of the liquid oxygen.

As was shown by a specially carried out

investigation, the sylvite plates which cover the window of the cryostat, do not introduce significant distortions in the results of the measurements; the light beam entering and leaving the cryostat fell almost normal to the surface of the plate.

To obtain a layer of sufficient thickness of antimony by vacuum precipitation on a clean glass surface was difficult because of recrystallization. Very good layers of antimony several microns thick were easily obtained by precipitation on a glass surface, which was first covered with a thin film of silver (100-150 A°). Such layers are opaque over all the investigated region, at least with an accuracy of 10^{-2}%.

4. RESULTS OF THE MEASUREMENTS

Measurements of the optical constants of antimony were made on four samples and gave very reproducible results. The values of the optical constants found in the various samples differ by no more than 5-8%. Control measurements, carried out by other methods [5], gave analogous results.

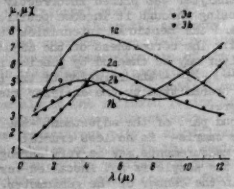

Fig. 3. Dependence of the indexes of refraction (a) and absorption (b) of antimony on wavelength. Temperatures (in °K) 1 - 290°, 2 - 110°, 3-room temperature for $\lambda = 2.45\mu$ according to Domanskii and Noskov.

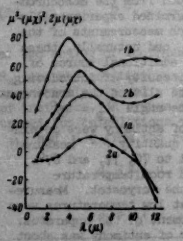

Fig. 4. Dependence of the real (a) and imaginary (b) part of the complex dielectric constant on wavelength. Temperature (in °K) 1-290°, 2-110°.

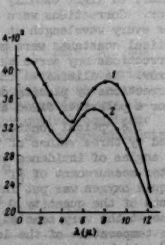

Fig. 5. Dependence of the energy coefficient of absorption on wavelength. Temperature (in °K) 1-290°, 2-110°.

In figure 3 is presented the dependence we found of the indexes of refraction and absorption of antimony on wavelength in the range from 1 to 12μ, at temperatures of 290° and 110°. Here also are given values of μ and $\mu\chi$ for antimony (points 3a and 3b) obtained at room temperature ($\lambda = 2.45\mu$) by Domanski and Noskov [6].

The dependence of the real $[\mu^2-(\mu\chi)]$ and imaginary $[2\mu(\mu\chi)]$ parts of the complex dielectric constant $\tilde{\varepsilon}$ on wave length was constructed from the sverage values of the optical constants at 290° and 110°. This dependence is presented in figure 4. With falling temperature a decrease of the quantity $\tilde{\varepsilon}$ and a displacement of the maximum to the long wave part of the spectrum is observed.

Knowing the optical constants μ and $\mu\chi$, one can calculate the value of the coefficient of energy absorption A with the help of the well-known formula

$$A = \frac{4\mu}{(\mu+1)^2+(\mu\chi)^2} \tag{3}$$

In figure 5 is presented the dependence $A = f(\lambda)$ for antimony. The curves presented have very evident maxima, which, it seems evident, should be ascribed to the presence of interband transitions. With a reduction of the temperature the absorption coefficient A increases, and the maximum absorption is shifted to the long wave part of the spectrum.

From the position of the maximum of A the quantity of the energy gap between bands, which corresponds to the quantum transition

$$\Delta E = \frac{hc}{\lambda} \tag{4}$$

where h is Planck's constant c is the speed of light and λ is the wavelength of maximum absorption. At room temperature the maximum of the absorption coefficient is 6.9 μ, and at a temperature of 110° - at 8.1μ. The values of ΔE at these temperatures equals 0.18 and 0.15 eV respectively. As shown in [7], layers of antimony precipitated in vacuum at room temperature are characterized, according to Moss, by a spacing between bands ΔE in the range from 0.05 to 0.20 eV.

The author wishes to take this opportunity to express hearty thanks to K. D. Sinel'nikov for kindness and interest in the work.

May 19, 1958

References

1. I. N. SHKLIAREVSKII, N. G. STARUNOV, V. G. PADALKA: OiS, 4, 792 (1958)
2. I. N. SHKLIAREVSKII, V. G. PADALKA: OiS, 6, 78 (1959) (See this journal, p. 45)
3. D. G. AVERY: Proc. Phys. Soc. B65, 425 (1952)
4. L. A. APANAS'EVA, M. M. NOSKOV, V. I. CHEREPANOV: FMM, 1, 566 (1955)
5. I. N. SHKLIAREVSKII, V. K. MILOSLAVSKII: OiS, 3, 361 (1957)
6. E. I. DOMANSKII, M. M. NOSKOV: FMM, 1, 567 (1955)
7. R. A. SMITH: Adv. Phys., 2, 321 (1953)

TOM VI, Vyp. 4 OPTIKA I SPEKTROSKOPIIA Aprel', 1959
VOL. VI, No. 4 OPTICS AND SPECTROSCOPY April, 1959

On the Influence of Thin Films on Total Reflection

P. G. KARD

Abstract: A theoretical analysis is made of the influence of a multilayer film between two media on the phase shift occuring in total (internal) reflection at the boundary of these media. A basic recurrence formula, convenient for numerical calculations, is derived. As an example a calculation is done for a one-layer and a two-layer film which in a broad spectral interval reduces to a minimum the difference in phase shifts of the components polarized in directions parallel to and normal to the plane of incidence.

In this article we are interested in the possibility of changing the amplitude coefficient of total (internal) reflection with the aid of multilayer films. The problem is of interest since total reflection plays an important role in a wide range of applications in which not only the energy coefficient of reflection but also the amplitude coefficient of reflection (i.e. the phase shift) is sometimes of substantial importance.

We know that the phase shift in total reflection depends on the angle of incidence and the relative index of refraction, and also on the polarization of the incident light. Let the light, which is polarized in directions parallel to and normal to the plane of incidence (super-scripts $\parallel$ and $\perp$) pass from the medium with index of refraction n to the medium having the smaller index of refraction n_o, and be incident on the boundary at an angle φ so that the condition for total reflection is fulfilled

$$n \sin \vartheta > n_o \tag{1}$$

The amplitude coefficient of reflection can be written in the form

$$r_o = \exp\left[-i\psi_o\right] \tag{2}$$

where ψ_o depends on the polarization as follows:

$$\tan\frac{\psi_o^{\parallel}}{2} = \frac{n\sqrt{n^2\sin^2\vartheta - n_o^2}}{n_o^2\cos\vartheta}, \tag{3}$$

$$\tan\frac{\psi_o^{\perp}}{2} = \frac{\sqrt{n^2\sin^2\vartheta - n_o^2}}{n\cos\vartheta}. \tag{4}$$

Let us assume that between two given media we have a thin film consisting of one or several transparent isotropic layers. Then, if the angle of incidence is the same as before, we will still have total reflection but the amplitude coefficient of reflection will be changed. The magnitude of the phase shift depends on the parameters of the film. In this publication we will derive a basic recurrence formula for the calculation of such layers and we will apply it to the solution of one particular problem.

Let us use the following notation: Let the lamina between the media consist of N layers having the indexes of refraction $n_1, n_2, \ldots, n_N$ (counting from the medium with index n_o, i.e. in the direction opposed to that of the incident light). Let us assume that

$$n \sin \vartheta < n_m, \quad m = 1, 2, \ldots N, \tag{5}$$

i.e. let none of the layers cause total reflection.* Furthermore, let k be the wave number in vacuu; h_m the thickness of the m^{th} layer; ϑ_m the angle of refraction in this layer and

$$\delta_m = kn_m h_m \cos\vartheta_m. \tag{6}$$

Finally, let us designate by ρ_m the amplitude coefficient of reflection at the boundary between the $(m+1)$ th and the m^{th} media [the initial medium is the $(N+1)$th]; and by $e^{-i\Psi_m}$ the amplitude coefficient of reflection for the light traveling at an angle ϑ_m from the m-th medium to the zero-th medium through the $(m-1)$-layer lamina, consisting of the first $m-1$ layers; and the amplitude reflection coefficient of the whole system by

$$r_N = \exp.\left[-i\Psi_N\right] \tag{7}$$

(obviously $\psi_N \equiv \varphi_{N+1}$). All these amplitude coefficients depend upon the polarization. Let us also introduce the auxiliary quantity

$$y_m = \frac{1-\rho_m}{1+\rho_m}, \quad m = 1,2, \ldots N, \tag{8}$$

where according to Fresnel's formulas

$$\left.\begin{aligned} y_m^{\parallel} &= \frac{\sin 2\vartheta_m}{\sin 2\vartheta_{m+1}}, \\ y_m^{\perp} &= \frac{\tan\vartheta_m}{\tan\vartheta_{m+1}}. \end{aligned}\right\} \tag{9}$$

In order to derive the recurrence formula which we need let us first investigate the case of one layer ($N = 1$). The simplest way to calculate r_1 is by using Vlasov's method [1] i.e. to take into account multiple reflections in the layer. Thus, in conformity with our notation we have:

$$r_1 = \exp\left[-i\Psi_1\right] = \frac{\rho_1 + \exp[i(2\delta_1 - \varphi_1)]}{1 + \rho_1\exp[i(2\delta_1 - \varphi_1)]} \tag{10}$$

* If we drop this condition, we undoubtedly would widen the possibilities of fulfilling diverse requirements with the aid of thin films; however, in this article we want to restrict ourselves to the simplest case as described in (5).

Let us calculate ψ_1. For this calculation we have from (10)

$$\frac{1 - r_1}{1 + r_1} = i \tan \frac{\psi_1}{2}, \tag{11}$$

$$\frac{1-r_1}{1+r_1} = iy_1 \tan \left(\frac{\varphi_1}{2} - \delta_1 \right). \tag{12}$$

and consequently

$$\tan \frac{\psi_1}{2} = y_1 \tan \left(\frac{\varphi_1}{2} - \delta_1\right) \tag{13}$$

Let us transform to the case of many layers and let us investigate the light traveling from the $(m+1)^{th}$ layer (at an angle ϑ_{m+1}) to the system of the first m layers (the zeroth medium included). Then, assuming the (m-1)-layer film (consisting of the first m-1 layers) to be a simple interface having a reflection index $e^{-i\varphi_m}$, from the m^{th} layer according to our notation, we find

$$\exp [-i\varphi_{m+1}] = \frac{\rho_m + \exp [i (2\delta_m - \varphi_m)]}{1+\rho_m \exp[i (2\delta_m - \varphi_m)]} \tag{14}$$

from which, as above, we obtain

$$\tan \frac{\varphi_{m+1}}{2} = y_m \tan\left(\frac{\varphi_m}{2} - \delta_m\right). \tag{15}$$

This is the recurrence formula we were looking for. Here $m = 1,2,\ldots N$ and $\varphi_{N+1} \equiv \psi_N$. The initial phase shift φ_1 and also all y_m depend upon the polarization; therefore all quantities $\varphi_2, \varphi_3, \ldots \varphi_{N+1} = \psi_N$ calculated successively depend in general on the polarization.

Let us now briefly examine one application of the theory above. We will require that

$$\psi_N^{II} - \psi_N^{I} = 0. \tag{16}$$

Of course, this condition can be fulfilled exactly only for certain wavelengths (since $\delta_1, \delta_2, \ldots \delta_N$ are related to the wavelength through k; here we will neglect dispersion). In addition we will require therefore that the difference $\psi_N^{II} - \psi_N^{I}$ be as small as possible in a given spectral interval. (For instance in the whole visible spectrum).

This problem has already been investigated by Lostis [2]. However, his article contains some inaccuracies and some erroneous conclusions which arose apparently from too complicated a method of calculation. Lostis gives a solution for a single layer* where the required condition $\psi_1^{II} - \psi_1^{I} \simeq 0$ is fulfilled in the interval $4000 \text{ Å} \leqslant \lambda \leqslant 7000 \text{ Å}$ with an accuracy of $\pm \frac{\lambda}{50}$ (i.e. $\sim \pm 7^\circ$). This solution is correct, but we will give another which is simpler and as accurate. Furthermore, we will investigate a two-layer film and we will show that, contrary to Lostis' opinion, it allows fulfillment of the required condition with almost twice the accuracy (a deviation of $\sim \pm 4^\circ$).

First let us investigate the one-layer film. In this case, according to (13), condition (16) leads to a quadratic equation in $\tan\delta_1$, the roots of which are real only when

$$\tan \frac{\varphi_1^{II} - \varphi_1^{I}}{2} \leqslant \frac{\left|n^2 - n_1^2\right|}{2nn_1}. \tag{17}$$

While investigating an analogous quadratic equation, Lostis arrives at the erroneous conclusion that the reality of the roots (in the case $n_o = 1$) requires that the refractive indices be $n \leqslant 1.46$, $n_1 \geqslant 2.6$ ** However, as can be seen from formula (17) where

$$\tan \frac{\varphi_1^{II} - \varphi_1^{I}}{2} = \frac{\cos \vartheta_1 \sqrt{n^2 \sin^2\vartheta - n_o^2}}{n_1 \sin^2\vartheta_1}, \tag{18}$$

this is not the case. Condition (17) can also be fulfilled for $n_1 < n$.

For instance it is fulfilled for $\vartheta = 45^\circ$; $n_o = 1$; $n = 1.8$; $n_1 \leqslant 1.385$. The simplest case is that where one of the equation becomes infinite (i.e. $\delta_1 = \frac{\pi}{2}$) For this case formula (13) gives

$$n_1 = \sqrt{nn_o}. \tag{19}$$

The other root of the equation is then:

$$\tan \delta_1 = \frac{(n + n_o)\sqrt{(n_o - n \sin^2\vartheta)(n^2 \sin^2\vartheta - n_o^2)}}{n[2n_o^2 - n(n+n_o)\sin^2\vartheta]}. \tag{20}$$

If we want condition (16) to be fulfilled approximately also for other wavelengths in a certain spectral interval, then one should choose the values of ϑ, n, and n_o such that two values of δ_1

---

* Lostis expresses the condition (16) in the form $\psi_N^{II} - \psi_N^{I} = \pi$ (in our notation). The reason for this difference is that Lostis uses Fresnel's reflection coefficient in the case of parallel polarization with a sign opposite to that in our article. If one takes this into account then Lostis agrees with us.

** In our notation

fulfilling this condition are separated by an interval sufficiently large but not too large. Without going into the details of a more exact analysis, let us present a numerical example. Let $n_o=1$; $n=1.75$; $\phi=45^\circ$; then $n_1 = 1.323$ and the values of $\psi_1^{II}-\psi_1^{\perp}$ calculated from these data are shown as a function of δ_1 in curve I of the figure. The graph shows that in the interval $76^\circ \leqslant \delta_1 \leqslant 133^\circ$, corresponding in the wavelength scale to the interval $7000\ \text{Å} \geqslant \lambda \geqslant 4000\ \text{Å}$, $|\psi_1^{II} - \psi_1^{\perp}|$ does not exceed 7°.

Let us now investigate the case of a two-layer film. Since in this case the calculation is much more involved let us assume for simplicity that

$$\delta_2=\delta_1$$

Then condition (16) will lead us to an equation of the 4^{th} order in $\tan\delta_1$ which is quite cumbersome. We will confine ourselves to only one numerical example in which the parameters of the film

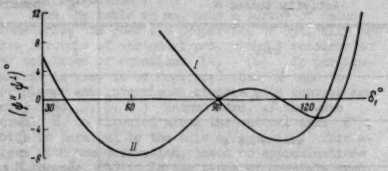

are mostly chosen at random. If we require that one of the solutions be $\delta_1 = \frac{\pi}{2}$ then we find:

$$\frac{n_1}{n_2} = \sqrt{\frac{n_o}{n}}. \tag{21}$$

Besides the point where $\delta_1 = \frac{\pi}{2}$ condition (16) is generally fulfilled for three wavelengths. Let us choose

$$n_1 = \sqrt[4]{n_o^3 n}\,. \tag{22}$$

$$n_2 = \sqrt[4]{n_o n^3}\,.$$

This choice satisfies equation (21) but due to practical considerations does not allow the choice $n_o = 1$. Therefore let us choose $n_o = 1.28$; $n = 1.92$; $\phi = 45^\circ$. Then we obtain $n_1 = 1.416$; $n_3 = 1.735$. The results of the calculation of the difference $\psi_2^{II} - \psi_2^{\perp}$ are shown in curve II of the figure. We can see that in the interval $77.5^\circ \leqslant \delta_1 \leqslant 135.6^\circ$, corresponding to the interval $7000\ \text{Å} \geqslant \lambda \geqslant 4000\ \text{Å}$, the value of $|\psi_2^{II}-\psi_2^{\perp}|$ scarcely exceeds 4° (i.e. $\frac{\lambda}{90}$). Of course we still have the unanswered question whether a further improvement of these results is possible by using just two layers.

In the case of three and more layers the calculation becomes more complicated. Naturally one assumes that the more layers we have the better we can fulfil any conditions established in advance. In any case our formula (15) gives us a convenient method of calculating the phase shifts of a system with given values of parameters.

Finally, let us note that in article [3] the condition $\psi_1^{II} - \psi_1^{\perp} = 0$ is used for the calculation of a light filter with total reflection, having no doublet structure of the transmission band.

April 17, 1958

References

1. A. G. VLASOV, et al.: Prosvetlenie optiki (Enlightenment of optics) Gostekhizdat, 1946
2. M. P. LOSTIS: J. Phys. et Rad., 18, 51S (1957)
3. P. G. KARD: OiS, 6, 389 (1959) (See this journal page 244)

TOM VI, Vyp. 4 OPTIKA I SPEKTROSKOPIIA Aprel', 1959
VOL. VI, No. 4 OPTICS AND SPECTROSCOPY April, 1959

On the Theory of Optical Activity in Crystals

III. General Equation of Normals

B. V. BOKUT' AND F. I. FEDOROV

Abstract: We obtain in invariant form a more general equation of normals for optically active crystals, taking account of magnetic terms. The theory indicates the possibility of three modes of propagation in optically active crystals; the phase velocity of the third mode may be very small compared with the velocity of light.

In two previous papers [1, 2] the phenomenological theory of optically active crystals was developed on an invariant basis for all types of symmetry. For optically active media the connection between the induction vectors $\vec{D}$, $\vec{B}$ and the fields $\vec{E}$, $\vec{H}$, is expressed by the relations [1]:

(1) $\vec{D} = \varepsilon\vec{E} + [\alpha\nabla, \vec{E}]$

(2) $\vec{B} = \mu\vec{H} + [\beta\nabla, \vec{H}]$

where α, β are respectively the electric and magnetic tensors of optical activity. Tensors α, β are real, generally non-symmetric tensors of the second order. A summary of the expressions obtained in [1] for tensors of electric activity α corresponding to all types of crystal symmetry is shown in the Table.

Expressions for the tensors of magnetic activity β are entirely analogous to those for α, differing only by scalar parameters.

Table

Expressions for the Activity Tensors of Optically Active Crystals

Symmetry	No.	Classes	Symmetric elements	Basic vectors	Activity tensor α	Tensor ε	Remarks
Cubic	1	Primitive axial	$4L_3\ 3L_2$ $3L_4\ 4L_3\ 6L_2$	—	$\alpha = a$	$\varepsilon = \varepsilon_0$	
tri-, tetra-, hexagonal	2	Planar	$L_n\ nP$ $(n=3,4,6)$	$e \parallel L_n$	$\alpha = ae^{\times}$ $\quad\lvert\alpha\rvert = 0$	$\varepsilon = \varepsilon_0 + (\varepsilon_0 - \varepsilon_0)\, e \cdot e$	$e^2 = e'^2 = e''^2 = 1,\ e'e'' = e''e = e'e = 0$ $\lvert e_0\rvert = +1,\ \lvert e\rvert = -1$
	3	Axial	$L_n\ nP$ $(n=3,4,6)$	$e \parallel L_n$	$\alpha = a_1 + a_2 e \cdot e$		
	4	Primitive	L_n $(n=3,4,6)$	$e \parallel L_n$	$\alpha = a_1 + a_2 e \cdot e + a_3 e^{\times}$		
	5	Inversion-planar tetragonal symmetry	$L_4 2L_2 2P$	$e \parallel L_4$ $e', e'' \parallel 2L_2$ $e_1, e_2 \perp 2P$	$a = a(e_0 \cdot e_0 + e_0^* \cdot e_0^*) = a(e' \cdot e' - e'' \cdot e'') = a(e_1 \cdot e_2 + e_2 \cdot e_1)$ $e_0 = \frac{1}{\sqrt{2}}(e' + ie''),\ e_1 = \frac{1}{\sqrt{2}}(e' + e''),\ e_2 = \frac{1}{\sqrt{2}}(e' - e'')$ $\quad\lvert\alpha\rvert = 0$		
	6	Inversion-primitive tetragonal symmetry	L_4	$e \parallel L_4$	$\alpha = ae_0 \cdot e_0 + c\, e_0^* \cdot e_0^{\times}$ $\quad\lvert\alpha\rvert = 0$		
Rhombic	7	Planar	$L_2 2P$	$e \parallel L_2$ $e', e'' \perp 2P$	$\alpha = a_1 e' \cdot e'' + a_2 e'' \cdot e' = a'e' \cdot e'' + a'e'^{\times} =$ $= a(e' \cdot e'' + e'' \cdot e') + be^{\times}$ $\quad\lvert\alpha\rvert = 0$	$\varepsilon = \varepsilon_0 + \varepsilon_0 \cdot e_0 \cdot e' \cdot e' + \varepsilon_0 e'' \cdot e''$	$e'^2 = e''^2 = e^2 = 1,$ $e'e'' = ee' = ee'' = 0$
	8	Axial	$3L_2$	$e, e', e'' \parallel 3L_2$	$\alpha = ae \cdot e + a'e' \cdot e' + a''e'' \cdot e'' = a + be' \cdot e' + ce'' \cdot e''$		
Monoclinic	9	Planar	P	$e \perp P$	$\alpha = a \cdot e + e \cdot a + b^{\times},\ ae = be = 0$ $\quad\lvert\alpha\rvert = 0$		
	10	Axial	L_2	$e \parallel L_2$	$\alpha = ae \cdot e + a' \cdot e' + a'' \cdot e',\ a'e = a''e = 0$		
Triclinic	11	Primitive	—	—	$\alpha = a \cdot e + a' \cdot e' + a'' \cdot e''$		

We note that for crystals of all classes the vector $\vec{e}$, parallel to an axis of symmetry, always appears as an eigenvector of all tensors α, β, ε and μ. For planar and inversional classes the tensors α, β become singular ($|\alpha| = |\beta| = 0$).

Let us consider plane harmonic electromagnetic waves

(3) $\vec{E}=\vec{E}_0 e^{i\varphi}$, $\vec{H}=\vec{H}_0 e^{i\varphi}$, $\vec{D}=\vec{D}_0 e^{i\varphi}$, $\vec{B}=\vec{B}_0 e^{i\varphi}$, $\varphi=\omega(\frac{1}{c}\vec{n}\vec{r}-t)$,

where $\vec{n}$ is the vector refractivity. With (3) Maxwell's equations and equations (1) (2) take the forms :

(4) $\vec{D} = -[\vec{n}\vec{H}]$, $\vec{B} = [\vec{n}\vec{E}]$,

(5) $\vec{D} = \varepsilon\vec{E} + i[\vec{a}\vec{E}]$,

(6) $\vec{B} = \mu\vec{H} + i[\vec{b}\vec{H}]$,

where $\vec{a}$ and $\vec{b}$ are respectively the electric and magnetic activity vectors, defined by

(7) $\vec{a} = k\alpha\vec{n}$, $\vec{b} = k\beta\vec{n}$

($k = \frac{\omega}{c}$ – is the wave number). These vectors, analogous to the gyro vector $\vec{G}$[3], appear as linear functions of the vector refractivity $\vec{n}$ (or the wave normal $\vec{n}$, because $\vec{n} = n\vec{n}$, where n is the index of refraction).

From the table we may make a series of deductions about the possible properties of optically active crystals of various types, without recourse to the solutions of equations (4) - (6). In particular, it is easy to be convinced that $\vec{a}$ and $\vec{b}$ for planar and inversional classes with central symmetry (No. 2, 5, 6) become zero, if the wave normal $\vec{n}$ is directed along the optical axis $\vec{e}$, which is parallel to the axis of symmetry. This agrees with the derivation, based on approximations in Reference [4]. In the types of crystals just mentioned light will be propagated along the axis of symmetry according to the same law as for non-active crystals. However, for an arbitrarily different direction the wave normal vectors $\vec{a}$ and $\vec{b}$ will differ from zero, and hence the optical properties of the crystals under consideration will differ from the optical properties of non-active crystals. According to the treatment presented in reference [2], we say that crystals No. 2, 5, 6 (see Table) are optically active, although they do not rotate the plane of polarization for any direction of wave propagation.

In crystals of the planar class with rhombic symmetry the activity vectors $\vec{a}$, $\vec{b}$, according to the Table, lie in a plane perpendicular to the axis of symmetry $L_2 \parallel \vec{e}$,

(8) $\vec{a} = kn(a_1\vec{e}''\vec{n}\cdot\vec{e}' + a_2\vec{e}'\vec{n}\cdot\vec{e}'')$,

$\vec{b} = kn(b_1\vec{e}''\vec{n}\cdot\vec{e}' + b_2\vec{e}'\vec{n}\cdot\vec{e}'')$.

It is evident that $\vec{a} = \vec{b} = 0$, only if $\vec{n}\vec{e}' = \vec{n}\vec{e}'' = 0$, i. e. $\vec{n}\parallel\vec{e}'\parallel L_2$; in this case the crystal properties do not differ from those of non-active crystals. For all remaining directions $\vec{n}$, in particular for $\vec{n}\parallel\vec{e}'$ or $\vec{n}\parallel\vec{e}''$, vectors $\vec{a}$ and $\vec{b}$ differ from zero, and hence the crystal exhibits optical activity even if the plane of polarization is not rotated. Thus, in rhombic planar crystals the directions of the three major axes $\vec{e}$, $\vec{e}'$, $\vec{e}''$ are different, in principle, with respect to the appearance of optical activity.

Let us derive the basic crystal-optic equation: - the equation of normals for optically active crystals. Equations (1) and (2) may be written in the form

(9) $\vec{D} = (\varepsilon + i\vec{a}^x)\vec{E}$,

(10) $\vec{B} = (\mu + i\vec{b}^x)\vec{H}$

where $\vec{a}^x$, $\vec{b}^x$, are tensors which are duals of the vectors $\vec{a}$, $\vec{b}$, respectively [5].

From equations (4) (9) (10), by eliminating $\vec{H}$ and $\vec{B}$, we obtain the equation for $\vec{E}$

(11) $\{(\varepsilon + i\vec{a}^x)(\mu + i\vec{b}^x)\vec{n}^x(\mu + i\vec{b}^x)^{-1}\vec{n}^x\}\vec{E} = 0$.

In order for non-zero solutions to exist it is necessary that

(12) $|(\varepsilon + i\vec{a}^x) + \vec{n}^x(\mu + i\vec{b}^x)^{-1}\vec{n}^x| = 0$.

After some calculations (see appendix) we obtain the general equation of normals for magnetically active nonconductive crystals

(13) $(\vec{n}[\vec{a}\vec{b}])^2 - \vec{n}\varepsilon\vec{n}\cdot\vec{n}\mu\vec{n} - [\vec{n}\vec{a}]\mu[\vec{n}\vec{a}] - [\vec{n}\vec{b}]\varepsilon[\vec{n}\vec{b}] + 2[\vec{n}\vec{a}]\varepsilon\vec{a}\cdot\vec{n}\mu\vec{b} - \vec{n}\mu(\varepsilon\mu - (\varepsilon\mu)_c)\vec{n} - (\vec{a}\varepsilon\vec{a} - |\varepsilon|)\vec{b}\mu\vec{b} - |\mu| = 0$.

Equation (13) does not change if electric and magnetic quantities are interchanged $\varepsilon \rightleftarrows \mu$ and $\vec{a} \rightleftarrows \vec{b}$ ($\alpha \rightleftarrows \beta$). For $\vec{a} = \vec{b} = 0$, i. e. in the absence of optical activity, we obtain from (13)

(14) $\vec{n}\varepsilon\vec{n}\cdot\vec{n}\mu\vec{n} + \vec{n}\mu(\varepsilon\mu - (\varepsilon\mu)_c)\vec{n} + |\varepsilon\mu| = 0$,

which agrees with the equation of normals for magnetically inactive crystals [5].

Taking into account [7], we see that in equation (13) the leading term $(\vec{n}[\vec{a}\vec{b}])^2$ depends on the 6th power of the vector refraction $\vec{n}$. Because $\vec{n}$ enters as an even power in all terms, equation (13) is a cubic in n^2. Thus generally it gives three values for the index of refraction, so that there are three modes of propagation in optically active crystals [6]. The coefficient of n^0, equal to $k^4(\vec{n}[\alpha\vec{n}, \beta\vec{n}])^2$, is very small because of the smallness of α and β; therefore one of the three roots of equation (13) is very large and the appropriate "third" mode is propagated with a very small phase velocity.

It is of considerable interest that the third mode can exist only for $\vec{a} \neq 0$ and $\vec{b} \neq 0$, i.e. for its analysis it is necessary to take into account magnetic as well as electric terms in the optical activity.

Thus, magnetic terms, which until now have been neglected, are highly significant for the optical activity phenomenon.

In some types of crystals the expression $\vec{n}[\vec{a}\vec{b}]$ becomes 0, and in those the third mode is impossible. The condition $\vec{n}[\vec{a}\vec{b}] = 0$ signifies that vectors $\vec{n}$, $\vec{a}$, $\vec{b}$ are coplanar. With the help of the Table it is easy to establish that the third mode must be completely absent in crystals of cubic symmetry, and also in crystals of the planar and axial classes with central symmetry (Nos. 1-3, 5 in the Table). In crystals of lower symmetry and also in the primitive classes with central symmetry, including the inversion-primitive class with tetragonal symmetry, the third mode can exist, but not however for all directions of

propagation. In particular, the third mode is absent if the wave normal is parallel or perdicular to the axis of symmetry or the plane of symmetry of the crystal. In addition it is evident that the third mode will be absent if the wave normal is parallel to an eigenvector of tensor α or β.

However, these deductions concerning the possibility of the third mode are essentially changed, if the form of the coupling equations characteristic of optically active media are changed. Leaving equation (1) unchanged we may take in place of equation (2)

$$\vec{H} = \mu^{-1}\vec{B} + [\beta'\nabla, \vec{B}]. \tag{15}$$

Such a form of coupling $\vec{H}$ and $\vec{B}$ has the advantage that the vector $\vec{B}$ now plays the role of an argument defining the value of the function $\vec{H}$. This corresponds to the well known proposition in electron theory, according to which the vector $\vec{B}$ plays a more fundamental role than $\vec{H}$, in as much as $\vec{B}$ is a direct result of averaging the microscopic magnetic field. Equation (15) is not equivalent to (2) but together with (1) leads to the law of conservation of energy in the form

$$\nabla\vec{P} + \dot{w} = 0,$$

where

$$w = w_e + w_m, \quad w_e = \frac{1}{8\pi}\vec{E}\vec{D}, \quad w_m = \frac{1}{8\pi}\vec{H}\vec{B}$$

and

$$\vec{P} = \frac{c}{4\pi}\left([\vec{E}\vec{H}] - \frac{1}{8\pi}\left(\vec{\alpha}[\vec{E}\vec{E}] - \vec{\beta}'[\vec{B}\vec{B}]\right)\right) \tag{16}$$

The only difference from formula (17) of [1] corresponding to using equation (2) is that the sign of β' is changed and $\vec{H}$ is replaced by $\vec{B}$ in the expression for $\vec{P}$.

The general equation of normals for plane waves, obtained using equations (1), (15), take the form

$$|\mu|\vec{n}\varepsilon\vec{n}\cdot(\vec{n}\vec{b}')^2 - \vec{n}\alpha\vec{n}\cdot\vec{n}\mu\vec{n} - [\vec{n}\vec{a}]\mu[\vec{n}\vec{a}] - 2|\mu|\vec{n}\vec{b}'\cdot\vec{n}\varepsilon\vec{a} + |\mu|\vec{a}\varepsilon\vec{a} - \vec{n}\mu(\varepsilon\mu - (\varepsilon\mu)_c)\vec{n} - |\varepsilon\mu| = 0,$$

where $\vec{b}' = k\beta'\vec{n}$. In contrast with (13), this relation is non-symmetric with respect to commutation of electrical $(\vec{E}, \vec{D}, \varepsilon, \alpha, \vec{a})$ and magnetic $(\vec{H}, \vec{B}, \mu, \beta', \vec{b}')$ quantities, which is related to the corresponding dissymmetry of (1) and (15). In addition, in equation (17) the term of third order in n^2 $\vec{n}\varepsilon\vec{n}\cdot(\vec{n}\vec{b}')^2$ does not vanish in those crystals (excluding planar classes of central symmetry, possessing magnetic optical activity ($\beta \neq 0$). Thus the magnetic terms in the coupling equations are entirely responsible for the presence of the third mode, which must exist in almost all optically active crystals.

It should be noted that the quantitative difference between the two variants of the theory considered is very insignificant, because in the case of plane waves the equations $\vec{B} = \mu\vec{H} + i[\vec{b}\vec{H}]$ and $\vec{H} = \mu^{-1}\vec{B} + i[\vec{b}'\vec{B}]$ follow one from the other to second order accuracy in the activity vectors $\vec{b}$ or $\vec{b}'$. In fact from $\vec{B} = (\mu + i\vec{b}^x)\vec{H}$ for small $\vec{b}$ it follows that $\vec{H} = (\mu + i\vec{b}x)^{-1}\vec{B} = (1 + i\mu^{-1}\vec{b}x)^{-1}\vec{B} \approx (1 - i\mu^{-1}\vec{b}x)\mu^{-1}B$, from which $\vec{b}'x = -\mu^{-1}\vec{b}x\mu^{-1}$ or $\vec{b}' = -\frac{1}{|\mu|}\mu\vec{b}$ (see [5]).

APPENDIX

To calculate the determinant in (12) it is convenient to make use of the formula (see [5]):

$$|\gamma + \delta| = |\gamma| + |\delta| + (\bar{\gamma}\delta)_c + (\gamma\bar{\delta}))_c \tag{18}$$

where $\bar{\gamma}$ is a matrix reciprocal to γ, and the subscript c, denotes a matrix trace. Condition (12) takes the form

$$|\varepsilon + i\vec{a}^x| + \{\overline{(\varepsilon + i\vec{a}^x)}\,\vec{m}^x(\mu + i\vec{b}^x)^{-1}\vec{m}^x\}_c + \{(\varepsilon + i\vec{a}^x)\,\vec{m}^x(\mu + i\vec{b}^x)^{-1}\vec{m}^x\}_c = 0. \tag{19}$$

Because $\vec{m}^x = \vec{m}\vec{m}$ and according to (18), $|\mu + i\vec{b}^x| = |\mu| - \vec{b}\mu\vec{b}$, the third term of (19) takes the form $\frac{1}{|\mu| - b\mu b}\vec{m}\varepsilon\vec{m}\cdot\vec{m}\mu\vec{m}$. Using the formula $\bar{\gamma} - \bar{\gamma}_c = \gamma(\gamma - \gamma_c)$ and $(\bar{\gamma})_c = \frac{1}{2}((\gamma_c)^2 - (\gamma^2)_c)$ (see [5]), we easily obtain

$$\overline{\gamma + \delta} = \bar{\gamma} + \bar{\delta} + (\gamma - \gamma_c)(\delta - \delta_c) + \delta\gamma - (\gamma\delta)_c \tag{20}$$

which gives $\overline{\varepsilon + i\vec{a}^x} = \varepsilon - \vec{a}\cdot\vec{a} + i(\varepsilon\vec{a}^x + \vec{a}^x\varepsilon - \varepsilon_c\vec{a}^x)$.

Because $\varepsilon\vec{a}^x + \vec{a}^x\varepsilon$ appears as an antisymmetric matrix, it is possible to write

$$\varepsilon\vec{a}^x + \vec{a}^x\varepsilon = \vec{c}^x \tag{21}$$

from which, after multiplying by $\vec{a}$, we find $[\vec{c} + \varepsilon\vec{a}, \vec{a}] = 0$ or $\vec{c} = -\varepsilon\vec{a} + c\vec{a}$. Multiplying (21) by $\vec{a}^x$ and taking the trace gives $c = \varepsilon_c$. Thus

$$\overline{\varepsilon + i\vec{a}^x} = \bar{\varepsilon} - \vec{a}\vec{a} - i(\varepsilon\vec{a})^x. \tag{22}$$

Substitution of this relation into (19) leads to equation (13).

March 15, 1959

References

1. F. I. FEDOROV: OiS, 5, 85 (1958)
2. F. I. FEDOROV: OiS, 5, 322 (1958)
3. M. BORN: Optiks, 1937
4. L. D. LANDAU, E. M. LIFSHITZ: Elektrodinamika sploshnykh sred. To be published as "Macroscopic Electrodynamics" by Pergamon Press, London and Addison-Wesley Publ. Co., Reading, Mass. GITTL, 1957
5. F. I. FEDOROV: OiS, 1, 926 (1956) (See LC translation)
6. F. I. FEDOROV, B. V. BOKUT': Report of the Theor. Physics Lab, IPM AN BSSR, Minsk, 1956

TOM VI, Vyp. 4 OPTIKA I SPEKTROSKOPIIA Aprel', 1959
VOL. VI, No. 4 OPTICS AND SPECTROSCOPY April, 1959

Determination of Spectral Coefficients of Diffuse Reflection of Infrared Radiation from Blackened Surfaces

B. P. KOZYREV AND O. E. VERSHININ

Abstract: A method is discussed of determining coefficients of diffuse reflection where scattered radiation is focussed on the receiver surface by means of a mirror hemisphere. This method can be employed to determine the absolute values of reflection coefficients if the losses of the reflected energy are eliminated. A description is given of the measuring apparatus which allowed the determination of the spectral coefficients of specular and diffuse reflection in the infrared region. Measurements were made of the spectral coefficients of reflection from metallic surfaces coated with different kinds of carbon black, Bi, Zn, Te, Sb blacks and other absorbing substances.

INTRODUCTION

For many calculations of radiative heat exchange between bodies one has to know the spectral coefficients of reflection. These coefficients play an important role in making thermal detectors of radiant energy: radiation thermopiles and bolometers. The spectral reflectivity of the detecting surfaces of these detectors is a measure of their selectivity, since energy losses and detector sensitivity depend on the magnitude of reflection. The methods of reflection spectroscopy are also applied to such problems as structure analysis of materials [1,2], determination of the width of the forbidden band of semconductors [3] and many others.

Reflection coefficients in the infrared band have been measured since 1910 [4-10], however, all of these investigations covered relatively few objects and the data published by different authors sometimes diverge radically.

Very often one has to determine the reflectivity of natural surfaces which have not been ground or polished. Reflection from such surfaces will be diffuse. However, in the long wavelength region one could observe a specular component also.

In measuring spectral coefficients of reflection in the infrared region, in which the radiation sources are of low energy and where the thermal detectors are not very sensitive one has somehow to collect the radiation scattered by diffuse reflection into the half-space, so that all of the radiant energy reflected by the sample as is possible will reach the receiver.

In order to do this one can employ a spherical mirror which will focus all rays emitted from its center in one point. However, if the radiation source is slightly off the center, then one finds the reflected radiation focussed in a point conjugate to that from which the rays are emitted.

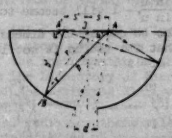

Figure 1. The effect of a hemispherical mirror A-the sample investigated A'-the radiation receiver.

For the determination of the reflection coefficients the investigated sample A is mounted near the center O) of the hemispherical mirror (fig. 1). The detector A' is mounted on the other side of the center in the conjugate point. If one illuminates the sample with radiation of the desired spectral composition through an opening cut into the hemisphere, then the reflected radiation will be focused by the hemisphere on the receiver. The reading of the measuring instrument connected with the detector will be proportional to the intensity of the reflected energy I_R. In order to measure the intensity of the radiation I_0 incident on the sample it is directed directly onto the receiver. The ratio of the values obtained will be equal to the reflection coefficient of the sample in the given spectral interval:

$$R = \frac{I_R}{I_0} \qquad (1)$$

Actually we obtain the value Rr where r is the reflection coefficient of the reflective plating of the hemisphere, however, the true value of the reflection coefficient of the sample can easily be calculated since the quantity r and its dependence on the wavelength can be determined in advance.

LOSSES OF THE REFLECTED RADIATION

Employment of the hemispherical mirror does not guarantee that we can obtain the absolute values of the coefficients as was assumed in the first measurements of diffuse reflection [4,5]. The general character of the spectral curves appears to be correct but the values of the coefficients are lower than their true values. We obtain this result due to losses of the reflected energy: in the measurement not all of the radiation reflected by the sample will reach the receiver but only part of it; often this fraction is uncertain.

The main reasons for losses are: a) escape of part of the reflected radiation beyond the boundaries of the hemisphere; b) aberrations of the optical system; c) screening effect of the detector holder.

Escape of Reflected Radiation. When reflection is diffuse, part of the reflected radiation escapes through the input opening and this leads to unavoidable losses of energy, however, the quantity lost is relatively small (about 3% of the reflected energy) and can easily be taken into account.

For completely specular reflection one can avoid these losses if the following condition is fulfilled:

$$s \geqslant \frac{d}{2} \qquad (2)$$

where s is the distance between the center of the hemisphere and the sample; d is the diameter of

the input opening for the radiation (Fig. 1).

In this case all of the reflected radiation hits the hemisphere and reaches the receiver. For small s part of the reflected energy falling on the opening leaves the hemisphere and is not recorded by the receiver.

As the distance between the center of the hemisphere and the sample increases the energy losses due to aberration will increase; therefore it is desirable to keep s as small as possible. At the same time one can not reduce the diameter of the input opening since this will lead to screening of the incident beam. Therefore, it is easier to eliminate the losses of the specular component by mounting the investigated sample at a certain inclination, so that the reflected beams would not fall on the opening (Fig. 2a). In this case all of the radiation reflected specularly is fully focussed by the hemisphere on the receiver and for diffuse reflection the losses through the opening will be of the same magnitude as for a horizontal disposition of the sample.

However, such a mounting of the sample leads to exaggerated values of the coefficients, especially noticeable when one investigates highly reflecting surfaces. The reason for this is that in the determination of the value of I_o the radiation is directed directly on the receiver and part of the radiation is reflected and escapes through the entrance beyond the hemisphere limits (Fig. 2b). Therefore the receiver records a smaller energy.

$$I_o = I_o(1-\rho). \tag{3}$$

where ρ is the reflection coefficient of the detector surface.

If one focuses the radiation on the investigated sample then the whole energy it reflects is focussed by the hemisphere on the receiver and even if part of the energy is reflected by the detector surface then this part will not strike the entrance but will be focussed by the hemisphere back onto the sample. If we do not take into account reflection by the hemisphere itself the detector will record the energy

$$I_R = I_o(R - R\rho + R^2\rho - R^2\rho^2 + \ldots) \tag{4}$$

Defining the ratio I_R/I_o as the reflection coefficient of the sample we get the exaggerated value:

$$R' = R(1 + R\rho), \tag{5}$$

which is different from the true value of R. Reflection from the receiver surface can amount to 18-20% (for instance a thermopile with a KRS-5 window), therefore for large R the correction will be 10 - 15%.

In order to obtain the true value of R it is necessary to mount the receiver in such a way that the radiation reflected specularly from it will not strike the entrance (Fig. 3). In this case for radiation directly incident on the receiver we will measure the value

$$I_o'' = I_o(1 - \rho + R\rho - R\rho^2 + \ldots) \tag{6}$$

and consequently $I_R/I_o = R$, i.e. the ratio of the instrument readings for radiation incident on the sample and on the receiver will give us the true value for the reflection coefficient of the sample.

Influence of Aberrations. Losses of the reflected energy due to aberrations can be especially noticeable if one employs thermal radiation detectors. In order to achieve a higher sensitivity and less inertness one tries to make the receiver platforms as small as possible. If the beam of the reflected radiation is larger than the dimensions of the receiving area of the detector then the latter will receive not the whole radiation but only part of it and the value of R will be understated.

One can not make the detector area smaller than the source image on the surface of the sample, however, one should make an effort not to have the sensitive area much larger than this image. The size of the reflected image should also not exceed that of the source image, i. e. the aberrations should be kept to a minimum. The condition for obtaining minimum aberrations can be determined from the law of sines. Designating all quantities as shown in Figure 1 we have

$$\frac{\rho}{\sin\varphi} = \frac{s}{\sin j} = \frac{r}{\sin u} \quad \text{and} \quad \frac{\rho}{\sin\varphi} = \frac{s}{\sin j} = \frac{r}{\sin u} \tag{7}$$

Consequently

$$\sin j = \frac{s}{r}\sin u \tag{8}$$

and

$$s = r\frac{\sin j}{\sin u} \tag{9}$$

The aberrations of the system are represented in the form

$$\delta s = s' - s = s\left(\frac{\sin u}{\sin u'} - 1\right), \tag{10}$$

i.e. they increase with increasing value of s. Therefore, as already noted, one should make s as small as possible. The lower limit of this quantity is determined by the dimensions of the investigated sample and of the receiver, since both the sample and the part of the receiver facing it must fit into the zone $s + s' = 2s$.

The magnitude of aberration is also determined by the term $\frac{\sin u}{\sin u'} - 1$ which is a function of s/r. A simple calculation shows [11] that for s/r 0.1 and for employment of broad beams the values of the quantity $\frac{\sin u}{\sin u'} - 1$ will become too large. Consequently one has to choose the dimensions of the hemisphere so that its radius is not less than 10 times the value of s.

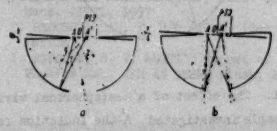

Figure 2. Mounting of the sample investigated in order to eliminate losses due to specular reflection.
a-path of reflected rays when the radiation is directed onto the sample; b-path of the rays when the radiation is directed onto the receiver.

Screening Effect of the Receiver Housing. A third kind of energy losses occurs only in diffuse reflection from the sample. These losses occur because part of the rays focussed by the hemisphere is incident on the receiver at large angles; such rays are not absorbed but are either reflected from the receiver surface or held back by its housing. Therefore not the whole reflected energy is measured but only that part of it within a cone with an angle less than 180° and the coefficients appear understated.

If the distribution of the reflected energy follows the cosine law then within a certain solid angle is included that part of the radiation flux which is equal to the ratio of the area cut by this solid angle out of the spherical surface to the total surface area of the sphere. From here it follows (see[11]) that if the detector receives the reflected energy only within a cone with an apex angle α then one loses the part of the radiation equal to:

$$(11) \quad \Delta I_R = I_R \cos^2 \frac{\alpha}{2}$$

Therefore for exact determination of the reflection coefficients one has to make corresponding corrections.

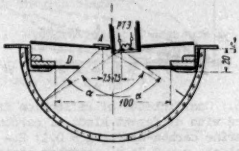

Figure 3. Apparatus for the investigation of the character of reflection.

A-sample D-iris diaphragm

To check expression (11) experimentally we measured the reflection from a magnesium oxide plate with artificial screening of part of the hemisphere. The discrepancy between experimental and calculated values did not exceed ± 1.5% which is quite satisfactory, taking into account the approximate determination of the screened area of the hemisphere.

DESCRIPTION OF EXPERIMENTAL SET-UP

The special features of reflectance measurements discussed above were taken into account in the design of the instrumentation which was made and tested in the Laboratory of Electro-Vacuum Engineering of the Leningrad Electrotechnical Institute.(Len).

A special radiation thermopile with a large detecting surface served as receiver. The dimensions of the thermopile did not permit making s smaller than 7.5 mm; therefore the mirror hemisphere was made 150 mm in diameter, i.e. the ratio s/r = 0.1.

The size of the reflected image in the plane of the great circle of the hemisphere was increased because of aberrations to approximately 3.0 mm for points near the center and to 4.5 mm for the most distant points. In the plane of best focussing the reflected image was of such a size that the energy was practically completely received by a thermopile with a sensitive area of 4 x 14 mm.

In order to eliminate radiation losses in specular reflection the detector and the sample were mounted at an angle 4° with respect to the plane of the great circle of the hemisphere. The design of the thermopile permitted recording radiation within a cone with an angle of ≈ 130°. Radiation beyond this cone was screened by the housing of the thermopile. Using expression (11) we could determine that the losses of energy amounted to about 18%. The losses due to the entrance in the hemisphere were ≈ 3%. Thus, when reflection was diffuse, ≈ 20% of the reflected radiation did not reach the receiver.

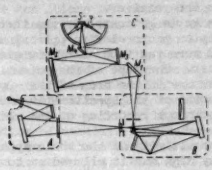

Figure 4. Diagram of set-up for the determination of the spectral coefficients of diffuse reflection.

The screening effect of the detector rim was vastly reduced by mounting special screens which limited the reflected beam by 20%, 30%, and so forth. The average value of the reflection coefficient of magnesium oxide thus obtained exceeded by 20% the same value obtained without the employment of screens. This again confirmed the 20% energy loss.

One can determine the character of the reflection of the sample investigated by varying the solid angle within which the reflected radiation is incident on the receiver: If the value of the reflection coefficient decreases steadily with decreasing solid angle then the sample reflects diffusely; however, if the reflection coefficient remains constant up to very small angles then the reflection is specular. Since the mounting of the screen requires a second adjustment of the instrument in order to measure the angle within which the radiation is received, our arrangement was provided with an iris diaphragm D with an opening diameter of 100 mm (Fig. 3). The diaphragm was mounted in such a manner that, when wide open, it did not introduce additional limitations to those induced by the rim of the receiver. (Acceptance angle 130°) However, when the diaphragm opening diameter was reduced the angle of acceptance decreased and when reflection was diffuse smaller and smaller amounts of radiation reached the receiver and consequently the value of the reflection coefficient obtained also decreased.

An experimental check, done with a magnesium oxide plate for the visible and near infrared regions, showed that when we changed the diaphragm diameter the calculated values of the reflection coefficients agreed with those obtained experimentally within ± 5%. At the same time for specular reflection, in particular from an aluminum mirror, the values of the coefficients remained unchanged when the diaphragm diameter was re-

duced up to 35-40 mm and began to fall rapidly only after this. Thus, a diaphragm mounted inside the hemisphere allowed us to determine the character of reflection from the samples investigated.

In order to measure the spectral coefficients of diffuse reflection our set-up was used in combination with an IKS-11 infrared spectrometer; a diagram of the whole assembly is shown in Figure 4. The radiation leaving the spectrometer slit was focussed by the hemispherical mirror M_2 from which a converging beam (after reflections from mirrors M_3 and M_4) travelled to the hemisphere. The last mirror, mounted at an angle of 45°, directed the radiation upward. It was thrown through the opening in the center of the hemisphere and, depending on the inclination of M_4, either on the sample or directly on the receiver.

The signals generated by the thermopile were amplified by an photo-electro-optical amplifier [12,13] and were fed into an EPP-09 electronic potentiometer. The tape of the potentiometer moved in synchronism with the drum of the apparatus of the wavelengths of the spectrometer and this provided a continuous recording of the reflected energy.

The sensitivity of the whole apparatus was sufficiently high and it allowed us to record radiation with a strength of 10^{-9}W. The accuracy of determining the reflection coefficients depends on many factors; one of these factors is the character of reflection, therefore one can only point out that in repeated measurements for the same sample the spread of values in all cases did not exceed $\pm$ 1.0%.

MEASUREMENT OF THE REFLECTIVITY OF BLACKENED SURFACES

The set-up described was employed to measure reflection of infrared radiation from blackened surfaces in order to determine the efficiency of different blacks. According to some data [4,5] the reflection of many blacks does not exceed 1-3% in a wide spectral band. In opposition to this more recent research [14,15] pointed out that many blacks become transparent for infrared radiation from $\lambda > 3$-4 μ on. Metallic surfaces coated with such blacks must have a high reflectivity. The low values for the reflection coefficients obtained in [4,5] can be explained by the fact that in these experiments the method of determination and the design of the measuring apparatus did not allow a record of the total energy reflected from the sample. Naturally, this resulted in values which were too low.

In this experiment the samples investigated were imitations of receiving surfaces of radiation thermopiles. The black tested was deposited on strips of metal foil 1 x 2 cm in size. The thickness of the deposited layer was checked by the weight of the layer in g/cm^2 of the sample surface; the accuracy with which the weight could be determined was not less than 0.025 mg/cm^2. Reflection from the foil itself for $\lambda > 3$ μ exceeded 90% (Fig5) and therefore it is obvious that partial transparency of the absorbing layer would result in a high value of the reflection coefficient of the whole sample.

Figures 5 and 6 show the results of investigations of reflection from surfaces coated with a layer of carbon black obtained from burning kerosene, turpentine and crystalline camphor and also from burning a stearine candle. All curves shown in this paper are not averaged but are chosen as the most typical from a large number of curves obtained experimentally.

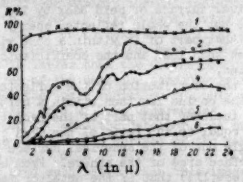

Figure 5. Coefficients of reflection from the surface of a metallic foil and from a foil blackened with kerosene carbon black.
1 - metallic foil, 2 - g = 0.025, 3 - 0,05
4 - 0.1, 5 - 0.18, 6 - 0.3 (g in mg/cm^2)

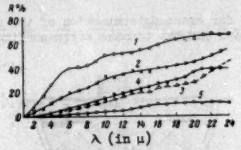

Figure 6. Coefficients of reflection from a foil blackened with different kinds of carbon black.
1 - stearine carbon-black g = 0.1; 2 - turpentine carbon black g = 0.2; 4 - camphor carbon black g = 0.1; 5 - camphor carbon black g = 0.2 (g in mg/cm^2)

Figures 5 and 6 show the results of investigations of reflection from surfaces coated with a layer of carbon black obtained from burning kerosene, turpentine and crystalline camphor and also from burning a stearine candle. All curves shown in this paper are not averaged but are chosen as the most typical from a large number of curves obtained experimentally.

The results confirm that thin layers of carbon black are transparent in the long-wave region of the spectrum. It is necessary to point out that with the exception of the thinnest layers (g = 0.025 mg/cm^2 and partly g = 0.025 mg/cm^2) all layers seem equally black to the eye and therefore a visual estimate of the quality of the black coating is impossible.

The reflection coefficient did depend on the conditions under which the absorbing layer was deposited. Using a high flame, giving large particles which could be detected with the unaided eye, we obtained layers reflecting 30 - 40 % of the radiation in the infrared region. The best samples with a uniform velvety layer, which resulted in a good and homogeneous absorption, were obtained from deposits of carbon black from a low flame.

From all the blacks of the same kind investigated and for the same weight of the deposited layer the surfaces coated with stearine black had the highest reflectivity those coated with camphor black had the lowest. The layer thickness corresponding to g = 0.2-0.3 mg/cm^2 was optimal since a further

increase in thickness increases the absorption only negligibly and at the same time increases the heat capacity of the layer.

The layer thickness of the black deposits on the receiving surfaces of the thermal radiation detectors has not been determined directly in this experiment . However, if we compare the times necessary to deposit these layers on the receiving surfaces and on the samples investigated we can see that the black layer usually deposited on the receiver surface has a thickness corresponding to $g = 0.2$ mg/cm^2. Thus such detectors can scatter in the long wave region up to 20% of the incident radiant energy.

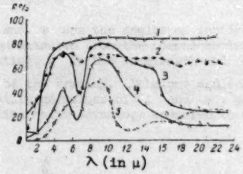

Figure 7. Coefficients of reflection from a foil coated with bismuth black.

1 - g = 0.1, evaporation at a pressure of p = 1.5;
2 - g = 0.2, p - 0.7; 3 - g = 0.8; p = 1.0;
4 - g = 0.8, p = 0.7; 5 - g = 0.9, p = 1.0
(g in mg/cm^2; p in mm Hg)

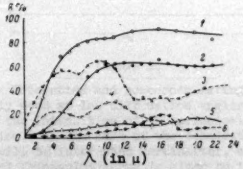

Figure 8. Coefficients of reflection from a foil coated with zinc black.

1 - g = 0.1, p = 2.5; 2 - g = 0.1, p = 0.5;
3 - g = 0.6, p = 5.0; 4 - g = 0.8, p = 0.5;
5 - g = 4.0, p = 0.5; 6 - g = 0.7, p = 1.0
(g in mg/cm^2; p in mm Hg)

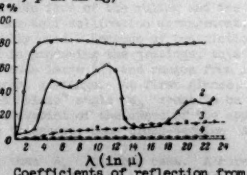

Figure 9. Coefficients of reflection from a foil coated with tellurium and antimony black.

1 - Te, g = 0.3 2 - Te, Te, g = 2.7
3 - Sb, g = 0.4; 4 - Sb, g = 1.0 (g in mg/cm^2)

Figures 7-9 show the results of our investigation of reflection from surfaces coated with bismuth, zinc, tellurium and antimony blacks.

Blacks from these metals were obtained by means of evaporation in an oxygen atmosphere.

All samples of this kind have in common that they reflect strongly radiation of the wavelength $\lambda > 3\mu$. Only antimony black is suitable as an absorbing layer. A g = 0.4 mg/cm^2 layer of this black reflected less than 10% in the band 1 to 15 μ and only for $\lambda > 15$ μ did reflection increase to 14%.

The high reflectivity of surfaces coated with oxides of Bi, Zn and Te could be expected. It had been known before [14] that metallic blacks are transparent in the infrared region.

The properties of these layers depend very much on the conditions of their preparation. Increasing the layer thickness leads usually to a higher absorptivity. However, the latter depends to a much higher extent on the pressure at which the black was prepared. Furthermore, we observed that the value of the reflection coefficient of the sample depends strongly on the rate of evaporation. Harris and co-workers [16, 17] showed that the properties of metallic blacks depend also on the composition of the atmosphere in which the evaporation is conducted: when 0.08 mm of air were added to an atmosphere consisting of nitrogen at 2 mm pressure (about 1% of oxygen) the layer of gold black which had been strongly absorbing in a wide spectral band became almost totally transparent for radiation of $\lambda > 2.5\mu$. The observed dependence of absorptive power of metallic black on the evaporation rate could also be connected with a change of atmosphere composition during the evaporation process.

Thus the absorptivity of metallic blacks depends on a large number of factors which cannot be taken into account easily: on the pressure at which the evaporation is conducted, the temperature of the substrate, the evaporation rate, the composition of the atmosphere, etc.. Therefore metallic blacks do not have any advantages over carbon black, especially because even the best black, antimony black - for the same layer weight gives us losses due to reflection which are not smaller than those of carbon black.

Other types of absorbing covering also do not have any noticeable advantage over those already discussed. As an example we can cite reflection from surfaces blackened with aquadag and several kinds of covering obtained by chemical processes.

Samples with thin layers of aquadag have a considerable reflectivity (53% at $\lambda = 21$ μ) which decreases with increasing layer thickness. However, if the thickness is increased beyond the values corresponding to g = 0.35 mg/cm^2 then the reflection is not changed and remains at the level of 15-18%, i.e. it probably does not depend on the transparency of the black layer but on reflection from the surface of the aquadag itself.

Coatings on metal surfaces obtained by chemical processes have a rather uniform absorptivity in a wide spectral band. On the other hand, surfaces coated with lacquers and paints had a more distinct selective absorptivity.

April 19, 1958

References

1. A. I. AVGUSTINIK, O. N. SETKINA, E. N. FEDOROVA: ZFKh, 28, 637 (1954)
2. S. ANDERSON: J. Am. Ceram. Soc., 33, 45 (1950)
3. P. D. FOCHS: Proc. Phys. Soc. B69, 70 (1956)
4. T. ROYDS: Phys. Z., 11, 316 (1910)
5. W. W. COBLENTZ: Nat. Bur. Stand. Bull., 9, 283 (1913)
6. V. G. VAFIADI: ZETF, 4, 809 (1934)
7. E. K. PUTSEIKO: ZETF, 15, 904 (1945)
8. J. A. SANDERSON: JOSA, 37, 771 (1947)
9. W. L. DERKSEN, T. I. MONAHAN: JOSA, 42, 263 (1952)
10. W. L. DERKSEN, T. I. MONAHAN:, A. J. LAWES: JOSA, 47, 995 (1957)
11. O. E. VERSHININ: Dissertation, LETI, 1955
12. B. P. KOZYREV: Materialy X Vsesoiuznyi soveshch. po spektr. (Materials of the X All-Union Conf. on Spectr.), 2, 125, 1959. L'vov Univ. Press
13. B. P. KOZYREV: UFN, 44, 173 (1951)
14. W. E. FORSYTHE (ed): Measurement of Radiant Energy, McGraw-Hill, N.Y., 1937
15. E. K. PLYLER, J. J. BALL: JOSA, 38, 988 (1948)
16. L. HARRIS, R. T. MC GINNIES, B. M. SIEGEL: JOSA, 38, 582 (1948)
17. L. HARRIS, J. K. BEASLEY: JOSA, 42, 134 (1952)

TOM VI, Vyp. 4 OPTIKA I SPEKTROSKOPIIA Aprel', 1959
VOL. VI, No. 4 OPTICS AND SPECTROSCOPY April, 1959

Use of an Echelette at Large Diffraction Angles

V. I. MALYSHEV, S. G. RAUTIAN

1. It is known that the angular dispersion $\frac{d\varphi}{d\lambda}$ and the theoretical resolving power R of diffraction gratings of any kind (echelon, echelle, echelette and others) increase with the diffraction angle and can be represented by the expressions (see [1] for example)

$$\frac{d\varphi}{d\lambda}=\frac{\sin\varphi+\sin\psi}{\lambda\cos\varphi}\ ;\quad R=\frac{A_0}{\lambda}(\sin\varphi+\sin\psi),$$

where ψ and φ are the angles of incidence and diffraction measured from the normal to the plane of the grating, λ is the wavelength and A_0 is the width of the grating. Echelons and echelles are used at large values of φ and ψ, which fact also explains their advantage compared to other gratings.

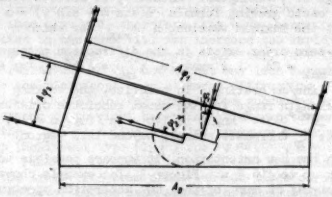

Figure 1.

Echelettes and nonconcentrating gratings are usually used at low diffraction angles, since otherwise the intensities of the principal maxima are very low. In the case of the echelette, in which we will be interested hereinafter, a non-symmetrical triangular shape is given to the grating ruling, and the principal maxima which have the greatest intensities are those which coincide with the mirror image from the faces of the ruling (the two "blaze" angles φ_1 and φ_2, fig. 1)[2]. Blaze angle φ_1, which corresponds to the reflection from the wider faces and equals the angle between the wide face of the ruling and the grating plane in the self-collimation arrangement, is the angle usually used. Because of restrictions encountered in producing the gratings, this angle cannot be made large [3] and ranges from 10° to 25° for different gratings. At first glance, use of the second "blaze" angle φ_2 seems to be unsuitable from the viewpoint of the speed of the apparatus, since the transverse beam cross-section A_{φ_2} is much less than A_{φ_1} in this case. A more careful analysis of the question shows, however, that the second method of orienting the grating can sometimes be of substantial advantage.

We have in mind the frequently encountered case of an investigation of the continuous spectrum by using a monochromator whose resolving power is limited by random errors of measurement.

Here the slit widths are much greater than normal and the flux isolated by the monochromator is defined by the expression (see [4], for example)

$$(2)\qquad \Phi=BT\frac{hH}{f}(\Delta\lambda)^2 k_\varphi A_\varphi\frac{d\varphi}{d\lambda}.$$

where B is the brightness of the emission source, referred to unit wavelength interval, H and A_φ are the height and width of the transverse cross-section of the diaphragmed beam of rays; h is the slit height, f the focal distance of the collimator; T the transmittance of the instrument and $\Delta\lambda=\frac{S}{f}\frac{d\lambda}{d\varphi}$ the spectral slit width. Formula (2) differs from the corresponding expression in [4] only by the explicit introduction of the factor k_φ defining the energy distribution over various orders of the diffraction pattern. Let us compare the flux magnitudes for the two blaze angles. These two cases differ only by the diffraction angle φ; among the characteristics of the instrument mentioned in (2), only k_φ, $\frac{d\varphi}{d\lambda}$ and A_φ depend on φ. Since $A_\varphi=A_0\cos\varphi$, then, denoting all the factors independent of φ_1 by c_1, we obtain for Φ:

$$(3)\qquad \Phi=c_1(\Delta\lambda)^2 k\varphi(\sin\varphi+\sin\psi)$$

or for the auto-collimating arrangement (or the similar Ebert-Fastie [5,6] and Pfund-Hardy [7,8] designs where $\varphi=\psi$

$$(4)\qquad \Phi=2c_1(\Delta\lambda)^2 k\varphi\sin\varphi.$$

If it is assumed that

$$(5)\qquad k_{\varphi_1}=k_{\varphi_2}$$

then it follows from (4) that the transition from one instrument to another for a given spectral slit width $\Delta\lambda$ leads to an increase of the flux by the ratio $\Phi_2/\Phi_1=\sin\varphi_2/\sin\varphi_1$, and to a decrease in the spectral slit width of

$$(6)\qquad \frac{\Delta\lambda_2}{\Delta\lambda_1}=\sqrt{\frac{\sin\varphi_1}{\sin\varphi_2}}$$

for a given magnitude of flux (i.e., for a constant "signal-to-noise ratio"). This is obviously related to the fact that as φ increases the dispersion increases more rapidly (as $\tan\varphi$) than the transverse beam cross-section decreases (as $\cos\varphi$).

These conclusions which are of practical importance, remain valid only when condition (5) is fulfilled. It is not difficult to show (for example, by using (9) from [9]) that this actually holds if the grating ruling has a triangular cross-section with ideally plane perpendicular faces, and if $\varphi=\psi$.

In the general case (angles different from the "blaze" angles, faces of the rulings not perpendicular, etc.) a theoretical analysis of the question would be very complicated and, apparently, insufficiently accurate. Moreover, the reasoning presented refers to a grating with ideally executed ruling surfaces. As a rule, in actual gratings the wider face of a ruling is of better quality than the short 'non-working' face. Consequently, the final solution of the question of the advantages of a new echelette instrument should be experimental; this does not exclude the possibility that the result will be different for different gratings.

2. The required measurements were made on a two-beam, DAIKS-F1 infrared grating spectrophotometer constructed in the FIAN Optical Laboratory.*

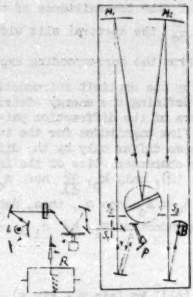

Figure 2.

The main monochromator follows the Ebert-Fastie [5,6] design (see fig. 2). Slits S_2 and S_3, (50 mm high) are located symmetrically with respect to the grating and have a 125 mm radius of curvature, which is equal to half the distance betwen the slits. Preliminary monochromatization is effected by a small prism monochromator with LiF or KBr prisms P. The lead-bismuth bolometer B [10] acts as light detector. The two-beam illuminator L and the recording apparatus R [11] were developed previously in the FIAN Optical Laboratory for the AIKS-F4 two-beam spectrophotometer and are used practically unchanged in the instrument being described.

The collimating mirrors M_1 and M_2 of the principal monochromator (250 mm diameter, 2000 mm focal length) were produced in the FIAN Optical workshop under a shadow method of contour control. Observation by microscope has shown that the slit image in the zero order has a clear diffraction structure without noticeable broadening or distortion an indication of the high quality of the focus optics.

The research was performed with a GOI 300 lines/mm grating which had an 18° blaze angle. In order to verify the theoretical conclusions, the rotational structure of the methane band in the 1.7μ region was first recorded with the usual echelette orientation in the minus first order. The spectral slit-width equalled $\Delta\nu_1 = 0.46$ cm^{-1}. Then the echelette was mounted in a new orientation (m = 3) and the geometric dimensions of the slit were enlarged until the previous value of the signal-to-noise ratio was reproduced. In this case, the spectral slit width turned out to be $\Delta\nu = 0.27$ cm^{-1}. The ratio is $\frac{\Delta\nu_2}{\Delta\nu_1} = \frac{1}{1.7}$, which is very close to the theoretical value $1/\sqrt{3}$ obtained from (6).

Similar measurements were made with lines of the mercury spectrum $\lambda = 1.3571$ μ (m = 4), 1.3954 μ (m = 4), 1.5299 μ (m = 3), 1.7114 μ (m = 3); the agreement with theory was completely satisfactory in all cases. Hence, the experiments described eliminate possible doubts related to the unknown parameter k_φ, and show graphically that the new orientation of the echelette has an explicit advantage from the viewpoint of the magnitude of the flux for a given value of $\Delta\lambda$ (or from the viewpoint of diminishing $\Delta\lambda$ for a given flux).

3. Let us consider certain other sides of the question. Another important advantage to working with large diffraction angles is the possibility of using the same grating effectively over a wider range of wavelengths. Actually, it follows from the basic grating formula $d(\sin\varphi + \sin\psi) = m\lambda$ that the maximum wavelength λ_{max} for which a non-zero order exists in the diffraction pattern is $\lambda_{max} = 2d$. For example, $\lambda_{max} = 6.66$ μ for a 300 line/mm grating. In practice, the working wavelength range for the usual echelette orientation and 18° "blaze" angle is 1.6 - 3μ (for m = 1), since k_φ decreases sharply beyond this region. With the new orientation, it appears possible to work up to ~6.5 μ. Figure 3, for example shows a tracing of part of the CO absorption spectrum near $\lambda = 4.56$ μ, obtained with a 300 line/mm grating in the new orientation.

The geometrical slit width is considerably greater in the new design than in the customary one. Consequently, there is a considerable relaxation of the accuracy required in producing the slit-jaws and of the accuracy of the rotating stage of the grating. Moreover, the wave aberration of the collimating mirrors and the overall dimensions of the apparatus are diminished because of the contraction of the transverse beam cross-section.

Along with the advantages enumerated, however, this echelette orientation can also have certain inadequacies. First of all, it is necessary to note that defects in the ruling of the grating which are not noticeable for small φ and m, can be substantial for large φ and m. Naturally, these factors play different roles in gratings of different types, or in gratings ruled on different ruling engines, or even in different samples of the same grating made by the same firm. For example, the focal plane of the spectrum furnished by our grating moved as the diffraction angle increased; the displacement reached 6 mm for the 11th order line $\lambda = 5461$ Å. This made it necessary to readjust exit slit S_3 of the principal monochromator.

We should also note that utilization of an echelette at large diffraction angles over a broad wavelength range is apparently possible only in the Ebert-Fastie design, since the curvature of the spectral line changes radically in other designs as $\varphi = 90°$.

*A.M. Surov helped to construct the instrument.

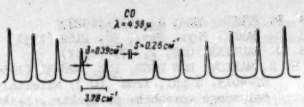

Figure 3.

It should also be noted that the angles of incidence and diffraction differ somewhat in the Ebert-Fastie arrangement. Consequently, the angular magnification $|W| = \frac{\cos\psi}{\cos\varphi}$ of the grating is different from unity. This fact is of greater importance, the greater the angle of diffraction. It leads to two effects. First, the geometric dimensions of the entrance and exit slits must be different ($S_3 = |W| S_2$). Therefore, these two slits must have independent opening mechanisms. Second, a third order coma [12] appears for $|W| \neq 1$, which is completely eliminated in the so-called Z-scheme for $|W| = 1$ [4]. However, it is essential that the transverse beam cross-section diminishes at the same time and, therefore, the wave aberration related to the coma will not increase too rapidly as φ increases. Apparently, this very fact is the reason why we did not detect any line asymmetry with the microscope even at large diffraction angles ($60 - 70^0$). For example, we succeeded in observing up to eight hyperfine structure components of the $\lambda = 5461$ Å line of a low pressure mercury lamp (Sosinskii type [13]) for $\varphi \approx 65^0$, m = 11.

Finally, it should be noted that a decrease in the transverse beam cross-section makes placing the detector in the beam all the more unsuitable, since it obstructs a relatively larger part of the beam; it is possible that an off-axis location of the light detector would be preferred.

4. The case of photoelectric recording of a continuous spectrum has been discussed in detail above. However, this does not delimit the range of problems for which the new echelette orientation is advantageous. The magnitude of the flux in the photoelectric recording of line spectra is given by an expression similar to (2) and (4) [4,14]

$$(7)\quad \Phi = B_\infty T \frac{hN}{f} \Delta\lambda\, k_\varphi A_\varphi \frac{d\varphi}{d\lambda} = 2c_2 \Delta\lambda\, k_\varphi \sin\varphi.$$

The difference from (2) and (4) is just that it is the integrated line intensity B_∞ which figures in (7), and the spectral slit width $\Delta\lambda$ is linear. Therefore, for a constant flux $\Delta\lambda \sim 1/\sin\varphi$, i.e., for a line spectrum the advantage of large φ is even more considerable than for a continuous spectrum (see [6]).

Of value in the photographic method of recording is the illumination, which is given by the expressions

$$(8)\quad E_c = B\,TH\Delta\lambda \frac{k_\varphi A_\varphi}{f^2},\quad E_l = B_\infty\, TH \frac{k_\varphi A_\varphi}{f^2}$$

for continuous and line spectra respectively. It follows from (8) that the transition from φ_1 to φ_2 leads to a decrease in the illumination because of the decrease in the transverse beam cross-section ($A_\varphi = A_0 \cos\varphi$). Therefore, a reorientation of the echelette in an existing instrument would admittedly be inadvisable from the light intensity viewpoint. However, the increase in angular dispersion can, in itself, be of interest. This fact should also be kept in mind in constructing new instruments. It is known that the resolving power of a spectrograph can be determined, to a considerable extent, by the function of the photosensitive surface in the apparatus. In order to diminish the role of this factor, it is necessary to increase the linear dispersion of the instrument, which is usually accomplished by increasing the focal distance of the camera objective, f. Since $E \sim 1/f^2$, it is natural to ask whether it is not more suitable, from the viewpoint of illumination, to achieve the same result by increasing the angular dispersion by a transition to the second blazed angle. Assuming constant linear dispersion $f \frac{d\varphi}{d\lambda} = \text{const}$, formula (8) becomes

$$E = c_3 k_\varphi \sin\varphi \tan\varphi$$

from which it is seen that the new echelette orientation is actually of substantial advantage in this case.

It must be remembered that the above analysis of the properties of actual echelettes concerned, basically, the coarse gratings used in the infrared. In the visible region (1200 and 600 line /mm gratings), where the photographic method is usually used, the situation can appear to be less favorable both in the sense of decreasing k_φ and also in the sense of a worsening of the quality of the image, related to the necessity of working in high orders. Consequently, an experimental verification of the practical suitability of the new echelette arrangement is required in each actual case.

CONCLUSIONS

1. The proposed echelette instrument should have an advantage in real resolving power when used as a monochromator, assuming an ideal grating. The measurements conducted verified this conclusion, it having appeared possible to double the resolving power.

2. The new echelette apparatus permits operation over a wider wavelength range at higher resolving power with the same grating.

3. An analysis of the advantages and disadvantages of the new echelette apparatus from the structural viewpoint also appears to be in its favor.

4. The measurements made showed that echelettes produced by F. M. Gerasimov in the GOI have a high enough quality so that they can be used at a second blaze angle.

April 19, 1958

References

1. G. R. HARRISON: JOSA, 39, 522 (1949)
2. H. A. ROWLAND: Phil. Mag. [5], 35, 397 (1893)
3. F. M. GERASIMOV, I. A. TEL'TEVSKII, S. V. NESMELOV, V. P. SERGEEV: Materialy X Vsesoiuznogo soveshchaniia po spektroskopii (Material from the X All-Union Conf. on Spectr.), 1, 394, 1957. L'vov Univ. Press
4. A. S. TOPORETS: Monokhromatory (Monochromators) GITTI, Moscow, 1955
5. H. EBERT: Wied. Ann., 38, 489 (1889)
6. W. G. FASTIE: JOSA, 14, 647 (1952)
7. A. H. PFUND: JOSA, 14, 337 (1927)
8. J. D. HARDY: Phys. Rev., 38, 2162 (1931)
9. S. G. RAUTIAN: OiS, 2, 279 (1957)
10. M. N. MARKOV: DAN USSR, 108, 428-31 (1956) (See RT-4613, 6 pp., from LC); Materialy X Vsesoiuznogo soveshch. po spektr., 1, 403, 1957.
11. M. N. MARKOV: ZTF, 24, 867 (1954)
12. I. V. PEISAKHSON: OiS, 4, 670 (1958)
13. M. L. SOSINSKII: Dissertation, MFTI, Moscow, 1955; IAN USSR FS, 17, 621 (1953)
14. P. JACQUINOT: JOSA, 44, 761 (1954)

TOM VI, Vyp 4 OPTIKA I SPEKTROSKOPIIA Aprel', 1959
VOL. VI. No.4 OPTICS AND SPECTROSCOPY April, 1959

On the Threshold Sensitivity of An Optical-Acoustic Radiation Detector

II. Nonuniform Heat Elimination in the Chamber Volume of a Selective Detector. High Modulation Frequency

A. O. SALL'

Abstract: We examine selective optical-acoustic radiation detectors in which the heat elimination is not proportional to the volume of the light-receiving chamber.

Formulas are obtained for defining the numerical magnitude of the threshold sensitivity of selective and non-selective radiation detectors, valid for a high modulation frequency. Formulas for the optimal length of the cylinder of a selective detector and the optimal concentration of absorbing gas are also obtained.

1. In the first part of this study [1] formulas were obtained for the threshold sensitivity of an optical-acoustic radiation detector, given the corresponding heat conductivity. However, the formulas used there for calculating the heat conductivity of a selective radiation detector are suitable only for the idealized situation in which heat elimination is proportional to the volume of the light-receiving chamber. In addition they are valid only for such a low modulation frequency that the depth of penetration of the temperature waves is larger than the chamber dimensions. We calculate here the heat conductivity for the case of nonuniform heat elimination over the chamber volume of a selective detector and examine the problem of the optimum concentration of absorbing gas in the chamber. We also obtain formulas to compute the heat conductivity which are valid for such high modulation frequencies that the depth of penetration of the temperature waves is less than the chamber dimensions.

2. Let us consider an actual case of a selective radiation detector in which heat elimination is not uniform over the chamber volume. To begin with we examine the case of a planar chamber, the thickness of which is considerably smaller than the diameter of the window. For the practical purposes of an approximate calculation we can assume that the radiation flux enters the detection cylinder of the chamber along the base cylinder axis and is reflected from the cylinder base also parallel to the axis, and that the illumination within the limits of the window of the chamber is uniform. Under the assumption of an exponential law for the absorption of radiation by the gas in the chamber, solution of the generalized equation of heat transfer [2] yielded a formula for ϑ. Comparing this formula with formula (9) of paper [1], we obtain

$$(1)\qquad G_{base} + i\omega C = \frac{2\lambda\left[(kl)^2 - \frac{i\omega c_p l^2}{\lambda}\right][1 + (\gamma - 1)\eta]}{l\gamma\left[\frac{2}{(kl)}\left(\frac{1 + \exp[-kl]}{1 - \exp[-kl]}\right)\eta\right]}$$

where G_{base} is the heat conductivity at the base of the cylinder, C the effective heat capacity, k the coefficient of radiative absorption by the absorbing component of the gaseous mixture filling the chamber, c the concentration of the absorbing component of the gaseous mixture, c_p specific heat per unit volume of the gas in the chamber.

The value of the function η is defined by the expression

$$(2)\qquad \eta = \frac{2\left\{1 - \exp\left[-(1+i)\sqrt{\pi c_p l^2 f \lambda^{-1}}\right]\right\}}{(1+i)\sqrt{\pi c_p l^2 f \lambda^{-1}}\left\{1 + \exp\left[-(1+i)\sqrt{\pi c_p l^2 f \lambda^{-1}}\right]\right\}}$$

In the case of a modulation frequency so low that the depth of penetration of temperature waves is larger than the chamber dimensions we obtain the following expression for the heat conductivity G_{base} by using (1) and (2):

$$(3)\qquad G_{base;l.f.} \simeq \frac{2\pi r^2 \lambda (1 - \exp[-kl])(kl)]}{l} \times$$

$$\times \left\{1 - 2\left(\frac{1 - \exp[-kl]}{kl}\right) + \exp[-kl]\right\}^{-1}$$

The heat conductivity at the side walls of the cylinder for a sufficiently low frequency was previously [1] obtained as

$$(4)\qquad G_{wall,\ l.f.} \simeq 8\pi\lambda l$$

Adding the heat conductivities as in Reference [1], we obtain the heat conductivity of the bounded cylinder

$$(5)\qquad G_{sel;l.f.} = G_{wall;l.f.} + G_{base;l.f.}$$

To calculate the threshold sensitivity ΔJ of the selective radiation detector it is necessary to take into account that due to the direction of radiation flux in the detector there is only partial absorption by the gas, equal to $(1-\exp[-2kl] - \psi(\exp[-kl]-\exp[-2kl]$. For a cylindrical chamber with reflecting base (see chamber 3 of Figure 6 in Reference [3] the coefficient ψ is equal to the coefficient of radiation absorption of the base with reflecting surface. In most cases, when a chamber with double window is used (see chamber 9, Figure 10 Reference [3]), the radiation flux passes through the chamber only once (successively through the 2 windows), and as an approximation $\psi \simeq 1$.

Considering, as in Reference [1], that $(\Delta Q)_2 < (\Delta Q)_1$, for sufficiently low modulation frequencies we obtain

(6) $$(\Delta J)_{sel;l.f.} \simeq$$

$$\simeq \frac{N\sqrt{1+(\omega\tau)^2}}{\beta(p\tau)}\left\{(1-\exp[-2kcl])-\psi(\exp[-kcl]-\exp[-2kcl])\right\}(\Delta Q)_1$$

$$\simeq \frac{N\sqrt{1+(\omega\tau)^2}}{\beta(p\tau)}\left\{(1-\exp[-2kcl])-\psi(\exp[-kcl]-\exp[-2kcl])\right\} \times$$

$$\times \frac{G_{sel.;\,l.f}}{G_{fl.;\,l.f.}} \sqrt{4kT^2 G_{fl.;\,l.f.}\Delta f}$$

where $G_{fl;l.f.}$ is the fluctuating heat conductivity.

Using Eq. (6) of [1] and Eqs. (3), (4) and (5) of the present paper we may show that if the product kcl does not exceed a value of the order of magnitude of a few units, then the optimum length of the cylinder is about 1.2r, as in the case where heat production is proportional to chamber value [1].

3. To obtain maximum sensitivity in a selective radiation detector the magnitude of the product kcl should be so large that a considerable portion of the radiation directed to the chamber would be absorbed by the gas filling it. An excessive increase in kcl, however, leads to an increase of the influence of the heat emission at the chamber window. Thus, there exists a definite value kcl, corresponding to maximum sensitivity. The optimum value of kcl when $l \ll r \ll \delta$, may be found from the expression

$$kcl \simeq 1.8 + 0.9\psi \tag{7}$$

4. We will find an expression for the conductivity G_{fl} of heat fluctuations valid at high frequencies (frequencies so high that the depth of penetration of the heat wave in the gas is considerably smaller than the chamber dimensions). The thermal conductivity $G_{fl;h.f.}$ and the thermal capacity $C_{fl;h.f.}$ appear as fixed coefficients in the conservation of energy equation for heat elimination in the chamber volume.

$$G_{fl;h.f.}\,\bar{\vartheta} + i\omega C_{fl;h.f.}\bar{\vartheta} + i\omega Pv = 0, \tag{8}$$

where v is an acoustic volume displacement.

To simplify further reasoning we shall, as before [2], consider the acoustic pressure uniform within the chamber. This is the case if the frequency ω is considerably smaller than the fundamental natural frequency of acoustic vibrations in the chamber volume. To calculate the thermal conductivity $G_{fl;\,l.f.}$ and heat capacity $C_{fl;l.f.}$ of a chamber with heat-conducting walls it is necessary to solve the generalized heat transfer equation.

$$\lambda\int_S \frac{\partial\vartheta}{\partial n}\,dS + i\omega C_v\vartheta + i\omega Pv = 0 \tag{9}$$

where λ is the thermal conductivity of the gas, ϑ the excess of the gas temperature over the wall temperature, S - the area of the chamber wall surface, n - the normal to the wall surface, C_v specific heat of the entire mass of gas (for constant volume).

If the chamber dimensions significantly exceed the depth of penetration of temperature vibrations then the solution of the generalized equation of heat transfer ϑ is equal to the sum of a constant component ϑ_0 and the temperature ϑ_1 of the wave being propagated from the heat conducting walls deep into the chamber [2]. The integral $\int\vartheta_1 dV$ actually extends over a very thin layer of gas near the wall surface, and it is possible to reduce it to an integral over the wall surface of the chamber. Taking into account the zero boundary conditions, we get

$$\bar{\vartheta} = \frac{\int(\vartheta_0+\vartheta_1)dV}{V} = \vartheta_0 - \frac{\vartheta_0 S}{V}\int_0^\infty \exp[-\frac{(1+i)x}{\delta}]dx$$

$$= \vartheta_0\left[1 - \frac{S\delta}{(1+i)V}\right] \tag{10}$$

where δ is the depth of penetration of the temperature vibrations, and x is distance from the chamber wall. Utilizing (10), we get

$$\lambda\int_S \frac{\partial\vartheta}{\partial n}\,dS = \frac{(1+i)S\lambda\bar{\vartheta}_0}{\delta} = \frac{(1+i)S\lambda\bar{\vartheta}}{\delta}\left[1_2\frac{S\delta}{(1+i)V}\right]^{-1}$$

$$\simeq \frac{(1+i)S\lambda}{\delta}\,\bar{\vartheta}. \tag{11}$$

If the expression thus found for the integral is substituted into (9), and the result compared with (8), we obtain

$$G_{fl;h.f.} \simeq \frac{\lambda S}{\delta}, \tag{12}$$

$$C_{fl;h.f.} \simeq C_v + \frac{\lambda S}{\omega\delta} \simeq C_v. \tag{13}$$

The depth of penetration of the temperature vibrations δ is found from the known heat capacity, heat conductivity, gas density and modulation frequency [2].

5. We now calculate the threshold sensitivity of a non-selective radiation detector for high modulation frequencies. Let the modulation frequency be such that the depth of penetration of temperature vibrations is considerably smaller than the chamber dimensions, and the heat capacity of the radiation absorbing film is considerably smaller than the heat capacity of its surrounding layer of gas, which has a thickness equal to the depth of penetration of the temperature vibrations. Then, utilizing Equations (5) and (15) mentioned in [1], and considering $(\Delta Q)_2 < (\Delta Q)_1$, we obtain

$$(\Delta J)_{non.sel.}\beta^{-1}\psi^{-1}N\sqrt{4kT^2 G_{fl;h.f.}\Delta f}$$

$$= \beta^{-1}\psi^{-1}N\sqrt{4kT^2 S\Delta f\sqrt{\kappa c_p f\lambda}}. \tag{14}$$

From (14) it follows that when the radiation detector sensitivity is limited by fluctuations of the gas temperature, then as the modulation frequency increases the sensitivity decreases. As the modulation frequency increases significantly the heat capacity of a gas layer of thickness δ enveloping the absorbing film will eventually begin to be considerably smaller than the heat capacity of the absorbing film. It can be shown that in this case, of the total quantity of heat eliminated in the film, the heating of the gas is accomplished only by the fractional part $(\lambda' c' \lambda^{-1} c_p^{-1} l+1)^{0.5}$ where c' is the heat capacity of the wall material per unit volume. In this case, considering that $(\Delta Q)_2 < (\Delta Q)_1$, we obtain

$$(15)\quad (\Delta J)_{\text{non. sel}} \simeq N\beta^{-1}\psi^{-1}\sqrt{4kT^2 S\lambda c\Delta f}\sqrt[4]{\pi\lambda^{-1}c_p^{-1}f}.$$

To calculate $(\Delta J)_{\text{non sel.}}$ in the last case it is necessary to take into account not only the surface of the chamber wall, but also the double surface of the film. The sensitivity of a non-selective radiation detector in this case can be several orders of magnitude less than the sensitivity of a selective detector having the same chamber size.

6. We examine next the question of optimum chamber size for selective radiation detectors in the case of high modulation frequencies. If radiation absorption by the gas of the ray receiving cylinder of a selective radiation detector were uniform over the whole volume, then for $G_{sel}{}' \simeq G_{fl;h.f.}$ and $(\Delta Q)_2 < (\Delta Q)_1$ the following relationship would hold:

$$(16)\quad (\Delta J)_{\text{sel; h.f.}} \simeq \frac{N\sqrt{1+(\omega\tau)^2}}{\beta(p\tau)}\left\{(1-\exp[-2kcl]) - \psi\,(\exp[-kcl]-\exp[-2kcl])\right\}\sqrt{4kT^2 S\Delta f}\sqrt[4]{\pi c_p \frac{f}{\lambda}}$$

Let the chamber be a finite cylinder of length $l = 0.5$ cm and a base radius of $r = 1$ cm. Taking $N = 10$, $\omega\tau \ll 1$, $\beta \simeq 1$, $p\tau \simeq 1$, $kcl > 1$, $\psi \ll 1$, $\Delta f = 1$ cps, $f = 10^3$ cps, $T = 300^\circ$ K for a chamber filled with carbon monoxide, we get

$$(\Delta J)_{\text{sel.; h.f.}} \simeq 1.2\cdot 10^{-8} \text{ watt}$$

(in the gas absorption band).

From a comparison of the numerical value of the threshold sensitivity just obtained with the value obtained previously [1] for a chamber of the same size, but for a lower frequency (3.10^{-9} watts), it follows that with increasing frequency the sensitivity decreases somewhat. For sufficiently high modulation frequencies the sensitivity is inversely proportional to the fourth root of the modulation frequency.

From an inspection of Eq. (16) it follows that in order to increase the sensitivity of the chamber it is necessary to decrease the wall area S of the chamber; i.e., to decrease the size of the chamber. However, the possible reduction is definitely limited. The length of the cylinder determines the width of the spectral region within which radiation is absorbed by the gas filling the cylinder. The base radius of the cylinder may also only be reduced to a size such that the radiation flux can still be focussed. It is evident that for selective detectors with heat elimination not proportional to chamber volume, it is also necessary to decrease the wall surface of the chamber to increase sensitivity.

7. We now consider the question of the optimum concentration of absorbing gas in the mixture filling the chamber, for the case of high modulation frequencies. The values of amplitude and phase of the acoustic pressure harmonics depend on the absorption coefficient of the gas. It is possible to show that there is a definite value of the absorption coefficient for which the amplitude of the acoustic pressure is a maximum. Consequently, if the maximum value of the absorption coefficient for any absorption line and the concentration of the absorbing component in the chamber is so large that a considerable portion of the radiation in the central region of the absorption line is absorbed in a distance smaller than the depth of penetration of the temperature vibrations, then the spectral sensitivity of the chamber in the central region of the line will be smaller than on the wings. The ratio of the spectral width of such a gap in the spectral sensitivity curve of a radiation detector to the half-width of the line is equal, in order of magnitude, to the square root of the product of the concentration of absorbing gas in the chamber, the maximum value of the absorption coefficient at the center of the line and the penetration depth of temperature vibrations.

Equation (7) obtained earlier to define the optimum value of kcl is valid only for low modulation frequencies. As the modulation frequency increases the thickness of the stationary layer near the chamber window decreases [2]. (We recall that the stationary layer is the layer at the chamber window in which the heat eliminated is delivered to the window and does not take part in the generation of acoustic vibrations [2]). This permits the magnitude of the product kcl to be increased without a significant increase in the loss in the stationary layer near the chamber window. Therefore, as the modulation frequency increases the value of kcl corresponding to the signal maximum also increases. For the ideal case $\psi = 0$ the optimum value of kcl, corresponding to maximum sensitivity is given by

$$(17)\quad (kcl) \simeq 1.0 + 1.7 \log\left(\frac{c_p f l^2}{\lambda}\right)$$

If $\psi \neq 0$ this value of kcl increases to

$$(18)\quad (kcl) \simeq 1.0 + 3.0 \log\left(\frac{c_p f l^2}{\lambda}\sqrt{\psi}\right)$$

Equation (18) holds only for such values of ψ which lead to larger values of kcl than does Eq. (17). In the opposite case (regardless of the numerical value of ψ) it is necessary to use Eq. (17). If calculations from Eqs. (17) or (18) give a value smaller than that given by Eq. (7) then the latter must be used to define the optimum value of kcl.

It must be noted that just as in the previous case of a low modulation frequency, substantial deviations of the product kcl from optimum values cause an unimportant decrease of the signal.

Suppose, for example that $c_v \varepsilon l^2 f \gg \lambda$. Then if we use Eq. (7) to determine the optimum value of kl, instead of (17) or (18), the decrease in sensitivity compared to the optimum case will amount to less than 10%. Therefore, to simplify calculation we may use Eq. (7) for all modulation frequencies.

Equations (7), (17) and (18), serving to define the optimum concentration of the absorbing component in the gas mixture filling the ray-receiving cylinder of the selective radiation detector, are obtained under the condition that maximum sensitivity is limited by fluctuations of gas temperature. It can be shown however that they are also valid when the threshold sensitivity of the radiation detector is limited by electrical noise at the amplifier input and by mechanical fluctuations of the movable system of the microphone.

8. We may generalize the results obtained to the case of an optical-acoustic gas analyser which makes use of nonmonochromatic radiation flux. We denote by u the product of the length of the working chamber (absorption cell), and the concentration of the component to be determined in it. Let us first take the case of such small values of u that the radiation absorption by the gas follows a linear law. If the absorption band of the component to be determined consists of absorption lines of identical intensity, then as calculation indicates, we would have $k \approx 0.5k_0$ where k_0 is the maximum value of the absorption coefficient in the absorption band of the component to be determined. In an actual case of a band consisting of lines of various intensities, the value of k will be smaller. For diatomic and linear polyatomic molecules, as calculation shows, $k \geqslant 0.25k_0$ (different methods of calculation give somewhat divergent results). In the range of values of u, for which the radiation absorption is proportional to $\sqrt{u}$, we find that the absorption coefficient is approximately $k \approx (0.5\text{-}1.0) \cdot u^{-1}$.

For large values of u, when saturation occurs in the absorption of radiation by the gas, the value of the equivalent absorption coefficient decreases to half the value of the general coefficient of an absorption band [4,5].

As experiments have shown, for an optical-acoustic gas analyser using quartz optics ($f = 6$ cps, $l = 26$ mm, $\psi = 0$), and methane at. $u = 30$ - 100mm %, the absorption coefficient is equal to $0.5 \cdot u^{-1}$. For carbon dioxide under the same conditions ($u = 30$ - 100 mm %) the value of the equivalent absorption coefficient is about $1.7\ u^{-1}$. The exaggerated value of the absorption coefficient is explained by saturation in the radiation absorption by the carbon dioxide in the ray-receiving cylinder of the microphonic chamber.

The optimum values of u, corresponding to maximum sensitivity of the gas analyser usually do not exceed 100 - 300 mm %.

9. The concentration of the absorbing component in the chamber of a selective detector may be adjusted [in accordance with (7), (17) and (18)] in such a way that the sensitivity is a maximum. Calculations of threshold sensitivities for this case give values close to that obtained by using formulas derived for the case of uniform heat elimination over the chamber volume. Hence, for approximate calculations we may take the heat elimination to be proportional to the chamber volume. Such an assumption, as we shall see in a continuation of the present paper, allows us to obtain comparatively simple expressions for the threshold sensitivity of chambers with complicated configurations.

May 9, 1958

References

1. A. O. SALL': OiS, 6, 219 (1959) (See this journal page 139)
2. A. O. SALL': ZTF, 26, 157 (1956) (See Soviet Physics Technical Physics)
3. M. L. VEINGEROV: ZL, 13, No. 4, 426 (1947)
4. W. M. ELSASSER: Heat Transfer by Infrared Radiation in the Atmosphere. Milton, Mass. Harvard University, Blue Hill Meteorol. Observ., 1942
5. K. IA. KONDRAT'EV: Perenos dlinnovolnovogo izlucheniia v atmosfere (Longwave radiation transport in the atmosphere). GITTL, Moscow-Leningrad, 1950

TOM VI, Vyp. 4 OPTIKA I SPEKTROSKOPIIA Aprel', 1959
VOL. VI, No. 4 OPTICS AND SPECTROSCOPY April, 1959

BRIEF REPORTS

On Processing Spectrograms Obtained on a Fabry Perot Interferometer

V. K. ABLEKOV

In the broad field of spectrographic research, which requires the use of high resolution spectroscopes, the problem of determining the contour and half-width of the spectral interval under study often arises.

Usually, practical determination of the contour and half-width of the spectral interval under study is very complicated. Actually, if $I(\nu)$ is the function giving the form of the spectral interval under study, $A(x)$ is the instrumental function, then the resulting distribution of intensity $W(\nu)$ can be written

$$W(\nu) = \int_{-\infty}^{\infty} I(\nu - x)\, A(x)\, dx, \tag{1}$$

where ν is the frequency (for the sake of simplicity we may consider $\nu = 0$) corresponding to one of the maxima of the interference plot $W(\nu)$.

Great mathematical difficulties are encountered in calculating the unknown function $I(\nu)$ in (1) in a whole series of cases important from a practical standpoint [1, 2] .

The present article proposes a simple method for determining the true half-width $I(\nu)$ when a Fabry-Perot interferometer is used, and for finding the intensity distribution of two spectral intervals which are superimposed one on the other.

1. In the case of a Fabry-Perot interferometer, the instrumental function [3] is

$$A(\nu) = \frac{I_0'}{1 + F \sin^2 \pi \frac{\nu}{[\Delta\nu]}}, \tag{2}$$

where

$$F = \frac{4R}{(1-R)^2},$$

$[\Delta\nu]$ is the free spectral range of the étalon (in cm^{-1}) and R is the reflection coefficient of the étalon mirrors. If (2) is substituted in (1) , then even in the case of a simple dispersion law for $I(\nu)$ the integral cannot be calculated simply. In order to circumvent this difficulty, (2) may be used as the sum of the dispersion distributions

$$\frac{I_0}{1 + (\frac{\nu}{\alpha})^2},$$

which are equidistant on the frequency axis (here α is the half-width *).

Then the resulting distribution will be expressed by the equation

$$W(\nu) = \sum_{n=-\infty}^{\infty} \int_{-\infty}^{\infty} I(\nu - x) \frac{I_0}{1 + (\frac{x + n[\Delta\nu]}{\alpha})^2}\, dx. \tag{3}$$

In a case where $I(\nu)$ is a dispersion function with the half-width β , the integral in (3) also gives the dispersion curve with the half-width

$$\gamma = \alpha + \beta. \tag{4}$$

The sum of these integrals for all orders of interference equals

$$W(\nu) = \frac{I_{max}}{1 + F_{eff} \sin^2 \pi \frac{\nu}{[\Delta\nu]}}, \tag{5}$$

where

$$I_{max} = I_0 \pi \frac{\gamma}{[\Delta\nu]} \operatorname{cth} \pi \frac{\nu}{[\Delta\nu]}, \tag{6}$$

$$F_{eff} = \operatorname{cth}^2 \pi \frac{\gamma}{[\Delta\nu]} - 1 \quad (F_{eff} \neq F). \tag{7}$$

Equations (5) - (7) make it possible to determine three unknowns F_{eff}, I_0 and γ from those determined by experiment, I_{max} and $W(\nu)$ or $I_{min} = W(\nu = \frac{[\Delta\nu]}{2})$.

Thus it is clear that in order to determine γ on the basis of (5) - (7) and then find the unknown half-width β from (4), it is sufficient to determine I_{max} and I_{min} on the visibility curve of intensity distribution on the spectogram. The instrumental half-width is determined from the equation

$$F = \operatorname{cth}^2 \pi \frac{\alpha}{[\Delta\nu]} - 1.$$

2. If a certain intensity distribution with respect to frequency is obtained on the spectogram and it is known beforehand that this distribution is the result of the superposition of two spectral regions of different half-widths, then in many cases it becomes necessary to clarify the quantitative distribution characteristics in each of the spectral regions separately ** .

In order to find the distribution in each of the two spectral regions (of known half-width) , it is sufficient to determine I_{01} and I_{02} , the intensities of the maxima of the unknown distributions.

Let us assume, as in the first case, that light consisting of two spectral intervals of width α_{01} and α_{02} falls on a Fabry-Perot interferometer, and in each of these intervals the dispersion law for frequency intensity distributions is operating, and each spectral interval is broadened according to the instrumental function of the spectroscope. The instrumental function of the spectroscope is assumed to be the dispersion function near the maximum of this function [3]. Applying the ideas of Mikusinskii [6] , equation (1) can be written as

$$\{W(\nu)\} = \{I(\nu)\} \{A(\nu)\}, \tag{8}$$

* It is interesting to note that if the Fabry-Perot interferometer is considered as a hollow resonator with plane-parallel faces, [4], the natural frequencies of this resonator are equidistant in distribution and coincide with the position of the maxima in (2).

** Such a problem arises, for instance, in studying the spectral distribution of light scattering (see [5]).

where the braces indicate that the functions from (1) inside them are to be written as Mikusinskii space operators. If (8) is considered as the functional equation relative to the half-width, then the solution of such an equation will be exponential. Then instead of (8) the equation may be written $e^{\alpha+\beta} = e^{\alpha} e^{\beta}$, where α and β are linear functions of the half-widths.

To determine the intensity maximum in each of the distributions under study we use the approximate equation

$$(9)\quad I_{01}\exp\left[\frac{\pi\alpha_{01}}{[\Delta\nu]}\right] + I_{02}\exp\left[\frac{\pi\alpha_{02}}{[\Delta\nu]}\right] = I_0 \exp\left[\frac{\pi\alpha_0}{[\Delta\nu]}\right];$$

$$I_{01} + I_{02} = I_0,$$

where α_0 is the half-width of the resultant distribution, and I_0 is the maximum intensity of the total distribution. Equation (9) makes possible the determination of the unknown values I_{01} and I_{02} and, consequently, the reproduction of all the distributions.

In conclusion, I would like to thank I. L. Fabelinskii, under whose direction this work was carried out.

July 14, 1958

References

1. M. M. SUSHCHINSKII: ZETF, 25, 87 (1953)
2. H. C. BURGER, P. H. VAN CITTERT: Zs. Phys., 79, 722 (1932); 81, 428 (1933)
L. S. ORNSTEIN, W. R. V. WYK: Zs. Phys., 78, 734 (1932)
3. S. TOLANSKY: High Resolution Spectroscopy. Methuen and Co., London, 1947 (IL, Moscow, 1955)
4. A. SOMMERFELD: Optik, Vorlesungen uber Theoretische Physik, Band 4. Dieterich'sche Verlagsbuchhandlung, Inh. W. Klemm, Wiesbaden, 1950 (English translation, Academic Press, New York, 1954. Russian translation, IL, Moscow, 1953)
5. I. L. FABELINSKII: UFN, 63, 355 (1957)
6. J. MIKUSINSKI: Rachunek operatorów Wyd. 2, Warszawa (Operational calculus), 1957.

TOM VI, Vyp. 4 OPTIKA I SPEKTROSKOPIIA Aprel', 1959
VOL. VI, No. 4 OPTICS AND SPECTROSCOPY April, 1959

Some Regularities in the Electron Paramagnetic Resonance Spectra of Alkyl Radicals

N. IA. CHERNIAK, N. N. BUBNOV, L. S. POLIAK
IU. D. TSVETKOV and V. V. VOEVODSKI

It has been found in systematic studies of the electron paramagnetic resonance (EPR) spectra of radicals, formed in frozen hydrocarbons when bombarded with gamma rays at 77° K, that the hyperfine structure (HFS) of these spectra undergoes a complete change through the homologous series. In Figure 1, are shown spectra of the radicals of normal paraffin hydrocarbons from $C_{11}H_{23}$ to $C_{16}H_{33}$, obtained under conditions described previously [1] (the purity of the samples being 97-98%).

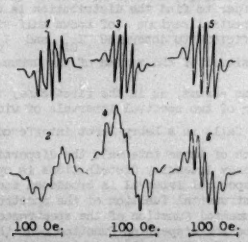

Figure 1. Electron paramagnetic resonance spectra of $C_{11}H_{23}$, to $C_{16}H_{33}$.

1- $C_{11}H_{23}$, 2- $C_{12}H_{25}$, 3- $C_{13}H_{27}$, 4- $C_{14}H_{29}$, 5- $C_{15}H_{31}$, 6- $C_{16}H_{33}$.

Figure 1 shows that the character of the HFS differs substantially for the even and the odd members of the series. Although, because of overlapping of the spectra of different radicals (especially among the lowest members of the series), an exact analysis is difficult, we can deduce that in hydrocarbons with odd numbers of carbon atoms the HFS is well defined and the intensities of the central components differ only slightly from each other. In the radicals of hydrocarbons with an even number of C atoms, the resolution is substantially worse, but the distribution of intensity in all cases is apparently close to binomial.

In the paraffins, from n-C_5 to n-C_{10}, spectra are more complicated and are very similar to one another (see Figure 2).

The spectra of the radicals of cyclic hydrocarbons (with five and six C atoms; see Figure 3) are in many respects analogous to the corresponding spectra of odd and even members of the series C_{11} — C_{16}.

Incidentally, note that the HFS of the spectrum of polyethylene bombarded at 77°K [2], is analogous to that of cyclo - C_6H_{12}.

It should also be noted that in obtaining the spectra of individual alkyl radicals, we ought to pay special attention to the influence of oxygen, whose presence brings about the formation of peroxide radicals of the type ROO [2]. The asymmetrical line which it produces distorts the symmetric spectrum of the radical R.

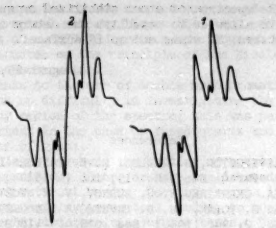

Figure 2. EPR spectrum of the radicals C_6H_{13} and C_7H_{15}.

The simplest spectrum is observed in the cyclo-C_6 case. The magnitude of the hyperfine splitting and the intensities of the components can be explained if we suppose that the spectrum represents a triplet (with a splitting of 37 Oe., and with the relative sizes of the components being 1:2:1), each component of which split in turn into 2 (splitting of 20 Oe.). It is possible to ascribe such a spectrum to the radical cyclo - C_6H_{11} (obtained from cyclo - C_6C_{12} by removal of an H atom). Besides, in accordance with Ingram's supposition [3], one must assume that only two of the four H atoms in the β position participate in the hyperfine splitting. This brings about the appearance of the triplet. The interaction with the H atom in the α - position produces doublet splitting of each component of the triplet.

In the case of cyclo-C_5H_{10}, by virtue of almost complete coplanarity, both H atoms of the

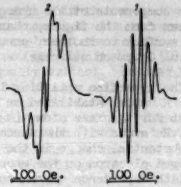

Figure 3. EPR spectra of the radicals Cyclo-C_6H_{11} and Cyclo-C_5H_9.

β CH_2 group in the radical must be equivalent relative to the vacant valence, and the number of HFS components must increase. The spectrum, shown in Figure 3, verifies this conclusion.

Investigation of the dependence of the EPR spectra of various radicals on the number of C atoms in the chain may turn out to be very profitable in explaining the structure and properties of these radicals.

The variations noted in the EPR spectra could likewise be used for analytical purposes.

August 28, 1958

References

1. N. IA. CHERNIAK, N. N. BUBNOV, V. V. VOEVODSKII, L.S.POLIAK, IU. D. TSVETKOV: DAN USSR, 120 No. 2, 346 (1958) (See OTS 59-11862 50¢);
2. IU. D. TSVETKOV, N. N. BUBNOV, M. A. MAKUL'SKII, IU. S. LAZURKIN, V. V. VOEVODSKII: DAN USSR, 122, 1053 (1958)
3. D. J. E. INGRAM, M. C. R. SYMONS, M. G. TOWNSEND: Trans. Farad. Soc., 54, 409 (1958)

TOM VI, Vyp. 4 OPTIKA I SPEKTROSKOPIIA Aprel', 1959
VOL. VI, No. 4 OPTICS AND SPECTROSCOPY April, 1959

On the Electron Paramagnetic Resonance Spectra of Hydrogen Atoms Stabilized on Solid Surfaces

N. N. BUBNOV, V. V. VOEVODSKII, L. S. POLIAK AND IU. D. TSVETKOV

In references [1, 2] some attention was devoted to the stabilization of H atoms formed on gamma bombardment of frozen hydrocarbons and other compounds on various surfaces.

It is of interest to clarify the influence of the character of the surface on a) the magnitude of the hyperfine splitting of the electronic paramagnetic resonance (EPR) spectrum of the H atoms and on b) the width of the EPR absorption line. For that purpose, we have investigated the EPR spectra of H atoms stabilized on quartz, silicagel and molybdemum glass. The H atoms were formed by gamma bombardment of the surfaces enumerated above at 77°K. One may assume that the formation of atoms in this case depends upon bond-breaking in H_2O molecules, absorbed on the surface, or in SiOH groups [3].

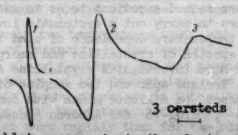

Doublet components in the electron paramagnetic resonance spectra of hydrogen atoms stabilized on different surfaces at 77° K.

1 - on quartz. 2 - on silicagel. 3 - on molybdemum glass.

The magnitude of the hyperfine splitting in all cases turned out to be close to 500 Oe., which differs very little from the magnitude of the splitting of the free H atom [4]. The

width of the components of the hydrogen doublet, as can be seen from the figure, changes substantially from one surface to another; on quartz, it is close to 0.8 Oe.; on silicagel - 2.4 Oe.; on glass - 4.5 Oe.

Since the hyperfine splitting in the EPR spectrum of H atoms stabilized on a surface is close to that for the free atom [4], the coupling of the H atoms with the surface takes place without a substantial change in the spin density of the unpaired electron on the atom. On the other hand, the width dependence of the components in the spectra of the different stabilizing surfaces points to the existence of a definite interaction of the unpaired electron with the surface. Experimental and theoretical research on the mechanism of relaxation (by way of measurement of the component width of the doublets and the saturation factor, as well as studies of the effect of temperature, chemical factors and surface properties on the EPR spectrum of atoms stabilized on surfaces all would allow us to establish the nature of the bond between H atoms and solid surfaces.

August 29, 1958

References

1. R. LIVINGSTON, H. ZELDES, E. H. TAYLOR: Disc. Farad. Soc., No. 19, 166 (1955)
2. N. IA. CHERNIAK, N. N. BUBNOV, V. V. VOEVODSKII, L. S. POLAK, IU. D. TSVETKOV: DAN USSR, 120, No. 2, 346 (1958) (See OTS 59-11862 50¢)
3. M. M. EGOROV, K. G. KRASIL'NIKOV, V. F. KISELEV: ZFKh, 32, 2448 (1958)
4. R. BERINGER, M. A. HEALD: Phys. Rev., 95, 1474 (1954)

TOM VI, Vyp. 4 OPTIKA I SPEKTROSKOPIIA Aprel', 1959
VOL. VI, No. 4 OPTICS AND SPECTROSCOPY April, 1959

Temperature Dependence of the Intensity of Stokes Bands in the Raman Spectra of Certain Solids

IA. S. BOBOVICH AND T. P. TULUB

The temperature dependence of the intensity of Raman bands has been the subject of many investigations [1 - 14]. These have been concerned most often with liquids and much more rarely with solids. In the case of liquids, the existence of a temperature anomaly has been shown quite conclusively; this is evinced in a decrease in the integrated band intensity with increasing temperature, instead of the increase predicted by theory. For solids, on the other hand, the results are much less definite [cf. 3, 5, 6, 8, 15]. This situation is explained by the numerous experimental difficulties which were characteristic of the early period of Raman investigations, the period to which almost all of the work on solids belongs. In light of the significant recent developments in the technique of exciting and recording Raman spectra, the difficulties of investigating solids have been completely eliminated. The new technique allows quantitative measurements to be carried out with precision. It therefore seemed expedient to us to use these new resources to carry out a systematic investigation of the temperature dependence of band intensities in the spectra of crystalline and amorphous solids.

We have investigated crystalline and fused quartz, Iceland spar and two samples of two-component glasses (a silicate glass with composition Na_2O-24, SiO_2-76 and a boron glass, BaO-20, B_2O_3-80) * over the temperature range 300 - 550°K. The glasses were prepared in the form of cylinders. Nichrome wire wound on the sample served as an electric heater. Accurate temperature points were determined in advance by the fusion of various crystalline substances placed on the sample, and corresponding currents in the heater circuit were read with an accuracy of ± 0.025 amp on an ammeter. A long time interval was always allowed for the sample to attain equilibrium. Subsequently, during the excitation and recording of the Raman spectra, the samples were mounted in an exactly similar manner, so that their temperatures could be estimated from the magnitude of the current in the heater circuit. We believe that the error in the determination of the temperature by this method amounts to at most ± 5-8° C, a magnitude entirely acceptable for our experiments.

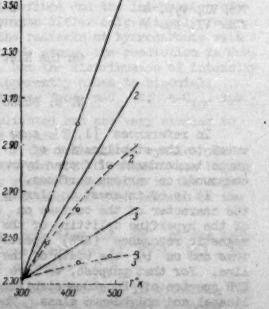

Figure 1. Variation of the intensity of the bands with temperature in the spectrum of crystalline quartz. The solid curves are theoretical, the dotted curves and points are obtained experimentally. Frequency (in cm^{-1}) : curve 1-125, curves 2 and 2'-200, curves 3 and 3'-460.

* As usual, the numbers show the mol percentages of the oxides.

The spectra of the samples were excited by low pressure spiral mercury lamps [16] and recorded by means of a DFS-12 grating spectrograph which is constructed on the principle of the Kiselev [17] double monochromator.

Thanks to the use of double monochromatization, there was no difficulty in investigating the low frequency region of the spectra; this was particularly important in the case of fused quartz and the two specimens of glass.

As is well known, the heating of substances is accompanied by a more or less rapid broadening of the vibrational bands. For this reason it is very important in temperature studies to measure the integrated intensities of the bands. To obtain reliable values for the integrated intensities, the bands were measured by a planimeter. Complex bands were divided up into component profiles; typical examples of this are shown in figures 2 and 4 below.

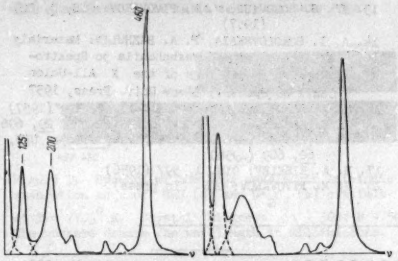

Figure 2. Spectrum of crystalline quartz at specimen temperatures of (a) 300, (b) 545°K. The numbers indicate the frequencies of the bands in cm $^{-1}$.

We will turn now to a description of the results obtained.

1) Crystalline quartz. In the spectrum of this substance we succeeded in observing the temperature behaviour of almost all the bands. A group of very weak bands in the region 800-1230 cm^{-1} did not change in intensity within the limits of error of the measurement ($\pm$ 7-8 %) on heating the sample to about 500°K . This agrees with theoretical deductions to the extent that the expected temperature effect for the lowest frequency band is only 9% ; that is, roughly equal to the error in our measurements. The intensity of other bands with frequencies 460 , 200 and 125 cm^{-1} increases with rising temperature, the increase being more rapid the smaller the magnitude of the vibrational quantum, although it is true that the first and second bands deviate from the theoretical trend.

For clarity, graphs of the change in intensity as a function of the temperature are shown in figure 1. Photoelectric recorder traces of the spectrum of crystalline quartz are reproduced in figure 2 for two temperatures of the sample. From these it is evident that the behaviour of crystalline quartz is qualitatively consistent with theoretical expectation.

2) Fused quartz. In this case the intensity of the bands also increases with increasing temperature of the sample and the relation between the observed effect and the magnitude of the vibrational quantum is equally evident. However, in contrast to crystalline quartz, the rate of change of the intensity of all the bands is noticeably greater than that predicted by theory. Curves showing the temperature variation * of the bands in the spectrum of fused quartz are shown in figure 3, and photoelectric recordings for two temperatures are reproduced in figure 4.

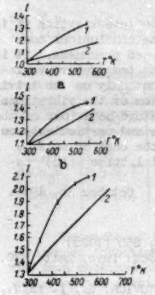

Figure 3.

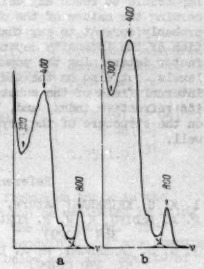

Figure 4.

Figure 3. Variation of the intensity of the bands in the spectrum of fused quartz with temperature. Frequency in cm^{-1} : (a) 800 , (b) 400, (c) 300 . No. 1 - experimental curves, No. 2 - theoretical curves. The line segments on the experimental curves indicate the scatter of the points.

Figure 4. Spectrum of fused quartz at sample temperatures of (a) 300°, (b) 540° K . The numbers indicate the frequencies of the bands in cm^{-1} .

Thus in the behaviour of the intensities for fused quartz we also observe only qualitative agreement with theory.

3) The glasses Na_2O-24, SiO_2-76 and BaO-20, B_2O_3-80. The Raman spectra of these substances were obtained for only two temperatures: 300 and 500°K. The increase of intensity in the spectra of the hot specimens was clearly evident, and was particularly great in the region of low frequencies. The high frequency bands showed no change in intensity. It is interesting that the intensity for the silicate glass rose much more rapidly than for the boron glass.

4) Iceland spar. The spectrum of the crystal of Iceland spar, in contrast to that of crystalline quartz, shows few bands. The most intense bands have the frequencies 155 , 280 and 1085 cm^{-1} .

* Since the broad low frequency band due to continuous scattering does not broaden noticeably on heating the specimen, the intensity values used in the frequency region 300 and 400 cm^{-1} were simply the ordinates of the spectrum tracing.

The first two belong to the external vibrations of the crystal lattice, the last to the totally symmetric internal vibration of the anion CO_3^{--}.

On raising the temperature of the specimen from room temperature to 550° K, the intensity of the bands at 155 and 280 cm^{-1} showed practically no change, whereas the intensity of the band at 1085 cm^{-1} decreased by approximately 30% in the same temperature interval. The average error in the measurements for the bands of this specimen did not exceed ± 5 %.

Thus in the spectrum of Iceland spar the intensities show a temperature anomaly similar to that observed in liquids.

At the present stage of the investigation it is impossible to reach any definite conclusions concerning the nature of the observed phenomena. It is probably correct to say that the temperature variation of the intensity depends not only on the trivial factor determining the population of the vibrational levels, but also on the temperature behaviour of the internal field of the substance and particularly on its refractive index, and, in the case of solids, on the structure of the crystal lattice [18] as well.

October 18, 1958.

References

1. K. S. KRISHNAN: Nature, 122, 650 (1928)
2. A. DADIEU, K. W. F. KOHLRAUSCH: Phys. Zeit., 30, 384 (1929)
3. G. S. LANDSBERG, M. A. LEONTOVICH: Zs. f. Phys., 53, 439 (1929)
4. F. G. BRICKWEDDE, M. F. PETERS: Phys. Rev., 33, 116 (1929)
5. G. S. LANDSBERG, L. I. MANDEL'SHTAM: Zs. f. Phys., 60, 364 (1930)
6. L. S. ORNSTEIN, J. J. WENT: Physica, 2, 503 (1935)
7. R. ANANTHAKRISHNAN: Proc. Ind. Acad. Sci., 7A, 196 (1938)
8. K. VENKATESWARLU: Proc. Ind. Acad. Sci., 13A, 64 (1941); 14A, 529 (1941); 16A, 45 (1942); 19A, 111 (1944); 21A, 24 (1945)
9. L. M. FISHKOVA: DAN USSR, 75, 523 (1950); Dissertation, Leningrad University, 1952
10. IA. S. BOBOVICH: DAN USSR, 98, 39-42 (1954) (See RT-4509, 4 pp.)
11. IA. S. BOBOVICH, V. M. PIVOVAROV: DAN USSR, 97, 801 (1954)
12. A. I. STEKHANOV, E. V. CHISLER: ZTF, 25, 2209 (1955) (See Soviet Physics, Tech. Phys.)
13. IA. S. BOBOVICH, V. M. PIVOVAROV: OiS, 3, 227 (1957)
14. A. I. SOKOLOVSKAIA, P. A. BAZHULIN: Materialy X Vsesoiuznogo Soveshchaniia po Spektroskopiia (Proceedings of the X All-Union Conf. on Spectr.) L'vov Univ. Press, 1957
15. M. HARRAND: Ann. Phys., Ser. 13, 2, 309 (1957)
16. IA. S. BOBOVICH, V. M. PIVOVAROV: ZETF, 29, 696 (1955) (See Soviet Physics, JETP); UFN, 60, 689 (1956)
17. B. A. KISELEV: OiS, 1, 597 (1956)
18. V. M. PIVOVAROV: OiS (In press)

TOM VI, Vyp. 4 OPTIKA I SPEKTROSKOPIIA Aprel', 1959
VOL. VI, No. 4 OPTICS AND SPECTROSCOPY April, 1959

Absorption Spectra of Certain Gallium Chalcogenide Crystals

E. F. GROSS, B. V. NOVIKOV, B. S. RAZBIRIN, L. G. SUSLINA

Investigations conducted in recent years on the absorption spectra of semiconducting crystals at low temperatures indicate the presence of a line structure for their long-wave intrinsic absorption edge. The first experiments in this region were made on cuprous oxide crystals [1], where a hydrogen-like series of narrow absorption lines was found at the temperature of liquid nitrogen. At the present time, a structure of the absorption edge which consists of discrete lines with, sometimes, a regular arrangement (Cu_2O, CdS for ex.) has been detected for a whole series of crystals (CdS, CdSe, ZnS, HgI_2, PbI_2, CuCl, CuBr, CuI [2-10] and others). Some authors relate this structure to the formation of exciton states in crystals, others - to superstoichiometric or foreign impurities in the crystal lattice.

Among the great variety of absorption spectra of semiconducting crystals, which are different in both the position of the absorption edge and in its structure, similar absorption spectra can be observed in a number of cases. Hence, it seems to us that a crystal-chemistry factor plays a large part. Thus, for example, an investigation of absorption in CdS, CdSe and ZnS crystals [2-4], which have the same hexagonal lattice and consists of components with similar chemical properties, discloses the similarity of their absorption spectra. An analogous similarity in the kind of absorption edge structure is also observed in copper halides [10], (the lattices of these compounds belong to the cubic system). It has also been remarked [11] that a change in the crystal lattice, with the stoichiometric relation of the components conserved (polymorphic transformation), influences the kind of absorption edge structure substantially.

In the light of the abovementioned considerations, we undertook investigations of the absorption spectra of gallium sulfide and selenide crystals which have the same hexagonal laminar lattice with comparable parameters [12]. Moreover, we investigated another stoichiometric relation of the components of β-Ga_2S_3 and Ga_2Se_3 crystals. The investigation of the crystals mentioned was also of independent interest since the absorption spectra of these substances had not yet been studied.

One of the authors synthesized the GaS and Ga_2S_3 crystals. The GaS crystals were obtained by the joint fusion of stoichiometric quantities of chemically pure gallium and sulfur in evacuated sealed quartz tubes. The synthesis temperature was 1000 - 1050° C. Especially fine crystals

(of thickness up to 1 μ) were obtained upon sublimation of GaS in a tube in which the temperatures of the upper and lower ends were 750 and 950°C, respectively [12]. Crystals of β-Ga_2S_3, whose lattice has a wurtzite (β-shape) structure, were also obtained by an analogous method, but, in contrast to the GaS, at a higher temperature (1200-1250°C). The production of GaSe and Ga_2Se_3 crystals (cubic system) has been described by Goriunova and her colleagues [13].

The GaS and GaSe crystals were investigated in the form of single crystals of 100 to several microns thickness.

At room temperature, the absorption edge of GaS is located at about 420 mμ. As the temperature is reduced to 77.3°K (fig. 1a), the absorption boundary is shifted toward the short wavelengths to 412 mμ. An absorption band of almost 2 mμ width with a maximum at 411 mμ is seen near this edge.

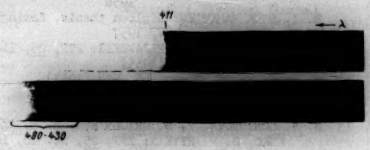

Figure 1. Spectra of the long wavelength intrinsic absorption edge of GaS (a) and Ga_2S_3 (b) crystals at T = 77.3° K. Crystal thickness: a - 30μ; b - 50μ. The numbers denote the wavelength in millimicrons.

The absorption spectrum of GaSe* is rather more complex. At room temperature, a 625 mμ band of almost 5mμ width is observed at the absorption edge. The band is located at the longwave edge of the weak absorption step which extends to the short wavelengths to the 550-560 mμ region from which the absorption starts to increase rather rapidly. As the samples are cooled to T = 77.3°K (fig. 2a), the whole picture is shifted toward the short wavelengths. The 625 mμ band is contracted to 3 mμ and it takes the position of 590 mμ. A second very weak doublet band 587-580 mμ appears at its shortwave side. In the thinnest samples (2-3 μ)the shortwave edge of the step is located near 500-510 mμ. A reduction of the temperature to 4.2°K contracts the whole band and displaces it still more toward the shortwave part of the spectrum, however no additional structure is detected here.

In contrast to GaS and GaSe, no structure was observed at the longwave absorption edges of Ga_2S_3 and Ga_2Se_3 crystals (thickness d≈50 - 100 μ). The absorption edge in Ga_2S_3 at room temperature is near 450-500 mμ and near 430-480 mμ at 77.3°K (fig. 1b); at room temperature in Ga_2Se_3 it is near 600-640 mμ and near 560-600 mμ at T = 77.3°K (fig. 2b). The absorption edges of both substances are washed out (particularly intensely in the Ga_2S_3) and are displaced toward the short wavelengths as the crystal thickness dimishes, which indicates the monotonic growth of the absorption coefficient in this region.

* One of the authors already reported on the presence of the structure and absorption spectrum of GaSe crystals [14].

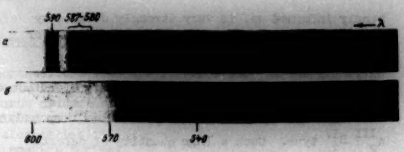

Figure 2. Spectra of the long wavelength intrinsic absorption edge of GaSe (a) and Ga_2Se_3 (b) crystals at T = 77.3°K. Crystal thickness: a-30μ; b-50μ. The numbers denote the wavelength in millimicrons.

Forbidden Band Width Δ E (in eV)

substance	From Optical measurements		From photoelectric measurements at room temperature
	T=290°K	T=77.3K	
GaS	2.9	3.0	
GaSe	1.98	2.09	1.95[13], 2.04[15]
β-Ga_2S_3	2.5-2.7	2.6-2.9	2.48[13]
Ga_2Se_3	1.9-2.1	2.1-2.2	1.75-1.9[13]

The width of the forbidden bands in the substances investigated can be estimated by using the data obtained about the absorption. The values of the forbidden bandwidths ΔE are compared in the table presented below with the results of other authors obtained from photoelectric measurements at room temperature.

It is interesting to note that in[15], where the spectral distribution of the photoconductivity in GaSe was investigated at room temperature and T = 100° C, a strong photo current peak was detected in the region of the structure we observed. It is possible that this maximum is related to the absorption structure noted above. The investigations conducted indicate that the crystallo-chemically similar crystals GaSe and GaS, with the exception of certain individual peculiarities, have generally similar absorption spectra, which verifies the strong effect of the lattice structure on the absorption edge spectrum.

As regards the nature of the observed absorption structures of GaS, GaSe crystals it is still not possible to give it a unique interpretation. On one hand, the good producibility of the structure in various samples and its position near the absorption edge seem to afford the possibility of relating it to the formation of exciton states in the crystal. On the other hand, because of the absence of any special check on the chemical composition of the substances obtained, the appearance of the structure discussed is possible because of foreign or hyperstoichiometric impurities.

It has already been remarked that a discrete structure of the absorption edge is not detected in a whole series of crystals [16]. All these crystals MoO_3, V_2O_5, Bi_2O_3, As_2S_3, $HgBr_2$, HgI_2 (yellow form) are in a class of low symmetry. However, even crystals such as β-Ga_2S_3 and Ga_2Se_3, which have higher forms of symmetry, do not have a line structure of the absorption edge. In this connection, it is interesting to note that the crystal lattice of these substances, as V.P. Zhuze

kindly informed us, is very strongly damaged by disorder defects. Thus, for example, the number of defects in the crystal lattice of Ga_2Se_3 is extremely large: one-third of the cation sites appear to be empty; here the defects are distributed statistically in the lattice [17]. A similar situation occurs in the lattices of other compounds of $A^{III}_2 B^{IV}_3$ type. Such a huge quantity of defects makes both the formation of excitons as well as their migration over the lattice extremely difficult. Excitons being formed under the influence of light will at once encounter defects in their paths as they move over the lattice and will be annihilated. Hence, the lifetime of the excitons in such lattices becomes very small because of the crystal imperfection, which can lead to the washing out of the exciton levels. In this case the exciton structure of the absorption edge can be absent.

The authors are grateful to N. A. Goriunova for kindly providing the GaSe and Ga_2Se_3 samples, synthesized in her laboratory, and also for valuable hints and comments on the preparation of GaS and Ga_2S_3 crystals.

November 27, 1958

References

1. E. F. GROSS, N. A. KARRYEV: DAN USSR, 84, 471 (1952)
M. HAYASHI, K. KATSUKI: J. Phys. Soc. Japan, 7, 599 (1952)
2. E. F. GROSS, M. A. IAKOBSON: DAN USSR, 102, 485 (1955)
3. E. F. GROSS, V. V. SOBOLEV: ZTF, 26, 1622 (1956) (See Soviet Physics, Tech. Phys.)
4. E. F. GROSS, L. G. SUSLINA: OiS, 6, 115 (1959) (See this journal, p. 70)
5. S. NIKITINE, L. COUTURE, M. SIESKIND, G. PERNY: C.R., 238, 1786 (1954)
S. NIKITINE, M. SIESKIND: C.R., 240, 1324 (1955)
6. S. NIKITINE, G. PERNY: C.R., 240, 64 (1955)
7. E. F. GROSS, A. A. KAPLIANSKII: ZTF, 25, 2061 (1955)
8. S. NIKITINE, L. COUTURE, G. PERNY, R. REISS: C.R., 241, 629 (1955)
9. S. NIKITINE, R. REISS: C.R., 242, 238, 1003 (1956)
10. B. S. RAZBIRIN: Diploma thesis, Leningrad Univ. 1956
R. I. SHEKHMAMET'EV: Diploma thesis, Leningrad Univ., 1957
11. E. F. GROSS, A. A. KAPLIANSKII: ZTF, 25, 1661 (1955)
12. H. HAHN: Angew. Chem., 65, 538 (1953)
H. HAHN, G. FRANK: Zs. f. anorg. u. allgem. Chem., 278, 340 (1955)
13. N. A. GORIUNOVA, V. S. GRIGOR'EVA, B. M. KONOVALENKO, S. M. RYVKIN: ZTF, 25, No. 10, 1675-1682 (1955) (See R-3692, 6 pp. from LC)
14. E. F. GROSS: J. Phys. et Rad., 17, 815 (1956)
15. S. M. RYVKIN, R. IU. KHANSEVAROV: ZTF, 26, 2781 (1956) (See Soviet Physics, Tech. Phys.)
16. E. F. GROSS, M. L. BELLE: ZTF, 25, 948 (1955)
A. A. KAPLIANSKII: Cand. Dissertation, LFTI, 1957
17. H. HAHN, W. KLINGLER: Zs. anorg. Chem., 259, 135 (1949)

ABBREVIATIONS OFTEN ENCOUNTERED AND USED HEREIN

DAN USSR	Doklady Akademii Nauk	(Reports of the Academy of Sciences of the USSR)
DAN UkrSSR	Dopovidi Akademii Nauk UkrSSR	(Reports of the Academy of Sciences of the Ukraine SSR)
DAN ArmSSR	Doklady Akademii Nauk ArmSSR	(Reports of the Academy of Sciences of the Armenia SSR)
IAN USSR	Izvestiia Akademii Nauk USSR	(Bulletin of the Academy of Sciences of the USSR)
	SF Seriia fizika	(Physics series)
	SM Seriia matematika	(Mathematics series)
	OKhN Otdelenie khimicheskikh	(Section of chemical sciences)
OiS	Optika i Spektroskopiia	(Optics and Spectroscopy)
PiTE	Pribory i Tekhnika Eksperimenta	(Instruments and Techniques of Experiment)
AE	Atomnaia Energiia	(Atomic Energy)
AZ	Astronomicheskii Zhurnal	(Astronomy Journal)
FMM	Fizika Metallov i Metallovedenie	(Physics of Metals and Metallography)
Radiotekh.	Radiotekhnika	(Radio Engineering)
RiE	Radiotekhnika i Elektronika	(Radio Engineering and Electronics)
UK	Uspekhi Khimii	(Progress in Chemistry)
UFN	Uspekhi Fizicheskikh Nauk	(Progress in Physical Sciences)
UFZ	Ukrainskii Fizichni Zhurnal	(Ukraine Physical Journal)
ZETF	Zhurnal Eksperimental'noi Teoreticheskoi Fiziki	(Journal of Experimental Theoretical Physics - JETP)
ZTF	Zhurnal Tekhnicheskoi Fiziki	(Journal of Technical Physics)
FTT	Fizika Tverkogo Tel	(Solid State Physics)
ZFKh	Zhurnal Fizicheskoi Khimii	(Journal of Physical Chemistry)
ZOKh	Zhurnal Obshchee Khimii	(Journal of General Chemistry
ZNKh	Zhurnal Neorganicheskoi Khimii	(Journal of Inorganic Chemistry)
ZPKh	Zhurnal Prikladnoi Khimii	(Journal of Applied Chemistry)
Tr.	Trudy	(Transactions, as for instance, Tr. FIAN)
FIAN	Fizicheskii Institut Akademii Nauk USSR	(P.N. Lebedev Physical Institut of the Academy of Sciences USSR)
Sb.	Sbornik	(Collection, as for instance, Fizich. sb. L'vovskogo Universitet) Fizich. sb. Fizicheskaia sbornik (Physics Collection)
Uch. Zap.	Uchenye Zapiskii	(Scientific Records)
Vestn.	Vestnik	(Herald or Messenger)
FTIAN	Fiziko-Tekhnicheskii Institut Akademii Nauk	(Physical-Technical Institute of the Academy of Sciences)
GOI	Gosudarstvennyi Opticheskii Institut	(State Optical Institute)
VEI	Vsesoiuznyi Elektrotechnicheskii Institut	(All-Union Electrotechnical Institute)
MFTI	Moskovskaia Fiziko-Tekhnicheskii Institut	(Moscow Institute of Physics and Technology)
NIZMIR	Nauchno-Issledovatel'skii Institut Zemnogo Magnetizma, Ionosfery i Rasprostraneniia	(Research Institute of Terrestrial Magnetism and Ionospheric Propagation)
GIFTI	Gor'kovskii Issledovatel'skii Fiziko-Tekhnicheskii Institut	(Gor'kii Research Institute of Physics and Technology)
NIFI	Nauchno-Issledovatel'skii Fizicheskii Institut	(Scientific Research Institute of Physics, Leningrad Univ.)
NIRFI	Nauchno-Issledovatel'skii Radio-fizicheskii Institut	(Scientific Research Institute of Radiophysics, Gor'kii Univ.)
GITTL	Gostekhizdat - Gosudarstvennoe Izdatel'stvo Tekhniko-Teoreticheskoi Literatury	(State Publishers of Technical-Theoretical Literature)
GIFML	Fizmatgizdat - Gosudarstvennoe Izdatel'stvo Fiziko-Matematicheskoi Literatury	(State Publishers of Physical-Mathematical Literature, formerly Gostekhizdat)
IL or IIL	Izdatel'stvo Inostrannoi Literatury	(Publishers of Foreign Literature)
Izd. AN USSR	Izdatel'stvo Akademiia Nauk USSR	(Academy of Sciences Press)
ZL	Zavodskaia Laboratoriia	(Factory Laboratory)
GOST	Gosudarstvennyi Obshchesoiuznyi Standart	(All - Union State Standard)
LIPAN USSR	Laboratoriia izmeritel'nykh priborov AN USSR	(Laboratory of Measuring Instruments)
IFAN UkrSSR	Institut Fiziki AN UkrSSR, KIEV	(Physics Institute AN Ukr SSR)
SFTI	Sibirskii Fiziko-Tekhnicheskii Institut, Tomsk	(Siberia Physical-Technical Institute)
IFAAN ESSR	Institut Fiziki i Astronomii AN ESSR, Tartu	(Institute of Physics and Astronomy)
IFA AN USSR	Institut fiziki atmosfery AN USSR	(Institute of the Physics of the Atmosphere)

AFFILIATIONS OF AUTHORS FROM ISSUE 4

V. I. DIANOV-KLOKOV	INSTITUT ELEMENTOORGANICHESKIKH SOEDINENII AN USSR
L. A. LYZINA A. T. VARTANIAN A. S. CHERKASOV T. M. VEMBER	GOI, LENINGRAD
Z. A. TRAPEZNIKOVA V. I. MALYSHEV S. G. RAUTIAN L. A. VAINSHTEIN I. I. SOBEL'MAN V. G. VESELAGO	FIAN USSR, MOSCOW
I. V. OBREIMOV E. V. IAMSHCHIKOV	MOSKOVSKII INZHENERNO-FIZICHESKII INSTITUT (MIFI)
I. N. SHKLIAREVSKII V. G. PADALKA A. A. AVDEENKO	KHAR'KOVSKII GOSUDARSTVENNYI UNIVERSITET
P. G. KARD	TARTUSKII GOSUDARSTVENNYI UNIVERSITET
F. I. FEDOROV B. V. BOKUT'	BELORUSSKII GOSUDARSTVENNYI UNIVERSITET, MINSK
B. P. KOZYREV O. E. VERSHININ	LENINGRADSKII ELEKTROTEKHNICHESKII INSTITUT (LETI)
A. O. SALL'	GOSUDARSTVENNOE SOIUZNOE KONSTRUKTORSKOE BIURO ANALITICHESKOGO PRIBOROSTROENIIA
IA. S. BOBOVICH T. P. TULUB	INSTITUT KHIMII SILIKATOV AN USSR
B. S. RAZBIRIN E. F. GROSS L. G. SUSLINA V. V. NOVIKOV	LENINGRADSKII GOSUDARSTVENNYI UNIVERSITET
N. IA. CHERNIAK N. N. BUBNOV L. S. POLIAK IU. D. TSVETKOV V. V. VOEVODSKII	INSTITUT KHIMICHESKOI FIZIKI, MOSCOW

SYMBOLS FOR SOURCES OF TRANSLATIONS

AIP
American Institute of Physics
335 East 45th Street
New York 17, New York

ATS
Associated Technical Services, Inc.
P.O. Box 271
East Orange, New Jersey

CB
Consultants Bureau, Inc.
227 West 17th Street
New York 11, New York

CCT
Consultants Custom Translations, Inc.
227 West 17th Street
New York 11, New York

CTT
Columbia Technical Translations
5 Vermont Avenue
White Plains, New York

HB
Henry Brutcher
P.O. Box 157
Altadena, California

LC
Photoduplication Service
Publication Board Project
Library of Congress
Washington 25, D. C.

MDF
Morris D. Friedman, Inc.
P.O. Box 35
New Newton 65, Mass.

NRCC
National Research Council, Library
Ottawa 2, Canada

OTS
Office of Technical Services
Department of Commerce
Washington 25, D.C.

PS
Primary Sources
11 Bleecker Street
New York 12, New York

RIS
Research Information Service
40 East 23rd Street
New York 10, New York

SLA
SLA Translation Center
The John Crerar Library
86 East Randolph Street
Chicago 1, Illinois

I. V. OBREIMOV, E. F. IAMSHCHIKOV
Krivye dispersii khloroforma i chetyrekhkhloristogo ugleroda v shirokom intervale temperatur 517

V. S. SUKHORUKIKH
Difraktsiia Frenelia ot uzkogo ekrana, shcheli i poluploskosti pri nesfericheskoi volne 523

I. N. SHKLIAREVSKII, A. A. AVDEENKO, V. G. PADALKA
Izmerenie opticheskikh postoiannykh sur'my v infrakrasnoi oblasti spektra pri temperature 290 i 110 528

P. G. KARD
O vliianii tonkikh plenok na polnoe otrazhenie 533

B. V. BOKUT'AND F. I. FEDOROV
K teorii opticheskoi aktivnosti kristallov. III. Obshchee uravnenie normalei 537

B. P. KOZYREV AND O. E. VERSHININ
Opredelenie spektral'nykh koeffitsientov diffuznogo otrazheniia infrakrasnoi radiatsii ot zachernennykh poverkhnostei 542

V. I. MALYSHEV, S. G. RAUTIAN
Ispol'zovanie esheletta pri bol'shikh uglakh difraktsii 550

A. O. SALL
O poroge chuvstvitel'nosti optiko-akusticheskogo priemnika radiatsii. II. Neravnomernoe vydelenie tepla po ob'emu kamery selektivnogo priemnika. Vysokaia chastota obtiuratsii 556

KRATKIE SOOBSHCHENIIA

V. K. ABLEKOV
Ob obrabotke spektrogramm, poluchennykh na interferometre Fabri-Pero 562

N. IA. CHERNIAK, N. N. BUBNOV, L. S. POLIAK, IU. D. TSVETKOV, V. V. VOEVODSKII
O nekotorykh zakonomernostiakh v spektrakh elektronnogo paramagnitnogo rezonansa alkil'nykh radikalov 564

N. N. BUBNOV, V. V. VOEVODSKII, L. S. POLIAK, IU. D. TSVETKOV
O spektrakh elektronnogo paramagnitnogo rezonansa atomov vodoroda, stabilizirovannykh na tverdykh poverkhnostiakh 565

IA. S. BOBOVICH, T. P. TULUB
Temperaturnaia zavisimost' intensivnosti stoksovykh polos kombinatsionnogo rasseianiia v spektrakh nekotorykh tverdykh tel 566

E. F. GROSS, B. V. NOVIKOV, B. S. RAZBIRIN, L. G. SUSLINA
Spektry pogloshcheniia kristallov nekotorykh khalkogenidov galliia 569

Dispersion Curves of Chloroform and Carbon-tetrachloride in a Wide Temperature Range 329

Fresnel Diffraction of a Non-spherical Wave by a Narrow Screen, a Slit and a Half-plane 332

Measurements of the Optical Constants of Antimony in the Infrared Region of the Spectrum at Temperatures of 290° and 110° 336

On the Influence of Thin Films on Total Reflection 339

On the Theory of Optical Activity in Crystals III. General Equation of Normals 342

Determination of Spectral Coefficients of Diffuse Reflection of Infrared Radiation from Blackened Surfaces 345

Use of an Echelette at Large Diffraction Angles 351

On the Threshold Sensitivity of An Optical-Acoustic Radiation Detector II. Nonuniform Heat Elimination in the Chamber Volume of a Selective Detector. High Modulation Frequency 355

BRIEF REPORTS

On Processing Spectrograms Obtained on a Fabry Perot Interferometer 359

Some Regularities in the Electron Paramagnetic Resonance Spectra of Alkyl Radicals 360

On the Electron Paramagnetic Resonance Spectra of Hydrogen Atoms Stabilized on Solid Surfaces 361

Temperature Dependence of the Intensity of Stokes Bands in the Raman Spectra of Certain Solids 362

Absorption Spectra of Certain Gallium Chalcogenide Crystals 364

Abbreviations Often Encountered and Used Herein 367

Affiliation of Authors from Issue 4 368

Instructions for Authors (Russian) 369

Letter from the Publisher 370

Lithoprinted in the U.S.A. by Blackburn Printing Co., West Concord, Mass.

TOM VI, Vyp. 4 OPTIKA I SPEKTROSKOPIIA Aprel , 1959
VOL. VI, No. 4 OPTICS AND SPECTROSCOPY April, 1959

SODERZHANIE

V Mezhdunarodnoi Ob edinennoi komissii po spektroskopii
Doklady na soveshchanii 429
G. HERZBERG
Lembovskie smeshcheniia osnovnykh sostoianii He^4 i He^3 429
W. F. MEGGERS
Sovremennoe sostoianie voprosa o spektrakh redkikh zemel' s eksperimental'noi tochki zreniia 433
CH. E. MOORE
Sovremennye dannye o spektrakh redkozemel nykh elementov (na avgust 1958 g.) 433
R. S. MULLIKEN
Issledovaniia, provodimye v Laboratorii molekuliarnoi struktury i spektrov v Chikago 437
L. A. VAINSHTEIN, I. I. SOBEL'MAN
Nestatsionarnaia teoriia shtarkovskogo ushireniia spektral'nykh linii v plazme 440
I. V. ORLOVA, I. N. GODNEV
O sviazi metoda Larnodi i metoda mulevykh priblizhenii El'iashevicha i Stepanova 447
V. G. VESELAGO
Opredelenie struktury i dipol'nogo momenta molekuly HDSE iz ee mikrovolnovogo spektra 450
V. I. DIANOV-KLOKOV
K voprosu o proiskhozhdenii spektra zhidkogo i szhatogo kisloroda (12,600 - 3000 Å) 457
G. A. KHACHKURUZOV
Kolebatel'nye postoiannye molekuly vody 463
G. S. DENISOV
Ob izmerenii intensivnosti sil nykh polos pogloshcheniia v infrakrasnykh spektrakh zhidkostei 475
M. S. KOZYREVA
Primenenie infrakrasnoi spektroskopii k issledovaniiu polimerizatsii poliizobutilenov 478
L. A. LYZLOVA, A. T. VARTANIAN
Vliianie parov vody na spektry pogloshcheniia vozognannykh sloev krasitelei 484
IU. V. NABOIKIN, B. A. ZADOROZHNYI, E. N. PAVLOVA
Osobennosti liuminestsentsii orto-dizameshchennykh aromaticheskikh uglevodorodov. II 492
A. S. CHERKASOV
O vliianii zameshchaniushchikh grupp na polozhenie spektrov pogloshcheniia i fluorestsentsii proizvodnykh antratsena 496
A. S. CHERKASOV, T. M. VEMBER
O vliianii kisloroda na fotokhimicheskie prevrashcheniia i kontsentratsionnoe tushenie fluorestsentsii nekotorykh proizvodnykh antratsena 503
Z. A. TRAPEZNIKOVA
O vzaimodestvii "golubykh" i "samarievykh" tsentrov v fosfore ZnS-Sm(Cl) 512

CONTENTS

V International Joint Commission on Spectroscopy
Reports at the Conference 273
Lamb Shifts of the Ground States of He^4 and He^3 273
The Present Status of Rare Earth Spectra from an Experimental Point of View 273
Modern Data on the Spectra of the Rare Earth Elements (August, 1958) 275
Research in Progress in the Laboratory of Molecular Structure and Spectra in Chicago 277
Non-Stationary Theory of the Stark Broadening of Spectral Lines in Plasmas 279
On The Connection Between Larnaudie's Method and the El'iashevich - Stepanov Method of Zero Approximations 284
Determination of the Structure and Dipole Moment of HDSe from its Microwave Spectrum 286
On the Question of the Origin of the Spectrum of Liquid and Compressed Oxygen (12,600 - 3,000 Å) 290
Vibrational Constants of the Water Molecule 294
On the Measurement of Intensities of Strong Absorption Bands in Infrared Spectra of Liquids 301
Application of Infrared Spectroscopy to the Investigation of Polymerization of Polyisobutylene 303
Influence of Water Vapors on the Absorption Spectra of Sublimated Layers of Dyes 307
Peculiarities of the Luminescence of Ortho-Disubstituted Aromatic Hydrocarbons: II 312
On the Influence of Substituting Groups on the Absorption and Fluorescence Spectra of Derivatives of Anthracene 315
The influence of Oxygen on Photochemical Transformations and the Concentration Quenching of Fluorescence of Some Anthracene Derivatives 319
On the Interaction of "Blue" and "Samarium" Centers in the Phosphor ZnS-Sm(Cl) 325